MECHANISM OF UBIQUITIN INDUCED ACTIVATION OF RIG-I LIKE

RECEPTORS IN ANTIVIRAL INNATE IMMUNITY

APPROVED BY SUPERVISORY COMMITTEE

Zhijian 'James' Chen, Ph.D.

James Brugarolas, Ph.D.

Lora Hooper, Ph.D.

Xiaodong Wang, Ph.D.

DEDICATION

To my Mom

MECHANISM OF UBIQUITIN INDUCED ACTIVATION OF RIG-I LIKE RECEPTORS IN ANTIVIRAL INNATE IMMUNITY

by

XIAOMO JIANG

DISSERTATION

Presented to the Faculty of the Graduate School of Biomedical Sciences

The University of Texas Southwestern Medical Center at Dallas

In Partial Fulfillment of the Requirements

For the Degree of

DOCTOR OF PHILOSOPHY

The University of Texas Southwestern Medical Center at Dallas

Dallas, Texas

November, 2011

MECHANISM OF UBIQUITIN INDUCED ACTIVATION OF RIG-I LIKE RECEPTORS IN ANTIVIRAL INNATE IMMUNITY

XIAOMO JIANG, Ph.D.

The University of Texas Southwestern Medical Center at Dallas, 2011

Supervising Professor: Zhijian J. Chen, Ph.D.

The innate immune response is the first line of defense against viral infections. Innate immune recognition is mediated by a set of host pattern recognition receptors that can recognize pathogen associated molecular patterns, and trigger the expression of immune response genes. Two proteins of the RIG-I like receptor family, RIG-I and MDA5, are essential for the detection of viral RNA in the cytoplasm. Upon viral recognition, RIG-I and MDA5 activate the mitochondrial signaling protein MAVS, and initiate downstream signaling pathways that activate the transcription factors NF-κB and IRF3. These transcription factors regulate the production of type I interferons and proinflammatory cytokines, which serve to keep virus infections under control.

RIG-I and MDA5 contain N-terminal tandem CARD domains. CARD domains in other proteins are known to mediate protein-protein interactions. MAVS also contain one CARD domain. It has been proposed that the activation of MAVS by RIG-I is mediated by homotypic interaction between their CARD domains. However, it is hard to detect stable interaction between the CARD domains of RIG-I and that of MAVS. Therefore, the underlying biochemical mechanisms of how activation signals are transduced from a cytosolic receptor, RIG-I, to a mitochondria signaling protein, MAVS, is not clear.

Protein ubiquitination have pivotal roles in diverse cell signaling pathways, including those in the immune system. A ubiquitin E3 ligase, TRIM25, promotes Lysine 63-linked polyubiquitination of RIG-I, and is essential for the RIG-I antiviral pathway. However, the biochemical mechanisms by which RIG-I is activated by ubiquitin remain poorly understood. In addition, whether ubiquitination is involved in MDA5 activation is unknown.

Here, I describe the development of an in vitro biochemical assay to detect MAVS activation by a cytosolic activator. Purification of this activator revealed an important role of ubiquitin in RIG-I activation. Biochemical characterization of the ubiquitin induced RIG-I activation process revealed a new mechanism by which ubiquitin regulates cell signaling that involves the formation of a polyubiquitin-induced tetrameric complex. In addition, polyubiquitin-induced oligomerization appears to be a conserved mechanism for both MDA5 and RIG-I activation.

TABLE OF CONTENTS

PRIOR PUBLICATIONS

1. Jiang, X., and Chen, Z.J. (2011). Viperin links lipid bodies to immune defense. Immunity *34*, 285-287.

2. Zeng, W., Sun, L., Jiang, X., Chen, X., Hou, F., Adhikari, A., Xu, M., and Chen, Z.J. (2010). Reconstitution of the RIG-I pathway reveals a signaling role of unanchored polyubiquitin chains in innate immunity. Cell *141*, 315-330.

3. Xia, Z.P., Sun, L., Chen, X., Pineda, G., Jiang, X., Adhikari, A., Zeng, W., and Chen, Z.J. (2009). Direct activation of protein kinases by unanchored polyubiquitin chains. Nature *461*, 114-119.

4. Skaug, B., Jiang, X., and Chen, Z.J. (2009). The role of ubiquitin in NF-kappaB regulatory pathways. Annu Rev Biochem *78*, 769-796.

5. Yan, J., Liu, X., Wang, Y., Jiang, X., Liu, H., Wang, M., Zhu, X., Wu, M., and Tien, P. (2007). Enhancing the potency of HBV DNA vaccines using fusion genes of HBV-specific antigens and the N-terminal fragment of gp96. J Gene Med *9*, 107-121.

LIST OF FIGURES

LIST OF TABLES

LIST OF APPENDICES

CHAPTER I

INTRODUCTION

This chapter introduces general background on the molecular basis of the mammalian antiviral innate immunity, as well as current knowledge on the diverse functions of ubiquitin in immunity.

I.1. Molecular Basis of Antiviral Innate Immunity

Viruses are the most abundant type of pathogens on earth. Viral diseases inflict great health and economical problems worldwide, and are major challenges for the biomedical field. The mammalian immune system has innate and adaptive components, both contributing to antiviral immunity. The innate immune system is an evolutionarily ancient form of host defense mechanism found in most multicellular organisms. Cells of the innate immune system play an essential role in initiating anti-microbial responses. They recognize infections with broad specificity for conserved and invariant features of microorganisms, rapidly activate conserved host signaling pathways that control the expression of a variety of immune response genes, and stimulate the adaptive immune response. The adaptive immune system, in turn, develops in a later phase of infection, mounts antigen-specific responses, and forms immunologic memory against the pathogen.

Knowledge about the immune system and host-pathogen interactions is vital to the development of effective protection against pathogens, and therapeutics for infectious diseases.

The foundation for innate immunity to virus infection is composed of the processes of pathogen recognition, and cellular signaling to induce immunological outcomes.

I.1.1. Pattern recognition and pathogen-associated molecular patterns

Innate immune recognition is a process of pattern recognition, i.e. molecular features of microorganisms, also known as pathogen-associated molecular patterns (PAMPs), by a set of host pattern recognition receptors (PRRs)[1]. Several features make PAMPs well suited targets for innate immune recognition[2] : 1) PAMPs represent molecular features of only microorganisms but not host cells, allowing distinction between self and non-self. 2) PAMPs are essential to the survival of microorganisms, so that pathogen evasion from the innate immune recognition through evolution is limited. 3) PAMPs are molecular features shared by large classes of microorganisms, not only providing broad specificity but also allowing the host to have limited number of germ-line encoded PRRs to recognize a vast variety of microorganisms. Upon virus infection, viral particles enter host cells, uncoat, and release genome components for processes essential for the viral life cycle, such as gene expression and genome replication. Each step presents viral specific proteins and nucleic acids as possible PAMPs.

Table 1.1 lists some viral PAMPs and host PRRs that recognize them. During viral entry, viral proteins can be recognized by cell surface receptors. Viral nucleic acids can be recognized based on specific structural and chemical features that are unique to viral RNA and DNA as well as on their location in the cell. Therefore, although all viral components are synthesized and assembled within host cells, the innate immune system can still efficiently recognize and distinguish self and non-self, and trigger immune defense responses.

I.1.2. Pattern recognition receptors and antiviral signaling pathways

To mediate pattern recognition, the innate immune system has three functional classes of pattern recognition receptors (PRRs): secreted, endocytic, and signaling. Secreted receptors are represented by the mannan-binding lectins which bind microbial carbohydrates, and initiate complement activation. Endocytic receptors occur on phagocytes, e.g. macrophage mannose receptors, and mediate the uptake and delivery of pathogens into lysosomes to be destroyed[3]. Both classes are essential for the direct clearance of pathogens. Signaling PRRs seem to have a major role in the induction of a variety of immune response genes, such as antimicrobial peptides and inflammatory and antiviral cytokines, and are discussed here in more detail.

There are several distinct groups of signaling PRRs that contribute to viral recognition (discussed below). Some Toll-like recpeotrs (TLRs) can recognize viral proteins; other TLRs, as well as RIG-I like receptors (RLRs) and NOD-like receptors

(NLRs), can recognize viral nucleic acids. Expression of some TLRs are highly restricted to specific tissues and cellular compartments, while nearly all nucleated cells can produce type I interferons (IFNs) (e.g. IFNα and IFNβ) after viral infection as the frontline of immune defense. With distinct distribution patterns among tissues and cellular compartments, RLRs, NLRs and TLRs contribute to different stages of antiviral defenses. In the following section, I first introduce background information on RLRs (which my project focuses on), and then introduce the other receptors (including TLRs, NLRs and other receptors), though the discovery of pattern recognition receptors is historically pioneered by the study of TLRs.

I.1.2.1. RIG-I like receptors

RIG-I-like receptors (RLRs), including RIG-I, MDA5 and LGP2, are essential for recognizing viral infection in the cytosol. RIG-I was originally identified as a retinoic acid inducible gene. Its role in antiviral immunity was discovered when RIG-I was identified in a cDNA expression cloning screen as a cytoplasmic protein that mediates type I IFN production induced by synthetic dsRNA poly[I:C][4]. MDA5 was originally isolated as an IFN-inducible putative helicase with melanoma growth-suppressive properties[5-7]. LGP2 was identified as a helicase-like protein encoded by the Stat3/5 locus with unknown functions[8]. All three members contain DExD/H box helicase domains, and C-terminal RNA binding domain (CTD). RIG-I and MDA5 both have at their N-termini two tandem CARD domains, which are lacking in LGP2 (Figure 1.1). Numerous studies

have shown that RIG-I and MDA5 play key roles in type I IFN induction after RNA virus infection, while LGP2 is thought to play a regulatory role.

Physiological importance

At the whole animal level, RIG-I deficiency in mice completely wipes out type I IFN response upon infection with certain RNA viruses, including paramyxoviruses (such as Sendi virus, SeV), Influenza virus, Japanese Encephalitis virus (JEV), Newcastle Disease virus (NDV), Vesicular Stomatitis virus (VSV), Hepatitis C virus (HCV) and Respiratory Syncytial virus (RSV) , whereas mice deficient in MDA5 have severely impaired type I IFN response to piconavirus infection, such as Encephalomyocarditis virus (EMCV), Theiler's ,virus and Mengo virus infection[9-12]. While TLRs function mostly in specific types of dendritic cells (DCs, also discussed later), RIG-I mediates type I IFN production in fibroblasts and conventional dendritic cells (cDCs), which are the cell types that are first exposed to local virus infection, explaining the importance of RIG-I in rapid and overall antiviral response at the whole animal level. RIG-I and MDA5 are expressed at low levels in many cell types, and can be further induced by type I IFN[4, 13, 14], so they are ready to combat an infection locally and rapidly. Splice variants of RIG-I and polymorphisms in the RIG-I gene in human populations have been examined[15-17], and linked to defective functions and altered antiviral immune responses.

RIG-I and MDA5 have also been studied in many specific cell types. MDA5 recognizes Murine Norovirus-1 (MNV-1) in DCs[18], a coronavirus Mouse Hepatitis Virus (MHV) in brain macrophages[19]. West Nile virus (WNV), SeV, Dengue virus-2 (DEN2),

and reoviruses have been shown to trigger both RIG-I- and MDA5-dependent innate immune responses in mouse fibroblasts[20-26]. Both RIG-I and MDA5 contribute to the induction of type I IFN in response to MHV infection in oligodendrocytes[27], and in measles virus-infected human epithelial cells[28]. The fact that RIG-I and MDA5 contribute to immune responses against distinct yet overlapping sets of viruses is likely due to: RIG-I and MDA5 have distinct, as well as overlapping, specificities for RNA ligands; one virus may produce multiple distinct PAMP features recognized by RIG-I or MDA5; RIG-I and MDA5 may have different cell-type specific expression patterns. Accordingly, some viruses have counteracting strategies that target RIG-I and/or MDA5[8, 29].

The physiological role of LGP2 is controversial. LGP2 was initially shown to be a negative regulator on IFN induction by SeV or NDV in cells[8, 30]. In LGP2 knockout ($^{-/-}$, or KO) mice, induction of type I IFN is augmented compared to wild type (WT) following infection with VSV, consistent with a negative regulatory role of LGP2 in the RIG-I pathway. However, LGP2 KO cells have defective in type I IFN induction in response to poly[I:C], and LGP2$^{-/-}$ cells and animals have a defect in the produce type I IFN following exposure to EMCV, which is recognized by MDA5[31]. Another group also generated LGP2$^{-/-}$ mice, and found that LGP2 is dispensable for IFN responses to poly[I:C] transfection, while LGP2 and its ATPase activity is required for type I IFN production induced by various RNA viruses, including EMCV (strongest defect, consistent with the other group's results), Mengo virus, VSV, SeV, JEV and Reo virus in cDC and macrophages[32]. The fact that both MDA5 and LGP2 are targeted by paramyxovirus supports the potential positive role of LGP2 in the MDA5 pathway[25].

RNA ligand

Although RIG-I was cloned as a cytosolic protein that promote poly[I:C]-induced IFNβ production, and can bind poly[I:C] in vitro[33], RIG-I$^{-/-}$ cells are not defective in IFNβ production in response to poly[I:C], but are defective in IFNβ production induced by in vitro-transcribed RNAs; while MDA5 is selectively activated by poly[I:C] transfection[9]. It was known that certain siRNA introduced to cells can induce IFNβ[34]. One study discovered that 5'-triphosphate (5'-ppp) on ssRNA, generated by in vitro transcription, induced IFNβ in cells[35]. Another study suggested that the recognition of short dsRNA with blunt ends was mediated by RIG-I in T98G cells, but the activation of RIG-I by blunt-end dsRNA without 5'-ppp was quite inefficient[36]. Using viral genomic RNA from Rabies virus, Influenza virus and VSV, as well as in vitro transcribed RNA, two groups identified 5'-pppRNA as RIG-I ligand that binds RIG-I and induces RIG-I-dependent IFNβ response[37, 38]. This is consistent with the fact that RNA transcripts of all positive-strand RNA viruses of the Flaviviridae family (recognized by RIG-I) start with an uncapped 5'-ppp, while the 5'-terminus of RNA from Picornaviridae (selectively recognized by MDA5) is masked by a covalently bound protein, VPg[39]. Processing of the 5'-termini of genomic RNA is thought to be used by some viruses to evade recognition by RIG-I[40].

Other features of RNA ligand contribute to their recognition by RIG-I. Some chemical modifications of RNA molecules, such as the incorporation of pseudourudine, 2-thiouridine, or 2' O-methylated uridine, ablate their ability to induce IFNβ production[37]. Certain nucleotide sequences can make a 5'-pppRNA molecule more potent in

stimulating IFN production[41, 42]. In addition, dsRNA without 5'-ppp (even with caps) was found to be a length-dependent RIG-I ligand: from 70 nt to 4000 bp, the longer the dsRNA is, the more dependent it is on MDA5 and less on RIG-I[43]. In this study, it was also shown that IFN-stimulatory RNA species from influenza-infected cells are mainly 5'-ppp ssRNA, and those from EMCV-infected cells are dsRNA, while VSV-infected cells generate both ssRNA and dsRNA. With chemically synthesized RNA, it was shown that 5′-ppp ssRNA with short blunt-end dsRNA structure, a structural feature also present in the genomes of negative-strand RNA viruses, most potently activates RIG-I[44, 45]. Blunt-end 5′-monophosphate dsRNA may be sufficient to support partial activation of RIG-I[44, 46]. Thus, RIG-I ligand seems to require both 5'-ppp and double-strandedness. By isolating RIG-I bound RNA from virus infected cells (by Influenza A virus or SeV), one group found that physiological RIG-I agonists seem to be the whole viral genome[47]. With the help of next generation sequencing technology, it was shown that in SeV-infected cells, RIG-I prefers defective interfering (DI) particles to full-length viral genomes; in Influenza-infected cells, RIG-I binds to short genome segments and DI particles[48]. In addition to viral RNA, small self-RNA generated by a host RNase, RNase L, was shown to amplify IFNβ induction in RIG-I and MDA5 pathways[49].

Long dsRNA stimulates the MDA5 pathway[43]. Experiments aiming at identifying endogenous RNA ligand for MDA5 revealed that, a dsRNA-specific antibody can pull down MDA5 from cells infected with EMCV (picornavirus, positive-strand ssRNA) and Vaccinia virus (DNA virus). Only the high molecular weight forms of MDA5-associated RNA have immunostimulatory activity[50]. MDA5 may also mediate the recognition of

some other features of viral RNA, including 2' O-methylation[51], and certain viral mRNA[52], although the molecular details await further elucidation.

RNA sensing by C-terminus domains of RIG-I like receptors

RIG-I C-terminus domain (CTD), when overexpressed in cells, could inhibit virus infection induced IFNβ production, and was originally called repression domain (RD). LGP2 CTD has an analogous repression activity, while MDA5 CTD does not[53].

RIG-I CTD domain was identified to be an RNA binding domain for 5'-pppRNA and synthetic dsRNA[46, 54]. RIG-I CTD may bind to bipartite molecular patterns, i.e. double-strandedness and 5'-ppp, through distinct sites[45]. Structure studies of RIG-I CTD alone (no ligand) revealed a basic groove that may interact with RNA and confer specificity to 5'-ppp. Structures of RIG-I CTD bound to short 5'-ppp dsRNA confirmed that RIG-I recognizes the termini of the dsRNA (a few nucleotides at both 5'- and 3'-termini) and that 5'-ppp interacts with the basic groove through extensive electrostatic interactions[55, 56]. Comparison of the ligand-free and ligand-bound forms of RIG-I CTD reveals local conformational changes. RIG-I CTD domain was also thought to facilitate RNA induced RIG-I dimerization and activation, although this is still controversial[46, 53, 54, 57-59].

It is likely that RIG-I uses both CTD and helicase domains to cooperatively recognize different PAMPs within the same RNA molecule[60], which is also supported by the most recent crystal structure of RIG-I containing the helicase-CTD fragment (discussed in Chapter VI).

Secondary structures are conserved among RIG-I, MDA5 and LGP2 CTDs, but the basic grooves in MDA5 and LGP2 CTDs are distinct from that of RIG-I CTD, possibly contributing to ligand specificty. Low-resolution electromicroscopic images of RNA-free or RNA-bound LGP2 (full length protein) suggest significant conformational changes upon RNA binding[61]. The crystal structures of LGP2 CTD in isolation and in complex with an 8 bp dsRNA revealed a highly conserved fold to that of RIG-I CTD, with some differences in loop regions[62, 63]. The structures also demonstrated that LGP2 specifically recognizes the blunt ends of dsRNA. In addition, the orientation of 5'-OH dsRNA bound to LGP2 CTD is different from that of 5'-ppp dsRNA bound to RIG-I CTD. Full-length LGP2 and LGP2 CTD have similar RNA binding affinity, indicating the CTD plays primary roles in RNA binding by LGP2.

The crystal structure of ligand free MDA5 CTD revealed a highly conserved fold similar to the structures of RIG-I and LGP2 CTDs[64, 65]. Like LGP2, MDA5 CTD preferentially binds dsRNA with blunt ends, but with significantly weaker affinity (μM range) compared with RIG-I or LGP2 (~100 nM range)[54, 63]. It has been proposed that the repression function of RIG-I and LGP2 CTDs might be mediated by competition for RNA ligand binding[57-59]. Therefore, the fact that MDA5 CTD does not have a repression function suggests that MDA5 CTD may bind RNA differently. It is speculated that MDA5 CTD may function in concert with other factors[46, 54].

In sum, RLR CTD domains have a similar overall fold and a basic surface for RNA interaction, with distinct structural features within the basic surface.

Helicase domains of RIG-I like receptors

The helicase domain of RIG-I was thought to play a role in long dsRNA binding[53]. Several studies support this idea. First, protease digest experiments showed that RIG-I assumes different conformations when bound to poly[I:C] compared with when it is bound to synthetic short dsRNA or 5'-pppRNA[46], suggesting different binding sites for different RNA. Second, poly[I:C] binds RIG-I stronger than short dsRNA or 5'-pppRNA[66], presumably by interacting with additional sites on RIG-I. Third, mutations in RIG-I helicase domain affect dsRNA binding more than they affect 5'-pppRNA binding[60]. Fourth, RIG-I helicase domain interacts strongly with double stranded regions of RNA ligand in competition binding assays, although its direct binding to RNA is very weak[45]. Fifth, while ATPase activity of full length RIG-I is stimulated significantly by both dsRNA and 5'-pppRNA, ATPase activity of the helicase domain alone is stimulated preferentially by dsRNA[54].

As to the enzymatic activities of the helicase domain, the ability of RNA ligands to activate RIG-I helicase activity inversely correlates with their immunostimulatory potential, while ATPase-inducing activity of RNA ligands is positively correlated to their immunogenic activity[46]. Thus the helicase domain is likely to be required for ATP-dependent conformational changes rather than RNA unwinding. Single molecule studies showed that RIG-I translocates on the dsRNA portion of RNA ligand while using ATP without unwinding the RNA duplex[67]. Translocation rate and ATPase acitivty of RIG-I helicase-CTD (lacking CARD domains) are high on both 5'-pppRNA (containing dsRNA portion) and dsRNA without 5'-ppp, while the translocation rate of full length RIG-I is lower on dsRNA than on 5'-ppp RNA, suggesting that preferred binding of CTD to 5'-

pppRNA exposes helicase domain, allowing for rapid translocation on RNA. However, the exact function of this RNA "translocase" activity awaits further investigation.

CARD domains of RIG-I and MDA5

CARD domains belong to the Death Domain (DD) superfamily, which also includes the death domain (DD), death effector domain (DED), and pyrin domain (PYD) subfamilies. Many proteins containing DD superfamily domains are involved in immunity, inflammation and cell death[68]. Some DDs within proteins are known to mediate homotypic interactions, and therefore play important roles in the assembly and activation of apoptotic and inflammatory complexes.

The N-terminal tandem CARD domains of RIG-I and MDA5 are essential for their signaling activity. RIG-I CARD domains can act as a constitutive activator of IFNβ production, while the signaling activity of the full length protein is stimulus-dependent. Conformational changes induced by RNA binding to RIG-I was proposed to expose CARD domains and enable RIG-I to interact with downstream adaptor protein Mitochondria antiviral signaling protein (MAVS) via homotypic interaction between their CARD domains, although stable interaction between RIG-I and MAVS is difficult to detect[69-72]. Mechanisms of RIG-I regulation via various CARD domain modifications have been proposed. RIG-I CARD domains, but not MDA5 CARDs, have been shown to be polyubiquitinated via Lysine 63 (K63) linkage by a RING-domain E3 ubiquitin ligase TRIM25[73]. Caspase-1 is important for immune response against West Nile virus (WNV), possibly by promoting RIG-I ubiquitination through yet unidentified mechanisms[74]. On the other hand, deubiquitination enzyme CYLD inhibits RIG-I signaling pathway

possibly by removing or inhibiting RIG-I ubiquitination[75, 76]. Autophagic regulator Atg3-Atg12 conjugate negatively regulates RIG-I pathway, perhaps by interacting with CARD domains of RIG-I and MAVS[77]. ISG15 conjugate likely regulates RIG-I protein level and ubiquitination level, although the exact mechanism is still unclear[78, 79]. Phosphorylation of RIG-I is also detected, and may affect its ubiquitination or other aspects of function[80]. Little is known about MDA5 regulation.

Signaling pathways downstream of RIG-I like receptors

Mitochondria anti-viral signaling protein MAVS (also known as IPS-1, VISA and Cardif) is critical for mediating the activation of transcription factors NF-κB and Interferon regulatory factor 3 (IRF3) to produce type I IFN downstream of RLR pathways[69-72]. MAVS knockout mice exhibit severely impaired type I IFN production in response to infection with several viruses that are detected by RIG-I or MDA5[81]. MAVS contain an N-terminal CARD domain, a middle proline rich (PR) region, and a C-terminal transmembrane (TM) domain. The TM domain contains a mitochondrial targeting sequence. Outer mitochondria membrane localization was thought to be critical for MAVS's function[71]. MAVS is also found on peroxisomes[82], a type of membrane bound-organelles, and peroxisomal MAVS is thought to play a key role in inducing the early rapid surge of antiviral response before mitochondria MAVS signals kick in for a sustained response. Early studies also proposed that TM domain might facilitate MAVS self-association in cells[83, 84], but this may be an indirect effect of mitochondria localization. Indeed, upon virus infection MAVS forms large aggregates capable of activating downstream signaling[85]. Recombinant MAVS protein spontaneously forms

prion-like aggregates that, remarkably, can convert endogenous MAVS into functional aggregates. In vitro, MAVS CARD domain alone is sufficient to form functional aggregates in the form of fibrils under electromicroscope, while in cells both mitochondria localization and CARD domain of MAVS are required for its conversion into aggregate forms.

Several pathways are activated downstream of MAVS, including the IRF3 pathway for IFNβ induction, and the NF-κB pathway for the induction of proinflammatory cytokines (Figure 1.2). For IRF3 activation, IRF3 is phosphorylated by its kinase TBK1. Phosphorylated IRF3 dimerizes and translocates to the nucleus. For NF-κB activation, kinase IKK phosphorylates IκB (inhibitor of κB) proteins, which then undergo ubiquitination and proteosomal degradation, releasing their inhibition on NF-κB proteins. The signaling events mediating these MAVS downstream pathways are under intense investigation.

Fas-associated protein with death domain (FADD) and receptor interacting protein 1 (RIP1), two signaling proteins for the relatively well-studied tumor necrosis factor receptor (TNFR) pathway, were shown to be involved in IRF3 activation by virus infection or intracellular dsRNA[86]. Another protein TNFR-associated death domain protein (TRADD), an adaptor protein in the TNFR1 pathway, was shown to be also important for both NF-κB and IRF3 pathway activation downstream of RIG-I and MDA5[87, 88]. TNFR-associated factor (TRAF) proteins are signaling proteins with E3 ligase activity involved in TNFR and Interleukin-1 receptor (IL1R) signaling pathways. MAVS contains binding sites for different TRAF proteins (TRAF2, 3, 5, 6) that may be

recruited to MAVS aggregates[85], though the exact function of these TRAF proteins in MAVS pathways are not well understood. CARD9 and Bcl10 were also recently shown to be required for NF-κB activation downstream of RIG-I and MDA5[89]. Further investigations are required to better understand how complex signaling networks are formed downstream of RLRs.

Regulation of RLR signaling pathways

Many studies proposed regulatory mechanisms of the RLR-MAVS pathways. A few cases suggest distinct regulatory mechanisms for RIG-I and MDA5. For example, a dihydroxyacetone kinase, DAK, associates with MDA5, but not RIG-I, and inhibits MDA5-mediated IFN production in overexpression experiments[90]. E3 ubiquitin ligases TRIM25 and REUL specifically ubiquitinate RIG-I, but not MDA5, and stimulate the RIG-I pathway[73, 91].

Additional ubiquitination-mediated mechanisms for RIG-I/MDA5 regulation have been proposed. Ring finger protein 125 (RNF125), when overexpressed, associates with RIG-I and MDA5 and promotes their degradation[92]. Riplet/RNF135 promotes K63-linked ubiquitination of RIG-I C-terminal region, possibly contributing to RIG-I activation[93]. CYLD is a deubiquitination enzyme that inhibits the RIG-I signaling pathway, possibly by removing polyubiquitin chains from RIG-I as well as from TBK1[76].

Several mitochondria proteins have been shown to regulate MAVS signaling function. RLR activation promotes mitochondria elongation which may promote MAVS downstream signaling. Forced mitochondria fragmentation appears to reduce MAVS

signaling. The link between mitochondria dynamics and MAVS signaling might be mediated by mitochondria fusion proteins[94-96]. Mitochondria proteins NLRX1 and receptor for globular head domain of complement component C1q (gC1qR) both interact with MAVS and inhibit MAVS mediated type I IFN induction[97, 98].

MAVS degradation induced by viral infection potentially serves as a viral evasion mechanism or as a negative feedback regulation to prevent excessive response. Two viral infection induced proteins have been implicated in MAVS ubiquitination and degradation. Poly(rC) binding protein 2 (PCBP2) interacts with MAVS and recruit E3 ligase AIP4 (also known as Itch) which mediates K48 linked ubiquitination and degradation of MAVS[99]. Proteasome subunit PSMA7 (α4) specifically associates with MAVS and decreases its protein level, thus negatively regulating antiviral response[100].

Deubiquitinating enzyme A (DUBA) is a K63-linkage specific DUB shown to inhibit RLR pathways as well as TLR pathways[101]. TRAF3 was proposed to be a possible target for DUBA's DUB activity. TRAF3 was also proposed to be the substrate for an E3 ligase Triad, which inhibits type I IFN production downstream of RLRs and TLRs. Triad-mediated TRAF3 ubiquitination induces TRAF3 degradation[102]. However, the role of TRAF3 in RLR signaling pathways is still unclear.

Other regulatory mechanisms of the RLR pathways have also been proposed. Tyrosine kinase c-Src, when overexpressed, associates with TRAF3, RIG-I and MAVS, and positively regulates the RIG-I pathway[103]. NLRC5, a protein belonging to the NOD-like protein family, inhibits NF-κB activation by blocking the phosphorylation and

activation of the IKK complex[104]. Phosphatase SHP-1 promotes type I IFN production, but inhibits NF-κB activation, downstream of RIG-I as well as TLR3 and TLR4, the exact mechanisms of which are unclear[105].

I.1.2.2. Toll-like receptors

The pioneering discovery in the field of PRRs was made in drosophila genetic studies. A gene called toll was found to be required for resistance to fungal infection in adult flies[106]. The toll gene encodes for a transmembrane protein Toll, which contains an extracellular domain (ECD) with leucine-rich repeats (LRR), and a cytoplasmic domain similar to that of the mammalian interleukin-1 (IL-1) receptor (IL1R), called Toll/IL-1 receptor (TIR) domain. Activation of both the IL-1R in mammals and Toll in drosophila lead to a cascade of signaling events that culminate in the activation of transcription factor NF-κB[107]. Structural and functional homologues of the drosophila Toll protein are referred to as Toll-like receptors (TLRs). Until now, 10 human TLRs and 13 murine TLRs have been identified that mediate innate immunity. Conservation between insects and mammals in the TLR pathways demonstrates the significance of the pathogen recognition systems, and points to a common ancestry of their innate immune systems.

Pattern recognition and physiological importance

TLRs are transmembrane proteins localized to the plasma membrane or the endosomal membrane. The ECD of various TLRs recognize a wide variety of pathogens

including bacteria, fungi, protozoa, and viruses [108, 109]. The cytoplasmic TIR domains are involved in downstream signaling through adaptor proteins containing TIR domains[110].

The first human TLR (TLR4) was cloned and found to induce proinflammatory cytokines[111]. The first TLR (also happened to be TLR4) in mouse was identified as the receptor for lipopolysaccharide (LPS), a Gram-negative bacteria cell wall component[112]. Activation of TLR4 leads to NF-κB and MAPK (mitogen-activated protein kinase) cascade activation resulting in the induction of a variety of cytokines and costimulatory molecules; TLR4 pathway also activate IRFs and leads to the induction of type I IFN.

The subfamilies of TLR1, TLR2 and TLR6 recognize gram-positive bacteria cell wall components, including lipid and carbohydrate compounds[113]. TLR5 recognizes bacteria flagellin proteins, and is responsible for gut immunity against pathogenic intestinal bacteria[114-116]. TLR11 recognize uropathogenic bacterial components[117], and profilin-like proteins from the parasite Toxoplasma gondii[118].

TLR3, TLR7, TLR8 and TLR9 localize to the endosomal compartment and recognize nucleic acid PAMPs. TLR3 recognizes dsRNA and induces both pro-inflammatory cytokines and type I IFNs[119]. However, TLR3 knockout mice recover normally after infection with several RNA viruses, including lymphocytic choriomeningitis virus (LCMV), vesicular stomatitis virus (VSV), and reovirus (ReV)[120]. It appears that IFN production in animals does not require TLR3 signaling, because most cell types, including fibroblasts, conventional dendritic cells (cDCs) and macrophages, rely on RLR pathways for IFN production. Because TLR3 pathway also induces an inflammatory response, virus infection in TLR3 knockout mice could result in a less

pathogenic phenotype despite a higher viral load than in WT mice[121]. Therefore, the physiological role of TLR3 in antiviral immunity likely depends on different types of viruses, cell types, and the specific types of responses generated.

TLR7 and 8 are mainly expressed in the endosomal compartments of plasmacytoid dendritic cells (pDCs) and myeloid dendritic cells (mDCs)[122]. They recognize ssRNA and certain small interfering RNA[123-125]. TLR9 also localizes in the endosomal compartment of pDCs, and recognizes the sugar backbone of DNA and unmethylated CpG-motif[126, 127]. pDCs are also called type I interferon-producing cells (IPCs), because they can rapidly produce large amounts of type I IFNs upon infection[128, 129]. The unique cell-type-specific expression of TLR7 and TLR9 in pDCs provides a parallel IFN inducing pathway to the RLR-dependent pathways in other cell types, allowing rapid IFN induction upon viral infection if the RLR pathway is impaired or bypassed by the virus[130].

TLR signaling pathways

Upon activation, TLRs recruit different combinations of TIR-domain containing adaptor proteins and activate specific signaling pathways. So far several such adaptor molecules have been characterized[131]: Myeloid differentiation primary response gene (MyD88), MyD88 adapter-like protein or TIR domain-containing adaptor protein (MAL/TIRAP), TIR domain-containing adapter protein inducing IFNβ or TIR domain-containing adapter molecule 1 (TRIF/TICAM1), TRIF-related adapter molecule or TIR domain-containing adapter molecule 2 (TRAM/TICAM-2), sterile alpha and armadillo motifs (SARM). MyD88 is involved in TLR1, 2, 4, 5, and 6 signaling pathways leading

to the activation of NF-κB and MAPK cascade to induce proinflammatory cytokines, and TLR7 and 9 utilize MyD88 to induce both proinflammatory cytokines and type I IFNs[132-134]. TIRAP is required to recruit MyD88 to TLR2 and TLR4[135]. TRIF is involved in NF-κB activation and IFN induction downstream of TLR3, and is also involved in the MyD88-independent branch of TLR4 pathways leading to IFN production and late phase NF-κB and MAPK activation[136]. TRAM is specifically involved in TRIF-dependent TLR4 pathways by recruiting TRIF to the receptor[137], after TLR4 is endocytosed and trafficked to the endosome[138]. SARM functions as an inhibitor of TRIF-dependent TLR signaling[139]. TLR pathways can be generally categorized into MyD88-dependent and TRIF-dependent pathways (Figure 1.3).

In MyD88-dependent pathways, MyD88 recruits IL receptor-associated kinases (IRAKs), via homotypic interactions between their DDs. The crystal structure MyD88-IRAK4-IRAK2 death domain complex reveals the assembly of a hierarchical "signaling tower", where MyD88 DD recruits the DDs of IRAK4 and then those of IRAK2 or IRAK1[140, 141]. Ubiquitination of IRAK1 is important for TLR-mediated NF-κB activation[142]. E3 ligase TRAF6 is subsequently recruited to the MyD88 signaling complex[133, 143-146], and mediates K63-linked polyubiquitin synthesis together with E2 enzymes Ubc13/Uev1A[147]. TAB2 and TAB3, regulatory components of the transforming growth factor-β-activated kinase 1 (TAK1) kinase complex, bind K63-linked polyubiquitin, and subsequently activate TAK1 kinase[148]. TAK1 is a MAP3K (MAP kinase kinase kinase) and can activate several MAP kinase cascades, as well as the IKK complex. NF-κB essential modulator (NEMO), the regulatory subunit of the IKK

complex, can also bind polyubiquitin chains, and mediates IKK activation and subsequent NF-κB activation[149-152].

In pDCs, MyD88 also mediates TLR7- and TLR9-induced type I IFN production[153]. The activation of type I IFN involves several adaptor proteins, including IRAK4, TRAF6, TRAF3, IRAK1 and IKKα, as well as the transcription factor IRF7, forming a transductional-transcriptional signaling complex[133, 146, 154-158].

In TRIF-dependent signaling pathways, TRAF3 functions downstream of TRIF and mediates the recruitment of TBK1, and the subsequent activation of IRF3 and type I IFNs production[146, 158]. For TRIF-dependent NF-κB activation, TRAF6 may be involved, but redundant E3 ligase may also exist[145, 159, 160]. In addition, RIP1 and TRADD are recruited to TRIF and are important for NF-κB activation downstream of TLR3 and TLR4[88, 161-163].

As described above, ubiquitination is repeated used as a regulatory mechanism in TLR pathways. In the next section Chaptor I.2, the TLR4 pathway is discussed in more detail as an example for ubiquitination-dependent regulatory mechanisms.

TLR-induced MAPK activation pathways are relatively less studied. MAPK cascades mediate inflammatory responses mainly by sequential phosphorylation and activation of kinases, leading to the activation of transcriptional regulators[164]. A MAP3K apoptosis signal-regulating kinase 1 (ASK1) is specifically required for TLR4-mediated activation of p38, but not JNK or NF-κB[165]. MAP3K tumor progression locus 2 (TPL2) mediates TLR-induced production of anti-inflammatory cytokine IL10, and pro-

inflammatory cytokine TNFα[166]. TPL2 is also a negative regulator for TLR-induced IFNβ production in macrophages and myeloid DCs[167].

I.1.2.3. NOD-like receptors

Nucleotide-binding domain, leucine-rich repeat-containing (or NOD-like Receptor, NLR) proteins are another set of intracellular receptors in immunity and inflammation. Members of this family usually contain an N-termial signaling domain, such as CARD, PYD, or baculovirus inhibitor repeat (BIR) domain, a central nucleoride-binding domain (NBD) that binds ATP and mediates oligomerization, and a C-terminal LRR region involved in sensing of PAMPs or autoinhibition.

NOD

Nucleotide-binding oligomerization domain 1 (NOD1) and NOD2 are among the first members of the NLR family. They detect bacterial peptidoglycan-derived molecules and mediate pathogen clearance by inducing proinflammatory cytokines[168]. Various mutations in NOD2 were found to associate with inflammatory diseases such as Crohn's disease and Blau syndrome[168-171], although the underlying molecular cause is still controversial[172]. NOD2 was also shown to mediate innate immune antiviral responses[173]. NOD2 recognizes viral ssRNA, and activates MAVS-dependent IRF3 activation pathway. The NBD and LRR domains of NOD2 are essential for interacting with MAVS (Figure 1.2).

In response to microbial invasion, NOD2 activation also induces several other pathways, including NF-κB and MAPK pathway, leading to the production of proinflammatory cytokines and chemokines. RICK/RIP2 is required for NF-κB activation downstream of NOD2[174-177]. RIP2 recruits E3 ligases cIAP1 and cIAP2, which mediate ubiquitination of RIP2[178]. Polyubiquitinated RIP2 then recruits the TAK1 complex, leading to IKK activation[179]. Conversely, DUB A20 inhibits NOD2 signaling by decreasing RIP2 ubiquitination[180]. CARD9 was required for NOD2-mediated MAPK activation and cytokine production after bacterial infection[181]. NOD2 may also coorperate with NLRP1 and/or NLRP3 and induce caspase-1 activation[177, 182], which leads to the processing of an important proinflammatory cytokine pro-IL1β into mature IL-1β[183].

NLRP3

NLRP3 mediates inflammation induced by certain chemicals, or by bacterial, fungal and viral infections[184-190]. NLRP3 mutations have been associated with a variety of autoinflammatory disorders[191]. Because NLRP3 responds to structurally diverse stimuli, it has been proposed that, instead of directly interacting with ligands, NLRP3 may function together with additional upstream receptors[192]. Upon activation, NLRP3 forms the NLRP3-inflammasome with its adaptor proteins apoptotic speck-like protein containing a CARD (ASC) and procaspase-1 to activate caspase-1. Activated caspase-1 is responsible for the proteolytic processing of proinflammatory cytokines IL-1β and IL-18[193].

I.1.2.4. DNA sensors

Several proteins have been identified as potential cytosolic DNA sensors to trigger innate immune responses[194, 195], such as DNA-dependent activator of IFN-regulatory factors (DAI), IFN-inducible protein 16 (IFI16), absent in melanoma 2 (AIM2), and RNA polymerase III (polIII).

DAI binds dsDNA in the cytoplasm, and triggers the activation of NF-κB and IRF3[196, 197], which is mediated by RIP1 and TBK1, respectively[198].

IFI16 is expressed in monocytes, binds to immunostimulatory dsDNA, and induces both IRF3 and NF-κB activation, which is likely mediated by stimulator of IFN gene (STING)[199]. STING is an endoplasmic reticulum (ER) adaptor protein that can activate both NF-κB and IRF3 pathways (Figure 1.2)[200-202]. An E3 ligase TRIM56 stimulates K63-linked ubiquitination of STING, and promotes the recruitment of the IRF3 kinase, TBK1[203]. STING also co-localizes with MAVS to the outer membrane of mitochondria, suggesting potential involvement in MAVS-dependent pathways.

AIM2 senses dsDNA and directly interacts with ASC and caspase-1 to form the AIM2-inflammasome and trigger caspase-1 activation after a DNA virus infection[204-207]. Interestingly, AIM2 have similar domain structures with IFI16.

PolIII in the cytosol can mediate the conversion of AT-rich viral or bacterial dsDNA into RIG-I ligand and triggers the RIG-I signaling pathway[208, 209].

I.1.3. Antiviral immune effectors

PRR mediated pathways produce multiple signaling outcomes. At the gene expression level, a plethora of immune response molecules are produced, including antiviral cytokines (e.g. type I IFN) and proinflammatory cytokines. At the cellular level, processes such as phagocytosis, antimicrobial-autophagy, and cell death can be induced. Collectively, these outcomes augment innate immune responses and induce adaptive immune responses to control or eliminate the infectious agents. This section focuses on the IRFs and type I IFN.

I.1.3.1 IRFs

Members of the IRFs family transcription factors commonly contain a helix-turn-helix DNA-binding motif, and play diverse roles in host defense. Two closely related IRFs, IRF3 and IRF7, are critical factors for type I IFN gene induction[210, 211]. They constitute part of a large protein complex called the IFNβ enhanceosome that also includes NF-κB, activator protein 1 (AP1), and co-activators CREB binding protein (CBP)/p300 to activate the transcription of IFNβ gene[212]. IFNβ transcription can be negatively regulated at the transcription factor level by a peptidyl-prolyl isomerase pin1[213], which induces ubiquitination and degradation of IRF3.

Both IRF3 and IRF7 are activated by stimulus-dependent phosphorylation, dimerization and nuclear transportation. IKK-related kinases TBK1/IKKε are the kinases for IRF3 and IRF7[214, 215]. NEMO, the regulatory subunit of the IKK complex, also associates with TBK1, and functions as an adaptor protein for both NF-κB and IRF

activation[216]. IRF7 activation in the TLR7/9 pathways is mediated by a different kinase, IKKα, in a tranductional-transcriptional complex that also includes MyD88, TRAF6, TRAF3, intracellular osteopontin (Opn-i), IRAK4, and IRAK1[133, 146, 154-158, 217]. IRF3 and IRF7 have different cell-type-specific expression patterns[218]. IRF3 is constitutively expressed in all cell types, whereas IRF7 is constitutively expressed in lymphoid cells and pDCs, and can be induced transcriptionally by IFN feedback loop in other cell types. IRF7 expression is also translationally controlled[219].

IRF5, IRF8 and IRF1 all play a role in innate immune cytokine production[220]. At the whole animal level, IRF5 is required for the induction of proinflammatory cytokines in TLR pathways[221]. Although the kinase for IRF5 is not yet identified, the activation of IRF5 is thought to be regulated by IKKα and K63-linked ubiquitination[222, 223]. IRF-8 is specifically required for the feedback phase of type I IFN transcription by functioning together with IRF7[224]. IRF-1 is required for TLR9- and TLR7-induced IFNβ production in myeloid dendritic cells[225, 226], as well as type I IFN induced by chronic TNF stimulation[227].

I.1.3.2. Type I IFN

IFNs are the first series of cytokines to be molecularly characterized. They have been extensively studied in the context of host defense against viral infection. Type I IFNs (IFNα and IFNβ) are produced by a variety of cells upon viral infection, while type II IFN (IFN-γ) is produced by activated T lymphocytes (T cells) and natural killer (NK)

cells. These two types of IFNs have a multitude of biological activities, including evoking an antiviral response through the stimulation of IFN receptors[228]. The binding of IFNs to IFN receptors triggers downstream signaling events, primarily mediated by the Janus kinase – signal transducer and activator of transcription (JAK-STAT) pathway, that induces a broad spectrum of interferon-stimulated genes (ISGs)[229, 230].

Type I IFN-mediated signaling triggers the expression of hundreds of ISGs that function together to establish an antiviral state for host cells[231, 232], by sabotaging viral life cycle, turning on cellular stress response, and modulating the activity of other antiviral proteins, and so on. Many PRRs and signaling proteins are themselves ISGs, forming a positive feedback loop to amplify antiviral responses. As a secreted factor, the effect of type I IFNs can reach many cells. Locally, IFNs promote the expression of vascular adhesion molecules and chemokines to attract leukocytes to the infection site. Systemically, pDCs circulate the system and produce type I IFN into the blood stream. Several types of interleukins are induced by type I IFN, and can promote DC maturation[233], as well as the activation of other immune cell types, such as natural killer (NK) cells[234-236]. Type I IFN can also directly stimulate T-cell mediated immunity, including controlling the differentiation, proliferation and survival of T cells[237-239], and cross-presentation of viral antigen to CD8 T cells[240].

I.2. Ubiquitin and Immune Defense

Ubiquitination is a widely used protein posttranslational modification that regulates many biological processes. The role of ubiquitin in immune regulation was originally uncovered through studies of antigen presentation and the NF-κB family of transcription factors, which orchestrate host defense against microorganisms. In recent years, many studies have revealed crucial roles of ubiquitination in many aspects of the immune system, including innate and adaptive immunity, antigen presentation and antimicrobial autophagy.

I.2.1. Introduction to ubiquitination

Ubiquitin is a highly conserved 76-amino-acid polypeptide in eukaryotes that can be covalently attached to other proteins through an enzymatic cascade involving three enzymes, E1, E2 and E3 (Figure 1.4)[241]. In humans, there are two E1 enzymes, ~ 40 E2 enzymes and hundreds of E3 enzymes. Ubiquitination can be reversed by de-ubiquitination enzymes (DUBs), which also form a large family, consisting of ~100 members in humans[242]. The ubiquitin "signal" is recognized by specific "ubiquitin receptors" that contain one or more ubiquitin-binding domains[243]. There are more than 20 different types of ubiquitin-binding domains that are embedded in a large variety of cellular proteins. Most ubiquitin-binding domains bind to ubiquitin with low affinity, which indicates that this binding is highly dynamic and specifically regulated. Thus, the ubiquitin conjugation and deconjugation systems, together with ubiquitin-binding

proteins, constitute the basic molecular machineries for ubiquitin-mediated regulation of diverse cellular processes.

A protein can be modified on one lysine residue with a single ubiquitin (mono-ubiquitination), or with a chain of ubiquitins (polyubiquitylation). In some cases, multiple lysine residues on a protein target can be modified by ubiquitin or ubiquitin chains. Non-linear polyubiquitin chains are linked through one of the seven lysine residues of ubiquitin. Lysine 48 (K48)-linked polyubiquitination usually targets proteins for proteasomal degradation, whereas K63-linked polyubiquitination is implicated in many areas of signal transduction, such as DNA repair and protein kinase activation. Linear ubiquitin chains, in which the carboxyl-terminus of one ubiquitin is linked to the amino-terminal methionine of the next ubiquitin, are also thought to function in signal transduction as well as protein degradation[244]. Polyubiquitin chains linked through other lysines of ubiquitin (K6, K11, K27, K29 or K33) have also been found in cells, but their functions are overall less well understood[245]. Many ubiquitin-like proteins, such as SUMO, NEDD8, ISG15, ATG8 (also known as LC3) and ATG12, also function by covalently modifying other target proteins[246].

The specificity of ubiquitination substrates, as well as the types of ubiquitin chains, is largely determined by E2 and E3 enzymes[247]. E3 enzymes typically contain either a RING (really interesting gene) or a HECT (homologous to E6AP C terminus) domain, which mediates E2 binding and ubiquitination. Many E3 enzymes form multi-protein complexes. For example, cullin RING ligases, which form the largest E3 family,

are composed of multiple subunits including one of the cullin proteins (CUL1–CUL7) and a RING subunit such as RING-box 1 (RBX1; also known as ROC1)[248].

I.2.2.Regulation of innate immunity by ubiquitination

I.2.2.1. Ubiquitination in Toll-like receptor pathways, as an example

As introduced earlier, each member of the TLR family recognizes a distinct type of PAMP, and together they can detect a broad array of pathogens, including bacteria, viruses, fungi and parasites[249]. Upon engagement by their respective ligands, different TLRs trigger specific signaling outcomes by recruiting various combinations of adaptor proteins, which then relay signals to specific downstream signaling molecules. TLR pathways can be largely categorized by the use of two main adaptor proteins, MYD88 and TRIF. MYD88-dependent pathways are used by all TLRs except TLR3, and generally lead to the induction of inflammatory cytokines. TLR7, 8 and 9, which are localized on the endosomal membrane, also use MYD88 for the induction of type I IFNs. TRIF-dependent pathways, which transmit signals from TLR3 and TLR4, lead to the induction of both type I IFNs and inflammatory cytokines.

Ubiquitination is involved in the activation of NF-κB and the mitogen-activated protein kinase (MAPK) cascade downstream of both MYD88- and TRIF-dependent pathways (Figure 1.3). Upon stimulation of MYD88-dependent pathways, MYD88

recruits kinases of the IRAK family[140], which then recruit TRAF6, a RING domain ubiquitin E3 ligase[147]. TRAF6 functions together with the ubiquitin E2 complex consisting of Ubc13 and Uev1A to catalyze the synthesis of K63-linked polyubiquitin chains. These polyubiquitin chains are recognized by the novel zinc finger (NZF) ubiquitin-binding domains of TAK1-associated binding protein 2 (TAB2) and TAB3, which are the regulatory components of the TAK1 complex[250, 251]. Binding of K63-linked polyubiquitin to TAB2 and TAB3 leads to TAK1 activation, which in turn activates the MAPK cascade. K63-linked polyubiquitin also binds to NEMO (also known as IKKγ), an essential regulatory subunit of the IκB kinase (IKK) complex that also contains the catalytic subunits IKKα and IKKβ[149, 150]. Binding of K63-linked polyubiquitin to both IKK and TAK1 complexes facilitates the phosphorylation of IKKβ by TAK1, leading to IKK activation. IKK phosphorylates inhibitor of NF-κB (IκB) proteins, which are then recognized by the F-box protein βTrCP, a subunit of the ubiquitin E3 ligase complex that also contains SKP1 (S-phase kinase-associated protein 1), CUL1 and RBX1. The βTrCP-containing E3 complex polyubiquitylates phosphorylated IκBs, which are subsequently degraded by the proteasome. This allows NF-κB to enter the nucleus to turn on target gene expression. The MyD88-dependent IL1R signaling pathway use very similar mechanism to activate NF-κB (Figure 1.5).

In TRIF-dependent pathways, receptor interacting protein 1 (RIP1) is recruited to TRIF[161], and undergoes K63-linked polyubiquitination by an E3 ligase of the pellino family, PELI1[252]. RIP1 ubiquitination then recruits TAB2 and NEMO, leading to NF-κB activation (as described above). TRIF-dependent pathways also lead to IRF3 activation

and type I IFN production. Another member of the TRAF family, TRAF3, is recruited to TRIF[146, 158]. TRAF3 mediates the recruitment and activation of IRF3 kinase, TBK1 and IKKε. However, the role of ubiquitination in this process is unclear.

Different types of polyubiquitination can function cooperatively to determine specific signaling outcomes. For example, in the TLR4-induced MAPK activation pathway, MYD88 is rapidly recruited to the receptor on the plasma membrane upon stimulation with the ligand lipopolysaccharide (Figure 1.3). MYD88 then recruits several ubiquitin E3 ligases including TRAF6, TRAF3 and cellular inhibitor of apoptosis protein 1 (cIAP1) and cIAP2. TRAF6 catalyzes K63-linked polyubiquitination and activates cIAPs, which in turn promote K48-linked polyubiquitination and proteasomal degradation of TRAF3[253]. Upon TRAF3 degradation, the signalling complex containing MYD88, TRAF6, cIAPs, UBC13 and TAK1 is released into the cytosol where it activates the MAPK cascade. IKKβ activation (and hence NF-κB activation), by contrast, does not require TRAF3 degradation.

In the IFN-inducing branch of TLR4 signalling, endocytosed TLR4 recruits TRAF3 and TRAF6, but not cIAPs, to the endosome (Figure 1.3). TRAF3 subsequently undergoes K63-linked polyubiquitination, which correlates with type I IFN induction. TRAF3 K63-linked polyubiquitylation was also shown to correlate with TLR9-induced and RIG-I-induced IFN production[101, 254], although the exact role of TRAF3 K63-linked ubiquitination in IFN induction is not yet clear. Interestingly, forced plasma membrane localization of TRAF3 confers the ability to induce IFNs to TLR pathways that normally do not induce IFNs (such as TLR2 stimulation)[138].

I.2.2.2. Negative regulation of innate immunity by ubiquitination and deubiquitination

Consistent with a key role of ubiquitination in activating immune signaling cascades, several deubiquitination enzymes (DUBs) have been shown to negatively regulate immune responses. A20 and CYLD are two DUBs that are best known for their inhibition of NF-κB activation in diverse signaling pathways, including PRR pathways[255-258]. A20 contains an ovarian tumor (OTU) domain that is known to catalyze deubiquitination. In addition, A20 contains multiple zinc finger domains that mediate ubiquitin binding and ubiquitin ligase functions[259, 260], both of which have been proposed to have a role in down-regulating NF-κB signaling. In several PRR signaling pathways, A20 interacts with specific adaptor proteins and inhibits NF-κB activation by removing or inhibiting the K63-linked ubiquitination of TRAF6[261, 262], RIP1[259] and RIP2[179, 180], thereby restricting the proinflammatory outcomes of PRR pathways[261, 262]. A20 can also prevent polyubiquitin chain synthesis by blocking the interaction between ubiquitin E3 ligases (such as TRAF6, TRAF2 and cIAPs) and their E2 enzymes (Ubc13 and Ubc5)[263]. As a significant regulator of NF-κB signaling, A20 also broadly controls the function of many immune cell types, including B and T cells and dendritic cells[264-270]. The function of A20 to restrict inflammatory responses is not only crucial for preventing exaggerated deleterious inflammation when combating microbial infections, but also important for maintaining homeostasis of the immune system under physiological conditions.

CYLD is a tumour suppressor whose loss of function has been linked to several skin tumours, including familial cylindromatosis and Brooke-Spiegler Syndrome. CYLD contains a ubiquitin protease (UBP) domain and it specifically cleaves K63-linked polyubiquitin chains. This catalytic activity negatively regulates IKK activation in several NF-κB signaling pathways including those downstream from the TNF receptor and RIG-I-like receptors, as well as T cell and B cell receptors[75, 76, 271-276]. Interestingly, a recent genetic study on CYLD uncovers an unexpected role of CYLD in antiviral immunity downstream of IFN receptor signaling, the exact mechanism of which is unclear[277]. Genetic studies have shown that A20 and CYLD have non-redundant physiological functions in the immune system, although they seem to target several common substrates. The difference in their physiological functions might be a result of differential regulation of their temporal and spatial expression patterns or their enzymatic activity and specificity, or might be due to the use of different adaptor proteins.

In addition to deubiquitination, ubiquitination can also negatively regulate innate immune responses by targeting intracellular signaling proteins for degradation by the proteasome. Examples of proteins targeted for proteasomal degradation include MYD88, TRIF[278], MAVS[99], TRAF3[102], TAB2 and TAB3[279], IRF3 and IRF7[280]. The degradation of these proteins can be controlled by cellular ubiquitination enzymes or by microbial proteins that have evolved to exploit the host ubiquitination and/or degradation machineries to evade host immune surveillance.

I.2.3. Role of ubiquitination in antimicrobial autophagy

Autophagy is a process by which eukaryotic cells dispose of intracellular organelles and large protein aggregates to maintain cellular homeostasis. Such activity can also target non-self entities such as microbial pathogens[281]. Autophagy involves the formation of a double-membrane structure, known as the autophagosome, which engulfs a portion of cytosolic constituents. ATG8 (also known as LC3), a ubiquitin-like protein, is conjugated to the membrane of autophagosomes. Autophagosomes then fuse with lysosomes to degrade the contents. It is not entirely clear what defines the substrate specificity for an autophagosome, but ubiquitin has emerged as a specificity factor for selective autophagy. Similar to the ubiquitin-proteasome pathway, whereby ubiquitinated cargos are recognized by ubiquitin receptors that deliver them to the 26S proteasome, ubiquitin-mediated recognition of autophagy targets is mediated by adaptor proteins, such as p62 and NBR1, that recognize both ubiquitinated cargo (through their ubiquitin-binding domains) and LC3 on autophagosomes (through their LC3-interacting regions)[282-286].

In addition to recognizing pathogen-associated ubiquitin targets, p62 also mediates the recruitment of certain ubiquitinated cellular proteins into autophagosomes, where they are processed into antibacterial peptides, such as peptides from the ribosomal protein RPS30[287].

I.2.4. Role of ubiquitination in antigen presentation to the adaptive immune system

Major histocompatibility (MHC) class II molecules on antigen-presenting cells (APCs) present antigenic peptides — such as those derived from extracellular pathogens that

enter APCs by endocytosis — to helper T cells. MHC class II molecules use intracellular protein trafficking pathways to communicate between different endosomal compartments and the plasma membrane[288]. Their expression at the cell surface is subject to regulation through endocytosis and delivery to lysosomes for degradation, a process regulated by ubiquitination of the cytoplasmic domains of these molecules. In mouse immature dendritic cells (DCs), the MHC class II β-chain cytoplasmic tail undergoes polyubiquitination by E3 enzyme MARCH1 (membrane-associated RING-CH 1), resulting in low levels of MHC class II surface expression in immature DCs[289-295]. Upon DC maturation, MHC class II molecules are no longer ubiquitinated, and as a result, mature DCs accumulate MHC class II at the cell surface, leading to enhanced capacity for antigen presentation.

Antigenic peptides generated from cytosolic proteins are translocated to the endoplasmic reticulum (ER) and presented by MHC class I molecules to cytotoxic T cells. Mature MHC class I complexes consist of a heavy chain, β2-microglobulin (β2m) and a peptide ligand. The folding and assembly of MHC class I complexes is under stringent quality control in the ER, such that misfolded MHC class I molecules undergo ER-associated degradation (ERAD), which involves ubiquitination and dislocation from the ER to the cytosol for proteasomal degradation. The physiological E3 enzymes involved in this process are still unclear[296-299]. Cell surface expression of MHC class I molecules is also controlled by endocytosis and endolysosomal degradation. Two E2 enzymes, Ubc5 and Ubc13, work sequentially to catalyze the initial monoubiquitination and subsequent polyubiquitination of MHC class I molecules.

I.2.5. Role of ubiquitination in adaptive immunity

Adaptive immunity is controlled by T and B cells. As discussed earlier, MHC molecules present antigenic peptides to T cells; the activation of T cells requires both T cell receptor (TCR)–peptide–MHC interactions and co-stimulatory signals. Adequately activated T cells then clonally expand and carry out effector functions such as cytotoxicity and/or cytokine secretion. B cells are activated through antigen interaction with B cell receptors (BCRs). Ubiquitination is important for the proper activation of adaptive immunity as well as for the prevention of autoimmunity.

T cell activation triggers a complex network of signalling pathways, among which are the NF-κB and MAPK pathways (Figure 1.6). TCR signaling activates the serine/threonine kinase PKCθ, which recruits a protein complex consisting of CARMA1, BCL10 and MALT1. Subsequent recruitment of TRAF6 to this complex activates the E3 ligase activity of TRAF6[300], leading to NF-κB and MAPK activation, and subsequent T cell proliferation, survival, and cytokine production. Another E3 ligase MIB2 is recently identified as a novel BCL10 interacting protein that plays a role in TCR signaling induced NF-κB activation, which may function redundantly with TRAF6 in NF-κB pathway activation[301]. TRAF6 also has a T cell-intrinsic role in inducing T cell anergy and suppressing spontaneous inflammation[302], the exact mechanisms of which remain to be determined.

TCR stimulation in the absence of costimulation leads to the induction of a tolerant state, known as anergy. In addition to TRAF6, several other E3 ligases, such as GRAIL, Itch and Cbl-b, have been implicated in the induction of T cell anergy in the absence of costimulation[303]. Recent studies indicate that these E3 enzymes can directly target components of the TCR complex. For example, GRAIL-deficient T cells are hypersensitive to TCR stimulation. This transmembrane RING-domain E3 ligase can down-regulate TCR cell surface expression after TCR activation[304], probably through endocytosis-mediated degradation, a process that involves recognition of ubiquitin modification by the endosomal sorting machinery[305]. Itch and Cbl-b cooperate to mediate K33-linked polyubiquitylation of TCRζ, which suppresses the recruitment of downstream signalling proteins in a proteasome- and endocytosis-independent manner[306]. Downstream signaling components are also regulated by ubiquitination. For example, deficiency if E3 ligase Peli1 result in T cell hyperactivation, possibly due to defects in the degradation of c-Rel, an NF-κB subunit important for T cell activation and the prevention of T cell anergy[307].

In B cells, ubiquitination-mediated mechanisms have been proposed for the activation of MAPK and non-canonical NF-κB signalling pathways downstream of CD40 and BAFF receptor (BAFF-R), two receptors of the TNF receptor superfamily[308, 309]. In these pathways, cIAPs and TRAF2 are recruited to the plasma membrane, where cIAPs are activated by TRAF2 through K63-linked polyubiquitination. cIAPs then induce K48-linked polyubiquitination and degradation of TRAF3, resulting in the release of a signaling complex containing MEKK1 (a MAPK kinase kinase) into the cytosol. MEKK1

then activates MAP kinase cascades. TRAF3 degradation also enables the kinase NIK (NF-κB inducing kinase) to dissociate from its E3 ligases cIAPs, thereby stabilizing NIK. Stabilized NIK phosphorylates and activates IKKα, which in turn phosphorylates the NF-κB precursor p100. p100 is subsequently polyubiquitinated by the βTrCP ubiquitin E3 ligase complex and processed to the mature p52 subunit by the proteasome. p52 then functions together with another NF-κB subunit RelB to turn on the expression of genes that are important for B cell survival, maturation and activation[310].

My thesis project focuses on how virus infection induces type I IFN production, more specifically, how RIG-I and MDA5 are activated once viral infection is detected. Experimental evidences point to the involvement of ubiquitin in the activation of these receptors.

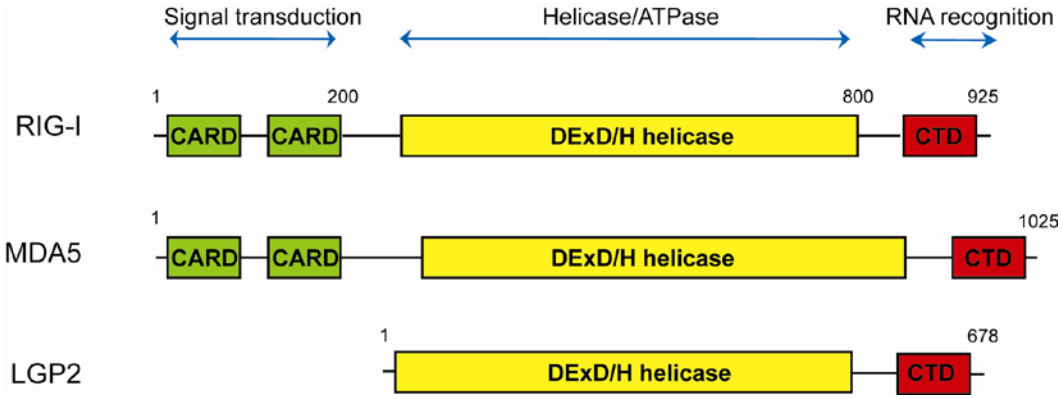

Figure 1.1. Domain structure diagrams of RIG-I like receptors.

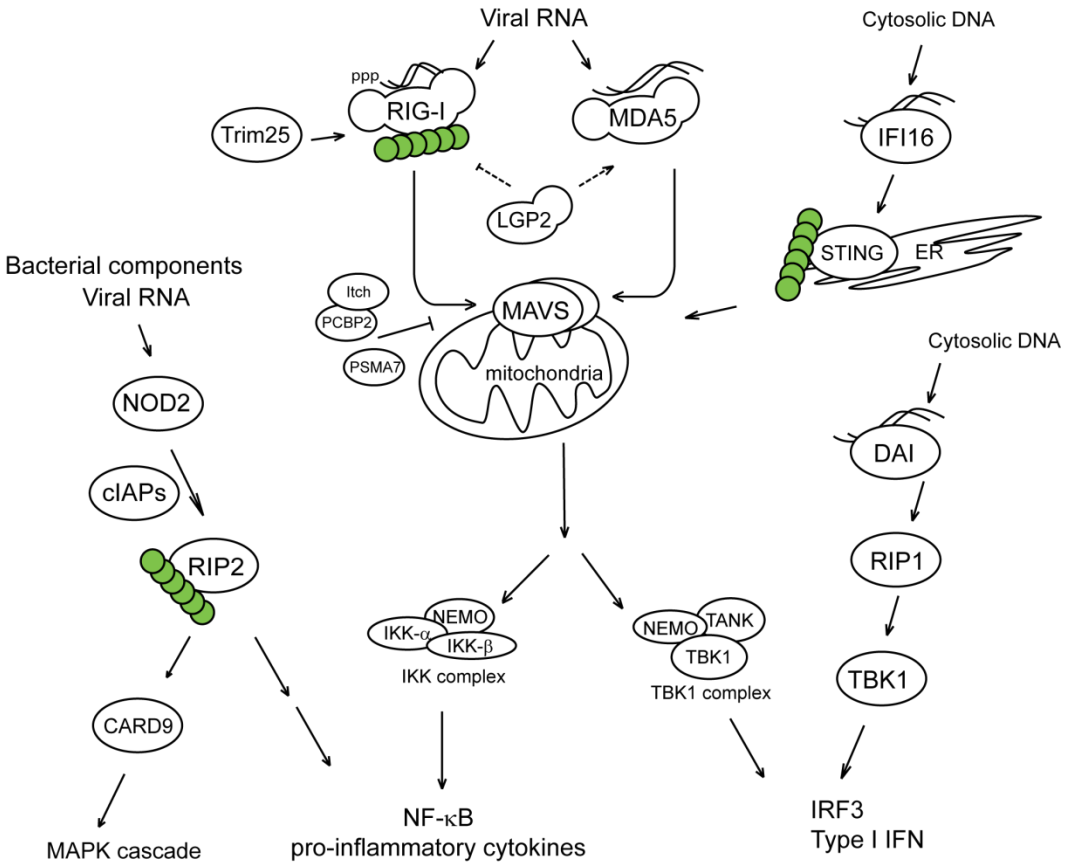

Figure 1.2. PAMPs in the cytosol are recognized by various PRRs, including NLR, RLR, and cytosolic DNA sensors, and trigger innate immune signaling pathways.

NOD2 senses bacterial peptidoglycans or viral RNA, and triggers RIP2 ubiquitination mediated by cIAPs, leading to the activation of MAPK and NF-κB pathways.

RIG-I and MDA5 sense viral RNA, and triggers MAVS-mediated signaling pathways, while LGP2 plays a regulatory role. E3 ligase Trim25 is essential for RIG-I activation. MAVS downstream signaling induces the activation of IKK and TBK1 complexes.

IFI16 and DAI recognize cytosolic DNA. STING-mediated intracellular DNA sensing pathways also involves ubiquitination.

Green circles represent important ubiquitination events.

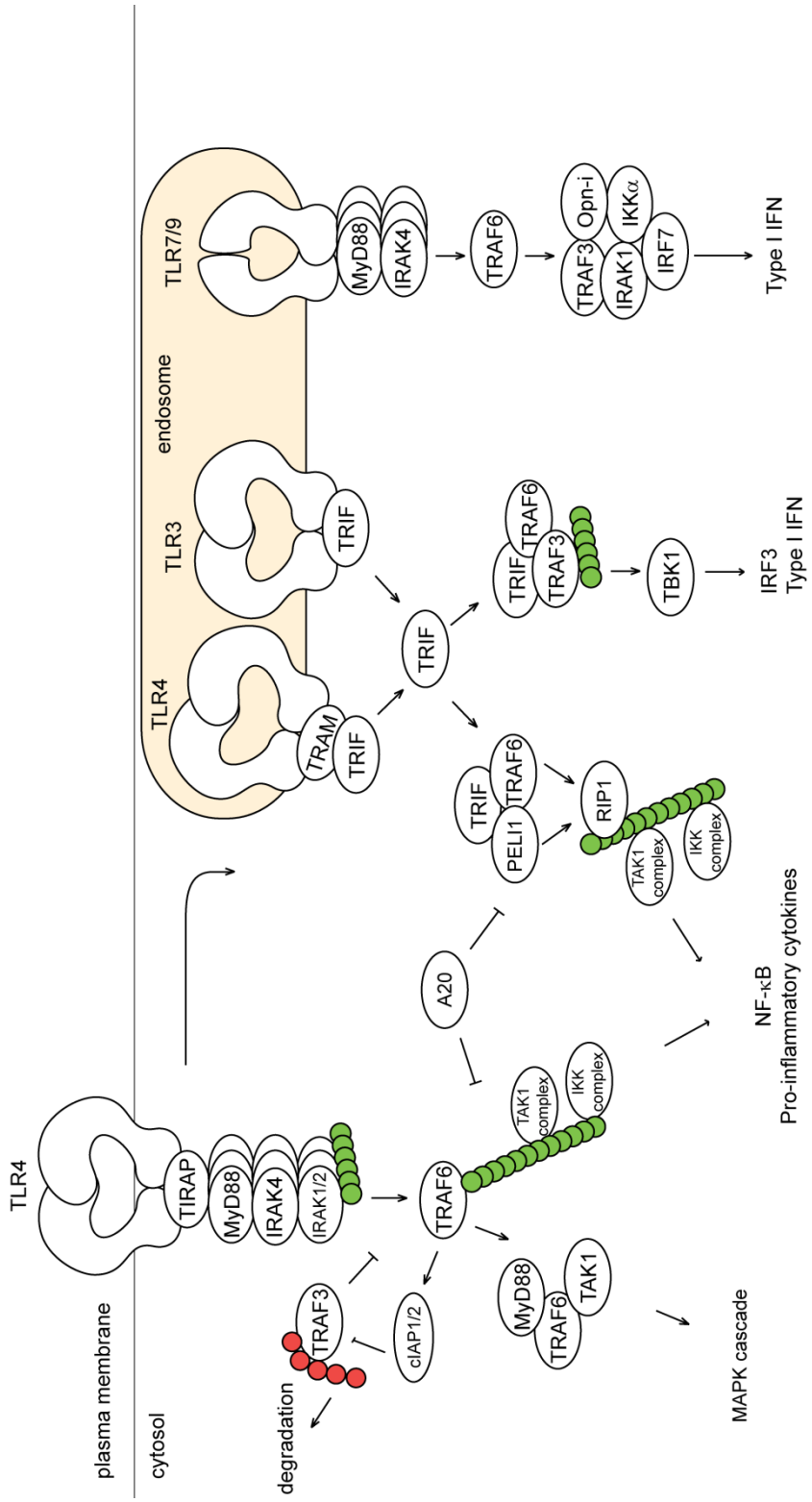
TLR4
TIRAP
MyD88
IRAK4
IRAK1/2
TRAF6
TRAF3
degradation
cIAP1/2
A20
TAK1 complex
IKK complex
MyD88
TRAF6
TAK1
MAPK cascade
NF-κB
Pro-inflammatory cytokines
plasma membrane
cytosol
endosome
TLR4
TLR3
TLR7/9
TRAM
TRIF
TRIF
TRIF
TRAF6
PELI1
RIP1
TAK1 complex
IKK complex
TRIF
TRAF6
TRAF3
TBK1
IRF3
Type I IFN
MyD88
IRAK4
TRAF6
TRAF3
IRAK1
IRF7
Opn-i
IKKα
Type I IFN

Figure 1.3. TLR signaling pathways.

TLR4 activated at the cell membrane recruits MyD88 through adaptor protein TIRAP. Signaling complexes containing MyD88, IRAKs and TRAF6 are formed at the plasma membrane. TRAF6 catalyze the synthesis of polyubiquitin, which then activates TAK1 and IKK complexes, leanding to NF-κB activation. TRAF6 activates E3 ligases cIAPs, which induce ubiquitination and degradation of TRAF3. Degradation of TRAF3 releases signaling complexes into the cytosol where additional components are recruited and activated.

Endocytosed TLR4 recruits TRIF via adaptor protein TRAM. TRIF also mediates TLR3 pathways. Through the action of several E3 ligases, PELI1, TRAF3 and TRAF6, and ubiquitination events of signaling proteins such as RIP1 and TRAF3, downstream pathways are activated leading to NF-κB activation and type I IFN induction. DUBs, such as A20, provide mechanisms for downregulation of various pathways, by disassembling polyubiquitin chains.

TLR7/9 pathway induced type I IFN production involves the assembly of a transductional-transcriptioanl signaling complex containing MYD88, IRAK4, TRAF6, TRAF3, Opn-i, IRAK1, IKKα, and IRF7.

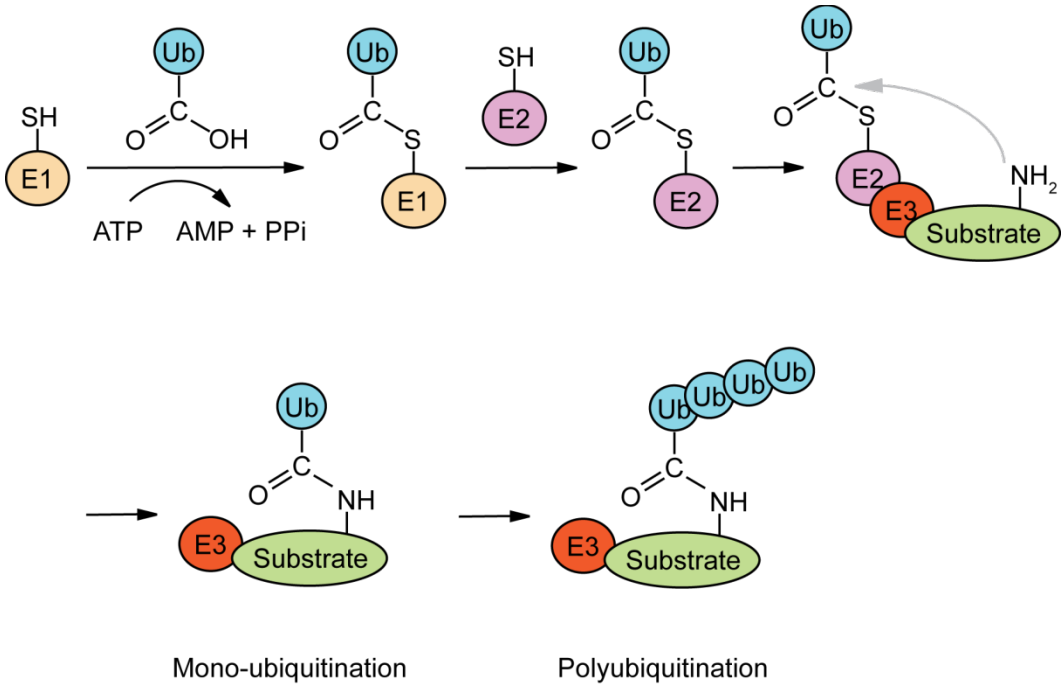

Figure 1.4. Ubiquitination reaction mediated by an enzymatic cascade involving E1, E2 and E3.

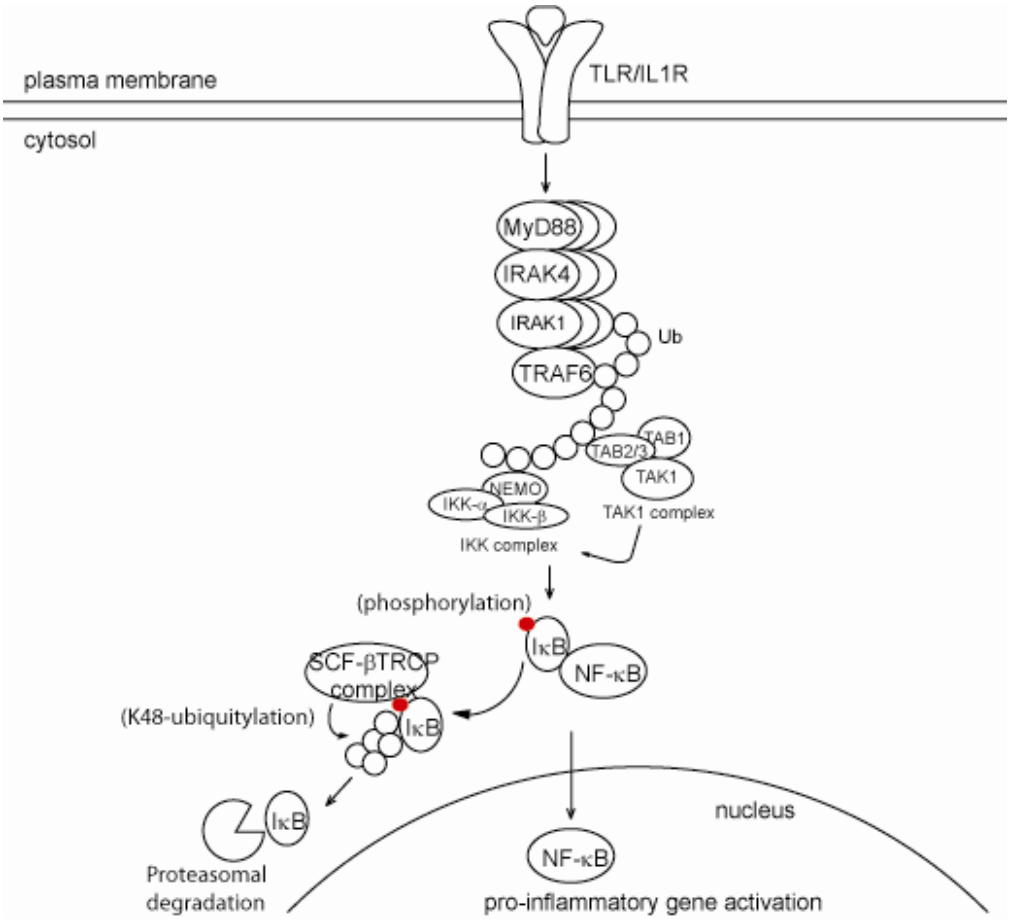

Figure 1.5. Role of ubiquitin in NF-κB activation in the IL1R/TLR pathway.

Activation of the IL1β receptor or TLR4 triggers the MYD88-dependent NF-κB activation pathway. MYD88, IRAKs and TRAF6 are recruited to the receptor. TRAF6 catalyzes the synthesis of K63-linked polyubiquitin chains. The polyubiquitin chains function as a scafoold to recruit the TAK1 and IKK complexes through binding to the regulatory subunits, TAB2 and NEMO, respectively. Recruitment of the kinase complexes facilitates autophosphorylation of TAK1 and subsequent phosphorylation of IKKβ by TAK1. IKK phosphorylates IκBα, which induces IκBα ubiquitination and degradation by the proteasome, and subsequent activation of NF-κB.

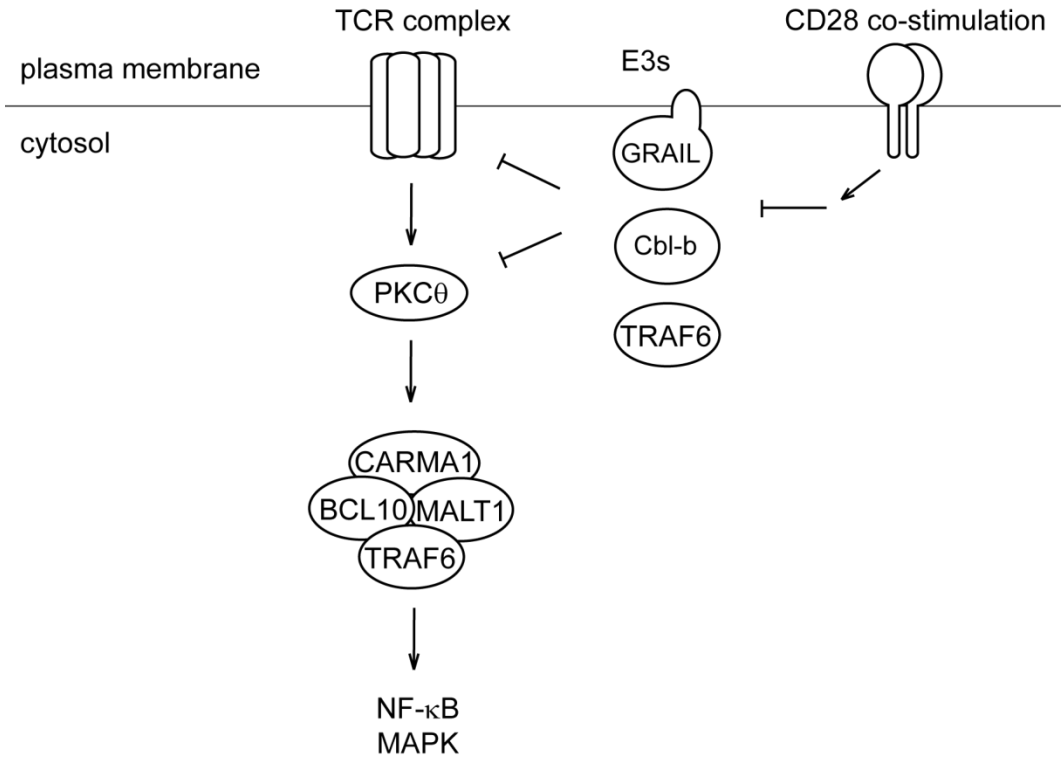

Figure 1.6. TCR activation induced NF-κB and MAPK activation pathways.

TCR signaling activates PKCθ, which recruits a protein complex containing CARMA1, BCL10 and MALT1. Subsequent recruitment of TRAF6 activates its E3 activity, leading to NF-κB and MAPK activation.

In the absence of co-stimulation, several E3 ligases, such as GRAIL, Cbl-b and TRAF6, are involved in the inhibition of TCR hypersensitivity and the induction of T cell anergy.

Table 1.1. Viral associated PAMPs and host PRRs that recognize them.

Location	Viral PAMPs	PRRs	References
Plasmamembrane	Viral Proteins	TLR2/4	[311-315]
endosome	ssRNA	TLR7/8	[119, 123, 126, 194, 316-318]
	dsRNA	TLR3	
	CpG DNA	TLR9	
cytosol	DNA	AIM2	[196, 197, 199, 204-207]
		DAI	
		IFI16	
	5'-pppRNA	RIG-I	[35, 209, 319-321]
	dsRNA	RIG-I, MDA5	
	lack of modification	RLR and TLR	
	5'-pppRNA converted from viral DNA	PolIII and RIG-I	

CHAPTER II

MATERIALS AND METHODS

II.1. Reagents and Standard Methods

Reagents

Antibodies were obtained from the following sources: Santa Cruz Biotech (mouse anti-ubiquitin); Sigma (mouse anti-Flag M2 and M2-agarose); Invitrogen (rabbit anti-GST). Generation and affinity purification of RIG-I antibody, native gel electrophoresis for detection of IRF3 dimerization, SDS-PAGE and immunoblotting procedures were described previously[71]. Rabbit anti-MDA5 antibody was generated by immunizing rabbits with recombinant protein MDA5(N) (amino acids 2-200) produced in *E. coli*., and was subsequently affinity purified using MDA5 antigen column, made by conjugating His-tagged MDA5(N) to NHS-activated sepharose (GE Healthcare) following manufacturer's instruction. ^{35}S-Methionine labelbed IRF3 (^{35}S-IRF3) is made by in vitro transcription and translation with rabbit reticulocyte lysate (Promega).

All chromatography columns were from GE Healthcare. Other chemicals and reagents were from Sigma unless otherwise specified. Sendai virus (Cantell strain, Charles River Laboratories) was used at 100 hemagglutinating (HA) units/ml culture media. EMCV was from ATCC.

5’-pppRNA was generated by in vitro transcription with MEGAscript® Kit (Ambion) using a T7 promoter driven-DNA template, according to manufacturer’s instruction. Sequence of the DNA template for 5’-pppRNA (135 nt) (including T7 promoter):

TAATACGACTCACTATAGGGAGAGAGAGAGAATTACCCTCACTAAAGGGAG

GAGAAGCTTATCCCAAGATCCAACTACGAGCTTTTTAACTGCAGCAACTTTAA

TATACGCTATTGGAGCTGGAATTACCGCGGCTGCTGTTCTAGAGGATC

Expression constructs, Protein Expression and Purification

pEF-GST-RIG-I(N), K172R, and 6KR (K99/169/172/181/190/193R) were kindly provided by Dr. Jae Jung (University of Southern California). cDNA encoding different fragments of MDA5 were inserted in-frame into pCMV-GST (Dr. Randall Reed[322]). Point mutations of RIG-I(N) and MDA5(N) were generated by site-directed mutagenesis. 14KR of RIG-I(N) contains the following mutations: K95/96/99/108/115/146/154/164/169/172/177/181/190/193R.

For proteins expressed in *E. coli*, cDNAs were cloned in-frame with appropriate tags into pGEX-4T1, or Gateway cloning vectors (Invitrogen). TEV cleavage sites were introduced between the N-terminal tag and insert cDNA. GST-MDA5-Flag, GST-RIG-I(N), GST-MDA5(N), His-tagged MDA5(N) and their various mutants and fusion proteins were expressed in *E. coli* BL21 pLyss cells. Cultures were grown at 37°C till OD600 = 0.6. Expression was induced with 0.5 mM IPTG (for GST-MDA5-Flag, 0.3

mM IPTG), and cells were subsequently incubated at 18°C overnight, with shaking. After harvesting, resuspended cells (in PBS, 1 mM DTT, and Roche protease inhibitor cocktail) were disrupted by sonication or with Emulsiflex (Avestin). GST fusion proteins were purified to homogeneity using glutathione affinity chromatography. GST tags were cleaved off with TEV protease unless otherwise indicated; resulting untagged recombinant proteins were purified using ion exchange, and gel filtration chromatography with standard protocols. For NZF fusion constructs, NPL4 NZF (residues 582-608)[251] were fused to the C-termini of RIG-I(N) or MDA5(N) by fusion PCR. Amino acid sequence of NZF: AMWACQHCTFMNQPGTGHCEMCSLPR.

GST-Nod1(N), GST-Nod2(N) and GST-caspase8(N) expression constructs were made by inserting cDNA encoding the following fragments in pGEX-4T1 vector: Nod1 amino acids 2-106; Nod2 amino acids 2-224; Caspase 8 amino acids 2-204.

His-tagged RIG-I, RIG-I-Flag, Trim25, and E1 were expressed and purified from insect cells, using baculovirus expression system (Invitrogen). His-tagged Ubc13 and Uev1A were expressed and purified from *E. coli*[147].

Cell culture methods

HEK293T cells were cultured in DMEM supplemented with 10% fetal calf serum (FCS, Hyclone Laboratories) and antibiotics. MEF cells and U2OS cells were cultured in DMEM supplemented with 10% fetal bovine serium (FBS, Invitrogen) and antibiotics. Thp1 cells were cultured in RPMI supplemented with 10% FBS and

antibiotics. Trim25 WT and KO MEF cells are from Dr. Jae Jung's group (University of Southern California). Primary MEF cells are prepared with standard protocol from Ubc13fl/fl mice from Dr. Shizuo Akira's group (Osaka University, Japan). For tetracycline-inducible expression system in U2OS cells, cells were treated with or without 1 μg/ml tetracycline for 3 (U2OS-shUb), 4 (U2OS-shUb-K63R), or 7 days (shUbc13) before used for experiments.

Transient transfection of DNA or siRNA (small interfering RNA) was carried out using calcium phosphate precipitation method in HEK293T cells. Lipofectamine 2000 (Invitrogen) method was used for transfection of RNA in HEK293T, MEF, U2OS, and Thp1 cells. For one well of cells in a 6-well plate, 1 μg RNA was transfected with 4 μl Lipofectamine 2000. For RNA transfection followed by gene expression analysis with quantitative PCR, total RNA was harvested 6 hours after transfection unless otherwise indicated.

Lentiviral vector construction and production

Lentivirus transducing vectors (pTY) were constructed to express both short hairpin RNA (shRNA) driven by U6 small nuclear RNA promoter, and cDNA (resistant to shRNA knockdown) driven by Elongation Factor 1α (EF1α) promoter. Lentivirus vectors were generated by transcient co-trasfection of pTY transducing vector and helper plasmids into HEK293T cells[323]. Twenty four hours after transfection, culture media were

collected, filtered with 0.22 μm filters (Millipore) and stored in aliquots at -80°C until use.

Table 2.1 lists shRNA or siRNA targeted sequences of indicated genes for knockdown.

Construction of stable cell lines

Target cells were transduced with lentiviral vectors in the presence of Polybrene (10 μg/ml). Cells were selected for the expression of drug resistance genes carried by lentivirus vectors (for example, puromycin, hygromycin) for seven days before experiments. For primary MEF cells, cells were transduced with lentiviral vector for RIG-I expression, and selected for hygromycin resistance for seven days. For Cre-recombinase-mediated gene deletion, cells were transduced with lentiviral vector for Cre expression, and selected for puromycin resistance for seven days before experiments.

U2OS cell lines with tetracycline-indicuble expression system used in this study were gifts from Dr. Ming Xu, and were described in published work[324].

Gene expression analysis by quantitative PCR (qPCR)

Total RNA was isolated using TRIzol (Invitrogen). 500 ng total RNA was reverse transcribed into cDNA using iScript cDNA synthesis kit (Bio-rad). The resulting

cDNA was used as template for quantitative PCR using SYBR Green method (Bio-rad) with primers listed in Table 2.2.

Luciferase reporter assay

HEK293T cells were plated in 6-well plates, and transfected with 50 ng to 500 ng indicated expression constructs, or 500 ng RNA, together with 25 ng IFNβ-luciferase reporter and 25 ng pRL-CMV as internal controls. Where indicated, HEK293T cells stably expressing IFNβ-luciferase reporter were used. Sixteen to thirty six hours after transfection, luciferase activity in cell lysate was measured using Promega Luciferase Assay system.

ATPase activity assay

Indicated proteins were incubated with RNA ligand in 1xMgATP buffer [20 mM Hepes-KOH (pH7.4), 2 mM ATP, 5 mM $MgCl_2$] at 37ºC for 1 hour. The concentration of released $(PO_4)^{3-}$ were measured with Biomol Green reagent (Enzo Life Scieinces) according to manufacturer instructions.

II.2. Special Experimental Procedures

Cellular fractionation

Hypotonic Buffer [10 mM Tris-HCl (pH 7.5), 10 mM KCl, 1.5 mM MgCl2, 0.5 mM EGTA, and Roche protease inhibitor cocktail] was used to make cytosolic fractions, and Isotonic Buffer (Hypotonic Buffer plus 0.25 M D-Mannitol) was used to make mitochondria fractions. Cells were collected and homogenized in appropriate buffers. Unbroken cells and nuclei were removed by centrifugation at 1,000 g for 5 min. The resulting supernatant was further centrifuged at 5,000 g for 10 min to separate pellet (P5, crude mitochondria fraction) and supernatant (S5, crude cytosolic fraction). P5 was washed once with Isotonic Buffer. Crude cytosolic fraction S5 was further centrifuged at 100,000 g for 1 hour to obtain supernatant (S100, cytosolic fraction).

Purification of a cytosolic activator of the MAVS-IRF3 pathway

S100 was subjected to chromatography columns including HiTrap Q, HiTrap Heparin, MonoQ, and Superdex-300pc. For HiTrap Q and MonoQ columns, samples were loaded onto columns equilibrated with Buffer A [20mM Tris-HCl (pH 7.5), 1 mM DTT], and eluted with NaCl gradient of 0 - 500 mM in the same buffer. For HiTrap Heparin, similar buffer was used except at pH 6.8. For Superdex-300pc, samples were loaded and eluted in Buffer B [20 mM Tris-HCl (pH7.5), 100 mM NaCl, 1 mM DTT]. For Flag affinity purification step, samples were incubated with M2-agarose beads at 4ºC for 2 hours, washed with 20mM Tris-HCl (pH7.5), 150mM NaCl, 1mM DTT, and eluted

with 0.2 mg/ml Flag peptide in Buffer A. Silver staining was carried out with silver staining kit (Thermo Scientific).

IRF3 dimerization assay

For IRF3 pathway activation by RIG-I or MDA5, proteins to be tested were added to reaction mixture containing, 0.5 mg/ml P5, 3 mg/ml S5, 1xMgATP buffer, and 0.02 mg/ml ^{35}S-IRF3. After incubation at 30°C for 1 hour, samples were centrifuged at 20,000 g for 5 minutes and supernatants were subjected to native PAGE to visualize IRF3 dimerization by autoradiography using PhosphorImager (GE Healthcare). ImageQuant was used to quantify signal intensity.

Ubiquitination reaction

Ubiquitination reaction was carried out with 0.1 μM E1, 1 μM Ubc13/Uev1a, 0.5 μM Trim25, 100 μM Ub, 1 mM DTT, in 1xMgATP Buffer at 30°C for 1 hour. 20 μM substrate [RIG-I(N) or MDA5(N)] was included where indicated.

Biochemical assay for RIG-I and MDA5 activation in vitro

For RIG-I(N) or MDA5(N) activation by ubiquitination, RIG-I(N) or MDA5(N) was subjected to ubiquitination reaction, and then 1 μl of the reaction mixture was used

in IRF3 activation assay described above. For RIG-I(N) or MDA5(N) activation by ubiquitin chains, 1 μl mixture containing 50 ng of RIG-I(N) or MDA5(N) and 50 ng of ubiquitin chains were incubated at 4°C for 30 minutes, and then tested in IRF3 activation assay. Five-fold serial dilution was used in titration experiments. For standard activation assays of full-length RIG-I or MDA5, 1 μl mixture containing 50 ng of RIG-I or MDA5, 50 ng poly[I:C] or 5'-pppRNA, 50 ng ubiquitin chains, in the presence of 1xMgATP Buffer, was incubated at 4°C for 30 minutes, and then used in IRF3 activation assay.

K63-linked ubiquitin chain synthesis

Methods for synthesizing K63-linked polyUb were described previously[148]. Briefly, K63-linked polyUb chains were synthesized in ubiquitination reactions without substrates. Reaction was stopped with 5 mM EDTA and reduced with 5 mM DTT at room temperature for 15 minutes, followed by 35 mM N-ethylmaleimide (NEM) treatment at room temperature for 15 min. Excess NEM was quenched with 20 mM DTT. Enzymes used in the reaction were then depleted with Ni-NTA beads. The mixture containing polyUb chains was buffer exchanged repeatedly into Buffer A. Short K63-, K48-, and mixed linkage ubiquitin chains (Ub2, Ub3, Ub4, Ub5, Ub6, Ub8, Ub3-7) were from Boston Biochem. Short K63-Ub chains were also synthesized in house according to published protocol[325].

Ubiquitin binding assay

For in vitro Ub binding assay, 0.1 mg/ml GST tagged proteins were mixed with 0.1 mg/ml polyUb in 20 mM Tris-Cl (pH7.5) at 4ºC for 30min. The mixture was then diluted 10 fold in Binding Buffer [20 mM Tris-Cl (pH7.5), 100 mM NaCl, 0.1% (v/v) NP-40 and 10% (v/v) glycerol]. GST proteins were pulled down with glutathione-sepharose (GE Healthcare), and washed three times in Binding Buffer. Associated proteins were analyzed by immunoblotting. When GST-proteins were expressed in HEK293T cells, cells were lysed with Lysis Buffer [20 mM Tris-Cl (pH7.5), 150 mM NaCl, 0.5% NP40, 1 mM DTT, protease inhibitor cocktail], and GST pull-down was performed with cell lysate in Lysis Buffer.

Semidenaturing Detergent Agarose Gel Electrophoresis

Semidenaturing detergent agarose gel electrophoresis (SDD-AGE) for analyzing MAVS oligomerization was performed according to published protocols with minor modifications[85, 326]. In brief, proteins from crude mitochondria (P5) were extracted by Hypotonic Buffer supplemented with 1% DDM (detergent), resuspended in a buffer containing 0.5xTBE, 10% glycerol, 2% SDS, and 0.0025% bromophenol blue, and loaded onto a vertical 1.5% agarose gel (Bio-Rad). After electrophoresis in the running buffer (1xTBE and 0.1% SDS) for 35 min with a constant voltage of 100 V at 4ºC, proteins were transferred to Immobilon membrane (Millipore) for immunoblotting.

Analytical Ultracentrifugation

Multisignal Sedimentation Velocity (SV) experiments were carried out as the following[327]. Concentrated stock solutions of RIG-I(N), K63-Ub3, -Ub4, -Ub5, and -Ub6 were prepared in 20 mM Tris-HCl (pH7.5), 20 mM NaCl, 0.5 mM TCEP, and diluted in the same buffer to final concentrations of 4-8 μM for RIG-I(N) or 20-40 μM for K63-Ub chains, separate or in combination. Samples were allowed to equilibrate for 16 hours at 4°C, and loaded into centrifugation cells equipped with charcoal-filled Epon centerpieces and sapphire windows; the cells were allowed to equilibrate at 20°C for two hours before centrifugation. 390 μl of sample in the sample sector and the same volume of buffer without proteins in the reference sector were centrifuged with Beckman Optima XL-I analytical ultracentrifuge in an An50Ti rotor at 50,000 rpm or 35,000 rpm, at 20°C, until all components apparently sedimented to the bottom of the cell. UV absorbance at 280 nm (ABS) and Rayleigh interferometry (IF) data were collected simultaneously using the Beckman control software, and analyzed with SEDPHAT using multiwavelength model[328]. Molar signal increments (ε) of all components were calculated (ε_{IF}) or refined by SEDPHAT from experimental data (ε_{ABS}), shown in Table 2.3. All values for buffer densities (ρ), buffer viscosities (η), and partial specific volumes ($\bar{\nu}$) of the proteins were estimated using SEDNTERP.

RIG-I oligomerization

For RIG-I in vivo oligomerization experiments, HEK293T cells stably expressing RIG-I-Flag were infected with SeV or mock treated for 16 hours. For MEF cells stably

expressing RIG-I-Flag, cells were infected with SeV or mock treated for 10 hours. Cell lysates were prepared in Lysis Buffer. RIG-I was immunoprecipitated from cell lysates with anti-Flag M2-agarose at 4°C for 2 hours. The agarose beads were washed three times with Lysis Buffer, and RIG-I was eluted with 0.2 mg/ml Flag peptide in Buffer A and concentrated. For RIG-I in vitro oligomerization experiments, RIG-I (0.1 mg/ml) was incubated in various combinations with ATP (provided as 1xMgATP Buffer), 5'-pppRNA (0.1 mg/ml), and K63-Ub6 (1 mg/ml) in Buffer B at 4ºC for 30 minutes. 50 µl of each sample was subjected to Superdex-200 gel filtration analysis with Buffer B as the elution buffer.

For RIG-I(N) oligomerization experiments, RIG-I(N) (0.5 mg/ml) was incubated with K63-Ub3, -Ub4, -Ub5 or -Ub6 (0.5 mg/ml) at 4ºC for 30 minutes. 50 µl of each mixture was loaded onto Superdex-200 gel filtration column with Buffer A. Gel filtration fractions were used for immunoblotting and IRF3 activation assay. For semi-quantitation, fractions containing RIG-I(N):Ub chain complexes were compared with purified RIG-(N) and Ub chains mixed at defined ratio with SDS-PAGE followed by Coommassie Blue staining. Gel band intensities were quantified with ImageQuant.

MDA5 oligomerization

For MDA5(N) oligomerization experiments, MDA5(N) (0.05 mg/ml) was incubated with K63-Ub6 (2 mg/ml) at 4ºC for 30 minutes. 50 µl of each mixture was

loaded onto Superdex-200 gel filtration column with Buffer A. Gel filtration fractions were used for immunoblotting and IRF3 dimerization assay.

Computational analysis

For cluster analysis of CARD domain subfamily sequences, CARD domain sequences were collected using PSI-BLAST[329] searches (E-value cutoff 0.01, limit 10 iterations) against the NR sequence database (posted Feb 24, 2010; 10,461,804 sequences) with query sequences corresponding to the MAVS CARD domain structure (gi|162330189, residues 385 to 477) and the Nod1 CARD domain structure (gi|161760910, residues 1 to 98). The resulting set of unique CARD domain sequences (1118) were clustered with the CLANS[330] program (first in 3 dimensions, and then in 2 dimensions) using all-against-all BLAST sequence similarities (cutoff 0.0001). Two-dimensional clustering map of CARD domain sequences was constructed. Each dot representing a CARD domain sequences were connected by pair-wise BLAST P-values.

To create a structure based distance tree, example CARD domain structures found in iterative BLAST searches were collected; known death domains structures from FADD and Pea-15 were also included. DaliLite[331] Z-scores were calculated for all-against-all pairwise comparisons of the following structures: MAVS (2vgq, residues 370-462), Apaf-1 (3ygsC, residues 1-95), ProCaspase9 (3ygsP, residues 1-97), Iceberg (1dgn, residues 2-90), Nlrp1 (3kat, residues 1379-1462), Pea-15 (1n3k, residues 1-91), FADD (2gf5, residues 1-90, and 2gf5, residues 91-191). Distances between structures were

calculated from the Dali Z-scores according to the following formula: 1/(ZscoreAB/Average[ZscoreAA, ZscoreBB]) -1. Trees were calculated from these distances using the FITCH program of the Phylip package[332], with global rearrangements option (-G).

Table 2.1. Targeted sequences by RNA interference.

Targeted gene	Targeted sequence	Targeting method
human MDA5	gcaaggagttccaaccattt	shRNA
human RIG-I	gaattatcccaaccgatat	shRNA
mouse MDA5	gccacagaatcagacacaagtt	shRNA
human MAVS	ccaccttgatgcctgtgaa	siRNA
eGFP	gtccgccatgcccgaaggc	siRNA

Table 2.2. Primers for qPCR.

Genes	Direction	Sequence
human IFNβ	forward	AGGACAGGATGAACTTTGAC
	reverse	TGATAGACATTAGCCAGGAG
human GAPDH	forward	AAAATCAAGTGGGGCGATGCT
	reverse	GGGCAGAGATGATGACCCTTT
human MDA5	forward	CCCTTCCTCAGATACTGGGAC
	reverse	CTCTGGTTGCATCTGCAATGGC
human RIG-I	forward	CTCCCGGCACAGAAGTGTAT
	reverse	CTTCCTCTGCCTCTGGTTTG
mouse IFNβ	forward	TCCGAGCAGAGATCTTCAGGAA
	reverse	TGCAACCACCACTCATTCTGAG
mouse β-Actin	forward	TGACGTTGACATCCGTAAAGACC
	reverse	AAGGGTGTAAAACGCAGCTCA
mouse MDA5	forward	GCTATGTCAAACCCACACTC
	reverse	CCTTCTGCACAATCCTTCTC

Table 2.3. Fixed IF signal increments and refined ABS signal increments used in this study.

Protein	ε_{IF} (fringes/M·cm)	ε_{ABS} (AU/M·cm)
RIG-I(N)	64784.8	45217.9
Ub3	70877.5	3841.26
Ub4	94381.4	5132.05
Ub5	117885.3	6220.40
Ub6	141389.1	7329.04

$\varepsilon_{IF} = 2.75M_c$ (M_c is the calculated molar mass)

CHAPTER III

PURIFICATION AND CHARACTERIZATION OF A CYTOSOLIC MAVS ACTIVATOR

III.1. Introduction

The RIG-I/MAVS pathway mediates type I IFN production induced by certain RNA viruses, including Sendi Virus (SeV). RIG-I directly detects viral RNA in the cytosol and activates the Mitochondria Antiviral Signaling protein MAVS, which in turn triggers the activation of downstream signaling cascade leading to the activation of transcription factors, including IRF3 and NF-κB. IRF3 is activated by its kinase TBK1. Phosphorylated IRF3 dimerizes and translocates to the nucleus. To identify additional factors in this pathway and dissect the biochemical mechanism mediating type I IFN production, our lab has previously established an in vitro reconstitution system that recapitulates signal transduction from MAVS to IRF3[333]. Cytosol and crude mitochondria are prepared from mammalian cells by differential centrifugation (Figure 3.1A), designated as P5 and S5, respectively. When crude mitochondria isolated from virus infected cells (P5*) and cytosol fraction from un-infected cells (S5) are incubated together at 30°C in vitro in the presence of magnesium (Mg), ATP, and radio-isotope labeled IRF3 protein (^{35}S-IRF3), robust IRF3 dimerization can be detected with native poly-acrylamide gel electrophorasis (PAGE) followed by autoradiography. Different

components of the in vitro system can then be manipulated to determine what factors are involved in the MAVS-IRF3 pathway.

Using this system we discovered important roles for ubiquitin in this pathway downstream of MAVS[333]. However, upstream of MAVS, it was not well understood how a cytosolic receptor RIG-I activates a mitochondria signaling protein MAVS. RIG-I and MAVS both have CARD domains, which may mediate homotypic interaction. RIG-I was shown to undergo conformational changes upon RNA binding that might lead to the exposure of the CARDs for interaction with downstream signaling components[46, 53, 54]. One can speculate that CARDs of RIG-I may mediate direct interaction with MAVS CARD domain. However, previous studies attempting at detecting RIG-I and MAVS interaction was all in overexpression settings[69-72]. Direct stable interaction between these two proteins was not apparent. So I decided to set up an in vitro reconstitution system to study the unknown signaling events upstream of MAVS activation.

In this chapter I describe a biochemical approach to understanding the mechanism of MAVS activation by RIG-I. Based on the MAVS-IRF3 reconstitution system, I set out to establish an in vitro assay system to recapitulate the upstream events leading to MAVS activation. I found by mixing cytosolic fractions from virus infected cells (S100*) with mitochondrial and cytosolic fractions from uninfected cells (P5 and S5), IRF3 dimerization could be observed (Figure 3.1B). Then by fractionating cytosolic fractions by various methods, this assay could be used to follow and purify the “MAVS activator” activity that can trigger the MAVS-IRF3 pathway activation.

III.2. In Vitro Reconstitution of MAVS Activation by a Cytosolic Activator

In HEK293T cells, the RIG-I-MAVS-IRF3 pathway mediates SeV-infection-induced type I IFN production[9, 71]. In SeV infected HEK293T cells, IRF3 forms dimers that can be detected by native PAGE (Figure 3.2A), indicating the RIG-I-MAVS-IRF3 pathway is activated upon SeV infection. When in vitro assays were carried out as described in Figure 3.1B, I found that cytosolic fractions from SeV infected cells (S100*) contained an activity that can trigger IRF3 dimerization in vitro when it was incubated with mitochondria fraction (P5) from uninfected cells and cytosolic fraction from uninfected cells (S5) (Figure 3.2B). This S100* activity was not due to direct kinase activity for IRF3 because it did not cause IRF3 dimerization directly without P5 fraction (Figure 3.2C). Thus, this S100* activity reflected an activation signal upstream of MAVS. The cytosolic activator also required additional cytosolic fractions from uninfected cells, probably because the amount of cytosolic proteins in S100* were not sufficient to support IRF3 activation by MAVS, since the amount of proteins from S100* used in the assay were much less than that from S5. To further confirm this in vitro assay mimicked the RIG-I-MAVS- IRF3 pathway, cellular fractions were prepared from cells where individual signaling protein was knocked-down by siRNA. When S100* from RIG-I siRNA cells, or P5 from MAVS siRNA cells were used, the activity was abolished (Figure 3.2D & E).

III.3. Purification of a Cytosolic MAVS Activator

The cytosolic activity upstream of MAVS could represent activated RIG-I or an intermediate activator between RIG-I and MAVS. To test whether the activator in S100* could be separated from RIG-I with chromatography method, S100* was fractionated on a HiTrap Q ion exchange column, and each fraction was tested for its ability to activate MAVS in the in vitro reconstitution assay. The S100* activity eluted from the HiTrap Q column at 260-340 mM NaCl. The distribution of S100* activity did not correlate with that of RIG-I, the majority of which eluted at 160-200 mM as indicated by RIG-I immunoblot (Figure 3.3A). Next, RIG-I was immuno-depleted from S100* with anti-RIG-I antibody. Surprisingly, S100* depleted of RIG-I lost its ability to activate MAVS in vitro (Figure 3.3B), indicating the cytosolic activator was likely to be a small fraction of activated RIG-I or tightly associated with a small fraction of RIG-I. Since S100* activity associated with RIG-I, S100* was then prepared from HEK293T cells stably expressing C-terminal Flag-tagged RIG-I. Cytosolic activity from S100* of HEK293T/RIG-I-Flag cells could be pulled down with Flag-antibody (Figure 3.3C), thus providing an efficient purification step of the RIG-I-associated MAVS activator.

To purify the S100* activator, S100* was subjected to tandem purification steps using additional purification steps (Figure 3.3D-G). From HiTrap Heparin column, most S100* activity eluted at 230-300 mM NaCl. Active fractions were then purified with Flag affinity pull down, Superdex-200 gel filtration column, and MonoQ column. Notably, the majority of RIG-I molecules were separated from the activity on multiple columns. For example, on Superdex-200, the activity eluted in fractions corresponding to higher

molecular weight than RIG-I monomer (calculated to be ~115 kDa); on MonoQ column, the activity distribution was different from RIG-I western blot. To further facilitate purification of the cytosolic activity, a second affinity purification method was employed by using RIG-I antibody to immuno-precipitate (IP) the activity. As shown in Figure 3.4, RIG-I antibody was able to deplete activity from MonoQ active fractions while rabbit IgG could not. RIG-I IP products were visualized with SDS-PAGE followed by silver staining (Figure 3.4B). Protein bands that correlated with the activity were cut off of the gel and analyzed by Mass Spectrometry (in collaboration with Dr. She Chen at National Institute of Biological Sicneces, Beijing). Similar experiments were repeated three times, with consistent protein identification in activity-associated bands to be RIG-I and ubiquitin. Ubiquitin western blot confirmed the presence of ubiquitin which associated with the cytosolic activity (Figure 3.4C). Given that the majority of RIG-I molecules did not associate with the cytosolic activity during the purification process, these results indicated that the S100* activity was likely due to a small fraction of RIG-I that was activated in the cytosol after virus infection, and that ubiquitin might be involved in RIG-I activation. For example, activated RIG-I could involve a specific modification (ubiquitination) and/or a specific conformation induced by the presence of ubiquitin. Next my project focused on the biochemical characterization of RIG-I activation.

III.4. Characterization of In Vivo Activated RIG-I

Characterization of RNA bound to activated RIG-I

RIG-I was known to bind RNA in vitro[4]. Purified RIG-I from virus infected cells could potentially associate with immunostimulatory RNA, which could also associate with the activity that I had been following. To test this hypothesis, first, I extracted RNA with Trizol reagent from RIG-I samples purified from virus infected or control cells, and transfected these RNA into HEK293T. Indeed, RIG-I from virus infected cells pulled down RNA that could stimulate IFNβ production when transfected into cells (Figure 3.5A). Later it was shown by another group that RIG-I associated with whole virus genome in the case of certain negative strand RNA viruses, such as influenza virus[47]. Thus, RNA virus genome may serve as ligands to activate RIG-I. However, how RNA ligands activate RIG-I was unclear. To determine if there was any RNA species associated with RIG-I that might be responsible for the S100* activity, purified RIG-I from SeV infected cells was treated with nucleases. Neither RNase nor DNase treatment affect the ability of activated RIG-I to activate the IRF3 pathway in vitro (Figure 3.5B), although RNase treatment did abolish the activity of RIG-I-associated RNA as shown by luciferase assays (Figure 3.5A). These results indicated that, once RIG-I was activated in vivo, nuclease treatment in vitro could not de-activate it.

Characterization of RIG-I cleavage event

It was noticed that upon SeV infection a low molecular weight band (around 30 kDa) appeared on RIG-I western blot, suggesting certain RIG-I cleavage event might correlate with RIG-I activation (Figure 3.6A). The RIG-I antibody used here was raised against the N-terminus CARD domains of RIG-I, indicating that upon virus infection a

RIG-I cleavage event generated an N-terminus fragment of the protein. In final fractions of S100* purification it was also noticed that there were a few low molecular weight bands (around 40-50kD) corresponding to the N-terminus of RIG-I and ubiquitin according to mass spectrometry identification as well as western blot (Figure 3.4C). This was potentially interesting because the N-terminus domains of RIG-I was known to mediate signaling activity[4].

To test whether RIG-I cleavage event generating the N-terminus fragment could activate RIG-I, bypassing the requirement for virus infection, I generated modified RIG-I cDNA constructs that were engineered to have a TEV protease cleavage site inserted after the CARD domains of RIG-I (N terminal 232 amino acids, designated as N232), as well as a Flag tag at either the N- or C-terminus. HEK293T stable cell lines were established expressing these RIG-I insertion proteins. Purified RIG-I(N232TEV)-Flag or Flag-RIG-I(N232TEV) from virus infected cells were able to activate IRF3 pathway in vitro (Figure 3.6B), indicating the TEV cleavage site insertion did not disrupt the normal function of RIG-I. To generate RIG-I N-terminal fragment in vitro (Figure 3.6C), RIG-I(N232TEV)-Flag was purified from SeV infected or uninfected cells with M2-agarose beads (Flag-antibody-conjugated agarose beads). After on-beads cleavage with TEV protease, N-terminal fragments of RIG-I were collected as flow through (TEV-FT). RIG-I N-terminal fragments from SeV infected cells could activate IRF3 in the in vitro reconstitution assay, however, forced cleavage of RIG-I in vitro without virus infection was not sufficient to activate RIG-I N-terminus (Figure 3.6C, right panel). To generate RIG-I N-terminal fragment in vivo (Figure 3.6D), Flag-RIG-I(N232TEV) was purified

from SeV infected or uninfected cells overexpressing TEV protease. N-terminal fragments of RIG-I (and uncleaved full length RIG-I) were then purified with M2 beads. RIG-I N-terminal fragments from SeV infected cells could activate IRF3 in the in vitro reconstitution assay, however, forced cleavage of RIG-I in vivo without virus infection was not sufficient to activate RIG-I N-terminus (Figure 3.6C, right panel). In both experiments in Figure 3.6C & D, RIG-I N-termini from uninfected cells did not associate with ubiquitin, unlike RIG-I N-termini from infected cells, again suggesting ubiquitin was involved in RIG-I activation.

Acute proteasome inhibitor treatment can deplete the cellular free ubiquitin reservoir, and affect certain ubiquitin-mediated cellular processes[334, 335]. To test whether proteasome inhibition could block RIG-I cleavage event, cells were treated with proteasome hinibitor MG-132, and then infected with SeV or mock treated. RIG-I purified from MG-132 treated cells lost the ability to activate the IRF3 pathway in vitro. Interestingly, MG-132 treatment also blocked RIG-I cleavage as well as its association with ubiquitin (Figure 3.6E). However, MG-132 treatment was not a specific inhibitor of the RIG-I cleavage event, and the nature and significance of the cleavage event were unclear. So I could not establish any casual relationship between RIG-I cleavage event and RIG-I activation. In the following work, I followed another lead and focused on how ubiquitin was involved in RIG-I activation.

III.5. Summary

The mitochondria antiviral signaling protein MAVS mediates type I IFN production in response to virus infection. I established an in vitro reconstitution assay system to mimic the activation of MAVS downstream pathway by a cytosolic activator upon virus infection. Purification of this cytosolic MAVS activator" activity revealed that it was tightly associated with a small portion of total RIG-I molecules in the cytosol, while the majority of RIG-I molecules did not associate with the activity. Activated RIG-I associated with ubiquitin and immunostimulatory RNA. Nucleic acids associated with activated RIG-I were not required for the "MAVS activator" activity in the in vitro assay system, suggesting that immunostimulatory RNA was dispensable or protected after RIG-I was activated. Thus, the cytosolic "MAVS activator" was likely an active form of RIG-I, and ubiquitin was associated with this active form of RIG-I.

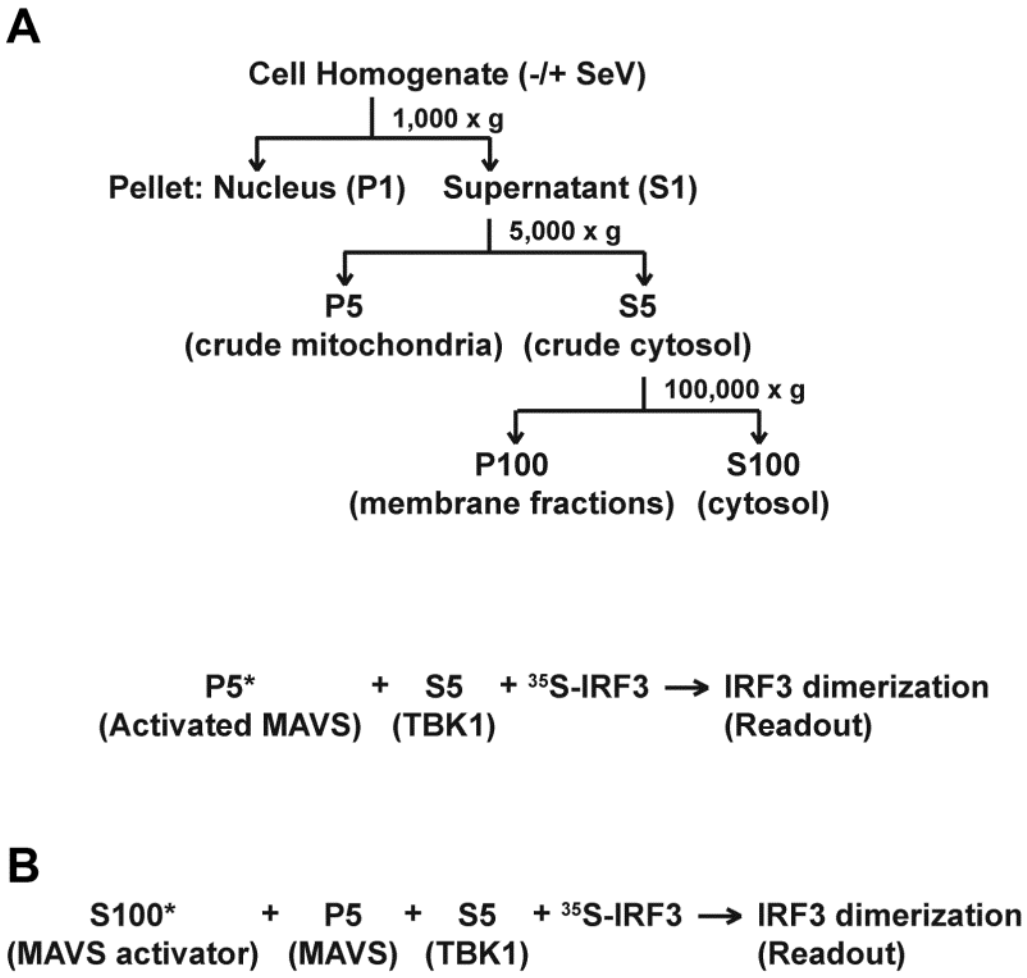

Figure 3.1. Schematic illustrations of an in vitro reconstitution system that recapitulates MAVS-mediated antiviral signaling pathways.

(A) Procedures for the isolation of crude mitochondria (P5) and cytosol (S5) by differential centrifugation, and the reconstitution of IRF3 activation by activated MAVS.

(B) Reconstitution of the MAVS-IRF3 pathway activation by a cytosolic MAVS activator.

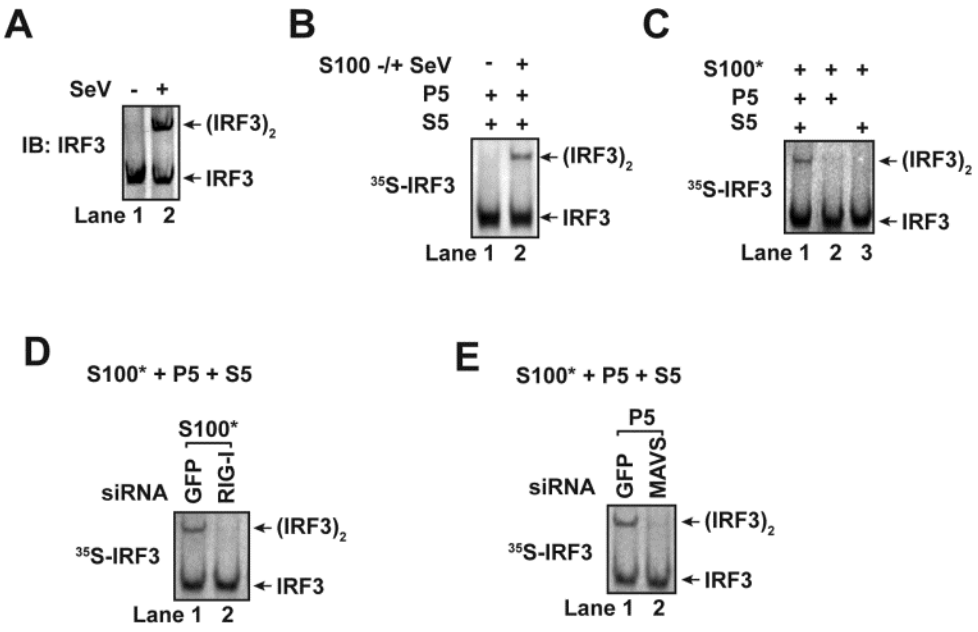

Figure 3.2. Establishment of an in vitro assay for the MAVS-IRF3 pathway activation by a cytosolic MAVS activator.

(A) Viral activation of IRF3 in vivo. Cysotolic extracts from mock treated or SeV infected HEK293T cells were analyzed with native PAGE followed by immunoblot (IB) for IRF3.

(B) Activation of MAVS-IRF3 pathway by a cytosolic MAVS activator in S100*. Cytosolic extracts (S100) from mock treated or SeV infected HEK293T cells was incubated with mitochondria fractions (P5) and cytosolic extracts (S5) from uninfected cells in the presence of ATP together with ^{35}S-IRF3. Dimerization of IRF3 was analyzed by native PAGE, followed by autoradiography.

(C) The cytosolic MAVS activator in S100* requires both mitochondria and cytosolic components to activate IRF3.

(D and E) RIG-I and MAVS are required for the activation of IRF3 in the reconstitution system. HEK293T cells were transfected with siRNA against GFP, RIG-I (D), or MAVS (E) and then infected with SeV (D), or left untreated (E). S100* or P5 from cells of indicated treatment were incubated with other components of the reconstitution system. Dimerization of IRF3 was analyzed by native PAGE, followed by autoradiography.

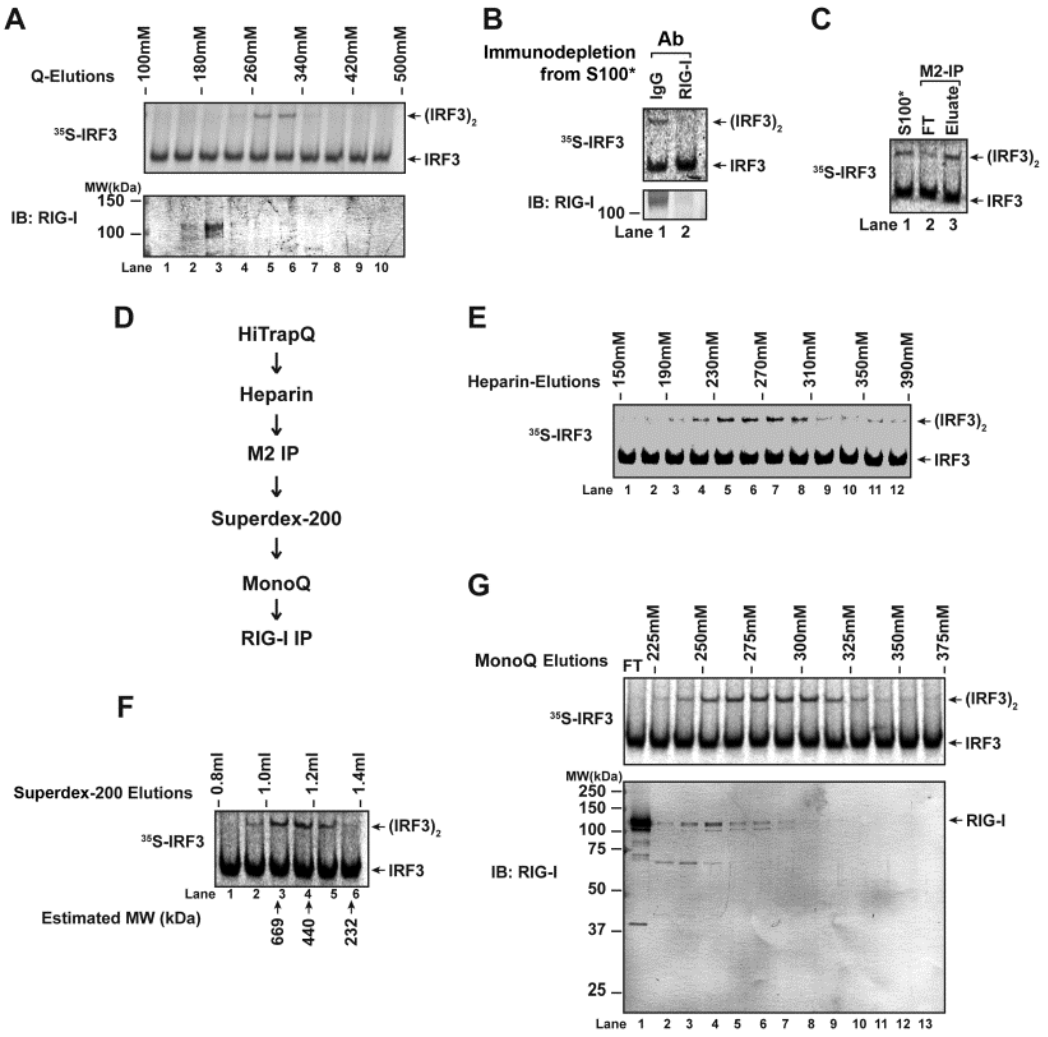

Figure 3.3. Purification of the cytosolic MAVS activator in S100*.

(A) Elution profiles of the MAVS activator activity in S100* and RIG-I on HiTrap Q ion exchange column. S100* was fractionated on HiTrap Q column, each indicated fraction was assayed for their ability to activate the MAVS-IRF3 pathway in vitro (top), as well as RIG-I immunoblot (bottom).

(B) Immunodepletion of the MAVS activator activity from S100* by RIG-I antibody. S100* was immunodepleted with rabbit IgG or RIG-I antibody, and the immunodepleted extracts were used to activate the MAVS-IRF3 pathway in vitro. Bottom panel shows the efficiency of RIG-I depletion.

(C) The MAVS activator activity in S100* can be pulled down by affinity purified RIG-I. S100* was prepared from HEK293T cells stably expressing RIG-I-Flag. RIG-I was immunoprecipitated (IP) with M2-agarose (Flag antibody conjugated agarose beads) and eluted with Flag peptide. Flow through (FT) and eluate of the pull down experiment were assayed for their ability to activate the MAVS-IRF3 pathway in vitro.

(D) Scheme of purification strategy for the MAVS activator in S100*.

(E-G) Elution profiles of the MAVS activator activity in S100* and RIG-I on Heparin column, Superdex-200 gel filtration column and MonoQ column.

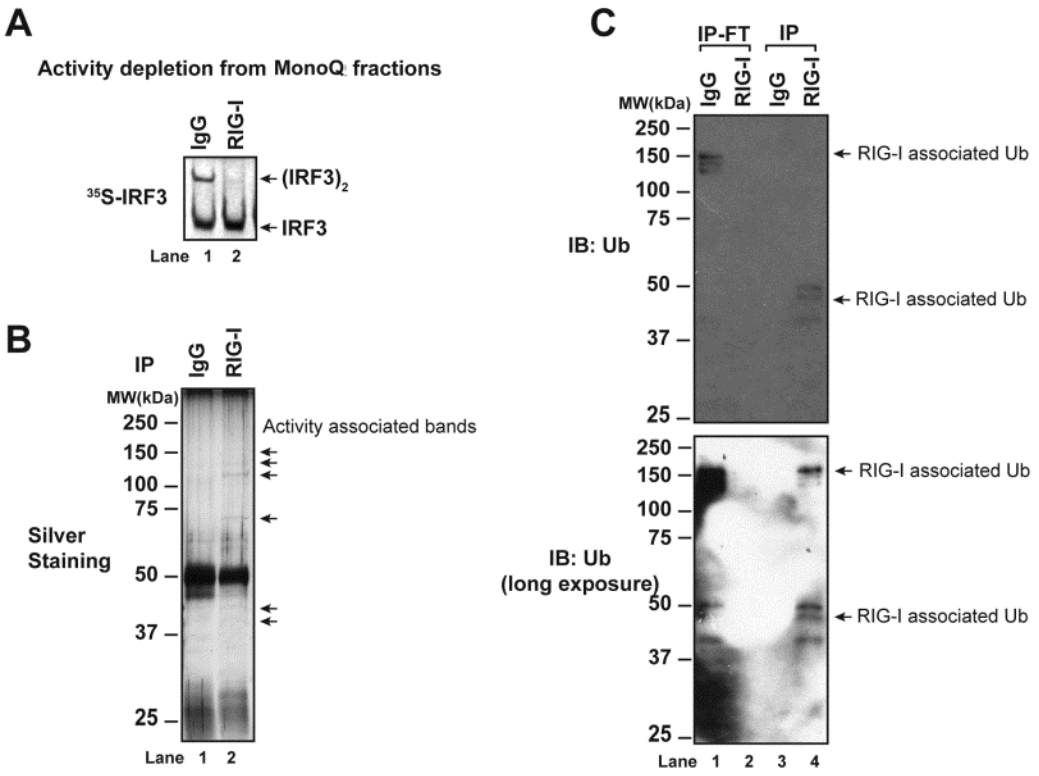

Figure 3.4. Ubiquitin and RIG-I correlate with the purified MAVS activator.

(A) Immunodepletion of the "MAVS activator" activity from MonoQ fractions.

(B) Silver staining of proteins bound to beads after IgG or RIG-I immunoprecipitation from MonoQ fractions. Arrows indicates gel bands cut out and analyzed with mass spectrometry identification.

(C) Ubiquitin immunoblot showing that RIG-I associated ubiquitin correlates with the "MAVS activator" activity.

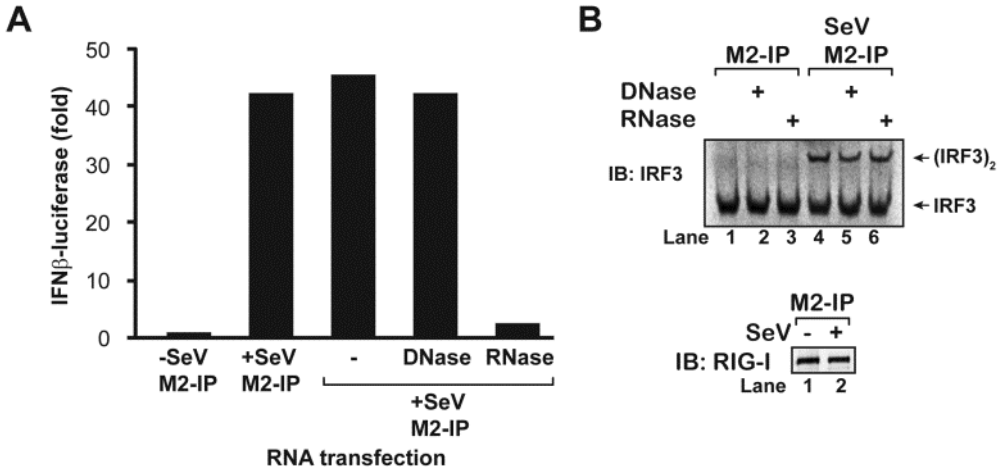

Figure 3.5. RNA associated with activated RIG-I is dispensable for the "MAVS activator" activity.

(A) RNA species were extracted from RIG-I pulled-down by M2-beads from SeV infected HEK293T cells or mock treated cells. RIG-I-associated RNA was treated with indicated nuclease, and then transfected into HEK293T cells together with IFNβ-luciferase reporter.

(B) RIG-I was purified by M2-beads pull-down from SeV infected or mock treated cells. Purified RIG-I was then treated with DNase or RNase before tested for its ability to activate the MAVS-IRF3 pathway in vitro.

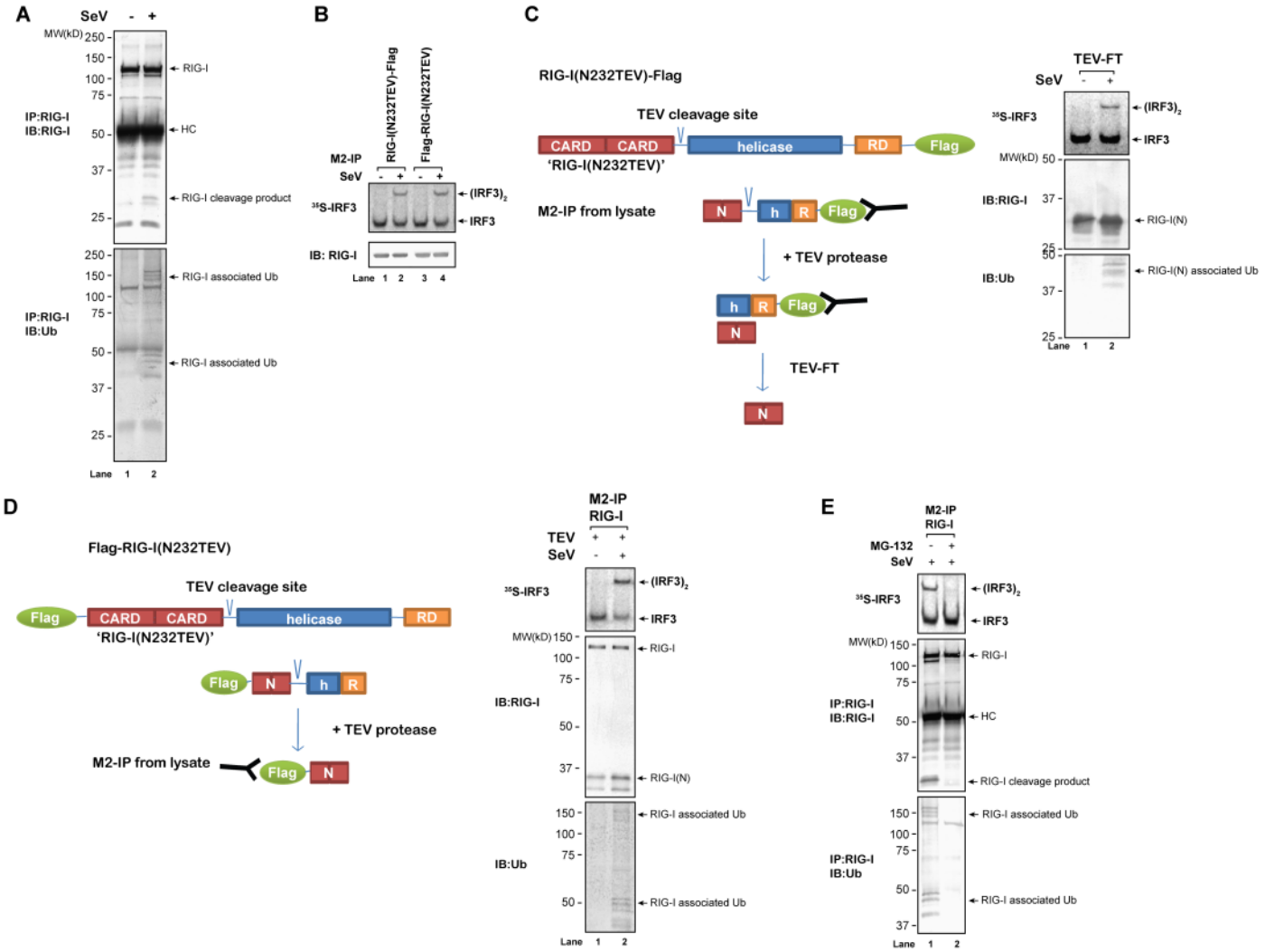
A
SeV - +
MW(kD)
250
150
100
75
50
37
25
RIG-I
HC
RIG-I cleavage product
IP:RIG-I
IB:RIG-I
RIG-I associated Ub
RIG-I associated Ub
IP:RIG-I
IB:Ub
Lane 1 2
B
RIG-I(N232TEV)-Flag
Flag-RIG-I(N232TEV)
M2-IP
SeV - + - +
35S-IRF3
(IRF3)2
IRF3
IB: RIG-I
Lane 1 2 3 4
C
RIG-I(N232TEV)-Flag
TEV cleavage site
CARD CARD helicase RD Flag
'RIG-I(N232TEV)'
M2-IP from lysate
N h R Flag
+ TEV protease
h R Flag
N
TEV-FT
N
TEV-FT
SeV - +
35S-IRF3
(IRF3)2
IRF3
MW(kD) 50
IB:RIG-I
37
RIG-I(N)
25
50
IB:Ub
37
RIG-I(N) associated Ub
25
Lane 1 2
D
Flag-RIG-I(N232TEV)
TEV cleavage site
Flag CARD CARD helicase RD
'RIG-I(N232TEV)'
Flag N h R
+ TEV protease
M2-IP from lysate
Flag N
M2-IP
RIG-I
TEV + +
SeV - +
35S-IRF3
(IRF3)2
IRF3
MW(kD) 150
RIG-I
100
75
IB:RIG-I
50
37
RIG-I(N)
150
RIG-I associated Ub
100
75
IB:Ub
50
RIG-I associated Ub
Lane 1 2
E
M2-IP
RIG-I
MG-132 - +
SeV + +
35S-IRF3
(IRF3)2
IRF3
MW(kD) 150
RIG-I
100
75
IP:RIG-I
IB:RIG-I
50
HC
37
RIG-I cleavage product
150
RIG-I associated Ub
100
75
IP:RIG-I
IB:Ub
50
RIG-I associated Ub
37
Lane 1 2

Figure 3.6. RIG-I cleavage product associates with activated RIG-I.

(A) RIG-I was immunoprecipitated from SeV infected or mock treated HEK293T cells. Immunoblots with both RIG-I and ubiquitin antibodies can detect bands around 40-50 kDa in SeV infected samples.

(B) TEV cleavage sites were inserted into RIG-I cDNA expression plasmids. These RIG-I insertion proteins were expressed in HEK293T cells. Purified RIG-I with inserted TEV cleavage sites were tested in the reconstitution system with P5 and S5, and IRF3 dimerization was analyzed.

(C and D) Forced cleavage in vitro (C) or in vivo (D) is not sufficient to activate RIG-I without virus infection. (C) Indicated RIG-I insertion protein was expressed and immunoprecipitated from SeV infected or mock treated HEK293T cells. After treatment with TEV protease on beads, cleaved N-terminal fractions were collected as flow through (TEV-FT), which were tested for their ability to activate IRF3 in vitro. (D) Indicated RIG-I insertion protein was co-expressed with TEV protease in HEK293T cells, which were then infected with SeV or mock treated. Flag-tagged RIG-I fragments were purified and tested for their ability to activate IRF3 in vitro.

(E) MG-132 treatment blocks virus infection induced RIG-I cleavage event. HEK293T cells expressing Flag-tagged RIG-I were treated with MG-132 for 1 hr, before SeV infection or mock treated for 12 hr. RIG-I was purified from these cells, and used for in vitro IRF3 dimerization assay, as well as immunoblot for RIG-I and ubiquitin.

CHAPTER IV

ROLE OF UBIQUITIN IN RIG-I ACTIVATION

IV.1. RIG-I Activation by Ubiquitination

Around the same time when I found ubiquitin was associated with active RIG-I, evidences from others suggested that ubiquitination of RIG-I CARD domains was important for the RIG-I-MAVS-IRF3 antiviral pathway. Gack et al. found by multi-dimensional liquid chromatography coupled with tandem mass spectrometry (LC/LC-MS/MS) that RIG-I N-terminus (RIG-I(N)) expressed and purified from HEK293T cells was modified by ubiquitination at several lysine residues, primarily with K63 linkage[73]. Mutation of lysine residue 172 to arginine (K172R) caused near-complete loss of ubiquitination. Concomitantly, K172R RIG-I(N) also had greatly reduced ability to induce IFNβ promoter activity when over-expressed in mammalian cells, whereas K172only RIG-I(N) (a multi-point mutant with five lysine to arginine mutations but not K172) was able to induce IFNβ promoter activity. RING-finger E3 ubiquitin ligase Trim25 was found to be associated with RIG-I(N), and could ubiquitinate RIG-I(N). In Trim25 knockout (KO) MEF cells, RIG-I mediated IFNβ expression was decreased compared to wild type (WT) cells.

To further characterize the role of ubiquitin in RIG-I activation, my project then focused on the biochemical characterization of the effect of ubiquitin on RIG-I. First, I

wanted to test the effect of in vitro ubiquitination reaction on RIG-I activity. To simplify the search, I started out by testing RIG-I(N) encompassing the tandem CARD domains, which are the signaling domains. GST-RIG-I(N), encoding GST tagged RIG-I amino acids 2-200, was expressed and purified from *E. coli*, which do not contain any ubiquitin genes (Figure 4.1A). GST-RIG-I(N) was mixed with ubiquitination reaction components, including recombinant E1, E2 (Ubc13/UeV1a complex), E3 (Trim25), and ubiquitin in the presence of Mg and ATP. An aliquot of this reaction was then tested in the in vitro reconstitution system containing P5 and S100 as described before, in place of S100* (Figure 4.1B), and IRF3 dimerization is monitored. Indeed, this reaction mixture was able to activate the MAVS-IRF3 pathway (Figure 4.1B, bottom panel).

IV.2. Direct Ubiquitin Fusion Does Not Activate RIG-I

One immediate possible explanation for the activity of RIG-I(N) after incubation with ubiquitination reaction is that ubiquitinated RIG-I(N) is the active form of RIG-I(N). Ubiquitination as a post-translational modification can modify protein function by providing docking sites for interaction partners. In some cases of ubiquitinated proteins, it was shown that simply appending ubiquitin molecules to target protein by N- or C-terminal fusion can mimic ubiquitinated protein function[289, 336-338]. To test whether ubiquitin fusion can enhance RIG-I(N) activity, I made several fusion constructs where one copy or three copies (in tandem) of ubiquitin cDNA were fused to either N- or C-terminus of RIG-I(N). These fusion proteins were expressed in *E. coli* and purified

(Figure 4.2A). RIG-I(N)-Ub, Ub-RIG-I(N), RIG-I(N)-triUb, and triUb-RIG-I(N) were able to be activated after incubation in the ubiquitination reaction, but none could activate IRF3 in vitro by itself, indicating that fusion of ubiquitin to RIG-I(N) was not sufficient to activate RIG-I(N) (Figure 4.2B). Mammalian expression constructs were made for ubiquitin fusion to RIG-I full length protein. RIG-I-Ub fusion proteins were expressed in HEK293T cells, and cells were mock treated or infected with SeV. Purified RIG-I, RIG-I-Ub, or Ub-RIG-I from SeV infected cells could activate IRF3 pathway in vitro, indicating ubiquitin fusion did not disrupt normal function of RIG-I full length protein. However, ubiquitin fusion RIG-I did not acquire constitutive activity to activate the IRF3 pathway without virus infection.

IV.3. K63 Polyubiquitin Binding Activates RIG-I CARD Domains In Vitro

I noticed, when His-MBP-RIG-I(N) was subjected to gel filtration column after it had been incubated in the ubiquitination reaction, the active fractions eluted in high molecular weight (HMW) fractions, while the majority of the protein were distributed in low molecular weight fractions (Figure 4.3). Western blot of RIG-I(N) protein did not detect any ubiquitination of RIG-I(N), indicating the majority of RIG-I(N) was not ubiquitinated. These results suggested that although the ubiquitination reaction promotes the activation of RIG-I(N), the mechanism through which ubiquitination functions might be something other than attaching polyubiquitination to RIG-I(N). One possible mechanism is that

RIG-I(N) binds to polyubiquitin and forms high molecular weight oligomers that are active.

To uncouple RIG-I(N) activation from ubiquitination reaction, the ubiquitination reaction step of the in vitro assay in Figure 4.1B was modified into two steps (Figure 4.4A, left panel). First, ubiquitination reaction was carried out with E1, E2, E3 enzymes, and Ub in the absence of RIG-I(N). Then the reaction was stopped by N-ethylmelanide (NEM), an irreversible thio-modifying agent that can react with the active sites cystein residues of ubiquitination enzymes. Ubiquitin itself does not contain any cysteins, therefore evading NEM modification. Next, this pre-synthesized polyubiquitin was incubated with RIG-I(N) at 4ºC for 30 min, and then the mixture was added to the in vitro reconstitution assay with P5 and S5. Interestingly, pre-synthesized polyubiquitin could activate RIG-I(N) (Figure 4.4A, right panel).

The fact that pre-synthesized polyubiquitin could activate RIG-I(N) led to two immediate questions. First, the ubiquitination reaction employed here was catalyzed by Ubc13/Uev1A E2 complex which was known to have specificity in making K63-linked ubiquitin chains. Does RIG-I(N) activation require K63-linkage specifically? Second, the fact that no ubiquitination reaction was required for polyubiquitin to activate RIG-I(N), and the fact that the active fractions of RIG-I(N) after being incubated with the ubiquitination reaction eluted in HMW fractions on a gel filtration column, led to the question whether RIG-I(N) could bind to polyubiquitin.

K63-linkage was known to play a role in signal transduction. To examine whether K63-linked polyubiquitin is important for RIG-I(N) activation, first I used lysine

63 to arginine mutant ubiquitin (K63R) and UbcH5 (also called Ubc5) as E2 in the ubiquitination reaction to prepare polyubiquitin, which was expected to contain polyubiquitin of mixed types of linkages but not K63-linkage. K63-linkage was found to be required for RIG-I(N) activation (Figure 4.4B). Next, using various Ub mutants that contain only one lysine to make polyubiquitin chains, I found that only WT and K63-only Ub could support RIG-I(N) activation (Figure 4.4C). Using presynthesized short ubiquitin chains of various lengths, it was found that short K63-ubiquitin chains containing more than two Ub, could activate RIG-I(N) in vitro efficiently (Figure 4.4D). Interestingly, Ub4 containing the K48-K63-K48 mixed linkage weakly stimulated GST-RIG-I(N), whereas Ub4 containing the K63-K48-K63 linkage was inactive, hinting that the K63 linkage in the center of Ub4 may be important (lanes 14-15).

To test if RIG-I(N) binds polyubiquitin, GST pull down experiments were carried out with GST-tagged RIG-I(N) recombinant protein and K63-linked short ubiquitin chains of different linkages. Indeed, RIG-I(N) was able to pull down K63-linked Ub3 but not K48-linked or linear-Ub3 (Figure 4.5).

IV.4. Polyubiquitin Binding is Essential for RIG-I to Activate IRF3 and Induce IFNβ

To delineate the regions in RIG-I(N) that are important for ubiquitin binding and IRF3 activation, I generated a series of deletion mutants of RIG-I(N). These mutants were expressed in *E. coli* as GST fusion proteins and affinity purified. The purified proteins

were tested for their binding to K63 polyubiquitin chains and their ability to activate IRF3 in the cell-free system. Both tandem CARD domains of RIG-I(N) are required for polyubiquitin binding, as well as its ability to activate IRF3 pathway in vitro (Figure 4.6).

To narrow down the functional boundaries of RIG-I(N), I generated progressive deletion mutants of RIG-I(N) with a few amino acids deleted from the N-terminus of the first CARD domain or the C-terminus of the second CARD domain, and tested their ability to bind polyubiquitin as well as their ability to activate IRF3 pathway in vitro (Figure 4.7). Overall, there was a good correlation between RIG-I(N) deletion mutants' ability to bind ubiquitin chains and their ability to activate IRF3. In particular, a RIG-I fragment containing residues 6-188 was capable of binding to K63 polyubiquitin chains and activating IRF3, and further removal of 2 amino acids from the C-terminus of the second CARD domain (6-186) abolished both activities. The truncation of the first 7 amino acids (8-190) also severely impaired RIG-I's activities.

Since MDA5 CARD domains were also found to bind polyubiquitin (described in more detail in the next chapter), I next identified several conserved residues in the CARD domains of RIG-I and MDA5 and across several vertebrate species, to further define the relationship between ubiquitin binding and IRF3 activation by RIG-I and MDA5. Sequence alignment of the CARD domains of RIG-I from human, mouse and zebrafish, as well as those of human and mouse MDA5, revealed several highly conserved residues (Figure 4.8A). These residues were mutated (highlighted by asterisks) and GST fusion proteins containing these mutations were expressed in *E. coli* and affinity purified. Results for MDA5 are described in detail in Chapter V. For RIG-I, strikingly,

among ten point mutants of RIG-I(N) tested, eight mutations (L58A, G68/W69A, D93A, L131A, K164A, W167A, P112A and E135A) abolished RIG-I(N)'s binding to K63 polyubiquitin chains as well as its ability to activate IRF3 in vitro (Figure 4.8B). One mutation, K164R, led to reduced ubiquitin chain binding as well as weakened IRF3 activation (Figure 4.8B, lane 8 on the left panel). Interestingly, another mutant, D122A, bound normally to ubiquitin chains but had reduced ability to activate IRF3 (Figure 4.8B, lanes 10-12 on the right panel). This result suggests that after RIG-I binds to K63 polyubiquitin chains, the D122A mutation impairs its ability to activate the downstream signaling cascade, possibly by affecting the interaction between RIG-I and MAVS. MAVS aggregates formation is a hallmark of MAVS activation[85]. When RIG-I(N) activated by polyUb was incubated with crude mitochondria (P5 fractions), MAVS aggregates were observed (Figure 4.9). RIG-I(N) mutants that could not be activated as probed by the in vitro IRF3 activation assay also failed to induce MAVS aggregates formation.

Overexpression of GST-RIG-I(N) in HEK293T cells led to a strong induction of IFNβ-luciferase reporter (Figure 4.8C). Importantly, all of the ubiquitin-binding defective mutants of RIG-I failed to induce IFNβ in this assay. These mutants also failed to pull down endogenous polyubiquitin chains from cells (Figure 4.8D). Similar to the in vitro experiments, RIG-I(N)-D122A bound to endogenous ubiquitin chains but its ability to induce IFNβ was reduced, suggesting a defect at a step downstream of ubiquitin binding (Figures 4.8C & D, left). Three mutants, K146R, E165A and N166A, which bound to polyubiquitin chains normally, were also capable of inducing IFNβ (Figure 4.8C & D,

right). Apparently, these mutants were also modified by ubiquitin chains. In general, there was a good correlation between RIG-I ubiquitination and IFNβ induction. However, our lab previously showed that the removal of ubiquitin chains from RIG-I by a deubiquitination enzyme (viral OTU) did not impair the ability of RIG-I to activate IRF3 [339]. Taken together, these results demonstrate that the binding to K63 polyubiquitin chains is essential for RIG-I to activate IRF3 and induce IFNβ.

IV.5. RIG-I Associated Polyubiquitin Chains Isolated from Human Cells Are Potent Activators of RIG-I

Overexpression of RIG-I(N) can pull down ubiquitin from cells as detected by ubiquitin western. These ubiquitin chains could associate with RIG-I through both covalent and non-covalent interactions. To test whether RIG-I(N) could pull down non-covalently bound ubiquitin, I tried to isolate and characterize RIG-I(N) bound ubiquitin. However, endogenous ubiquitin chains isolated from cells are rather labile, because there are many deubiquitination enzymes (DUBs) in cell lysates, making in vitro characterization of these ubiquitin chains challenging. Interestingly, we found that RIG-I(N) can protect in vitro synthesized polyubiquitin chains from the treatment of two DUBs (Figure 4.10A, compare lanes 6 and 9 to lanes 13 and 14; Figure 4.10B), isopeptidase T (IsoT) and viral OUT (vOTU). IsoT specifically cleaves free polyUb chains[340], while vOTU can cleave polyUb chains from target proteins as well as free ubiquitin chains[148, 341]. Therefore we hypothesized that RIG-I might also protect endogenous polyUb. We devised a protocol to

isolate the RIG-I-bound ubiquitin chains from HEK293T cells by employing two strategies (Figure 4.11A). First, cells were lysed in the presence of NEM to inactivate most of the deubiquitination enzymes. Ubiquitin contains no cysteine, therefore evading modification by NEM. Second, as ubiquitin is known to be relatively stable at high temperatures, RIG-I(N):polyUb complex were heated at 75°C which could denature RIG-I(N) but preserve the structure and function of ubiquitin chains. Following centrifugation that precipitated denatured protein aggregates, the supernatant was expected to contain polyUb chains and could be tested for its ability to activate IRF3 in the presence of fresh RIG-I(N). Indeed, the supernatant containing polyUb chains released from the RIG-I(N) complex at 75°C were capable of activating IRF3 when supplied with fresh GST-RIG-I(N) (Figure 4.11B, lane 2).

To determine whether the supernatant of the heated GST-RIG-I(N) complex contained unanchored polyUb chains and whether these chains were responsible for activating the RIG-I pathway, the endogenous ubiquitin chains were incubated with IsoT and then their activity in the IRF3 dimerization assay were measured. Importantly, the IsoT treatment completely abolished the ability of the supernatant to activate IRF3 in the presence of GST-RIG-I(N) (lane 3). However, if the order of incubation with GST-RIG-I(N) and IsoT was reversed, the activity was protected (lane 4). To determine if the endogenous unanchored polyUb chains are linked through K63 of ubiquitin, the heat-resistant supernatant was treated with the K63-specific deubiquitination enzyme CYLD. This treatment markedly diminished the ability of the supernatant to activate RIG-I (lane 5); pre-incubation with GST-RIG-I(N) also protected the activity from CYLD treatment

(lane 6). Parallel control experiments showed that unanchored K63-polyUb chains were sensitive to IsoT and CYLD treatment but became resistant after preincubation with GST-RIG-I(N) (lanes 7-12).

IV.6. Ubiquitin Binding Rescues RIG-I CARD Domain Mutants

Previous studies showed that K172R mutation of RIG-I impairs its ubiquitination and IFNβ induction[73]. However, we found that this mutation also abrogates the binding of RIG-I to polyubiquitin chains. To determine whether ubiquitin binding or ubiquitination of RIG-I is important for its signaling functions, I fused RIG-I CARD domain mutants to the novel zinc finger (NZF) domain of NPL4[342], which is known to bind polyubiquitin chains (Figure 4.12A). Remarkably, the NZF domain rescued the ability of RIG-I(N)-K172R to activate IRF3 in vitro in the presence of K63, but not K48, polyubiquitin chains (Figure 4.12B, lane 7). The activity of a RIG-I(N) mutant containing six-lysine mutations (K99, 169, 172, 181, 190 & 193; termed 6KR) was also restored by NZF fusion (Figure 4.12B, lane 5). In contrast, a RIG-I(N) mutant containing 14-lysine mutations (14KR) was inactive even after NZF fusion, indicating that mutations of some of the lysines affect RIG-I structure or functions (Figure 4.12C). This experiment also ruled out the remote possibility that the NZF domain alone could activate the RIG-I pathway. Interestingly, the NZF domain restored the binding of K172R and 6KR to both K63 and K48 polyubiquitin chains (Figure 4.12D & E), suggesting that even when K48 ubiquitin chains are forced to bind to RIG-I, they cannot activate the pathway.

The NZF domain also restored the ability of RIG-I(N)-K172R and 6KR to induce IFNβ-luciferase in HEK293T cells (Figure 4.13A & B, top). GST pull down from these cells revealed that RIG-I(N)-K172R-NZF and 6KR-NZF were able to pull down endogenous polyubiquitin chains, whereas their ubiquitination was much weaker than that observed for RIG-I(N)-NZF (Figure 4.13A & B, bottom). Taken together, these results provide the direct evidence that polyubiquitin binding by RIG-I is critical for its signaling functions.

IV.7. Ubiquitin-Induced Oligomerization Activates RIG-I CARD Domains

To understand how polyubiquitin binding activates RIG-I(N), I performed gel filtration analysis of RIG-I(N) following its incubation with K63 ubiquitin chains of different lengths. In these experiments, RIG-I(N) did not contain the GST tag, which could have confounded the results due to GST-mediated dimerization. Ub3, Ub4, Ub5 and Ub6, but not Ub, caused a shift of RIG-I(N) into high molecular weight (HMW) fractions (Figure 4.14A-E). Furthermore, the HMW complexes containing RIG-I(N) and ubiquitin chains were highly potent in activating IRF3 in the cell-free system. Titration experiments using the RIG-I(N)/Ub4 complex (fraction 5 in Figure 4.14B) showed that the half maximal effective concentration (EC50) of this complex was ~404 pM (Figure 4.14F; this is likely an underestimate as it does not take into account of the dissociation of the complex during the reaction).

I estimated the stoichiometry of RIG-I(N):Ub chain complex by comparing the intensity of Coomassie blue-stained bands in the complex eluted from the gel filtration column with that of RIG-I(N) and Ub chains mixed at 2:1, 1:1 and 1:2 ratios (Figure 4.15). Such estimates, although imprecise, revealed that RIG-I(N) and Ub chains had a stoichiometry of approximately 1:1 irrespective of the Ub chain lengths [ratio of RIG-I(N) to Ub3: ~0.8:0.7; to Ub4: 1.4:1.4; to Ub5: 1.2:1.1; to Ub6: 1.1: 0.9].

IV.8. Polyubiquitin Binding Promotes the Formation of RIG-I Tetramer

To more precisely measure the stoichiometry and sizes of the RIG-I:Ub chain complexes, I performed sedimentation velocity analytical ultracentrifugation (AUC) (Figure 4.16). Calculation of sedimentation coefficients and frictional ratios of RIG-I(N) and K63-Ub4 alone revealed their molar masses of 24.1 g/mol and 32.7 g/mol, respectively, consistent with their theoretical values (Figure 4.16A). In the sample where RIG-I(N) was incubated with a large molar excess of K63-Ub4, a faster-sedimenting population appeared with a molar mass of 231.6 g/mol (Figure 4.16B). Multisignal sedimentation velocity analysis [327] showed that RIG-I(N) and Ub4 in this complex had a stoichiometry of 1:1, consistent with gel filtration experiments. Thus, the molar mass and stoichiometry measurements revealed that RIG-I(N) and Ub4 likely formed a complex containing 4 molecules of RIG-I(N) and 4 molecules of Ub4. Similar analyses using K63-Ub3, -Ub5 and -Ub6 were consistent with the conclusion that RIG-I(N) formed complexes with these ubiquitin chains with a stoichiometry of approximately 4:4 irrespective of chain lengths (Figure

4.16C-E; Figure 4.17). The distribution of species during the sedimentation process showed few intermediate species, suggesting that RIG-I(N) and the Ub chains form hetero-tetrameric complexes in a highly cooperative manner.

IV.9. RNA and Polyubiquitin Induce Oligomerization and Activation of Full-length RIG-I

The model of RIG-I activation at the time was that RIG-I RD domain binds to RNA, which then triggers conformational changes that open up the CARD domains for downstream signaling, although the exact structural details were unknown. Our in vitro reconstitution system was then modified to mimic the activation of full length RIG-I by RNA and ubiquitin. Full-length RIG-I can be activated in vitro when incubated with 5'-ppp-RNA ligands and K63 polyubiquitin chains in the presence of ATP (Figure 4.18)[339].

To determine if full-length RIG-I forms oligomers after binding to K63 polyubiquitin chains, I carried out gel filtration analyses using purified RIG-I, and K63-Ub6 (Figure 4.19). RIG-I alone eluted from the column with the peak fraction corresponding to molecular weight between 75kDa and 158kDa (Figure 4.19A, top panel, lane 12; Figure 4.19D), suggesting that it is a monomer. Incubation with 5'-pppRNA (containing 135 nucleotides) caused a shift in RIG-I elution peak to fractions corresponding to ~230 kDa, which may represent a RIG-I dimer with bound RNA. Incubation with K63-Ub6 alone did not change RIG-I distribution, because polyubiquitin binding to RIG-I requires both RNA and ATP[339]. Interestingly, when incubated with

RNA, K63-Ub6 and ATP, some RIG-I shifted to HMW fractions that were larger than 400kD. A small fraction of K63-Ub6 also co-migrated with RIG-I to the HMW fractions when the mixture contained RNA and ATP (Figure 4.19B). The fractions with molecular weights larger than 600 kDa were most potent in activating IRF3 in the in vitro assay (Figure 4.19A, lanes 2-5; bottom). These HMW complexes could be composed of RIG-I tetramers with bound RNA and Ub6.

IV.10. Virus Infection Induces RIG-I Oligomerization and Activation In Vivo

To determine if RIG-I forms oligomers in cells in response to viral infection, I used a HEK293T cell line stably expressing RIG-I-Flag previously established in the lab, and purified RIG-I-Flag from these cells infected with Sendai virus or uninfected. The RIG-I protein was fractionated by gel filtration chromatography (Figure 4.20). RIG-I from uninfected cells eluted from the column with an elution profile suggestive of a monomer (top panel, lanes 11-12). While the majority of RIG-I from the virus-infected cells also eluted as a monomer that was incapable of activating IRF3, a small fraction eluted as HMW complexes that potently activated IRF3 (lanes 4-8). The heterogeneity of these active complexes may reflect RIG-I tetramers bound to heterogeneous viral RNA and ubiquitin chains in cells.

IV.11. K63 Ubiquitination and RIG-I Ubiquitin Binding Are Important for Virus-Induced RIG-I Oligomerization and Activation In Vivo

To determine whether Ub binding of RIG-I is essential for its antiviral activity in cells, I established RIG-I KO MEF cell lines reconstituted with WT RIG-I or several Ub binding point mutants. These cells were infected with SeV, and IFNβ induction was measured as an indicator for the RIG-I-MAVS-IRF3 pathway activation. WT RIG-I rescued IFNβ induction in response to SeV infection, while point mutants L58A, D93A, K164A, K164R, W167A, and 6KR could not rescue (Figure 4.21A & B). Further, to determine whether the defects of ubiquitin binding mutants were upstream of MAVS, I tested the ability of mitochondria fractions (P5) from SeV-infected cells to activate IRF3 dimerization in the in vitro reconstitution system. P5 from WT RIG-I reconstituted RIG-I KO cells could activate the IRF3 pathway, while P5 from K164A RIG-I reconstituted cells had little activity; D93A and 6KR mutants were not able to activate MAVS (Figure 4.21C). These results demonstrated that the defects of these cell lines were upstream of MAVS activation. As a control, several RIG-I mutants and WT RIG-I proteins were purified from the reconstitution cell lines, and were shown to have normal ATPase activity induced by RNA (Figure 4.22).

To determine whether ubiquitin binding is important for RIG-I oligomerization and activation, RIG-I KO cells reconstituted with WT RIG-I or Ub binding mutants were infected with SeV, and then RIG-I oligomerization status were examined in the cytosolic extracts of these cells by gel filtration analysis. Upon SeV infection, a small fraction of

WT RIG-I oligomerized into HMW fractions that were able to activate the IRF3 pathway in the in vitro reconstitution system, while K164A and 6KR did not oligomerize (Figure 4.23).

Using shRNA knockdown technology, results from our lab suggested that both Ubc5 and Ubc13 are involved in the activation of MAVS by RIG-I in response to viral infection[333]. Ubc5 is a family of E2s comprised of highly homologous isoforms (Ubc5a, b, and c; putative Ubc5d in human) that catalyze the synthesis of polyUb chains linked through various lysines of ubiquitin, including K63[324]. In contrast to Ubc5, the E2 complex consisting of Ubc13 and Uev1A is highly specific in synthesizing K63-polyUb chains[147, 343]. We obtained mice with loxP-flanked Ubc13 alleles ($Ubc13^{fl/fl}$ mice)[344]. I used $Ubc13^{fl/fl}$ primary MEF cells to examine the role of Ubc13 in RIG-I activation in vivo. In these cells, the Ubc13 gene was left intact or deleted by introducing Cre recombinase via a lentiviral vector. RIG-I was purified from SeV infected or uninfected cells, and its oligomerization and activation were examined. In WT MEF cells, upon SeV infection, RIG-I was able to activate the IRF3 pathway in vitro (Figure 4.24A). Further, a small fraction of RIG-I oligomerized into HMW fractions that were able to activate the IRF3 pathway in the in vitro reconstitution system (Figure 4.24B & C). In contrast, in Ubc13 KO MEFs, RIG-I was inactive and did not oligomerize. These results strongly suggest that K63 ubiquitination and ubiquitin-binding-induced RIG-I oligomerization are essential for RIG-I activation.

IV.12. Summary

Studies in this chapter provide insights into how ubiquitin plays a role in RIG-I activation. After incubation with ubiquitination reaction, RIG-I(N) can activate the MAVS-IRF3 pathway in vitro. Interestingly, RIG-I(N) activation does not require covalent ubiquitin conjugation on it. Instead, pre-synthesized K63 polyubiquitin chains containing more than two ubiquitin can activate RIG-I(N). RIG-I(N) binds K63 polyubiquitin, and both CARD domains of RIG-I(N) are required for polyubiquitin binding. Ubiquitin binding is important for RIG-I function. Mutations of conserved residues in RIG-I(N) that abolish ubiquitin binding also impair its ability to activate IRF3 in vitro and in vivo. Conversely, fusion of a heterologous ubiquitin binding motif to RIG-I(N) ubiquitin binding mutants can rescue their signaling activity. RIG-I(N) is able to protect polyubiquitin from DUBs, and can also pull down from inside the cell endogenous K63 polyubiquitin chains that have the ability to activate RIG-I(N) in vitro.

Biochemical characterization of the interaction between RIG-I(N) and short polyubiquitin chains have revealed interesting features of their interaction. Binding to short K63 polyubiquitin chains leads to the formation of RIG-I(N) tetramer, which is highly potent in activating MAVS and the downstream pathway. Interestingly, the stoichiometry of the RIG-I(N)/polyubiquitin complex is 4:4 irrespective of ubiquitin chain length, as long as the ubiquitin chains contain more than two ubiquitins linked through K63.

Full length RIG-I can be activated by RNA, ATP and K63 polyubiquitin chains in vitro. Remarkably, RNA and polyubiquitin induces step-wise oligomerization of full

length RIG-I, that correlates with RIG-I activation. Furthermore, virus infection leads to the formation of a HMW RIG-I complex, and only this complex, but not the lower molecular weight forms of RIG-I, is capable of activating IRF3 in the cell-free system. Mutations that disrupt ubiquitin binding (such as K164A and 6KR) abolish the ability of RIG-I to activate downstream signaling in vitro and in vivo. Importantly, RIG-I with these mutations fail to form oligomer, and therefore are not active. Ubc13, an E2 enzyme that specifically catalyzes the synthesis of K63-linke ubiquitin chains, is essential for virus infection induced RIG-I oligomerization and activation.

Based on these results, a model of RIG-I activation is proposed, in which sequential binding to viral RNA and endogenous K63 polyubiquitin chains leads to the oligomerization of RIG-I, resulting in its activation (Figure 4.25). The oligomerization of RIG-I likely promotes the formation of CARD domain clusters, which presumably interacts with the CARD domain of MAVS on the mitochondrial surface, leading to MAVS activation.

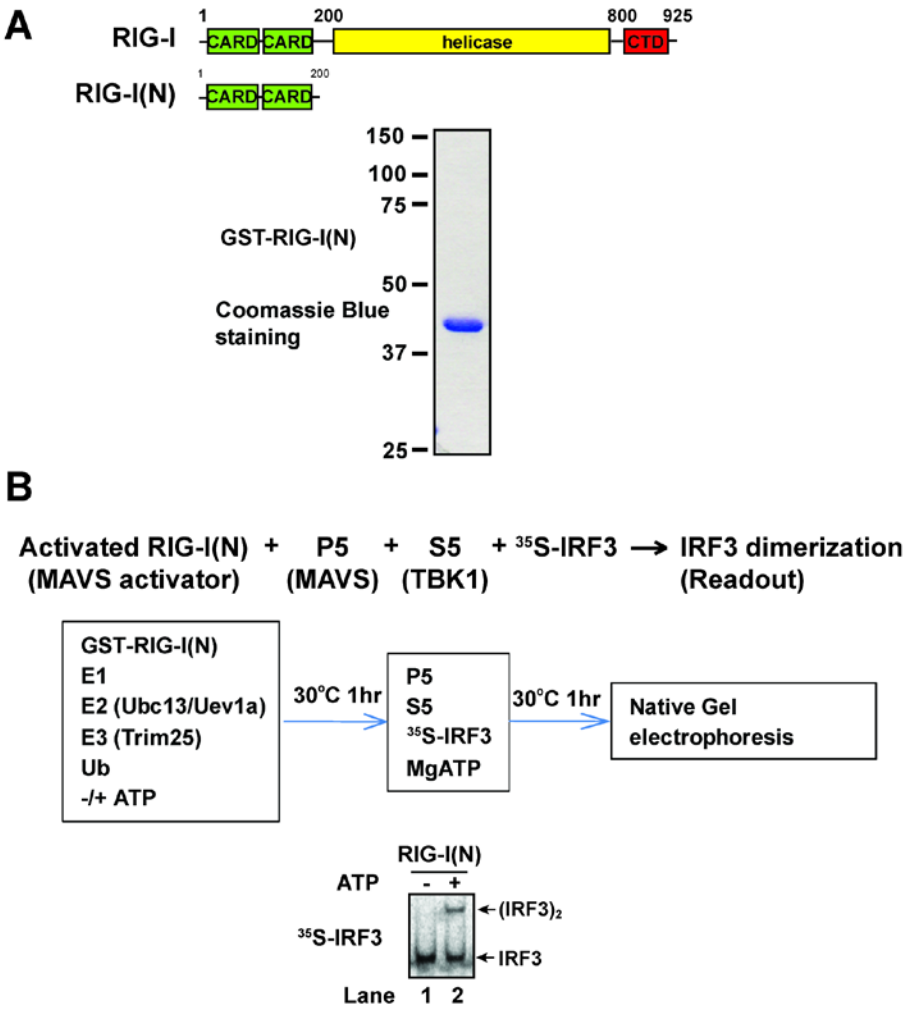

Figure 4.1. RIG-I CARD domains activates IRF3 in a cell-free system through a ubiquitination-dependent mechanism.

(A) Diagram of RIG-I protein (top); Coomassie blue stained gel of RIG-I(N) (bottom).

(B) GST-RIG-I(N) was incubated with ubiquitination components as shown in the diagram. Aliquots of the reaction mixtures were further incubated with mitochondria (P5) and cytosolic extracts (S5) together with ^{35}S-IRF3 and ATP. IRF3 dimerization was analyzed by native gel electrophoresis.

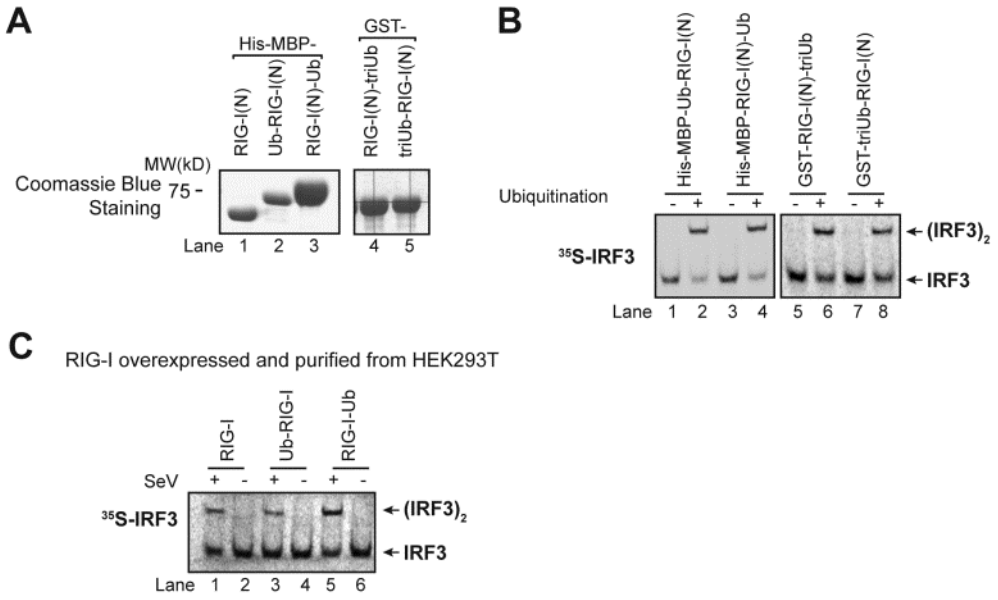

Figure 4.2. Direct fusion of ubiquitin does not activate RIG-I.

(A) Coomassie blue staining of indicated RIG-I(N) and ubiquitin fusion RIG-I(N) proteins expressed and purified from *E. coli*.

(B) Indicated RIG-I(N) and ubiquitin fusion RIG-I(N) proteins were incubated with ubiquitination reaction containing E1, Ubc13/UeV1A (E2), Trim25 (E3), and ubiquitin, in the presence or absence of Mg-ATP. Aliquots of the reactions were tested for their ability to activate IRF3 dimerization in vitro.

(C) RIG-I and ubiquitin fusion RIG-I proteins were expressed and purified from HEK293T cells that had been infected with SeV or mock treated, and their ability to activate the MAVS-IRF3 pathway was measured in the in vitro reconstitution system.

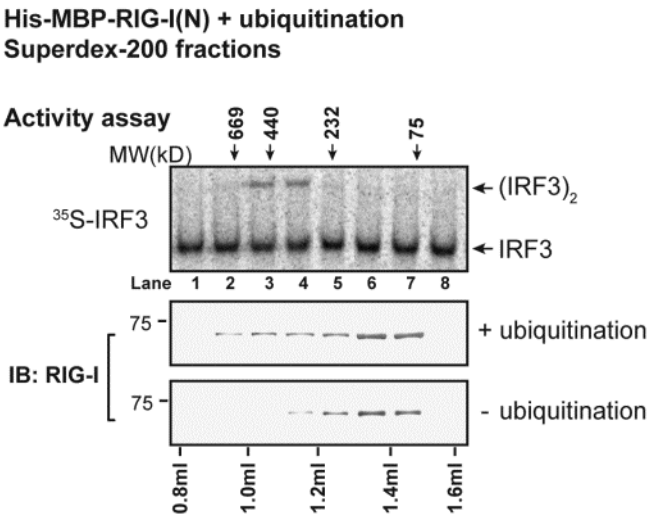

Figure 4.3. Incubation with ubiquitination reaction induces oligomerization of RIG-I CARD domains.

His-MBP-RIG-I(N) was incubated with ubiquitination reaction described in Figure 4.2B, and then subjected to Superdex-200 gel filtration column. Each fraction where analyzed for its ability to activate IRF3 in vitro, as well as RIG-I immunoblot.

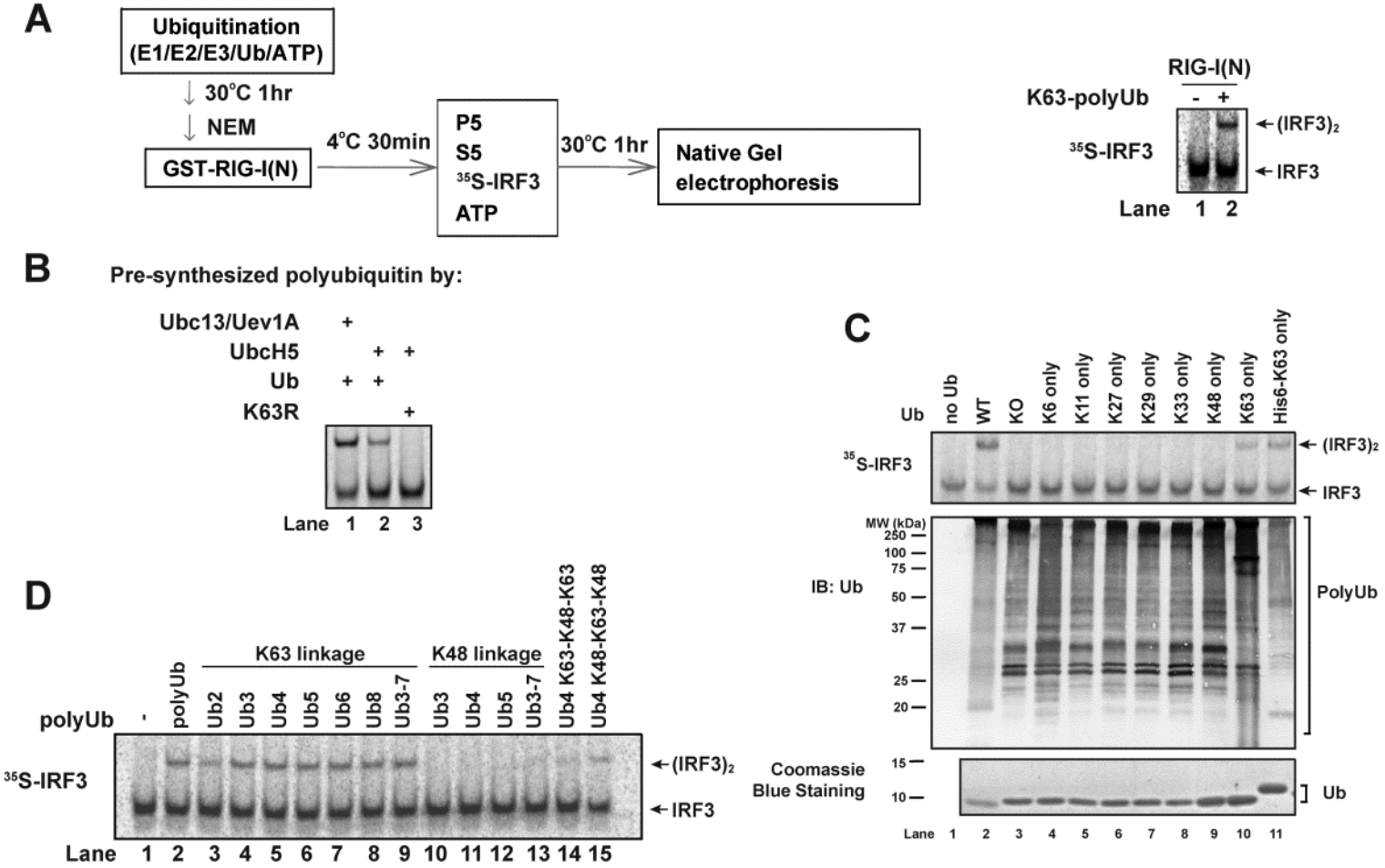
A
Ubiquitination
(E1/E2/E3/Ub/ATP)
30°C 1hr
NEM
GST-RIG-I(N)
4°C 30min
P5
S5
35S-IRF3
ATP
30°C 1hr
Native Gel
electrophoresis
RIG-I(N)
K63-polyUb
- +
35S-IRF3
(IRF3)2
IRF3
Lane 1 2
B
Pre-synthesized polyubiquitin by:
Ubc13/Uev1A +
UbcH5 + +
Ub + +
K63R +
Lane 1 2 3
C
Ub
no Ub
WT
KO
K6 only
K11 only
K27 only
K29 only
K33 only
K48 only
K63 only
His6-K63 only
35S-IRF3
(IRF3)2
IRF3
MW (kDa)
250
100
75
50
37
25
20
IB: Ub
PolyUb
15
10
Coomassie
Blue Staining
Ub
Lane 1 2 3 4 5 6 7 8 9 10 11
D
polyUb
-
polyUb
K63 linkage
Ub2
Ub3
Ub4
Ub5
Ub6
Ub8
Ub3-7
K48 linkage
Ub3
Ub4
Ub5
Ub3-7
Ub4 K63-K48-K63
Ub4 K48-K63-K48
35S-IRF3
(IRF3)2
IRF3
Lane 1 2 3 4 5 6 7 8 9 10 11 12 13 14 15

Figure 4.4. Pre-synthesized K63 polyubiquitin chains activate RIG-I CARD domains in vitro.

(A) Ubiquitination reactions was carried out as shown in the diagram with E2 (Ubc13/UeV1A), E3 (Trim25) as E2 and E3. The reaction was then inactivated by N-ethylmaleimide (NEM). An aliquot of the resulting polyubiquitin mixture was then incubated with RIG-I(N), then further incubated with mitochondria (P5) and cytosol (S5) to measure IRF3 dimerization.

(B) Polyubiquitin chains were synthesized similar to (A), except with indicated E2 enzymes, and indicated ubiquitin (WT Ub or K63R mutant ubiquitin). The synthesized polyubiquitin chains were then used to activate RIG-I(N), similar to (A).

(C) Similar to (A), except that ubiquitination reactions were carried out in the presence of Ubc5c, Trim25, and various ubiquitin mutants as indicated.

(D) Ubiquitin chains of defined lengths and linkages were incubated with RIG-I(N), and then IRF3 dimerization assay was carried out by incubating the mixtures with P5 and S5 in the presence of Mg-ATP. IRF3 dimerization was visualized by native PAGE and autoradiography.

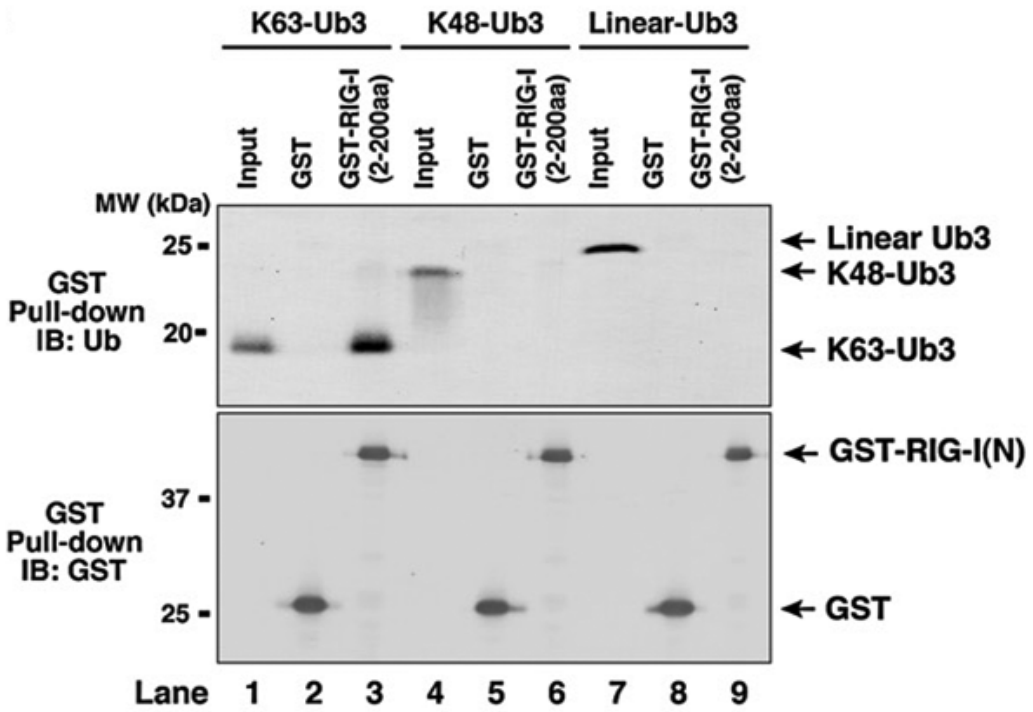

Figure 4.5. RIG-I CARD domains bind specifically to K63-linked ubiquitin chains.

GST or GST-RIG-I(N) was incubated with Ub3 containing K63, K48, or linear linkage, and then pulled down with glutathione Sepharose beads (GST Pull-down), followed by immunoblotting. Input represents 10% of Ub3 used in the pull-down experiments.

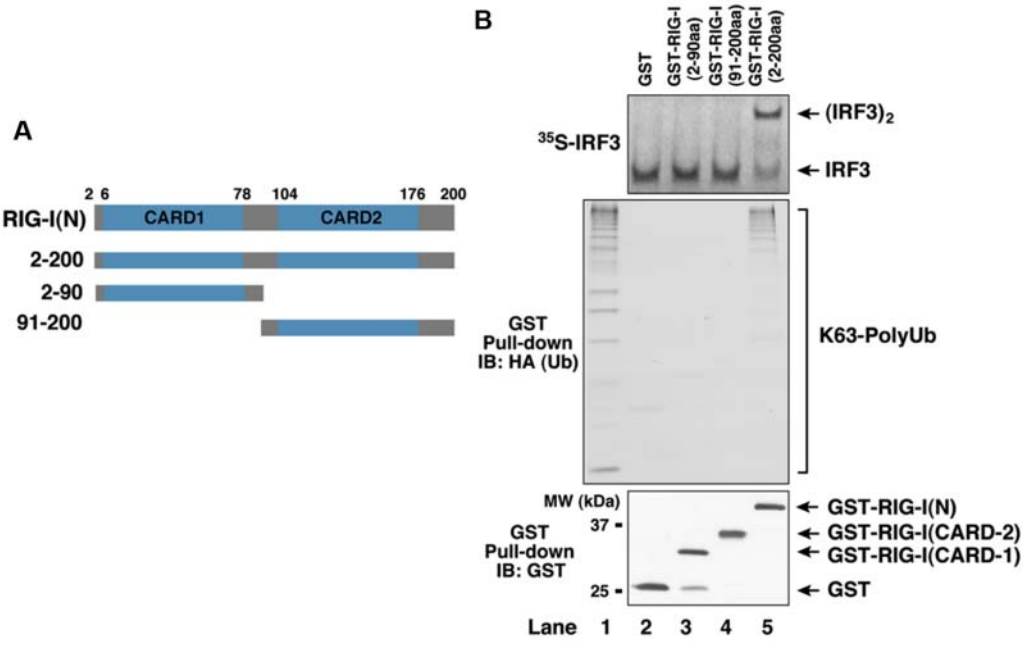

Figure 4.6. Both CARD domains of RIG-I are required for K63-polyubiquitin chain binding and IRF3 activation.

(A) Diagram of RIG-I(N) fragments containing one or two CARD domains.

(B) GST or GST-RIG-I(N) fragments were expressed and purified from *E. coli*, and incubated with presynthesized free K63 polyubiquitin chains composed of HA-Ub. The incubation mixture was used for IRF3 dimerization assay (top), and GST pull-down experiments (middle and bottom). Proteins on the beads were detected with an antibody against HA or GST. Lane 1 contained 1% of polyubiquitin chains used in the GST pull-down experiments.

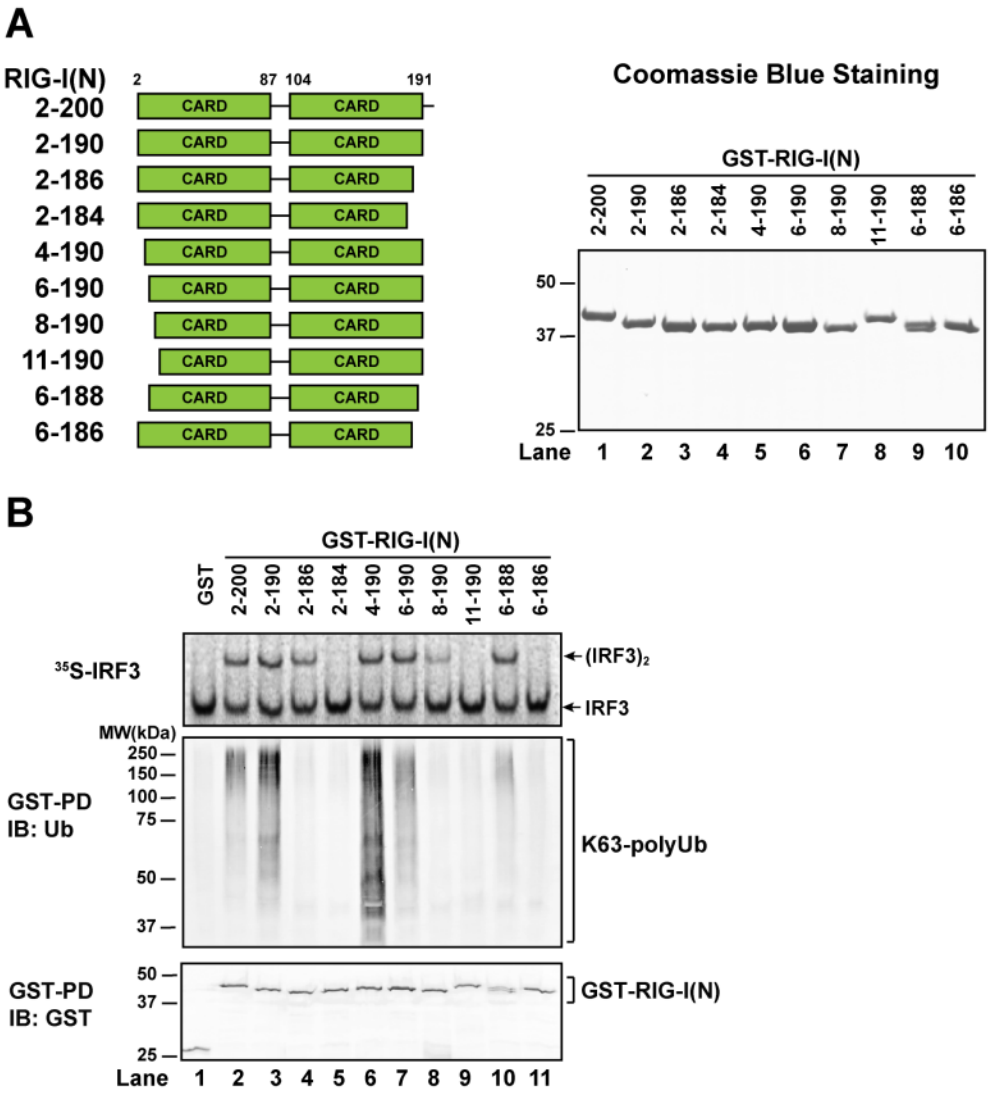

Figure 4.7. Correlation of the functional boundaries for the two activities of RIG-I CARD domains: ubiquitin binding and IRF3 activation.

(A) Diagram and Coomassie blue stained gel of RIG-I(N) fragments.

(B) Fragments of RIG-I(N) protein shown in (A) were tested for polyUb binding by GST pull-down (GST-PD) and IRF3 activation in the cell-free assay containing mitochondria and cytosolic extracts.

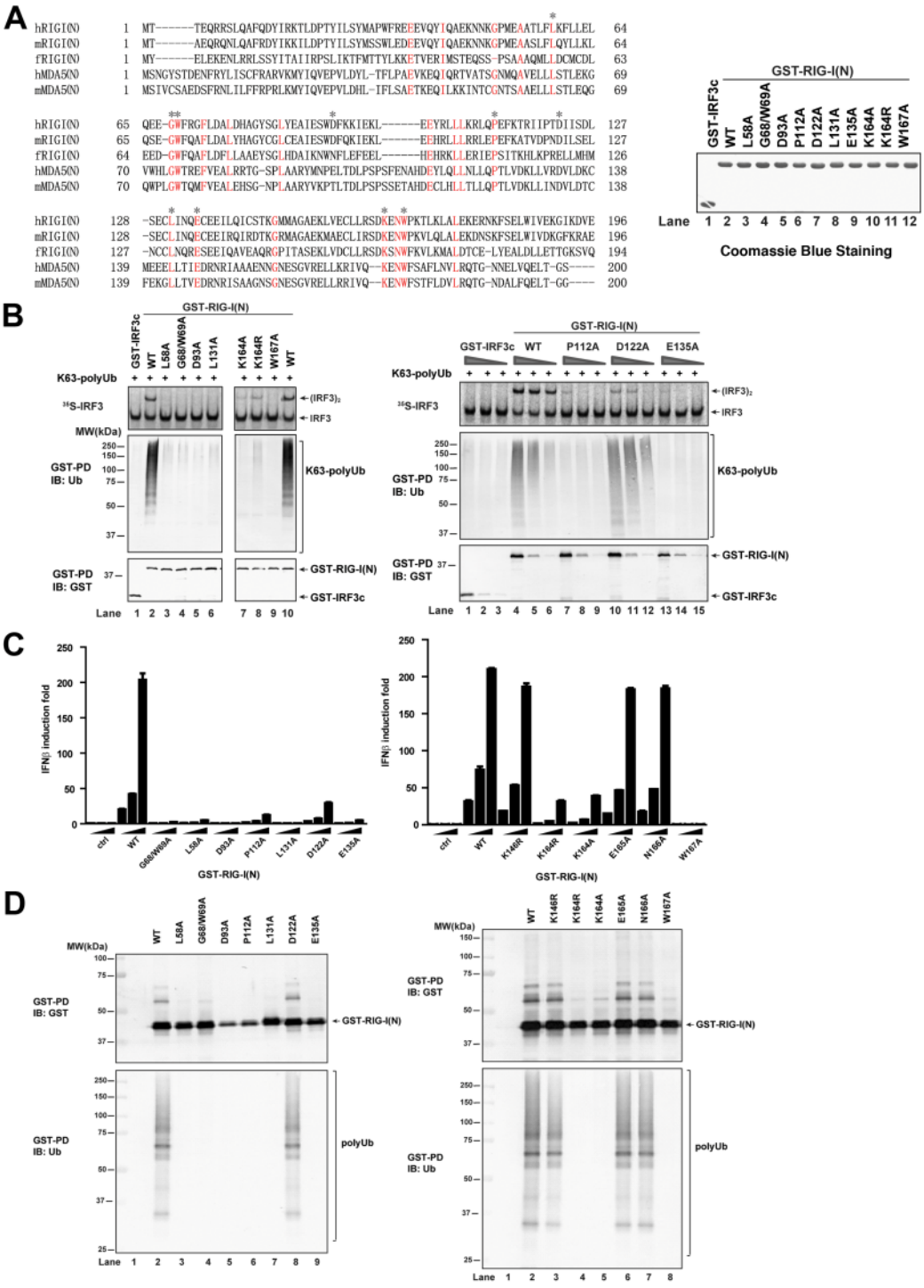
A
hRIGI(N)
mRIGI(N)
fRIGI(N)
hMDA5(N)
mMDA5(N)
GST-RIG-I(N)
GST-IRF3c
WT
L58A
G68/W69A
D93A
P112A
D122A
L131A
E135A
K164A
K164R
W167A
Lane 1 2 3 4 5 6 7 8 9 10 11 12
Coomassie Blue Staining
B
K63-polyUb
35S-IRF3
(IRF3)2
IRF3
MW(kDa)
GST-PD IB: Ub
K63-polyUb
GST-PD IB: GST
GST-RIG-I(N)
GST-IRF3c
Lane 1 2 3 4 5 6 7 8 9 10
GST-IRF3c WT P112A D122A E135A
Lane 1 2 3 4 5 6 7 8 9 10 11 12 13 14 15
C
IFNβ induction fold
ctrl
WT
G68/W69A
L58A
D93A
P112A
L131A
D122A
E135A
K148R
K164R
K164A
E165A
N166A
W167A
GST-RIG-I(N)
D
MW(kDa)
GST-PD IB: GST
GST-RIG-I(N)
GST-PD IB: Ub
polyUb
Lane 1 2 3 4 5 6 7 8 9
Lane 1 2 3 4 5 6 7 8

Figure 4.8. Ubiquitin binding is essential for RIG-I activation.

(A) Sequence alignment of the N-termini of RIG-I and MDA5 from human (h) and mouse (m) as well as zebrafish (f) RIG-I N-terminus. Asterisks indicate the residues to be mutated. Shown on the right are the GST-RIG-I(N) mutant proteins expressed and purified from *E. coli*.

(B) Point mutants of RIG-I(N) were incubated with K63 polyUb, and tested for polyUb binding by GST pull-down (GST-PD) and IRF3 activation in the cell-free assay containing mitochondria and cytosolic extracts.

(C and D) Expression vectors for GST-RIG-I(N) mutants were transfected into HEK293T cells stably expressing IFNβ-luciferase reporter. Cell lysates were assayed for luciferase activity (C) or pulled down with glutathione Sepharose followed by immunoblotting (D).

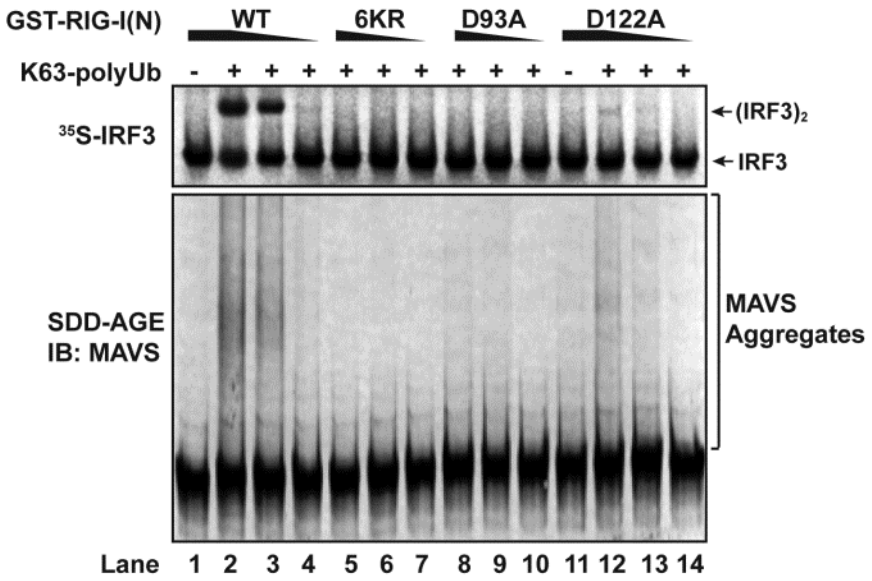

Figure 4.9. RIG-I CARD domains activated by K63 polyubiquitin induce MAVS aggregation and activation on the mitochondrial membrane.

GST-RIG-I(N) and mutants was incubated with K63 polyubiquitin chains, and then the mixtures were incubated with mitochondria from HEK293T cells. Top panel, mitochondria extracts were analyzed for its ability to activate IRF3 dimerization by incubating with S5 in the presence of Mg-ATP (like in Figure 3.1A). Bottom panel, mitochondria extracts were analyzed with semi-denaturing detergent agarose gel electrophoresis (SDD-AGE) for MAVS aggregation, a hallmark of MAVS activation.

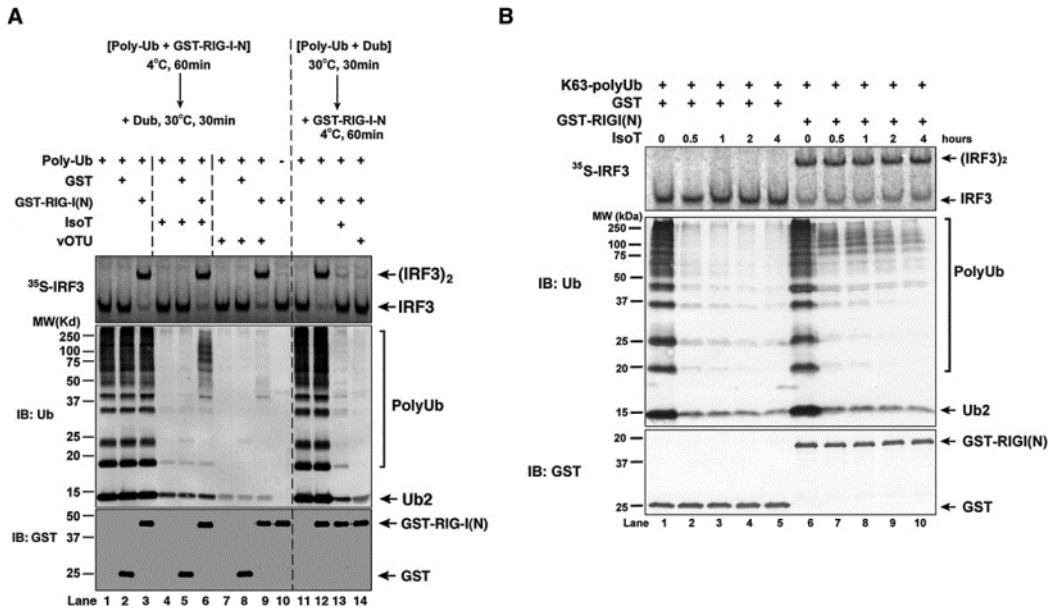

Figure 4.10. RIG-I CARD domains protect polyubiquitin from deubiquitination enzymes (DUBs).

(A) K63-polyUb chains were preincubated with GST-RIG-I(N) or GST before treatment with IsoT (lanes 4–6) or viral OTU (lanes 7–9) or mock-treated (lanes 1–3). Alternatively, the polyUb chains were pretreated with IsoT (lane 13) or vOTU (lane 14) before incubation with GST-RIG-I(N). The ability of GST-RIG-I(N) to stimulate IRF3 dimerization was then examined in the in vitro reconstitution assay.

(B) Similar to (A), except that a time course of IsoT treatment was performed.

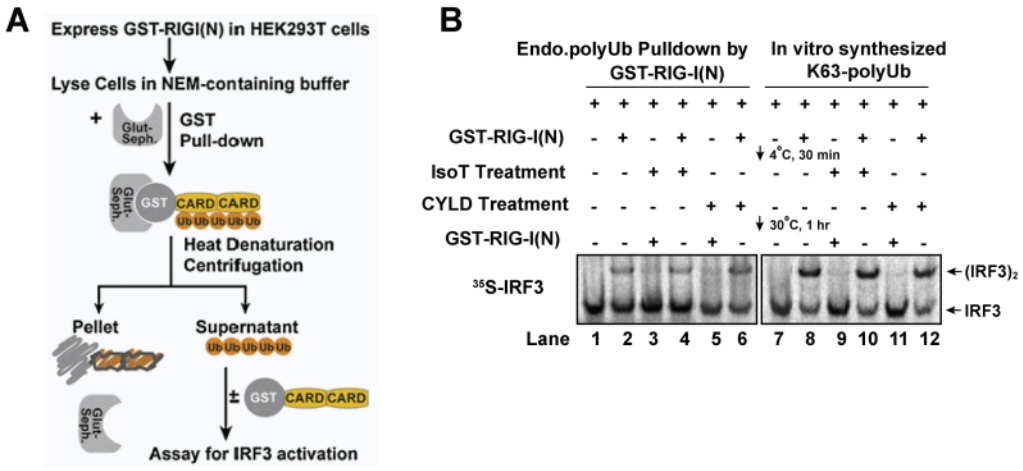

Figure 4.11. Endogenous free K63 polyubiquitin chains activate the RIG-I pathway.

(A) Scheme for isolating functional endogenous polyUb chains in human cells.

(B) As described in (A), GST-RIG-I(N) was expressed in HEK293T cells and pulled down with glutathione Sepharose. Polyubiquitin chains associated with GST-RIG-(N) were captured and released at 75ºC. The heat-resistant supernatant was incubated with fresh GST-RIG-I(N), and treated with IsoT or CYLD in the orders as indicated (lanes 1-6). The activity of GST-RIG-I(N) was then measured by in vitro IRF3 dimerzation assays. Parallel experiments were carried out with in vitro synthesized free K63 polyubiquitin chains (lanes 7-12).

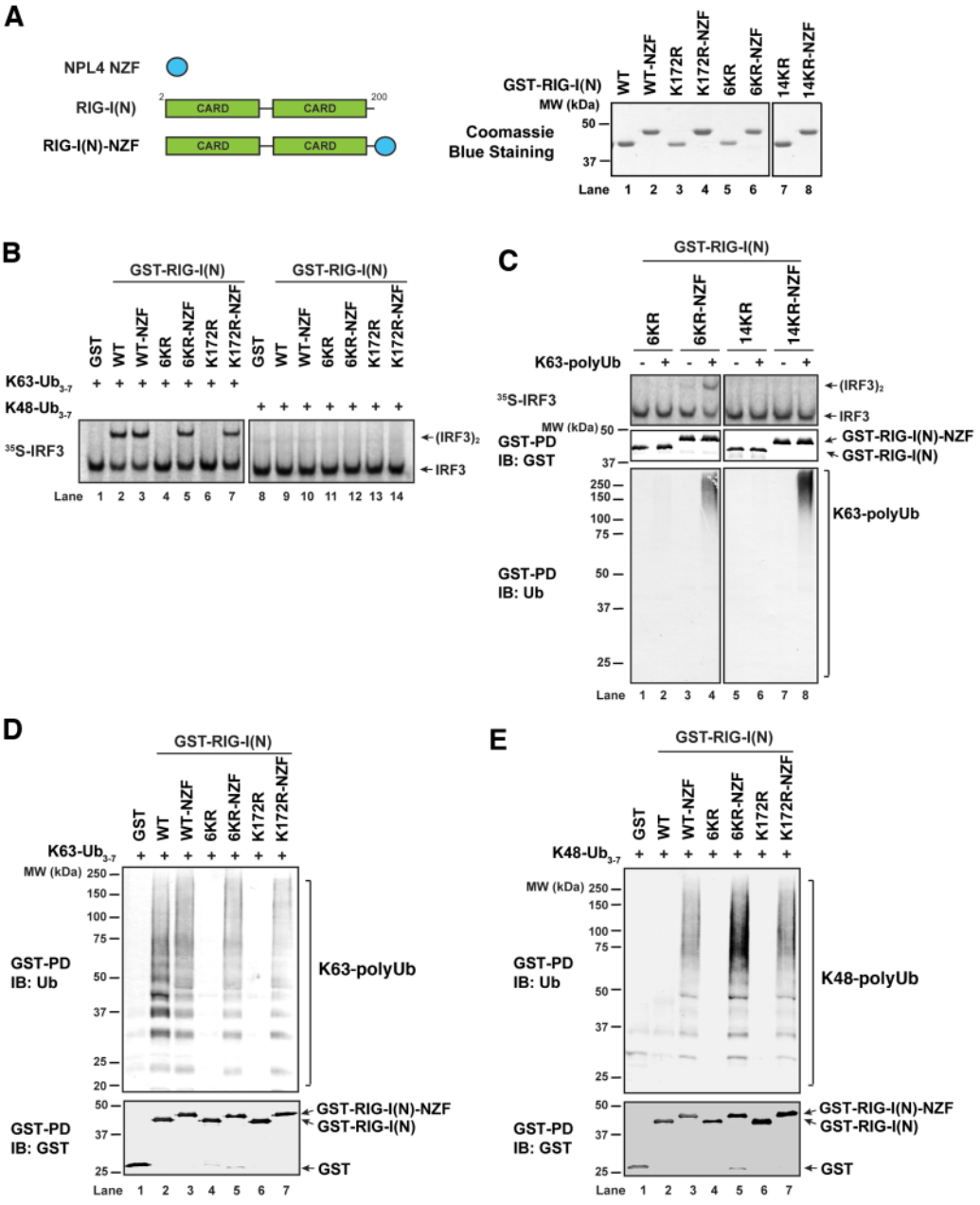
A
NPL4 NZF
RIG-I(N)
RIG-I(N)-NZF
CARD
CARD
GST-RIG-I(N)
WT
WT-NZF
K172R
K172R-NZF
6KR
6KR-NZF
14KR
14KR-NZF
MW (kDa)
Coomassie Blue Staining
Lane
B
GST-RIG-I(N)
K63-Ub3-7
K48-Ub3-7
35S-IRF3
(IRF3)2
IRF3
C
K63-polyUb
GST-PD IB: GST
GST-PD IB: Ub
GST-RIG-I(N)-NZF
GST-RIG-I(N)
K63-polyUb
D
GST-PD IB: Ub
GST-PD IB: GST
K63-polyUb
GST-RIG-I(N)-NZF
GST-RIG-I(N)
GST
E
K48-Ub3-7
K48-polyUb

Figure 4.12. A heterologous ubiquitin binding domain fused to RIG-I ubiquitin binding mutants rescues their ability to bind ubiquitin and to activate IRF3 in vitro.

(A) Diagram depicting the NPL4 novel zinc finger (NZF) ubiquitin binding domain and its fusion to RIG-I(N). The right panel shows GST-RIG-I(N) mutants and the NZF fusion proteins.

(B-E) GST-RIG-I(N) and various mutants were incubated with K63- or K48-ubiquitin chains, and then analyzed for their ability to activate IRF3 dimerization in vitro (B and C), and their ability to bind polyubiquitin chains (C-E).

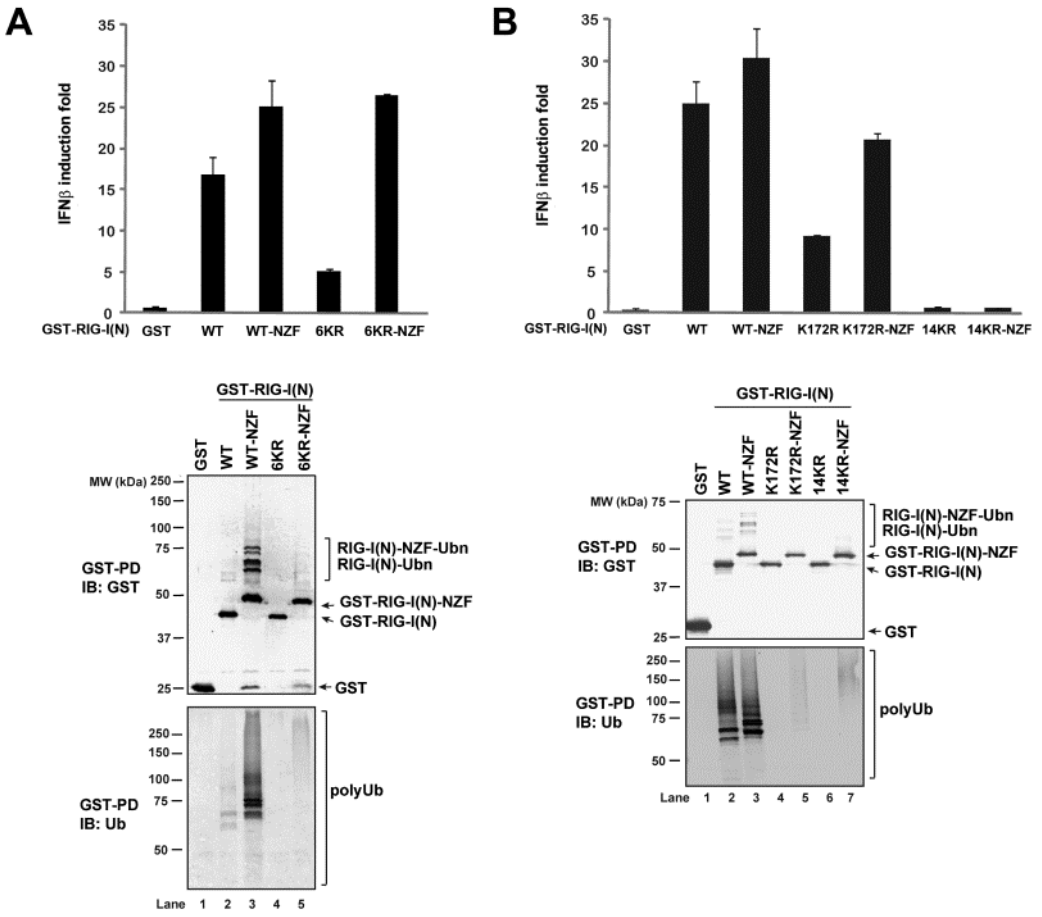

Figure 4.13. A heterologous ubiquitin binding domain fused to RIG-I ubiquitin binding mutants rescues their ability to induce IFNβ in vivo.

(A and B) RIG-I(N)-NZF fusion rescues the ability of 6KR and K172R, but not 14KR, to activate IFNβ reporter in vivo. Expression vectors for GST-RIG-I(N) proteins are transfected into HEK293T cells with IFNβ-luciferase and pRL-CMV reporter vectors. Cell lysates were assayed for luciferase activity (top) or pulled down with glutathione Sepharose followed by immunoblotting (bottom).

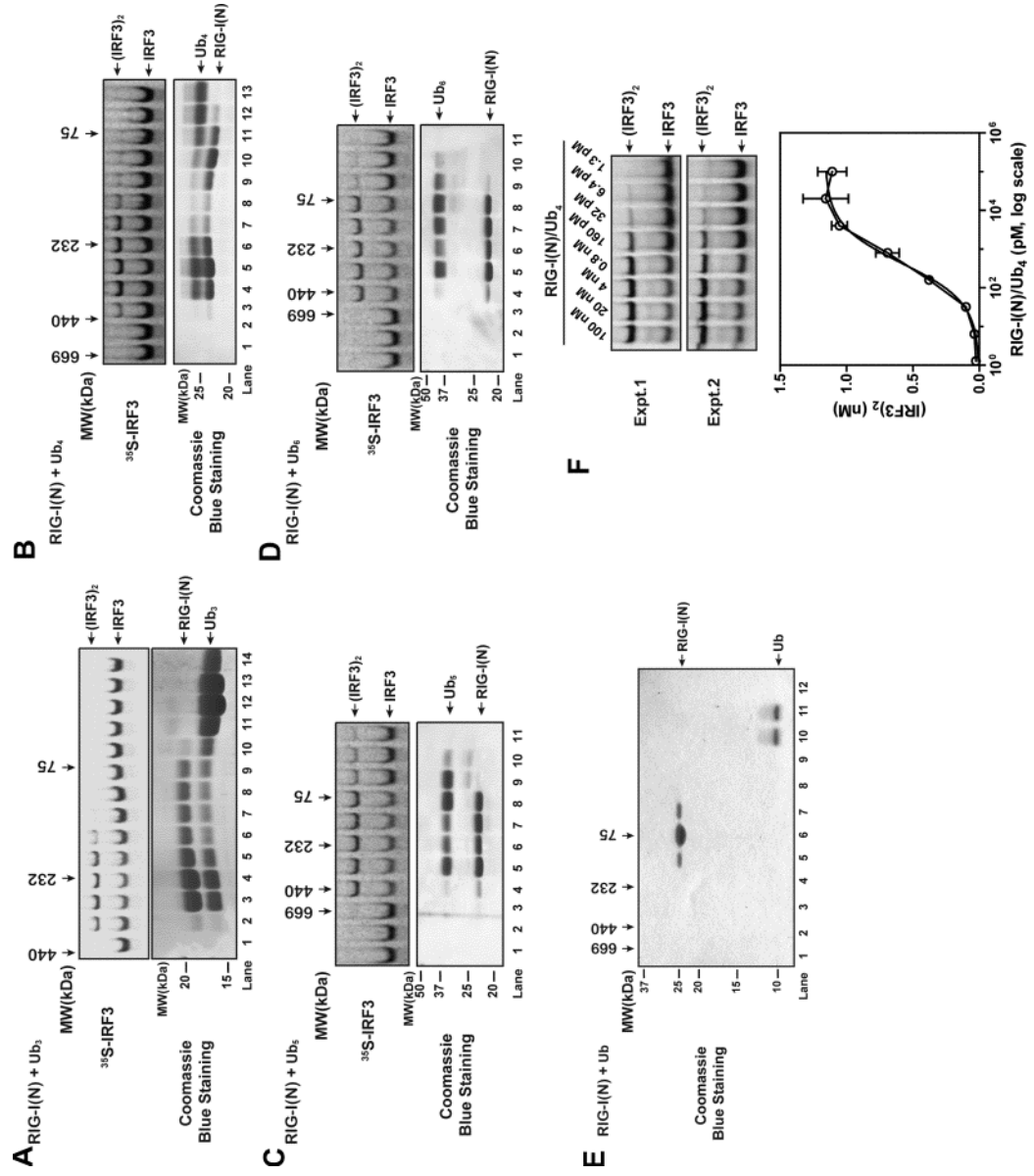
A
RIG-I(N) + Ub3
MW(kDa)
440
232
75
(IRF3)2
IRF3
35S-IRF3
RIG-I(N)
Ub3
Coomassie Blue Staining
Lane 1 2 3 4 5 6 7 8 9 10 11 12 13 14
B
RIG-I(N) + Ub4
MW(kDa)
669
440
232
75
(IRF3)2
IRF3
35S-IRF3
Ub4
RIG-I(N)
Coomassie Blue Staining
Lane 1 2 3 4 5 6 7 8 9 10 11 12 13
C
RIG-I(N) + Ub5
MW(kDa)
669
440
232
75
(IRF3)2
IRF3
35S-IRF3
Ub5
RIG-I(N)
Coomassie Blue Staining
Lane 1 2 3 4 5 6 7 8 9 10 11
D
RIG-I(N) + Ub6
MW(kDa)
669
440
232
75
(IRF3)2
IRF3
35S-IRF3
Ub6
RIG-I(N)
Coomassie Blue Staining
Lane 1 2 3 4 5 6 7 8 9 10 11
E
RIG-I(N) + Ub
MW(kDa)
669
440
232
75
RIG-I(N)
Ub
Coomassie Blue Staining
Lane 1 2 3 4 5 6 7 8 9 10 11 12
F
RIG-I(N)/Ub4
100 nM
20 nM
4 nM
0.8 nM
160 pM
32 pM
6.4 pM
1.3 pM
Expt.1
(IRF3)2
IRF3
Expt.2
(IRF3)2
IRF3
(IRF3)2 (nM)
RIG-I(N)/Ub4 (pM, log scale)

Figure 4.14. Polyubiquitin binding induces oligomerization of RIG-I CARD domains.

(A-D) RIG-I(N) (no GST tag) was incubated with K63-linked ubiquitin chains of indicated lengths, and then fractionated using Superdex-200 gel filtration column. Aliquots of the fractions were analyzed for their ability to activate IRF3 dimerization in vitro, and by SDS-PAGE followed by Coomassie Blue staining.

(E) RIG-I(N) was incubated with ubiquitin, then fractionated by gel filtration followed by SDS-PAGE and Coomassie blue staining.

(F) Varying concentrations of RIG-I(N)/Ub4 complex (lane 5 in B) were analyzed by IRF3 dimerization assay. Signal intensity of IRF3 on the autoradiograph was quantified by ImageQuant. Results from duplicated experiments are shown.

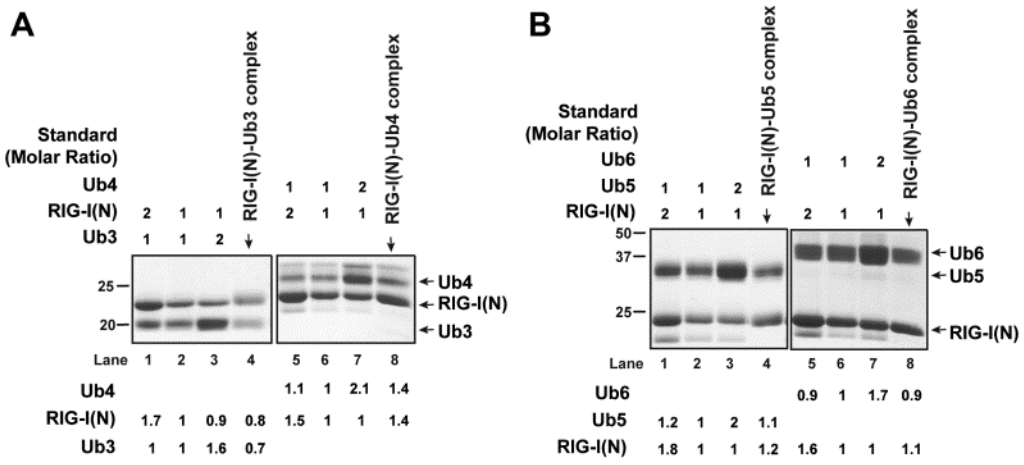

Figure 4.15. Estimation of RIG-I(N)/K63 Ub chain complex stoichiometry.

(A-B) Gel filtration fractions containing complexes of RIG-I(N)/Ub3, RIG-I(N)/Ub4 (A), RIG-I(N)/Ub5, or RIG-I(N)/Ub6 (B) were compared by Coomassie blue staining with RIG-I(N) and various Ub chains mixed at indicated ratio. Relative intensity of gel bands are shown below each lane.

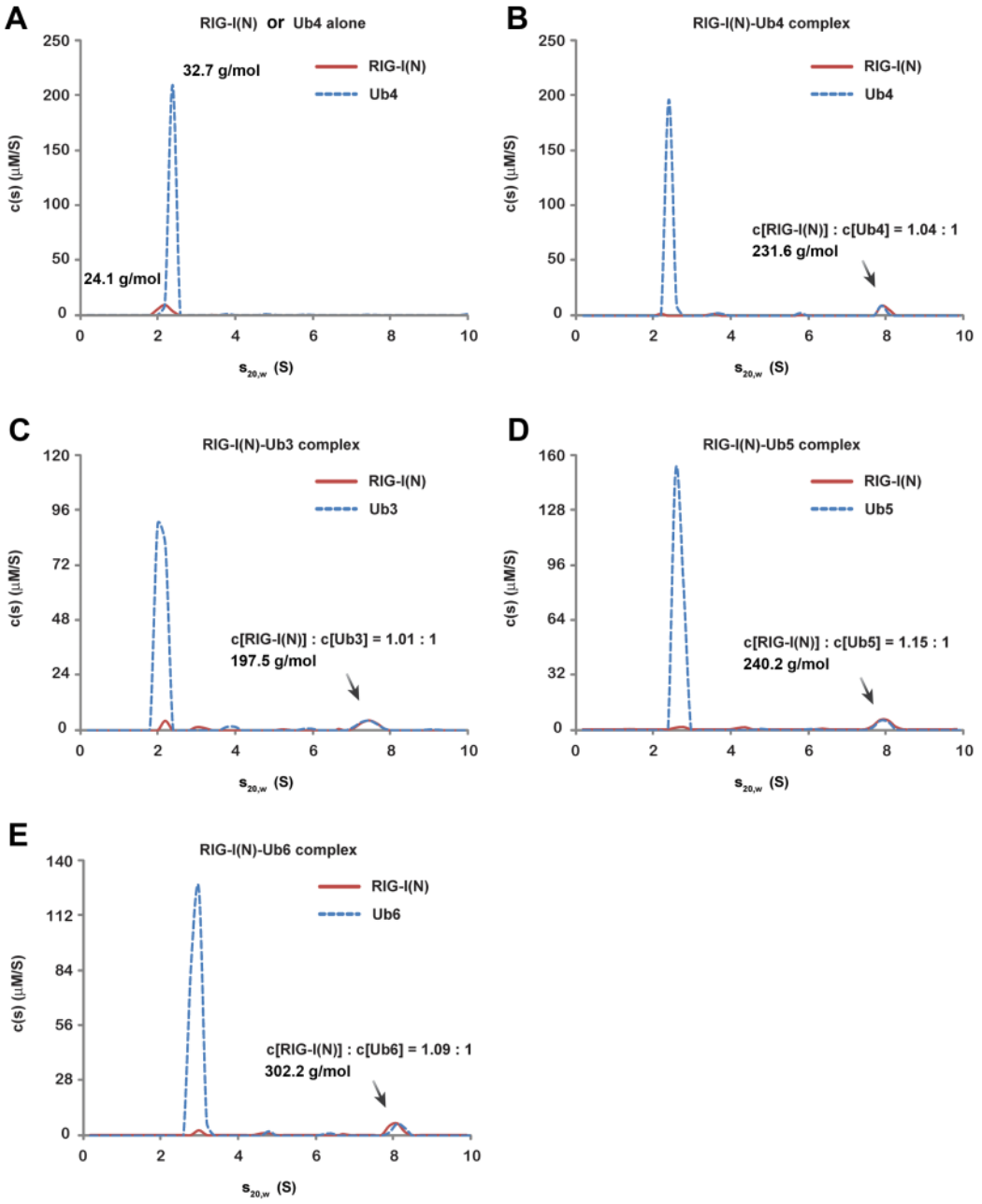
A
RIG-I(N) or Ub4 alone
32.7 g/mol
24.1 g/mol
RIG-I(N)
Ub4
c(s) (μM/S)
s20,w (S)
B
RIG-I(N)-Ub4 complex
c[RIG-I(N)] : c[Ub4] = 1.04 : 1
231.6 g/mol
C
RIG-I(N)-Ub3 complex
Ub3
c[RIG-I(N)] : c[Ub3] = 1.01 : 1
197.5 g/mol
D
RIG-I(N)-Ub5 complex
Ub5
c[RIG-I(N)] : c[Ub5] = 1.15 : 1
240.2 g/mol
E
RIG-I(N)-Ub6 complex
Ub6
c[RIG-I(N)] : c[Ub6] = 1.09 : 1
302.2 g/mol

Figure 4.16. K63 polyubiquitin chains induce the formation of RIG-I tetramer.

(A) Analytical ultracentrifugation of RIG-I(N) or K63-Ub4 alone was performed. Absorbance at 280 nm and Rayleigh interferometry results were analyzed using SEDPHAT. Sedimentation coefficient distribution of either RIG-I(N) or K63-Ub4 is shown on the same graph for comparison.

(B-E) RIG-I(N) was mixed with K63 ubiquitin chains of indicated lengths and then analyzed by analytical ultracentrifugation. Sedimentation coefficient distributions of RIG-I(N) and K63 ubiquitin chains are shown.

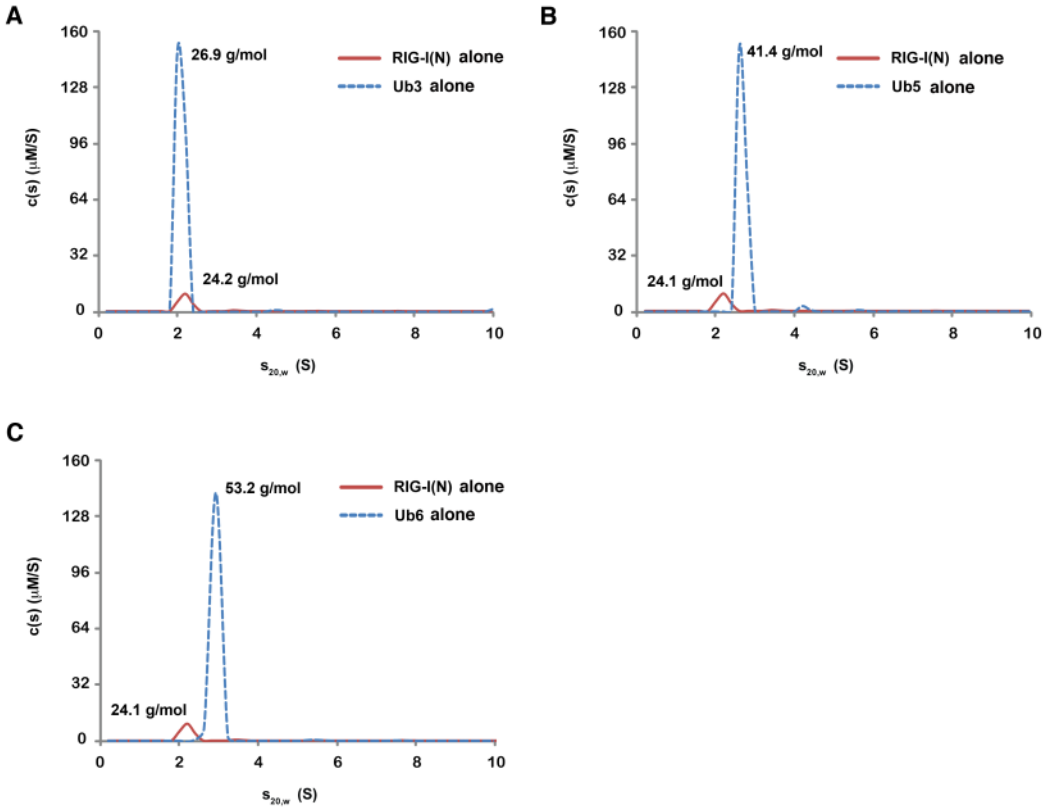

Figure 4.17. Sedimentation coefficient distributions of RIG-I(N) and K63 Ub chains of various lengths.

(A-C) Multisignal sedimentation velocity experiments were performed with RIG-I(N), K63-Ub3 (A), K63-Ub5 (B), or K63-Ub6 (C) alone. Sedimentation coefficient distributions of RIG-I(N) and K63 Ub chains are shown on the same graph for comparison.

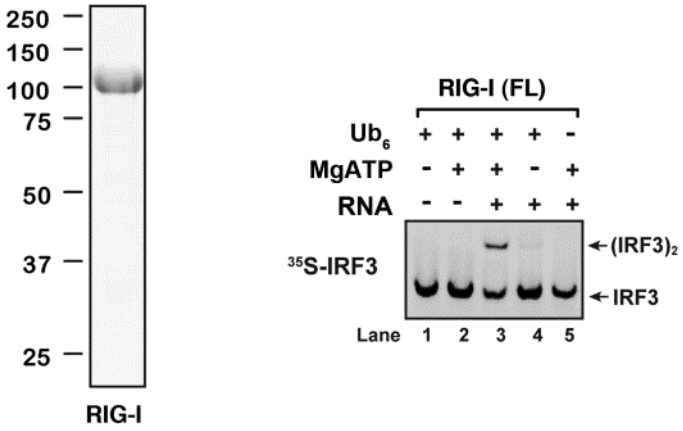

Figure 4.18. In vitro reconstitution of the RIG-I pathway.

Full-length (FL) RIG-I was incubated with K63-Ub6, MgATP, and 5'-pppRNA ligand as indicated. Shown on the left is a Coomassie blue stained gel containing RIG-I protein.

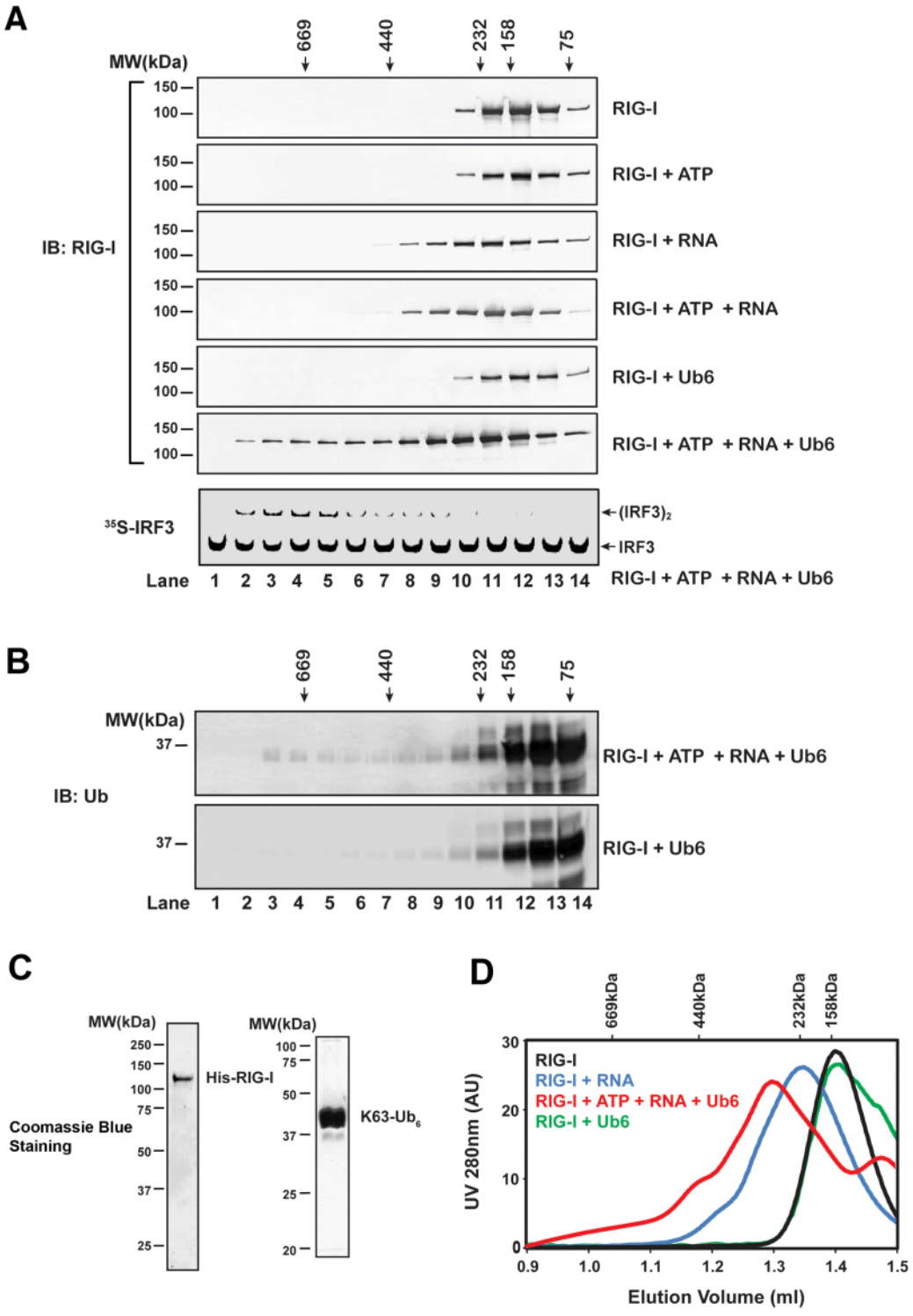
A
MW(kDa)
669
440
232
158
75
150
100
IB: RIG-I
RIG-I
RIG-I + ATP
RIG-I + RNA
RIG-I + ATP + RNA
RIG-I + Ub6
RIG-I + ATP + RNA + Ub6
35S-IRF3
(IRF3)2
IRF3
Lane 1 2 3 4 5 6 7 8 9 10 11 12 13 14
RIG-I + ATP + RNA + Ub6
B
MW(kDa)
37
IB: Ub
RIG-I + ATP + RNA + Ub6
RIG-I + Ub6
C
MW(kDa)
250
150
100
75
50
37
25
Coomassie Blue Staining
His-RIG-I
MW(kDa)
100
75
50
37
25
20
K63-Ub6
D
669kDa
440kDa
232kDa
158kDa
UV 280nm (AU)
30
20
10
0
RIG-I
RIG-I + RNA
RIG-I + ATP + RNA + Ub6
RIG-I + Ub6
0.9
1.0
1.1
1.2
1.3
1.4
1.5
Elution Volume (ml)

Figure 4.19. RNA and polyubiquitin chains induce oligomerization and activation of full-length RIG-I.

(A) RIG-I was incubated with ATP, 5'-pppRNA and/or K63-Ub6 as indicated. The mixtures were fractionated by gel filtration using Superdex-200. Aliquots of the fractions were analyzed by immunoblotting with a RIG-I antibody or by in vitro IRF3 dimerization assay as indicated. Only RIG-I incubated with ATP, 5'-pppRNA and K63-Ub6 had IRF3 stimulatory activity.

(B) In the indicated mixture analyzed by gel filtration, polyubiquitin co-eluted with RIG-I oligomer in the mixture containing RIG-I, ATP, RNA and Ub6 (top), but not when ATP and RNA were omitted (bottom).

(C) Coomassie blue staining of the proteins used in this experiments.

(D) UV (280 nm) absorption chromatographs of indicated mixtures analyzed by Superdex-200 gel filtration column.

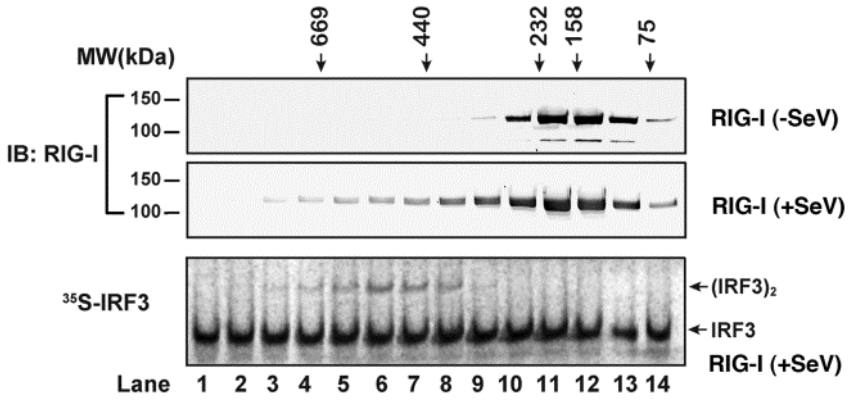

Figure 4.20. Virus infection induces oligomerizaiton and activation of RIG-I in vivo.

HEK293T cells stably expressing RIG-I-Flag were infected with SeV for 16 hours (+SeV) or not infected (-SeV). RIG-I-Flag was affinity purified, and then fractionated by gel filtration using Superdex-200. Aliquots of the fractions were analyzed by immunoblotting (top two panels), or in vitro IRF3 dimerization assay (bottom).

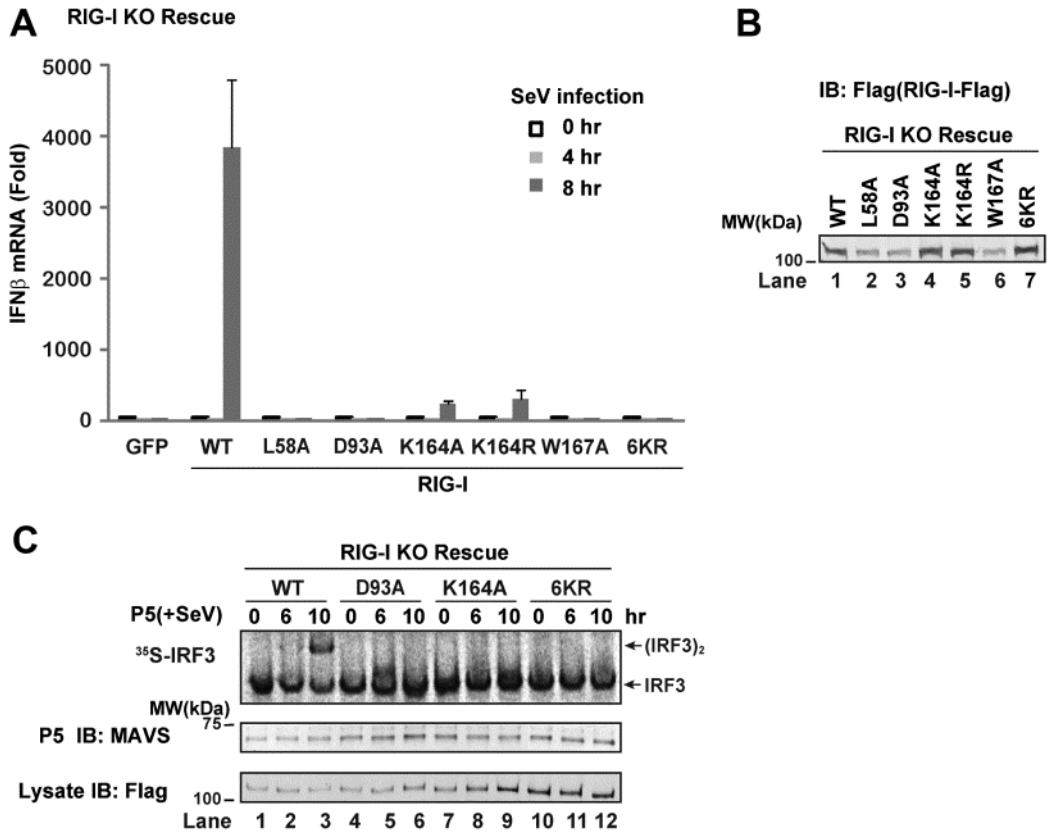

Figure 4.21. Ubiquitin binding by RIG-I is essential for virus infection induced RIG-I activation and IFNβ production in cells.

(A) RIG-I WT, but not ubiquitin binding mutants, rescues IFNβ production in response to SeV infection in RIG-I KO MEF cells. RIG-I WT or ubiquitin binding mutants were stably expressed via lentiviral expression vectors in RIG-I knockout (KO) MEF cells (RIG-I KO Rescue cell lines). Cells were infected with SeV, and IFNβ production was measured by quantitative PCR.

(B) Immunoblot showing RIG-I expression in cells used in (A).

(C) Cells were infected with SeV, and then mitochondria fractions (P5) were incubated with cytosol from uninfected cells (S5) in the presence of ATP and ^{35}S-IRF3. IRF3 dimerization was measured. MAVS and RIG-I immunoblots were also shown.

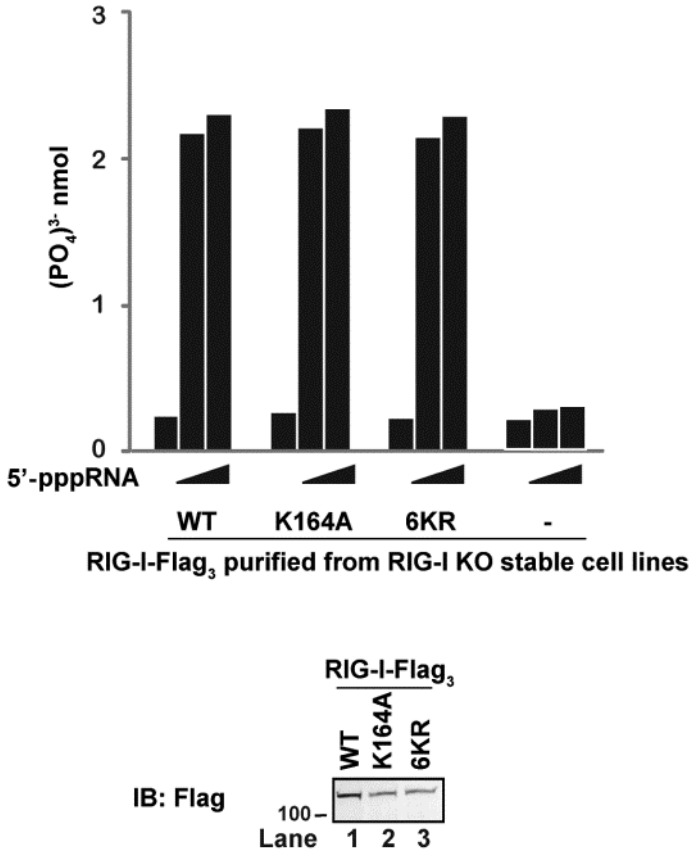

Figure 4.22. ATPase activity of RIG-I WT and mutant proteins.

RIG-I WT and mutant proteins were affinity purified from RIG-I KO rescue cell lines. 100 ng of each protein was incubated with 0, 50 ng, 200 ng 5'-pppRNA in the presence of Mg-ATP. End point concentration of $(PO_4)^{3-}$ was measured using BioMol Green reagent as an indicator for RIG-I ATPase activity. Immunoblot for the proteins used were also shown.

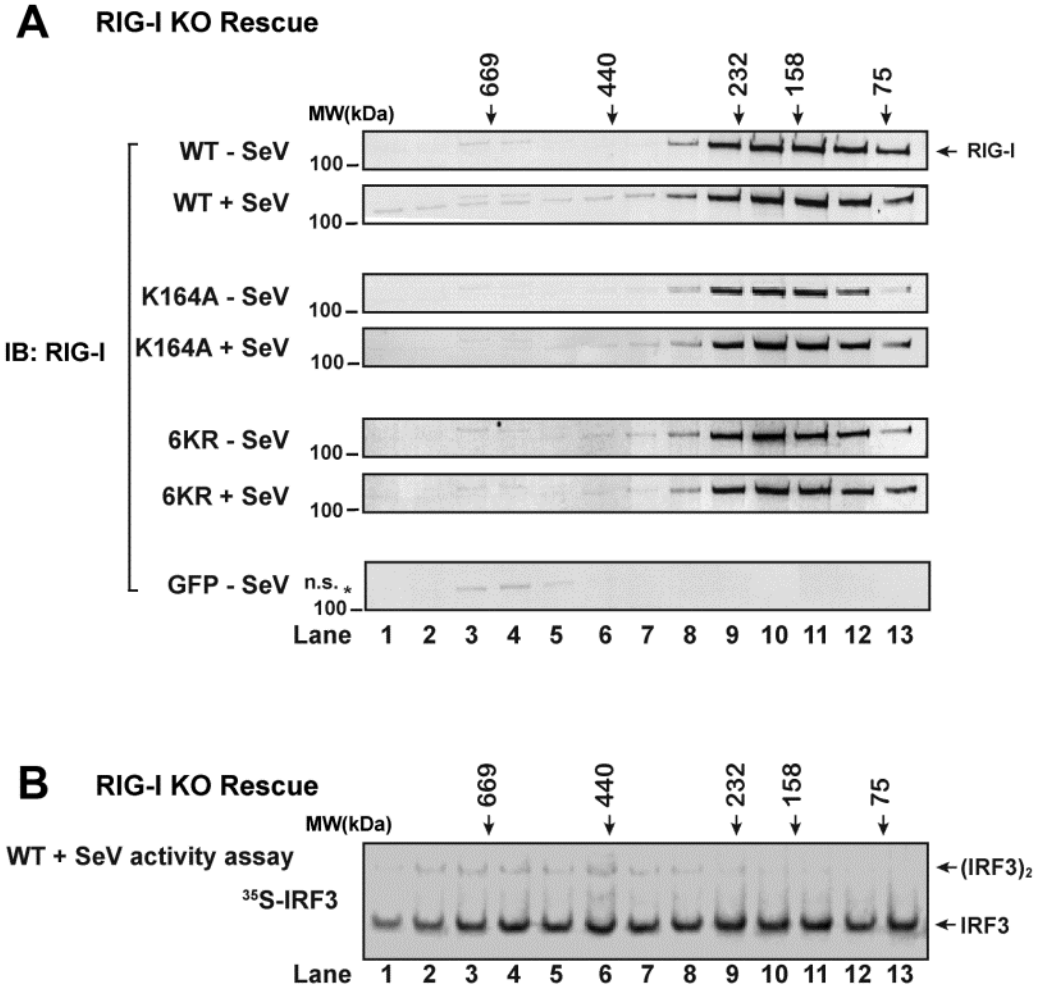

Figure 4.23. Ubiquitin binding is important for virus infection induced oligomerization and activation of RIG-I in cells.

(A) RIG-I KO MEF cells stably expressing RIG-I WT, K164A, 6KR or GFP were infected with SeV for 14 hours (+SeV) or mock treated (-SeV). Cytosolic extracts were prepared from each cell line, and analyzed with Superdex-200 gel filtration column followed by immunoblot for RIG-I. Asterisk indicates a non-specific band (n.s.).

(B) RIG-I KO MEF cells stably expressing WT RIG-I were infected with SeV for 14 hours. Cytosolic extracts were analyzed with Superdex-200 gel filtration column. Each fraction was tested for its ability to activate the MAVS-IRF3 pathway in vitro.

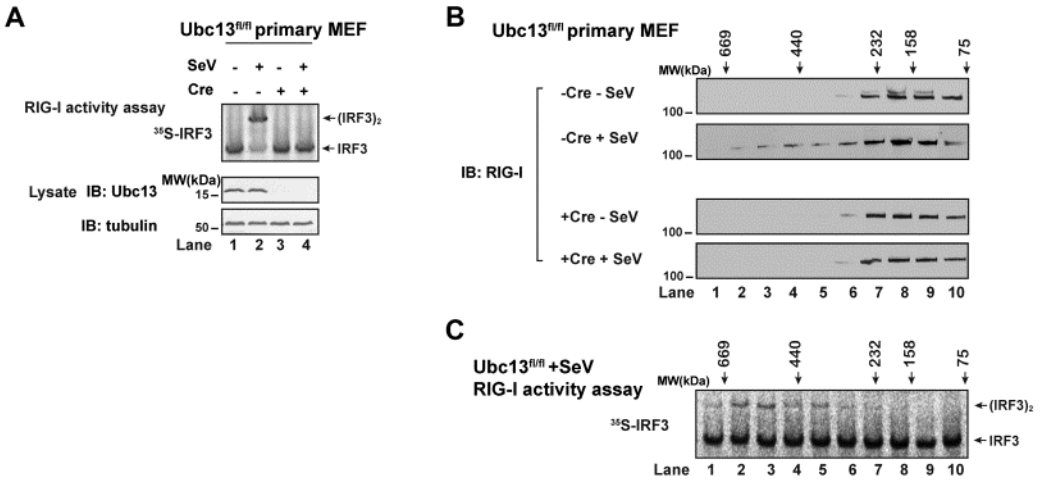

Figure 4.24. Ubc13 is essential for virus infection induced RIG-I oligomerization and activation.

(A) In Ubc13$^{fl/fl}$ primary MEF cells expressing Flag-tagged RIG-I, the Ubc13 gene was left intact or deleted by introducing lentivirus expressing Cre recombinase. The efficiency of Ubc13 depletion was shown by immunoblotting (bottom two panels). Cells were infected with SeV or mock treated, and then RIG-I was affinity purified, and tested for its ability to activate IRF3 dimierization in the in vitro reconstitution system.

(B) RIG-I purified from indicated cells were analyzed with Superdex-200 column followed by immunoblotting.

(C) Gel filtration fractions of RIG-I from SeV infected WT cells were used in the in vitro reconstitution system.

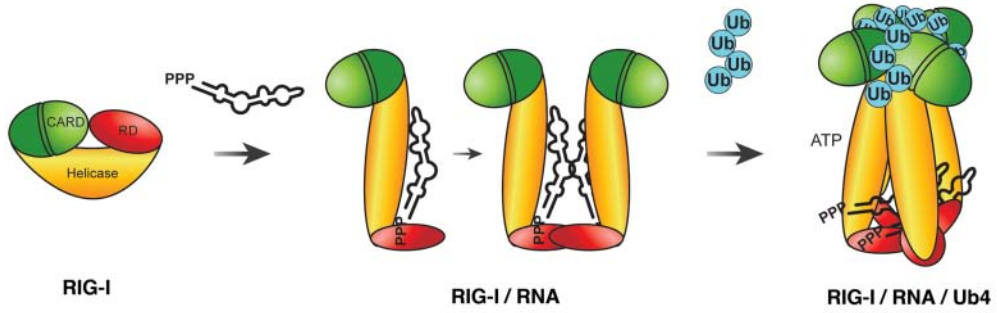

Figure 4.25. A model of RIG-I activation through polyubiquitin-induced oligomerization.

Sequential binding of RNA ligand and K63 polyubiquitin induce RIG-I oligomerization and activation.

CHAPTER V

ROLE OF UBIQUITIN IN MDA5 ACTIVATION

V.1. Introduction

While MDA5 is known to play crucial roles in immune responses against many RNA viruses, especially piconarviruses[345], little is known about how MDA5 is activated and how it activates the downstream pathways leading to type I IFN production. The C-terminus of MDA5 is distinct from the RD of RIG-I and it does not bind to 5'-pppRNA[8, 64, 65]. Although long double-stranded RNA analogue poly[I:C] has been shown to induce IFNβ in a MDA5-dependent manne[43], the physiological ligand of MDA5 has not been defined. A previous study found that RIG-I, but not MDA5, is ubiquitinated by TRIM25, and that a putative ubiquitination site of RIG-I (K172) is not conserved in MDA5, raising the question of whether ubiquitination plays any role in MDA5 activation[73].

This chapter describes my work aiming at understanding the molecular mechanism of MDA5 activation. I found that ubiquitin is important for MDA5 activation by setting up an in vitro reconstitution assay mimicking MDA5 pathway activation similar to that used for studying RIG-I activation. Mutations in the conserved residues of MDA5 CARD domains that disrupt its binding to ubiquitin chains also impair its ability to activate IRF3. MDA5 CARD domains bind polyubiquitin and forms active oligomers. The CARD domains of RIG-I and MDA5 share a conserved mechanism of ubiquitin-

binding induced oligomerization and activation, and may represent a unique class of ubiquitin sensing CARD domains. For MDA5 function in vivo, previous works on MDA5 activation in vivo were limited to end-point readouts such as virus infection induced IFNβ production. I established a cell-based model for MDA5 activation by virus infection that is amenable for interrogating MDA5 activation both genetically and biochemically. Using in vivo MDA5 activation models, I provided evidences supporting the hypothesis that K63-ubiquitination and MDA5 ubiquitin binding is essential for MDA5 activation in vivo.

V.2. Ubiquitin-Dependent Activation of the MDA5 Signaling Cascade in a Cell-Free System

We have previously shown that RIG-I N-terminus containing the CARD domains [RIG(N)] binds K63 polyubiquitin chains, and that this binding triggers a signaling cascade that leads to the activation of IRF3 in a cell-free system consisting of mitochondria and cytosolic extracts. To investigate if MDA5 CARD domains [MDA5(N)] could also activate IRF3 through a similar mechanism, I expressed GST-MDA5(N) in *E. coli*, purified it, and incubated it in a ubiquitination reaction containing E1, Ubc13/Uev1A (E2), TRIM25 (E3) and ubiquitin in the presence or absence of ATP (Figure 5.1A & B). Afterwards, the reaction mixtures were incubated with mitochondria (P5) and cytosolic extracts (S5) together with ^{35}S-IRF3 and ATP, followed by native gel

electrophoresis to detect IRF3 dimerization. Like RIG-I(N), MDA5(N) was capable of causing IRF3 dimerization following the ubiquitination reaction (Figure 5.1B).

To determine if ubiquitination of MDA5(N) was involved in its activation, we carried out the ubiquitination reaction as described in Figure 5.1B except that GST-RIG-I(N) or MDA5(N) was omitted from the reaction. The thio-modifying agent N-ethymaleimide (NEM) was added to the reaction mixture to inactivate E1 and E2, and then the reaction mixture, which contained mostly unanchored K63 polyubiquitin chains[148], was incubated with GST-RIG-I(N) or GST-MDA5(N). Like GST-RIG-I(N), GST-MDA5(N) gained the ability to activate IRF3 after incubation with K63 polyubiquitin chains (Figure 5.1C). We have previously shown that unanchored K63 ubiquitin chains could directly activate RIG-I(N). Similarly, incubation of K63 chains containing four or more ubiquitin with GST-MDA5(N) led to IRF3 activation in the in vitro assay (Figure 5.1D). In contrast, K48 ubiquitin chains had no activity. In addition, Ub4 containing the K48-K63-K48 mixed linkage weakly stimulated GST-MDA5(N), whereas Ub4 containing the K63-K48-K63 linkage was inactive (lanes 14-15), this activation pattern was reminiscent to that of RIG-I(N) as well. Linear Ub4, in which the N-terminal methionine of one ubiquitin is conjugated by the C-terminus of the preceding ubiquitin, did not activate MDA5(N) (Figure 5.3A).

Full-length MDA5 is activated by long poly[I:C] as well as by undefined ligands associated with certain RNA viruses such as those of picornaviridae[345]. To determine if full-length MDA5 could lead to IRF3 activation in the in vitro reconstitution system, MDA5 expressed and purified from *E. coli* was tested. Similar to RIG-I (Figure 4.18),

incubation of MDA5 with poly[I:C], ATP and K63 polyubiquitin chains led to strong activation of IRF3 in the cell-free system (Figure 5.1E).

V.3. MDA5 CARD Domains Bind K63 Polyubiquitin Chains

Our previous study showed that both CARD domains of RIG-I are required for binding to K63 polyubiquitin chains and the single CARD domain of MAVS does not bind to these chains[339]. Similar to GST-RIG-I(N), GST-MDA5(N) bound to K63 polyubiquitin chains, but not K48-Ub4 or Linear-Ub4 (Figure 5.2B).

To delineate the regions in MDA5 that are important for ubiquitin binding and IRF3 activation, I generated a few deletion mutants of MDA5(N) (Figure 5.3A). These mutants were expressed in *E. coli* as GST fusion proteins and affinity purified. The purified proteins were tested for their binding to K63 polyubiquitin chains and their ability to activate IRF3 in the cell-free system (Figures 5.3B). There was a good correlation between their ability to bind the ubiquitin chains and their ability to activate IRF3. The functional boundaries of MDA5(N) aligned with those of RIG-I(N), both roughly corresponding to the boundaries of their tandem CARD domains, supporting the notion that they use similar structural units (both CARDs of the tandem CARD domains) for ubiquitin binding and activation.

CARD domains belong to the death domain (DD) superfamily, which also includes the death domain (DD), death effector domain (DED), and pyrin domain (PYD)

subfamilies. Many proteins of the DD superfamily are involved in immunity, inflammation and cell death[68]. Our findings that RIG-I and MDA5 CARD domains bind to K63 polyubiquitin chains raise the question of whether the CARD or DD domains of some other proteins are also ubiquitin-binding domains. To begin to address this question, we carried out bioinformatics analysis of the CARD domain subfamily (in collaboration with Dr. Lisa Kinch). CARD domain subfamily sequences were collected by PSI-BLAST. Clustering analysis based on sequence homology shows that the CARD domains of RIG-I (two CARD domains), MDA5 (two CARD domains) and MAVS form a distinct cluster that is distantly related to other CARD domains, such as those present in NOD1, NOD2 and RIP2, which are important in innate immunity (Figure 5.4A). Although all DD superfamily domains share a conserved six-helical bundle fold, the CARD domain subfamily is also distinct from DD and DED subfamilies based on structural-based homology analysis (Figure 5.4B).

The determine whether RIG-I and MDA5 CARD domains are unique in their ubiquitin binding ability among other members of the DD superfamily, I purified DD of several closely related protein and tested whether they could bind ubiquitin. NOD1 and NOD2 were chosen because they were two PRRs in innate immunity. Caspase8 was chosen because it had two tandem DED domains. In contrast, the CARD domain of NOD1, tandem CARD domains of NOD2, and tandem DED domains of caspase 8 did not exhibit detectable ubiquitin chain binding activity (Figure 5.4C). Although these results do not exclude the possibility that some other proteins in the DD superfamily can

bind ubiquitin chains, they suggest that the CARD domains of RIG-I and MDA5 are unique in their ability to bind specifically to K63 polyubiquitin chains.

V.4. Polyubiquitin Binding is Essential for MDA5 to Activate IRF3 and Induce IFNβ

To further define the relationship between ubiquitin binding and IRF3 activation by RIG-I and MDA5, I identified key residues in the CARD domains that are important for their functions. Sequence alignment of the CARD domains of RIG-I from human, mouse and zebrafish, as well as those of human and mouse MDA5, revealed several highly conserved residues (Figure 4.8A). These residues were mutated (highlighted by asterisk) and GST fusion proteins containing these mutations were expressed in *E. coli* and affinity purified. RIG-I(N) mutants were described in Chapter Four. For MDA5(N), among seven point mutants tested, four mutations (G74/W75A, D101A, K174A, P123A) abolished MDA5(N)'s binding to K63 polyubiquitin chains as well as its ability to activate IRF3 in vitro (Figure 5.5A). Other mutations, D133A, E135A, K174R, led to reduced ubiquitin chain binding as well as weakened IRF3 activation.

Overexpression of GST-MDA5(N) in HEK293T cells led to a strong induction of IFNβ-luciferase reporter. Importantly, all of the ubiquitin-binding defective mutants of MDA5 failed to induce IFNβ in this assay. These mutants also failed to pull down endogenous polyubiquitin chains from the transfected cells (Figure 5.5B). In contrast to

RIG-(N), there is no apparent ubiquitination of MDA5(N). Furthermore, MDA5 does not contain a conserved lysine known to be ubiquitinated in RIG-I and there is no evidence that MDA5 is ubiquitinated[73]. Taken together, these results demonstrate that the binding to K63 polyubiquitin chains is essential for MDA5 to activate IRF3 and induce IFNβ.

V.5. MDA5 Binds to Polyubiquitin In Vivo

Similar to RIG-I(N), overexpression of MDA5(N) can pull down ubiquitin from cells as detected by ubiquitin western, although relatively weaker compared to RIG-I(N). As noted above, for MDA5(N), this associated ubiquitin is more likely to be non-covalently bound, because there has been no evidence that MDA5 is ubiquitinated[73] and MDA5 does not contain a conserved lysine known to be ubiquitinated in RIG-I. To isolate MDA5-associated endogenous ubiquitin from cells, I used similar strategies used for isolating RIG-I(N) bound ubiquitin (Figure 4.11A). In brief, cells overexpressing GST-MDA5(N) were lysed in the presence of NEM to inactivate most of the deubiquitination enzymes, and MDA5(N):polyUb complex were pulled-down from cell lysates and heated at 75°C which could denature MDA5(N) but preserve the structure and function of ubiquitin chains. Following centrifugation that precipitated denatured protein aggregates, the supernatant was expected to contain polyUb chains and could be tested for its ability to activate IRF3 in the presence of fresh RIG-I(N) or MDA5(N). Indeed, the supernatant containing polyUb chains released from the MDA5(N) complex at 75°C were capable of

activating IRF3 when supplied with fresh GST-RIG-I(N) or GST-MDA5(N) (Figure 5.6A).

To determine whether the supernatant of the heated GST-MDA5(N) complex contained unanchored K63-linked polyUb chains and whether these chains were responsible for activating the MDA5 pathway, I incubated the endogenous ubiquitin chains with IsoT or CYLD (a free ubiquitin chain specific DUB and a K63-ubiquitin chain specific DUB), and then measured their activity in the IRF3 dimerization assay (Figure 5.6B). Indeed, the heat supernatant of MDA5(N) complex behaved similarly to that of RIG-I(N) complex. Both IsoT and CYLD treatment abolished the ability of the supernatant to activate IRF3 in the presence of GST-RIG-I(N) (lanes 9 and 11). However, if I reversed the order by incubating the supernatant with GST-RIG-I(N) first and then with the DUB enzymes, the activity was protected and IRF3 dimerization was observed (lanes 10 and 12).

V.6. Ubiquitin-Induced Oligomerization Activates MDA5

To examine whether ubiquitin binding also induces MDA5(N) oligomerization similar to ubiquitin induced RIG-I(N) oligomerization, I performed gel filtration analysis of MDA5(N) following its incubation with K63 ubiquitin chains of different lengths. In these experiments, MDA5(N) were prepared by cutting off GST tag from GST-MDA5(N) with TEV protease. I also used a relatively larger amount of Ub6 in these experiments (as

compared to experiments done with RIG-I(N)), because, compared to RIG-I(N), the formation of MDA5(N) with short ubiquitin chains are relatively weaker in the same condition, which might reflect a preference for longer ubiquitin chains. A readily detectable amount of HMW complex was formed as detected by MDA5 and Ub western blots (Figure 5.7A). Furthermore, the HMW complexes containing MDA5(N) and Ub6 are highly potent in activating IRF3 in the cell-free system (Figure 5.7B).

V.7. Ubiquitin Binding Rescues the Activity of an MDA5 CARD Domain Mutant

Although for MDA5, the distinction between ubiquitination and ubiquitin binding is less of a question than for RIG-I(N), I was still interested in the effect of ubiquitin binding domain fusion to a ubiquitin binding mutant of MDA5(N). I fused MDA5(N) mutants to the novel zinc finger (NZF) domain of NPL4^{342}. However, out of a few mutants tested, NZF fusion could not rescue their ability to activate IRF3 in vitro, although ubiquitin binding was rescued (data not shown). RIG-I(N) and short ubiquitin chain were shown to form complexes of a defined stoichiometry (described in Chapter IV), so CARD domains and ubiquitin likely form defined complexes with multiple interacting surfaces. It is conceivable that various mutations may disrupt the formation of CARD/Ub complex in different ways, for example, some mutants may disrupt the binding surface between CARD and Ub, others may disrupt the binding surface between individual CARD domains within one tandom CARDs molecule, or between two CARD domains that belong to two different molecules. Therefore, it was not surprising that certain ubiquitin

binding mutants could be rescued (such as K172R and 6KR for RIG-I), while others could not be rescued in the same way.

I made additional point mutants of MDA5(N), in which all the lysine residues were mutated to arginine, individually. Other than the K174R mutation shown earlier, only K68R abolished MDA5(N)'s ability to activate IRF3 in vitro (Figure 5.8A). NZF fusion to K68R mutant rescued its ability to activate IRF3 in vitro (Figure 5.8B). Overexpression of MDA5(N)-K68R-NZF also enhanced its ability to induce IRF3 activation in vivo by luciferase reporter assay (Figure 5.8C). GST pull down from these cells revealed that MDA5(N)-K68R-NZF was able to pull down endogenous polyubiquitin chains. Taken together, these results support the notion that polyubiquitin binding by MDA5 is critical for its signaling functions. It was noted that K68R mutation did not completely abolish MDA5(N)'s ability to induce IFNβ in vivo, which might be due to its incomplete loss of ubiquitin binding in vivo. An end point read out like IFNβ induction is the result of the activation of the complete signaling pathway, which includes multiple amplification steps, and therefore may not accurately reflect the amplitude of activation signal at the beginning of the pathway. Another caveat of this experiment is that K68R mutant retained some ubiquitin binding activity in vivo but not in vitro. I could reasonably speculate several possible explanations. This particular mutation may exhibit strong ubiquitin binding in vitro with purified proteins, but in vivo, in the presence of other cellular proteins (possibly endogenous WT protein), the defect might be compensated. Another possible explanation was that the difference in experimental

conditions between in vitro and in vivo experiments may contribute to the different detection thresholds of ubiquitin binding.

V.8. Establishing Cell-Based Systems for Studying the MDA5 Signaling Cascade In Vivo

To better understand the MDA5 pathway, I tried to establish an in vivo model for MDA5 activation induced by virus infection. EMCV infection was shown to induce IFNβ in a MDA5-dependent manner in MEF cells and conventional dendritic cells[345]. I found that transfection of total RNA prepared from EMCV-infected HEK293T cells (designated as 293EMCV) was a much stronger inducer of IFNβ in MEF cells compared to EMCV infection (Figure 5.9A). It is possible that viruses have mechanisms to suppress the activation of the MDA5 pathway. Thus, I next tested in several cell lines the use of 293EMCV transfection to mimic virus-infection-induced activation of the MDA5-IFNβ pathway.

In MEF cells, 293EMCV transfection induced IFNβ in a MDA5-dependent manner, while 293SeV (RNA prepared from SeV-infected HEK293T cells) induced IFNβ independent of MDA5 (Figure 5.9A & B). In HEK293T cells, I found that neither EMCV infection nor 293EMCV transfection induced any IFNβ (not shown), although cytopathic effects were observed. Interestingly, in HEK293T cells stably expressing MDA5, 293EMCV transfection strongly induced IFNβ (Figure 5.10A), while EMCV

infection did not induce IFNβ (not shown), which might reflect a viral evasion mechanism that isolated RNA ligand did not have. In Thp1 cells, transfection of 293EMCV also activated IFNβ transcription. This was dependent on endogenous MDA5 as shown with Thp1 cells stably expressing shRNA targeting MDA5 (Thp1/shMDA5) (Figure 5.10B). In contrast, 293SeV transfection induces IFNβ in a RIG-I dependent manner in Thp1 cells (Figure 5.10C). Similarly, in U2OS cells, 293EMCV transfection also induced MDA5-dependent IFNβ production (Figure 5.10D).

V.9. Polyubiquitin Binding is Essential for MDA5 Activation In Vivo

Once the cell-based systems were set up for investigating MDA5 activation in vivo, I tested whether MDA5-K174A, a mutation that disrupts ubiquitin binding, could abolish MDA5 activation in response to 293EMCV transfection. I tested this in two cell lines. In HEK293T cells stably expressing MDA5-K174A (HEK293T/MDA5-K174A), 293EMCV transfection did not induce IFNβ as in HEK293T cells expressing WT MDA5 (Figure 5.11A). The response to 293SeV transfection was still normal in HEK293T/MDA5-K174A cells, indicating the MDA5 mutation did not affect the RIG-I pathway and its downstream components, such as MAVS, and TBK1. Further, I showed that mitochondria fractions (P5) from 293EMCV transfected HEK293T/MDA5 cells could activate IRF3 in an in vitro reconstitution system similar to that described in Figure 3.1, in which P5 fractions from stimulated cells were used to activate cytosolic fractions

(S5) from uninfected cells (Figure 5.11B). However, P5 from stimulated HEK293T/MDA5-K174A cells were not active. In Thp1 cells where endogenous MDA5 was stably knocked down by shRNA (Thp1/shMDA5), introducing WT MDA5 resistant to shRNA knock-down could rescue IFNβ activation, while MDA5-K174A mutant could not rescue this defect (Figure 5.11C). As a control, both WT and K174A mutant MDA5 proteins, purified from HEK293T stable cells, were shown to have normal ATPase activity induced by RNA (Figure 5.12, right). Thus, these results demonstrated that ubiquitin binding is essential for MDA5 to activate IRF3 and induce IFNβ in vivo.

V.10. ATPase/Helicase activity is Important for MDA5 Activation In Vivo

Previous work on RIG-I showed the the ATPase activity of RIG-I was required for its antiviral function[4]. To determine whether this was the case for MDA5, I introduced ATPase/helicase mutants of MDA5 into stable shRNA knockdown background (Figure 5.11D), and found that E444Q, K335A and D443N could not rescue IFNβ production in response to 293EMCV transfection. ATPase activity defects of these mutants were confirmed by ATPase assays performed with purified MDA5 proteins from HEK293T stable cell lines expressing each mutant (Figure 5.12, left). Therefore, MDA5 ATPase/helicase activity is required for its function in vivo.

V.11. K63 Ubiquitination, Ubc13 and Trim25 Are Required for MDA5 Activation In Vivo

To further investigate the role of K63 polyubiquitination in the MDA5 pathway in cells, I used recently developed U2OS cell lines in which endogenous ubiquitin is knocked down with shRNA (shUb) and replaced with transgenes of ubiquitin through a tetracycline-inducible strategy[324]. Like in HEK293T cells, EMCV infection did not induce any IFNβ (not shown), however, I found that 293EMCV transfection induced IFNβ transcription in U2OS cells (Figure 5.10D). Depletion of endogenous ubiquitin severely impaired IFNβ induction (Figure 5.13A, left). This defect could not be rescued by the expression of K63R mutant ubiquitin transgene, suggesting K63-linkage is important for MDA5 pathway activation. I further showed that the mitochondria isolated from ubiquitin knockdown cells as well as K63R Ub replacement cells ("ubiquitin knockdown; K63R rescue", shUb/K63R +Tet) failed to activate IRF3 in vitro (Figure 5.13C, right), strongly suggesting that K63 polyubiquitination is essential for the activation of MDA5 pathway upstream of MAVS.

Next I used U2OS cell lines stably integrated with tetracycline-inducible shRNA targeting Ubc13 (shUbc13). Cells depleted of Ubc13 failed to induce IFNβ in response to 293EMCV transfection (Figure 5.13B). Further, it was showed that the defects of Ubc13 knockdown cells were upstream of MAVS activation by in vitro assay using mitochondria fraction (P5) from stimulated cells to activate cytosolic IRF3 (Figure 5.13C, left). Therefore, Ubc13 is important for MDA5 activation in vivo.

Trim25 associates with overexpressed GST-RIG-I(N), and was found to be an important E3 for RIG-I activation[73]. I found that Trim25 could also be pulled down by GST-MDA5(N) overexpressed in HEK293T cells (Figure 5.14A). To determine whether Trim25 was involved in MDA5 activation, I treated Trim25 WT and Trim25 KO MEF cells with RNA transfection (293EMCV and 293SeV) as well as virus infection (EMCV and SeV) (Figure 5.14B). Trim25 KO MEF cells had severe defects in IFNβ induction in response to both EMCV infection and 293EMCV transfection. Further, mitochondria fraction (P5) from Trim25 WT MEF cells, activated either by 293EMCV transfection or by SeV infection, could activate the IRF3 pathway in vitro, while P5 from Trim25 KO MEF cells could not (Figure 5.14C). Thus, Trim25 is involved in MDA5 pathway activation upstream of MAVS.

V.12. MDA5 Binds to K63-Linked Free Polyubiquitin Chains When Activated In Vivo

To examine whether 293EMCV transfection induces the formation of polyUb chains associated with full-length MDA5 in cells, HEK293T cells expressing MDA5-Flag (HEK293/MDA5) were transfected with 293EMCV or mock treated, and then MDA5 was immunoprecipitated and heated at 75ºC to release polyUb chains. The heat supernatant prepared from the 293EMCV transfected cells, but not mock-treated cells, stimulated IRF3 dimerization in the presence of freshly added RIG-I(N) (Figure 5.15, lane 2). This activity was diminished by IsoT treatment and CYLD treatment (lanes 3 and

5), indicating that the supernatant contained unanchored K63 polyUb chains. It should be noted that the activity associated with full-length MDA5 was much lower than that associated with RIG-I(N) or MDA5(N), possibly because the activation of full-length MDA5 is limited by its accessibility to ligand RNA.

V.13. Activated MDA5 Forms High Molecular Weight Oligomers In Vivo

To determine if MDA5 forms oligomers in cells in response to 293EMCV transfection, I purified Flag-tagged MDA5 by affinity purification from HEK293T/MDA5 cells transfected with 293EMCV or mock treated. Purified MDA5 was analyzed by gel filtration chromatography (Figure 5.16). MDA5 from mock treated cells eluted from the column between 232 kDa and 440 kDa molecular weight markers (Figure 5.16A, top). This is larger than the expected molecular weight of a monomeric MDA5 (calculated to be around 120 kDa, and at ~150 kDa on SDS-PAGE), suggesting MDA5 might be in a complex at resting state. MDA5 from mock treated cells was not able to activate IRF3 in the in vitro reconstitution system (not shown). While the majority of MDA5 from 293EMCV transfected cells eluted at the same volume as MDA5 from mock treated cells, a small fraction eluted as HMW complexes that could activate IRF3 in vitro (Figure 5.16A, bottom; B). The heterogeneity of these active complexes may reflect MDA5 bound to heterogeneous ligand RNA and ubiquitin chains in cells. It was noted that the activity of MDA5 which had been activated in vivo was relatively weak compared to RIG-I from SeV-infected cells. This could be due to several reasons. MDA5 activation in

vivo was mimicked by 293EMCV transfection, which might be in limited quantities inside the cell and might not recapitulate bona fide viral RNA ligand as well. MDA5 might also require other factors to achieve optimal activivation in vivo, which might not be recapitulated in our in vitro assay system.

V.14. Summary

In this chapter, I describe a cell-free system in which MDA5 CARD domains can be activated by pre-synthesized K63 polyubiquitin chains, and lead to the activation of IRF3; full length MDA5 leads to the activation of IRF3 in a manner that depends on RNA ligand and K63 polyubiqutin chains. MDA5 CARD domains bind to K63 polyubiquitin chains and that this binding is important for IRF3 activation. I have identified several conserved residues within MDA5 and RIG-I CARD domains that are required for K63 polyubiquitin chain binding. Mutations that disrupt ubiquitin binding also impair the ability of MDA5 to activate IRF3 and induce IFNβ. Collectively, these results provide a unified mechanism of RIG-I and MDA5 signaling that involves the binding of K63 polyubiquitin chains through the tandem CARD domains.

An extensive bioinformatics analysis was carried out on proteins harboring known and putative domains belonging to the death domain superfamily, including the CARD domains. We grouped these proteins based on their sequence homology and available structural information, and found that RIG-I and MDA5 CARD domains form a unique cluster. I have tested several CARD domains for their ability to bind K63

polyubiquitin chains, but so far only closely related RIG-I and MDA5 tandem CARD domains have the ubiquitin binding activity. This limited analysis by no means rules out the possibility that some other domains of the DD superfamily could be functional ubiquitin binding domains. Nevertheless, it appears that the CARD domains of RIG-I and MDA5 have acquired the new ubiquitin-binding function and utilize the labile ubiquitin chains as an endogenous ligand to regulate their signaling functions.

Polyubiquitin binding induces the oligomerization of the CARD domains of RIG-I and MDA5, which seems to be a conserved mechanism of activation for RIG-I and MDA5. To our knowledge, this is the first example of ubiquitin binding leading to protein oligomerization. In vitro, short K63 polyubiquitin chains form high molecular weight oligomers with MDA5 CARD domains, resulting in its activation. In vivo, stimulation of the MDA5 pathway also leads to the formation of MDA5 complexes containing K63-linked free polyubiquitin. Only the HMW complexes of MDA5, but not the lower molecular weight forms of MDA5, are able to activate IRF3 in the cell-free system. In summary, MDA5 and RIG-I activation appear to use conserved mechanisms of polyubiquitin binding induced oligomerization.

I have also established cell based models to study the MDA5 signaling cascade in vivo. Transfection of total RNA isolated from EMCV infected cells is able to induce IFNβ production in an MDA5-dependent manner in a number of cell lines, including mouse cell line MEF (embryonic fibroblast), and human cell lines HEK293T (fibroblast), Thp1 (monocytic leukemia) and U2OS (osteosarcoma). Through molecular and genetic manipulation of these cell lines, I provide in vivo evidence that polyubiquitin binding by

MDA5, as well as its ATPase/helicase activity, are important for its activation. In addition, by testing candidate E2 and E3 enzymes that have been implicated in antiviral signaling pathways, I show that an E3 ligase, Trim25, and a K63-specific E2 enzyme, Ubc13, are essential for MDA5 activation in vivo.

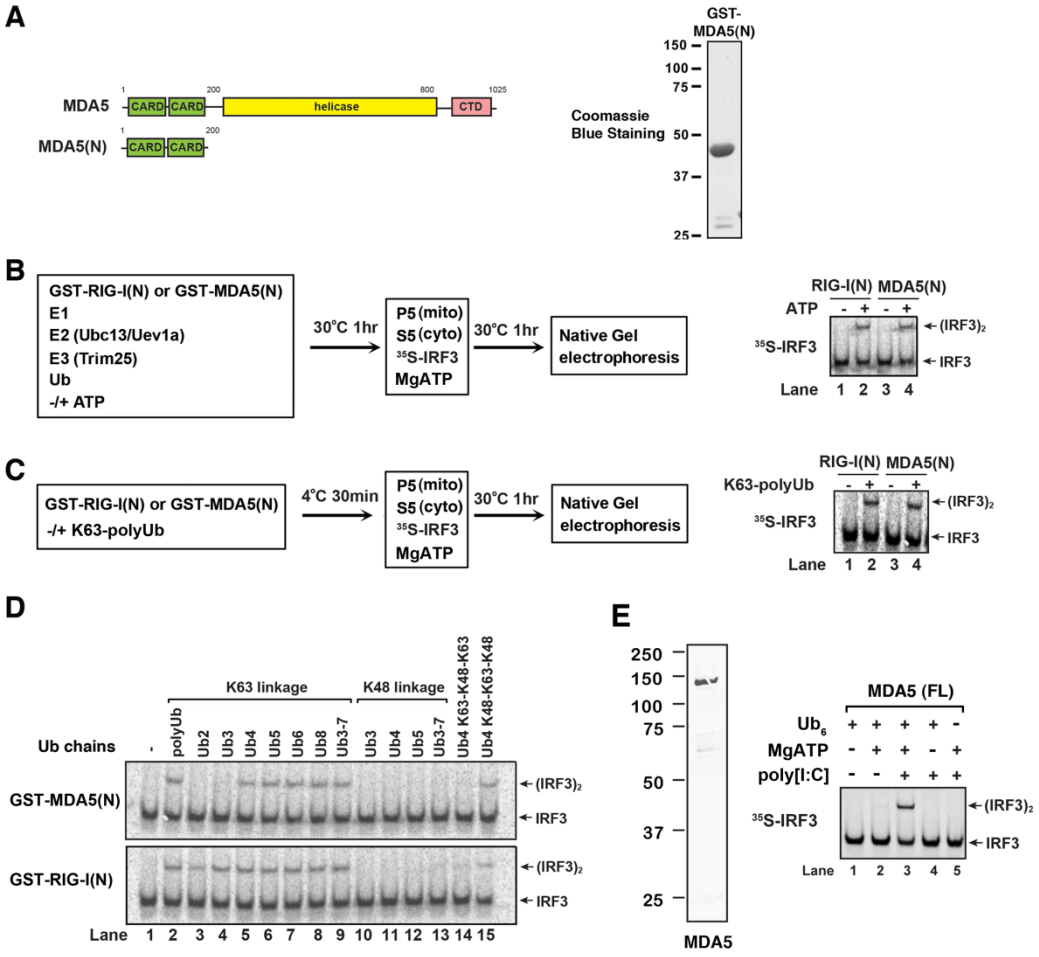

Figure 5.1. MDA5 activates IRF3 in a cell-free system through a ubiquitin-dependent mechanism.

(A) Diagram of MDA5 (left); Coomassie blue stained gel of MDA5 N-terminal CARD domains (right).

(B) GST-RIG-I(N) or GST-MDA5(N) was incubated with ubiquitination components as shown in the diagram. Aliquots of the ubiquitination reaction mixtures were then added to mitochondria (P5) and cytosolic extracts (S5) together with 35S-IRF3 and ATP. IRF3 dimerization was analyzed by native gel electrophoresis.

(C) Similar to (B), except that RIG-I(N) or MDA5(N) was incubated with polyubiquitination mixtures in which E1 and E2 had been inactivated by NEM.

(D) Similar to (C), except that RIG-I(N) or MDA5(N) was incubated with free ubiquitin chains of different lengths and linkages as indicated.

(E) Similar to (C), except that full-length (FL) MDA5 was incubated with K63-Ub6, MgATP, and poly[I:C] as indicated. Shown on the left is Coomassie blue stained gel of MDA5 protein.

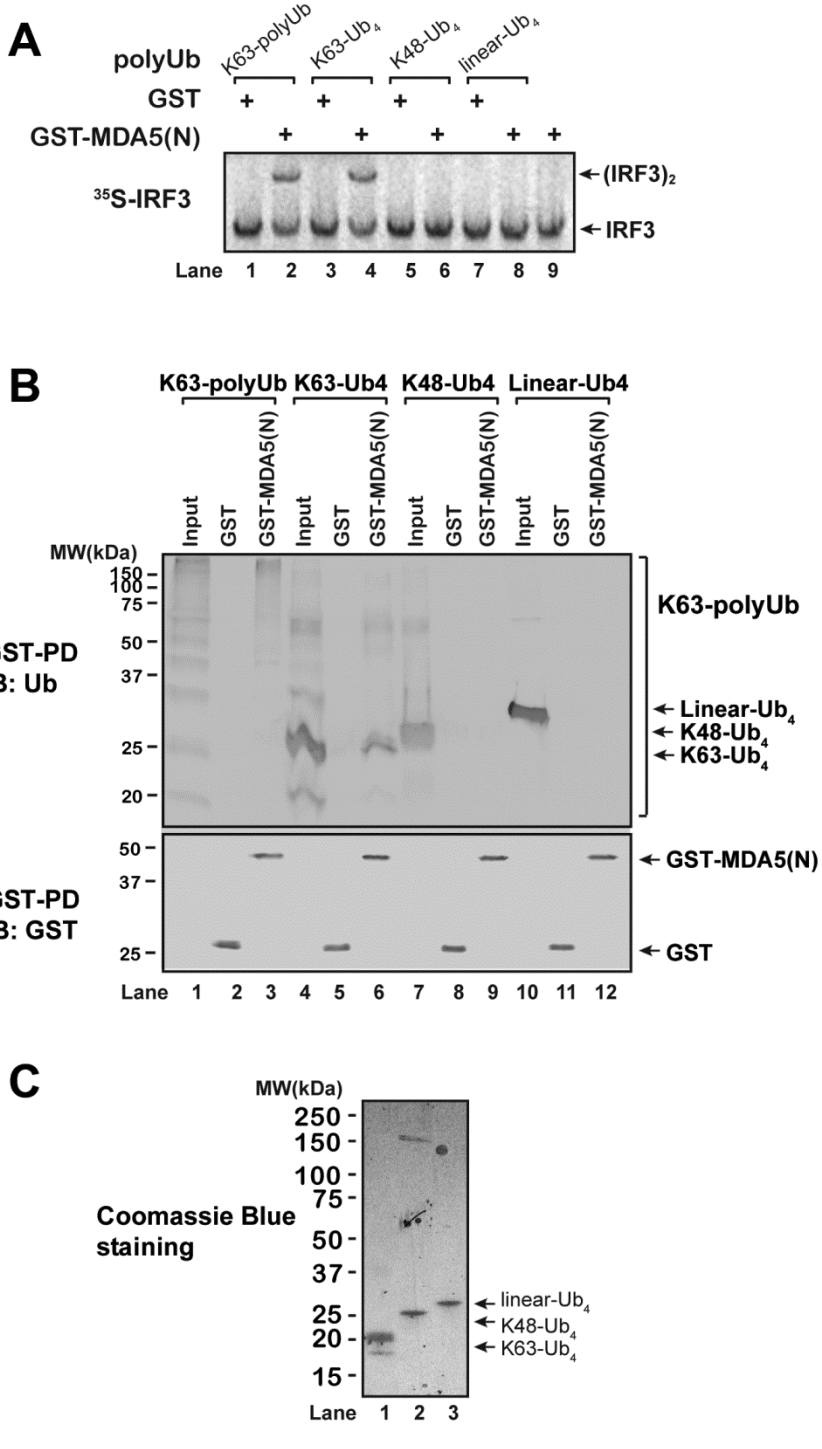
A
polyUb
K63-polyUb
K63-Ub4
K48-Ub4
linear-Ub4
GST
GST-MDA5(N)
35S-IRF3
(IRF3)2
IRF3
Lane 1 2 3 4 5 6 7 8 9
B
K63-polyUb K63-Ub4 K48-Ub4 Linear-Ub4
Input GST GST-MDA5(N)
MW(kDa)
150
100
75
50
37
25
20
GST-PD
IB: Ub
K63-polyUb
Linear-Ub4
K48-Ub4
K63-Ub4
GST-PD
IB: GST
GST-MDA5(N)
GST
Lane 1 2 3 4 5 6 7 8 9 10 11 12
C
MW(kDa)
250
150
100
75
50
37
25
20
15
Coomassie Blue
staining
linear-Ub4
K48-Ub4
K63-Ub4
Lane 1 2 3

Figure 5.2. K63 polyubiquitin chains bind and activate MDA5 CARD domains.

(A-B) GST or GST-MDA5(N) was incubated with ubiquitin chains of indicated lengths and linkages, and then assayed for its ability to activate the MAVS-IRF3 pathway in the in vitro reconstitution system (A), and its ability to bind ubiquitin chains by GST pull-down (GST-PD) experiments (B). Input represents 10% of polyubiquitin used for GST-PD experiments.

(C) Coomassie blue staining of polyubiquitin chains used in (A) and (B).

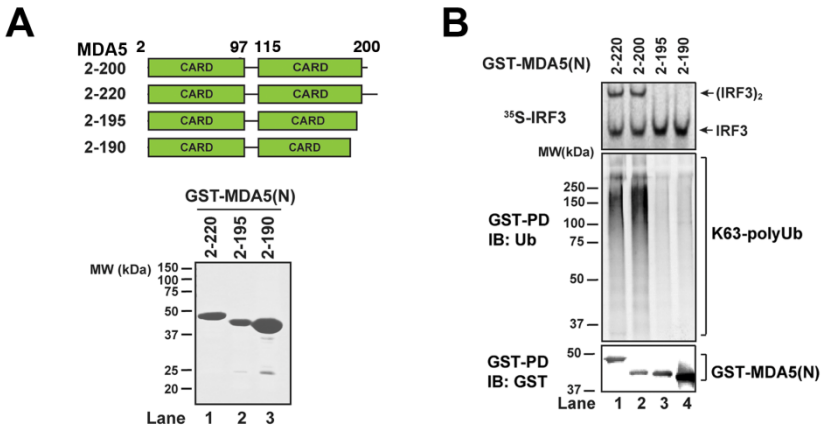

Figure 5.3. Correlation of the functional boundaries for the two activities of MDA5 CARD domains: ubiquitin binding and IRF3 activation.

(A) Diagram and Coomassie blue stained gel of MDA5(N) fragments.

(B) Fragments of MDA5(N) protein shown in (A) were tested for polyUb binding by GST pull-down and IRF3 activation in the cell-free assay containing mitochondria and cytosolic extracts.

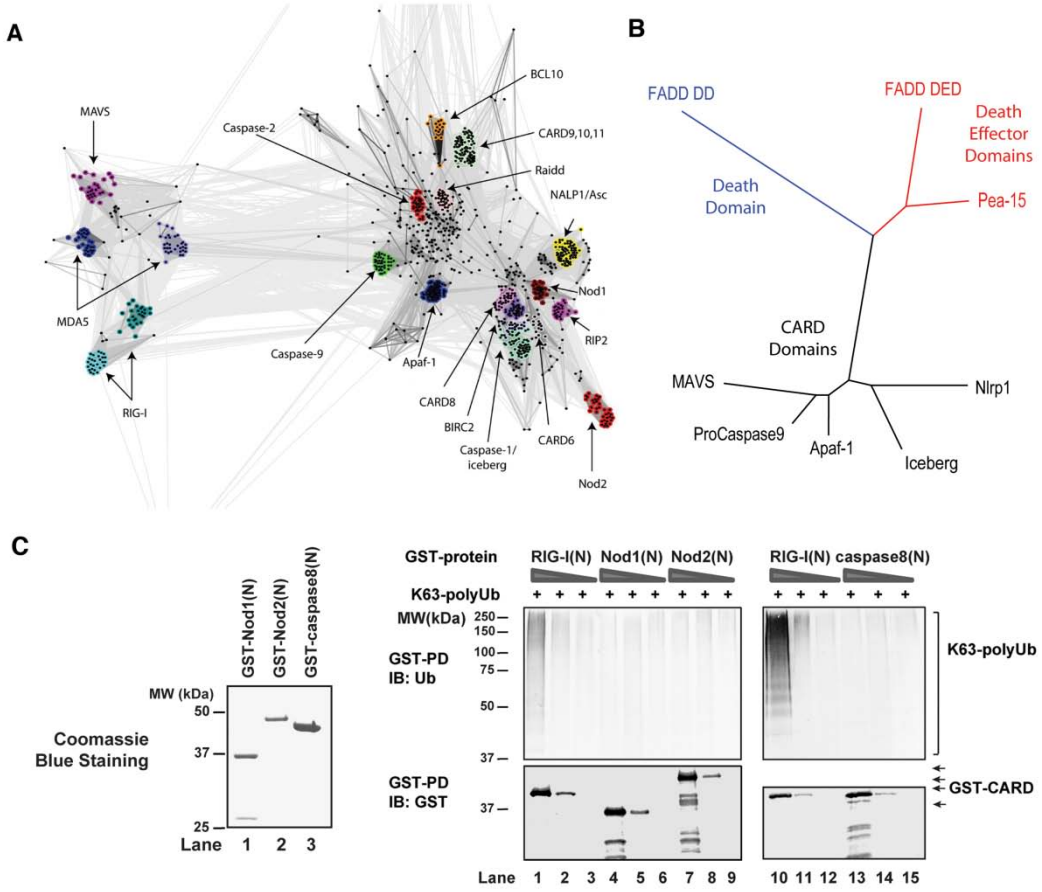

Figure 5.4. Unique polyubiquitin binding activity of RIG-I and MDA5 CARD domains.

(A) Clustering analysis of CARD domains based on their sequence homology and evolutionary distance. Each dot indicates a protein domain in the database, and the lines indicate evolutionary distances between the domains.

(B) Structure-based distance tree of example CARDs, DEDs and DDs.

(C) GST-tagged CARD domains of Nod1 and Nod2, and DED domains of caspase8 were expressed and purified from *E. coli*, incubated with K63 polyubiquitin chains and tested for their ability to bind polyubiquitin by GST pull-down experiments.

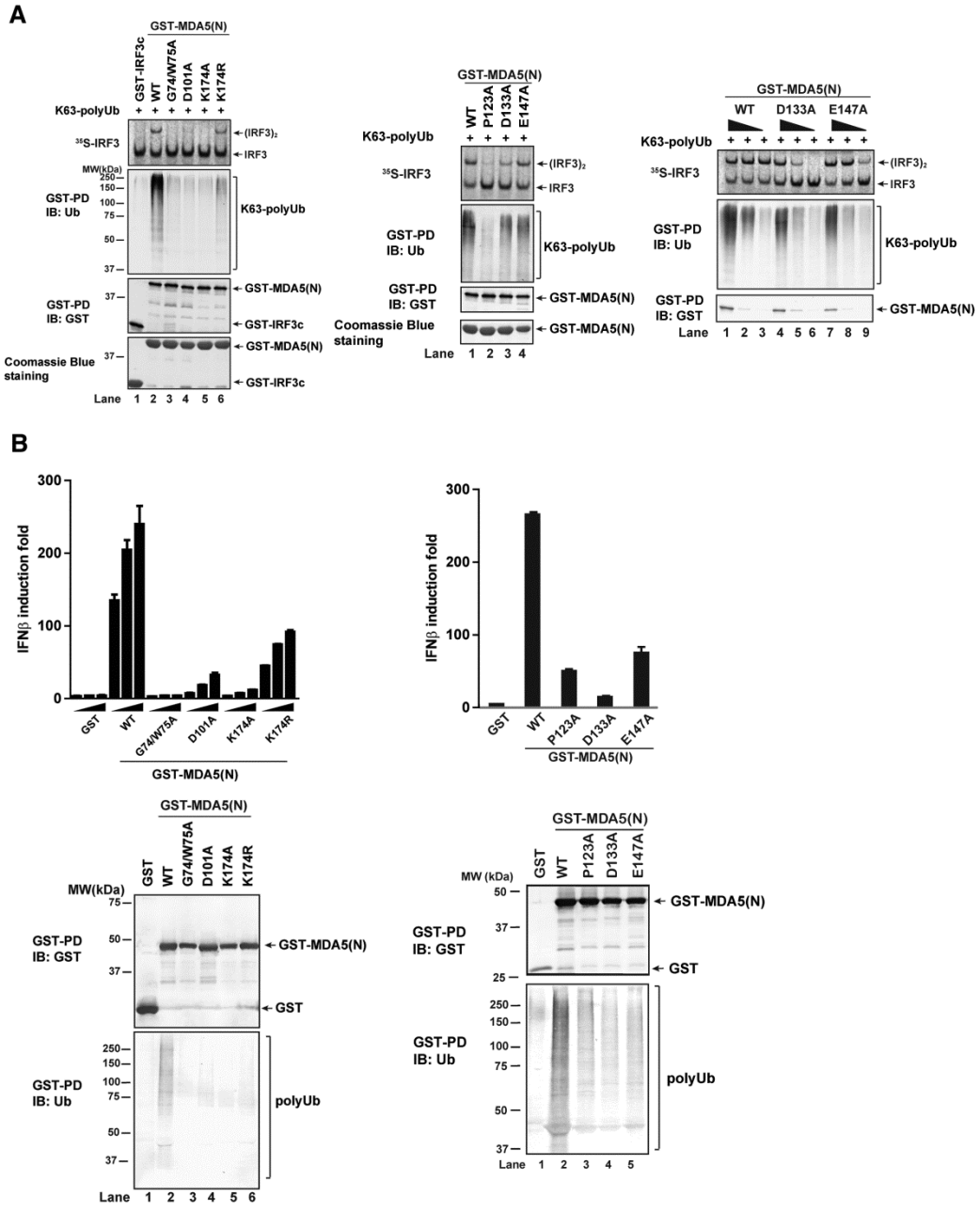
A
GST-MDA5(N)
GST-IRF3c
WT
G74/W75A
D101A
K174A
K174R
K63-polyUb
35S-IRF3
(IRF3)2
IRF3
MW(kDa)
GST-PD IB: Ub
K63-polyUb
GST-PD IB: GST
GST-MDA5(N)
GST-IRF3c
Coomassie Blue staining
Lane 1 2 3 4 5 6
WT
P123A
D133A
E147A
Lane 1 2 3 4
Lane 1 2 3 4 5 6 7 8 9
B
IFNβ induction fold
GST
GST-MDA5(N)
MW(kDa)
polyUb
Lane 1 2 3 4 5 6
MW (kDa)
Lane 1 2 3 4 5

Figure 5.5. Ubiquitin binding is essential for MDA5 activation.

(A) Conserved residues of MDA5(N) were mutated (see also Figure 4.8A), and mutant proteins were expressed and purified from *E. coli*. Point mutants of MDA5(N) were incubated with K63 polyUb, and tested for polyUb binding by GST pull-down and IRF3 activation in the cell-free assay containing mitochondria and cytosolic extracts.

(B) Expression vectors for GST-MDA5(N) were transfected into HEK293T cells together with IFNβ-luciferase and pRL-CMV reporter vectors. Cell lysates were assayed for luciferase activity (top) or pulled down with glutathione Sepharose followed by immunoblotting (bottom).

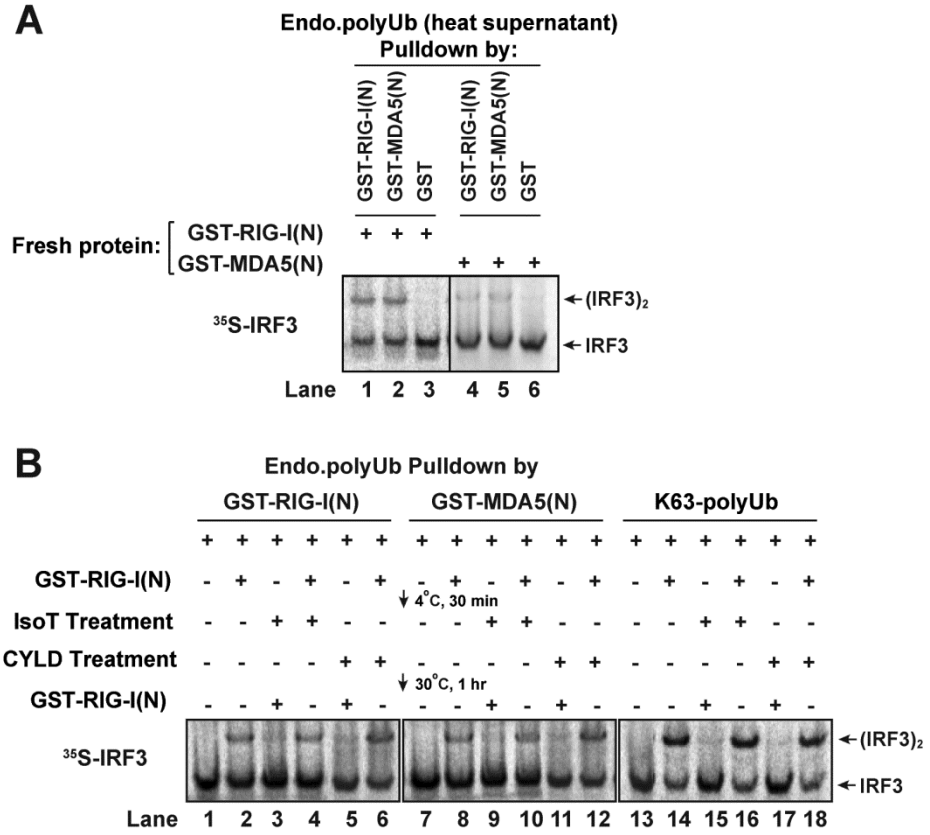

Figure 5.6. MDA5 CARD domains associate with endogenous free K63 polyubiquitin chains from human cells.

(A) Similar to Figure 4.11A, GST, GST-RIG-I(N) or GST-MDA5(N) was expressed in HEK293T cells and pulled down with glutathione Sepharose. Associated polyubiquitin chains were captured and released at 75ºC. The heat-resistant supernatant was incubated with fresh GST-RIG-I(N) or GST-MDA5(N). RIG-I(N) and MDA5(N) was then tested for their ability to activate IRF3 dimerzation in vitro.

(B) Endogenous polyUb pulled down by GST-RIG-I(N) or GST-MDA5(N) were incubated with fresh GST-RIG-I(N), and treated with IsoT or CYLD in the orders as indicated (lanes 1-12). The activity of GST-RIG-I(N) was then measured by in vitro IRF3 dimerzation assays. Parallel experiments were carried out with in vitro synthesized free K63 polyubiquitin chains (lanes 13-18).

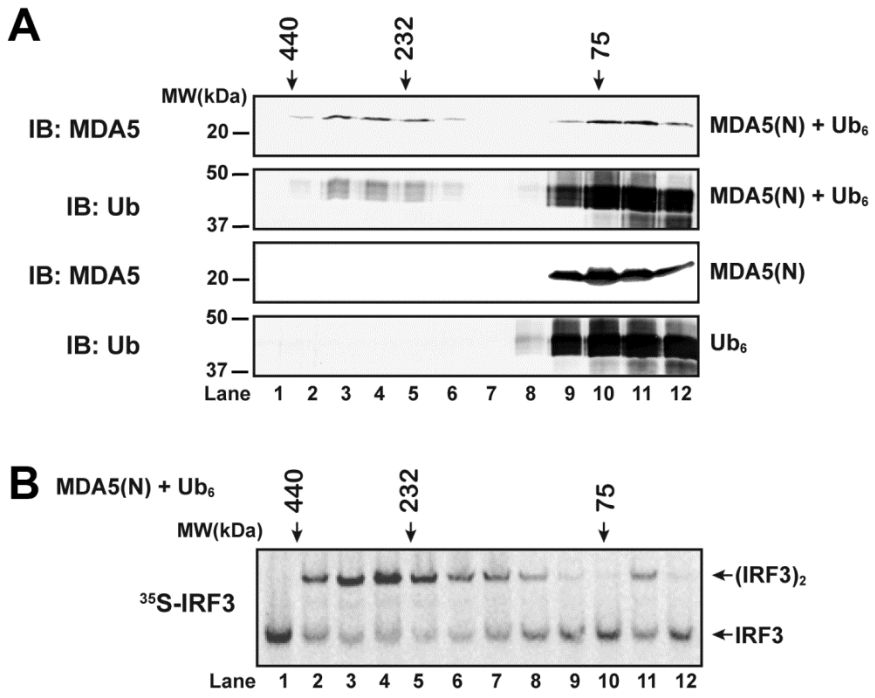

Figure 5.7. Polyubiquitin binding induces oligomerization of MDA5 CARD domains.

(A-B) MDA5 (no GST tag) was incubated with K63-linked Ub6, and then fractionated using Superdex-200 gel filtration column. Aliquots of the fractions were analyzed for MDA5 and Ub6 oligomerization with SDS-PAGE followed by immunoblotting (A), and for their ability to activate IRF3 dimerization in vitro (B).

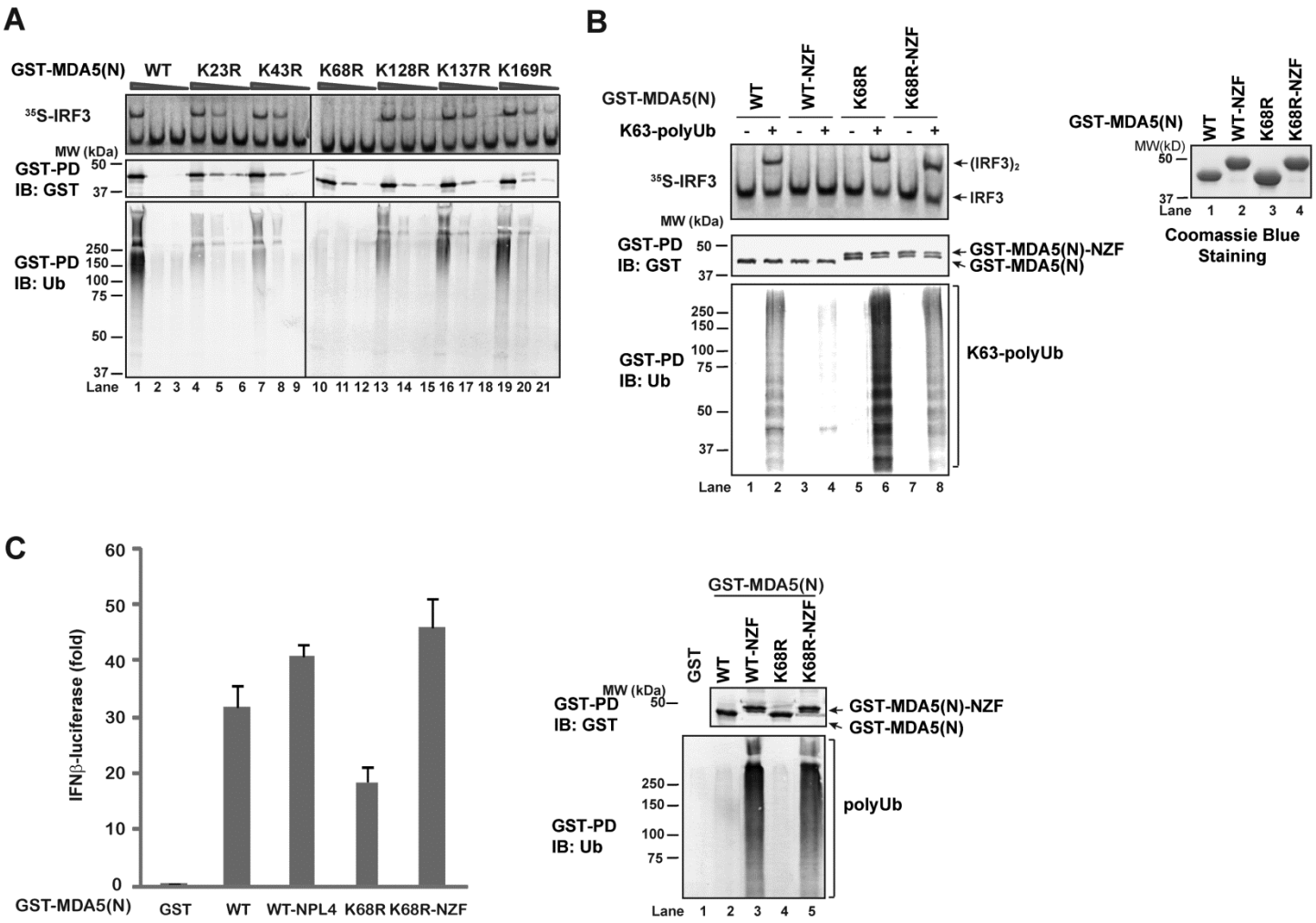
A
GST-MDA5(N) WT K23R K43R K68R K128R K137R K169R
35S-IRF3
MW (kDa)
GST-PD IB: GST
50
37
GST-PD IB: Ub
250
150
100
75
50
37
Lane 1 2 3 4 5 6 7 8 9 10 11 12 13 14 15 16 17 18 19 20 21
B
GST-MDA5(N) WT WT-NZF K68R K68R-NZF
K63-polyUb - + - + - + - +
35S-IRF3
(IRF3)2
IRF3
MW (kDa)
GST-PD IB: GST
50
37
GST-MDA5(N)-NZF
GST-MDA5(N)
GST-PD IB: Ub
250
150
100
75
50
37
K63-polyUb
Lane 1 2 3 4 5 6 7 8
GST-MDA5(N) WT WT-NZF K68R K68R-NZF
MW(kD)
50
37
Lane 1 2 3 4
Coomassie Blue Staining
C
IFNβ-luciferase (fold)
60
50
40
30
20
10
0
GST-MDA5(N) GST WT WT-NPL4 K68R K68R-NZF
GST-MDA5(N)
GST WT WT-NZF K68R K68R-NZF
MW (kDa)
GST-PD IB: GST
50
GST-MDA5(N)-NZF
GST-MDA5(N)
GST-PD IB: Ub
250
150
100
75
polyUb
Lane 1 2 3 4 5

Figure 5.8. NZF ubiquitin binding domain fusion to MDA5 ubiquitin binding mutant rescues its ability to activate IRF3 and induce IFNβ.

(A) Point mutants of MDA5(N) were expressed and purified from *E. coli*, and tested for their ubiquitin binding activity and for their ability to activate the IRF3 pathway in vitro.

(B) MDA5(N) WT and K68R and their NZF fusion proteins were tested for ubiquitin binding and for their ability to activate the IRF3 pathway in vitro. The right panel shows GST-MDA5(N) Wt and K68R mutant and their NZF fusion proteins.

(C) MDA5(N)-NZF fusion enhances the ability of K68R to activate IFNβ reporter in vivo. Expression vectors for GST-MDA5(N) proteins are transfected into HEK293T cells with IFNβ-luciferase and pRL-CMV reporter vectors. Cell lysates were assayed for luciferase activity (left) or pulled down with glutathione Sepharose followed by immunoblotting (right).

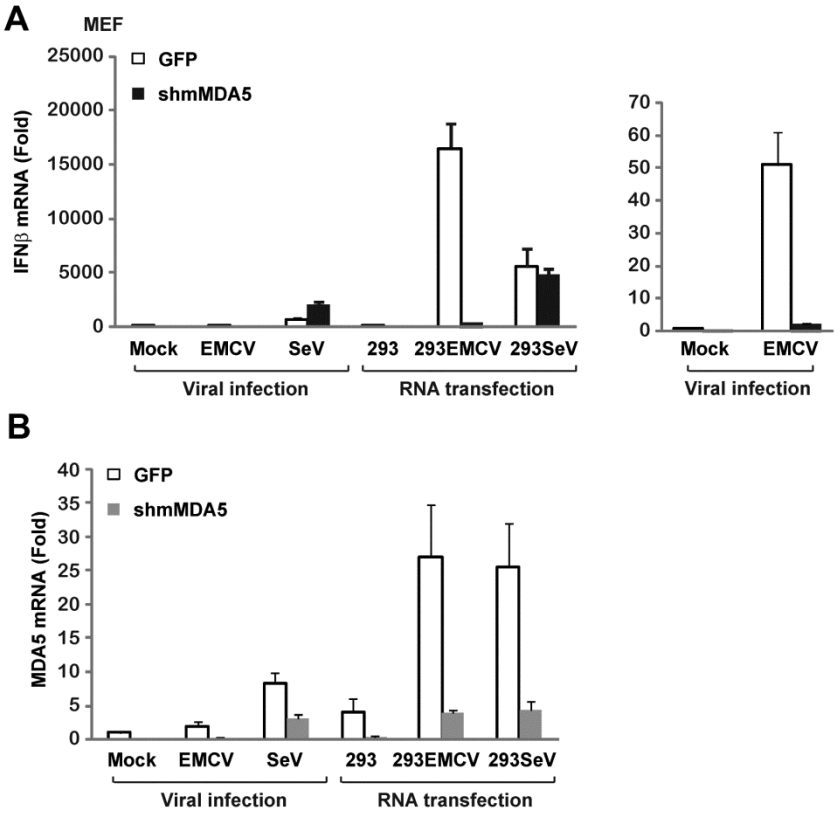

Figure 5.9. Transfection of RNA isolated from EMCV infected cells induces IFNβ in a MDA5-dependent manner in MEF cells.

(A) MEF cells stably expressing GFP or shRNA targeting mouse MDA5 (shmMDA5) were treated with virus infection (EMCV or SeV) or RNA transfection (with RNA from normal HEK293T cells virus infected HEK293T cells). IFNβ induction was measured by quantitative PCR. The right panel shows a zoomed-in view of part of the left panel.

(B) Experiments were carried out as in (A), and MDA5 mRNA levels were measured by quantitative PCR.

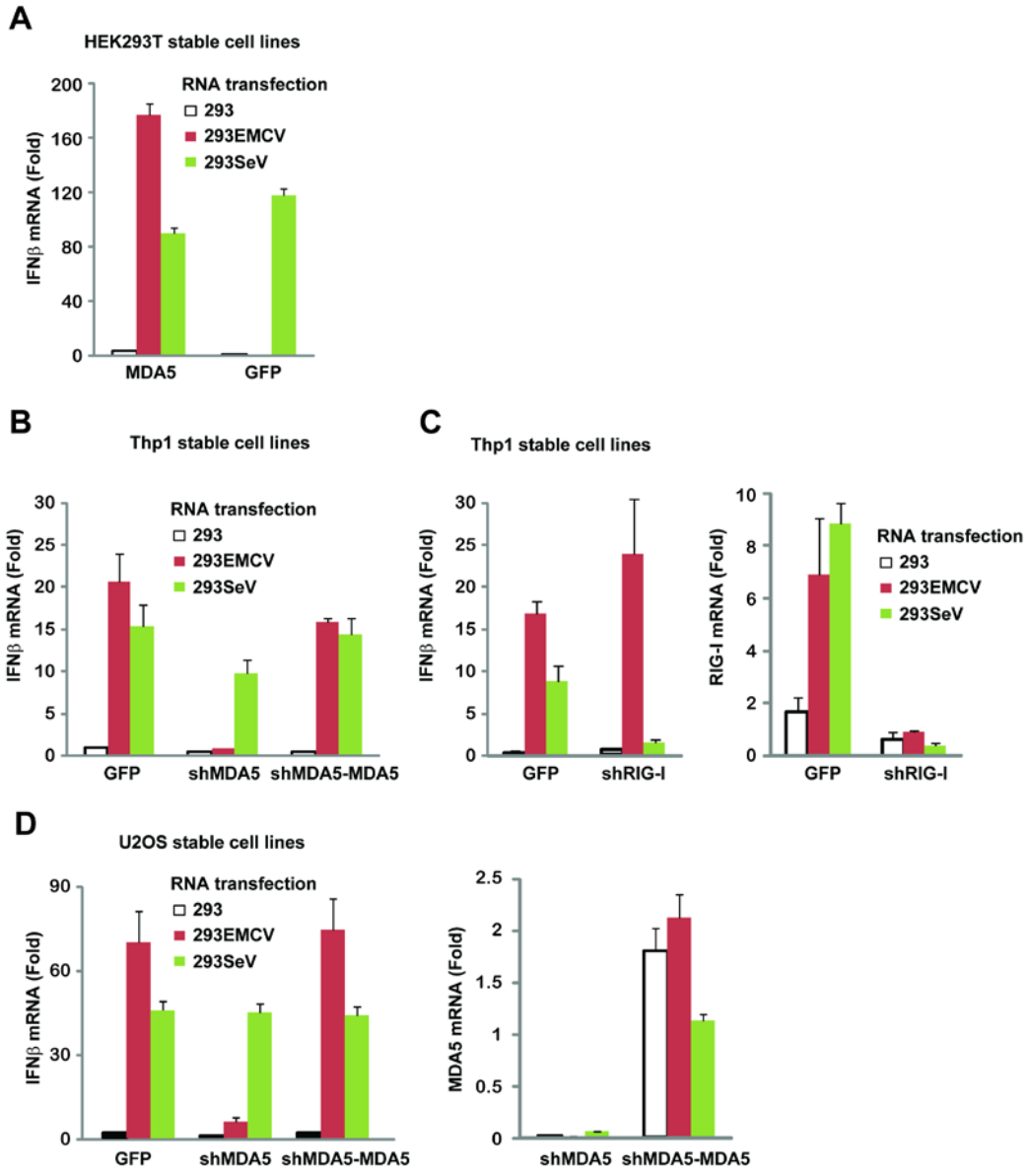

Figure 5.10. Establishment of cell based models to mimic virus infection induced IFNβ production mediated by MDA5.

(A) HEK293T cells stably expressing GFP or MDA5 were transfected with RNA isolated from normal HEK293T cells (293) or from HEK293T cells that had been infected with EMCV or SeV (293EMCV or 293SeV). IFNβ induction was measured by quantitative PCR.

(B-C) Thp1 stable cells were established to express GFP, or shRNA targeting MDA5 (shMDA5), or to contain a rescue construct expressing both shMDA5 and MDA5 cDNA that is resistant to shMDA5 knockdown (shMDA5-MDA5) (B). Cells expressing shRNA targeting RIG-I (shRIG-I) were also established (C). Cells were transfected with indicated RNA. IFNβ induction was measured by quantitative PCR. RIG-I knockdown were also monitored (C, right).

(D) Similar to (B), except in U2OS cells.

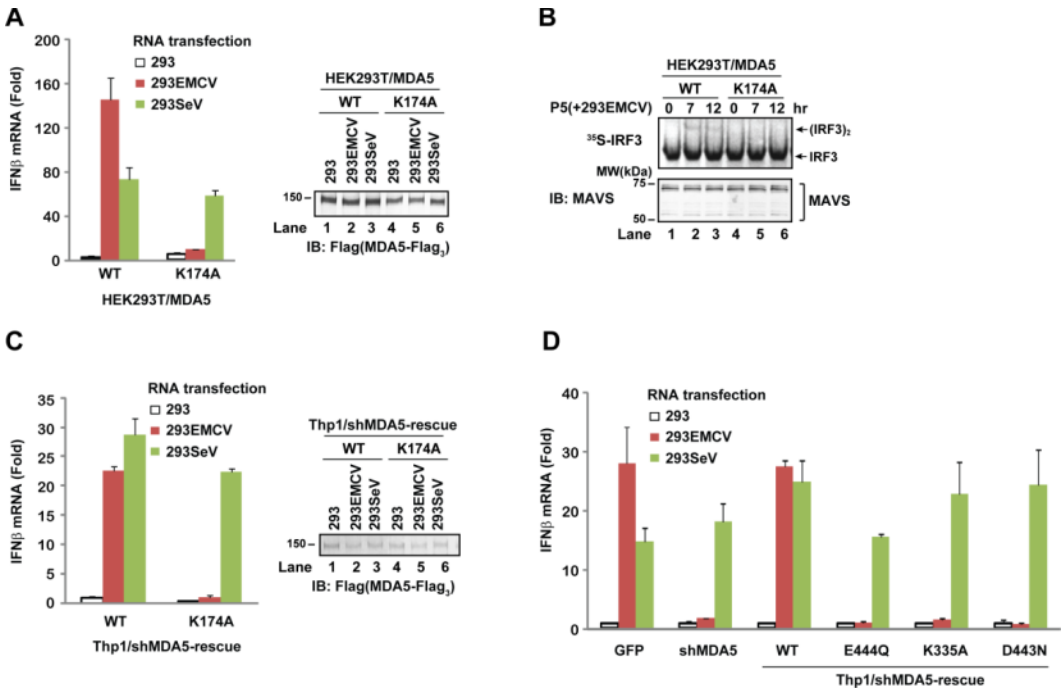

Figure 5.11. Ubiquitin binding is essential for MDA5 activation in cell based virus infection models.

(A) In HEK293T cells stably expressing MDA WT or K174A, indicated RNA was transfected, and IFNβ production was measured by quantitative PCR. MDA5 expression was shown in the right panel.

(B) RNA transfection experiments were carried out as in (A), and then mitochondria fractions (P5) were tested for their ability to activate the IRF3 pathway in vitro.

(C) Thp1 stable cells were established to express shMDA5 and MDA5 cDNA (Thp1/shMDA5-rescue cell lines). RNA transfection was carried out as in (A), quantitative PCR and western blots show IFNβ production and MDA5 expression level.

(D) Similar to (C), with indicated Thp1/shMDA5-rescue cell lines expressing MDA5 ATPase mutants.

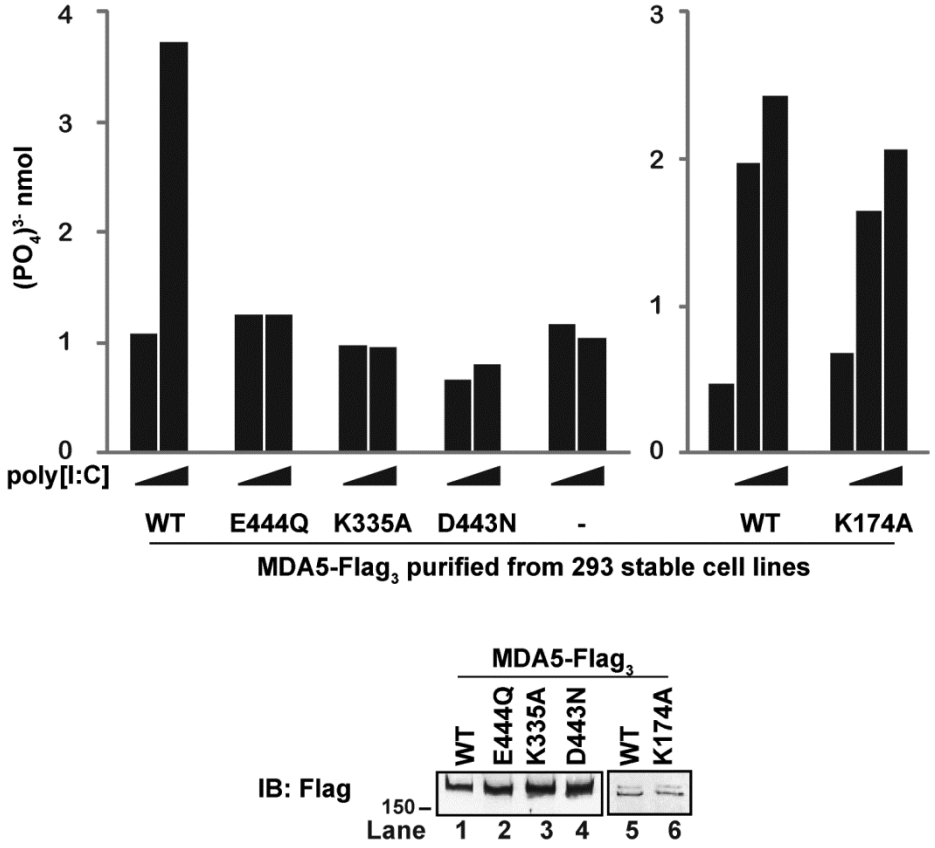

Figure 5.12. ATPase activity of MDA5 WT and mutant proteins.

MDA5 WT and mutant proteins were affinity purified from HEK293T stable cell lines expressing each protein. 500 ng of each MDA5 protein was incubated with 0, 500 ng (left), or 0, 200 ng, 500 ng (right) poly[I:C] in the presence of Mg-ATP. End point concentration of $(PO_4)^{3-}$ was measured using BioMol Green reagent as an indicator for MDA5 ATPase activity. Immunoblot for the proteins used were also shown.

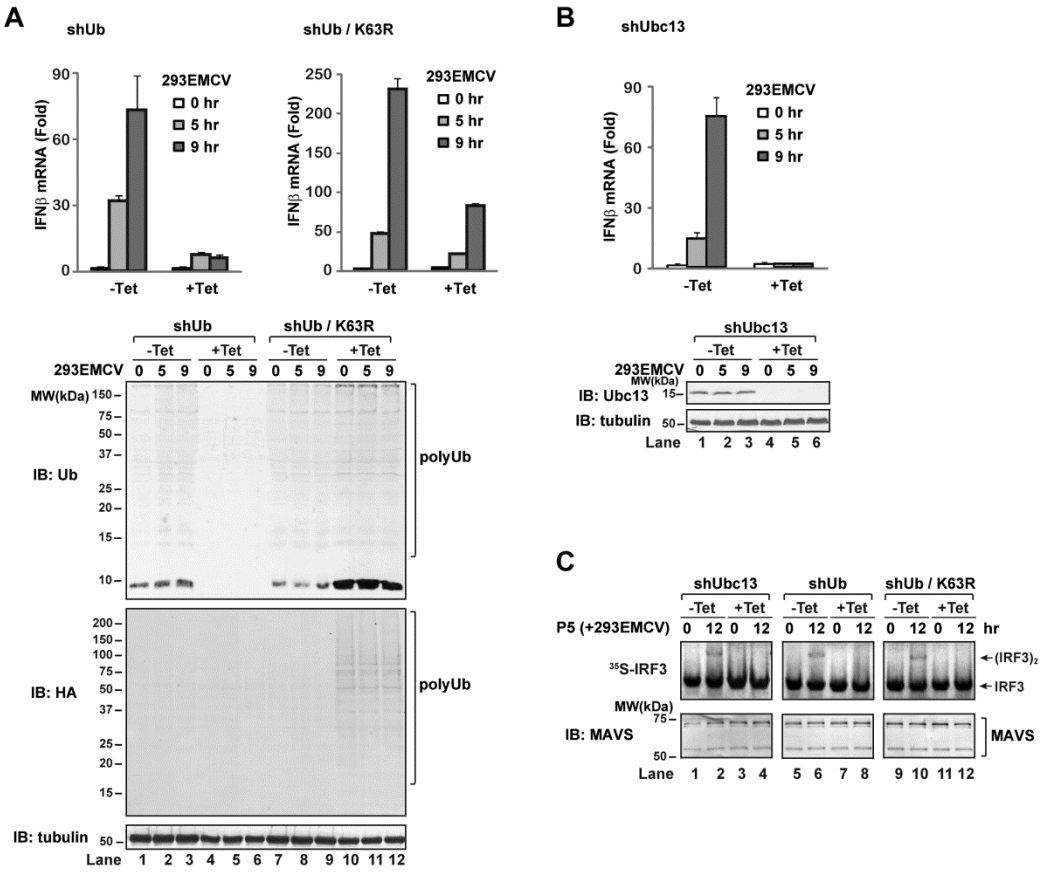

Figure 5.13. K63 ubiquitination is essential for MDA5 activation in cell based virus infection models.

(A) K63 of ubiquitin is important for MDA5 activation in vivo. U2OS cells stably integrated with tetracycline-inducible shRNA against ubiquitin (shUb, left), and cells with an additional tetracycline-inducible rescue expression vector for K63R mutant of ubiquitin (shUb/K63R, right), were treated with or without tetracycline (Tet). After transfection of 293EMCV for the indicated time, IFNβ production was measured by quantitative PCR. Knockdown efficiency was shown with immunoblotting for ubiquitin and HA (HA-K63R).

(B) Ubc13 is essential for MDA5 activation in vivo. Similar to (A), except with U2OS integrated with tetracycline-inducible shRNA against Ubc13 (shUbc13).

(C) RNA transfection experiments were carried out as in (A) and (B). Mitochondria fractions (P5) of cells were tested for their ability to activate IRF3 dimerization in vitro.

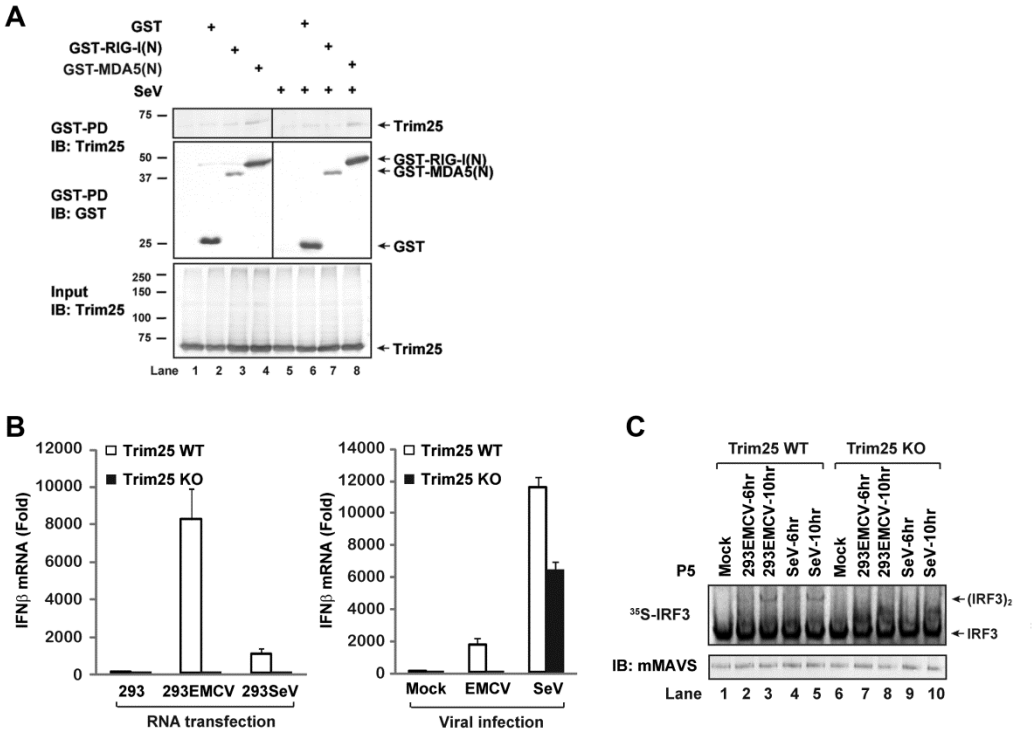

Figure 5.14. Trim25 is essential for MDA5 activation in vivo.

(A) MDA5 CARD domains associate with Trim25. GST, GST-RIG-I(N), or GST-MDA5(N) were overexpressed in HEK293T cells. Cells were infected with SeV or mock treated. GST pull-down experiments were performed followed by immunoblotting. Cell lysates input were used for immunoblotting Trim25.

(B) Trim25 WT or KO MEF cells were transfected with indicated RNA(left), or infected with virus (right). IFNβ production was measured by quantitative PCR.

(C) RNA transfection experiments were carried out as in (B). Mitochondria fractions (P5) of cells were tested for their ability to activate IRF3 dimerization in vitro.

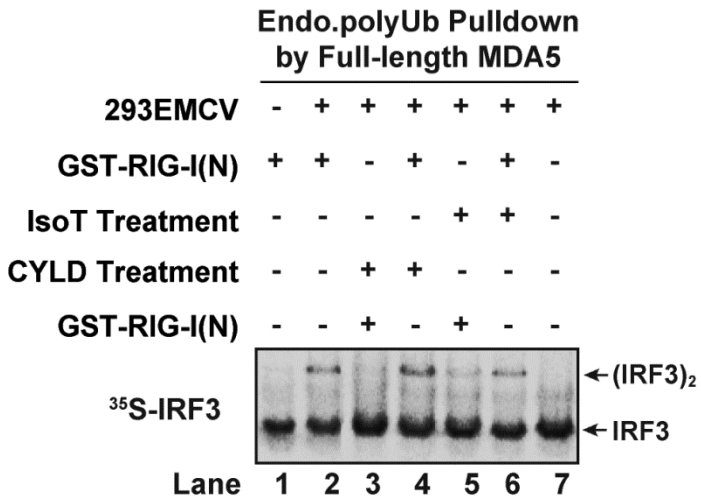

Figure 5.15. Endogenous free K63 polyubiquitin chains associate with activated MDA5.

Similar to Figure 4.11 and Figure 5.6, endogenous polyUb chains associated with MDA5 were isolated from human cells. HEK293T cells stably expressing MDA5 were transfected with 293EMCV or mock treated. Flag-tagged MDA5 was immunoprecipitated with M2-agarose. Associated polyubiquitin chains were released by heating at 75ºC. The heat-resistant supernatant was incubated with fresh GST-RIG-I(N), and treated with IsoT or CYLD in the orders as indicated. The activity of GST-RIG-I(N) was then measured by in vitro IRF3 dimerzation assays.

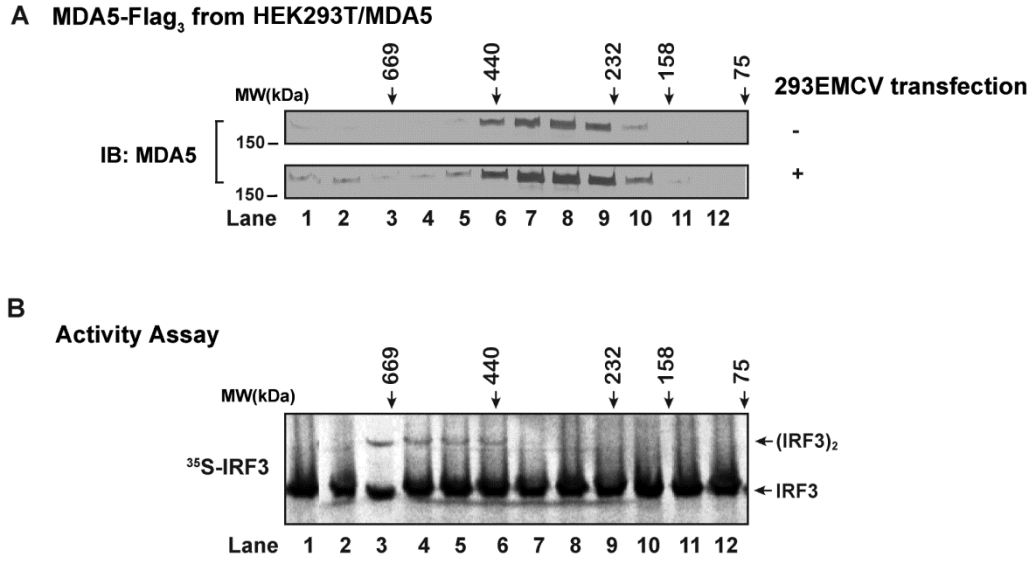

Figure 5.16. Activated MDA5 forms high molecular weight oligomers in vivo.

(A) MDA5 was purified from HEK293T/MDA5 cells that had been transfected with 293EMCV or mock treated, and then analyzed with Superdex-200 gel filtration column followed by immunoblotting.

(B) Superdex-200 fractions of activated MDA5 as in (A) bottom panel were tested for their ability to activate the MAVS-IRF3 pathway in vitro.

CHAPTER VI

DISCUSSION AND FUTURE DIRECTIONS

VI.1. Conclusions

In this dissertation, I describe the mechanisms of how ubiquitin is involved in the activation of RIG-I and MDA5, two important intracellular receptors detecting foreign RNA.

Based on an in vitro biochemical assay system for the activation of mitochondria antiviral signaling protein MAVS, I set out to purify a cytosolic MAVS activator. The correlation between RIG-I and ubiquitin with the purified "MAVS activator" activity, as well as evidence from on-going development in the field, suggested ubiquitin plays an important role in the activation of RIG-I. Biochemical characterization of the interaction between RIG-I CARD domains and polyubiquitination led to the discovery that polyubiquitin binding induced RIG-I CARD domains oligomerization and activation. The ubiquitin-induced oligomerization-activation mechanism was also observed with full length RIG-I protein. RIG-I detects foreign RNA, and activates MAVS. This study uncovered an additional step in RIG-I activation, that is, sequential binding to RNA ligand and polyubiquitin induces stepwise assembly of the activate RIG-I complex. In vivo data also support the importance of ubiquitin binding for RIG-I oligomerization and activation induced by virus infection.

The family of intracellular RIG-I-like receptors (RLRs) also includes MDA5 and LGP2. I have extended the study of CARD domain activation to MDA5, and showed that MDA5 CARD domains also undergo ubiquitin-binding induced oligomerization. In vitro characterization showed that ubiquitin-binding is important for the activation of MDA5 CARD domains. In vivo data also support the importance of K63 ubiquitination and MDA5 ubiquitin binding for MDA5 activation.

VI.2. Structural Understanding of RIG-I Activation

The structure of RIG-I and MDA5 C-terminal domains (CTD) were determined by several groups[54-56, 62, 346]. More recently, crystal structures were determined for RIG-I (one for duck RIG-I helicase domain, and another two for duck or human RIG-I without CARD domains, i.e. helicase-CTD) in complex with different RNA ligands, as well as ligand-free structures for duck RIG-I helicase domain, CARDs-helicase, and full length protein[57-59]. Another crystal structure for MDA5 helicase subdomain (HEL1) is to be published (PDB accession code 3b6e). These structures revealed that RNA binding to RIG-I is mediated by multiple domains, including two helicase subdomains (HEL1 and HEL2), an insertion helicase subdomain (HEL2i), a V-shaped pincer domain connecting helicase and CTD, and the CTD (name changed from RD to CTD, because based on the recent structures it is not likely directly involved in auto-repression). RNA binding to RIG-I results in dramatic structural rearrangements and conformational changes among these domains. Specifically, in resting state, the overall structure of RIG-I helicase-CTD

domains is likely in an extended and flexible conformation with auto-suppressive interaction between the helicase domain and the CARD domains, hindering dsRNA binding to the helicase domain and polyubiquitin binding to the CARDs, while CTD is available for specific binding to 5'-pppRNA. Initial binding of 5'-pppRNA to CTD triggers co-operative binding of dsRNA and ATP to the helicase domain. Dramatic conformational changes occur and the helicase-CTD domains assume a compact formation surrounding dsRNA, probably resulting in the release of CARD domains.

Of particular interest, one study solved two structures containing CARD domains in the context of other parts of duck RIG-I, without any ligand (PDB accession codes: 4a2q for dRIG-I CARDs-helicase, 4a2w for full-length dRIG-I). These structures revealed the interactions between the two CARD domains (CARD1 and CARD2), and between CARD2 and the insertion helicase domain (HEL2i). There is intimate contact between CARD1 and CARD2 (Figure 6.1A). The structure strongly suggests that the tandem CARDs form an essentially rigid functional unit, consistent with the fact that both CARDs are required as one intact functional unit for signaling. The CARD1-CARD2 interface contact is mediated by conserved residues. Notably, two residues characterized in this study, E135 and K164 of human RIG-I, might position close to this interface when mapped to homologous residues on duck RIG-I (Figure 6.2).

CARD2's extensive contact with the HEL2i domain, its proximity to the HEL1 domain, and possibly its proximity to the linker between CARD2 and the helicase domains would sterically hinder CARD2 interactions with other macromolecules (Figure 6.1B). Two residues important for polyubiquitin binding characterized in this study,

K172 and P112 in human RIG-I, corresponds to Q170 and A111 in duck, which locate close to the CARD2-HEL2i interface. Thus, in the inactive conformation, there is probably significant steric hindrance for these residues to interact with other proteins. Upon RNA binding, these residues might open up to interact with other proteins, such as polyubiquitin, ubiquitination enzymes, or another molecule of RIG-I. Residues characterized in this study that may mediate potential interactions were summarized in Figure 6.3.

One has to keep in mind that the current structure may reflect the conformation of CARD domains of duck RIG-I in the resting state. How the two CARD domains coordinate their conformation upon RIG-I activation (and ubiquitin binding) is not yet known. It is tempting to speculate that individual ubiquitin in a chain bind to one or both of the tandem CARD domains, and the longer ubiquitin chains may actually 'chain' or 'cross-link' different RIG-I CARD domains together. Alternatively, the binding of K63 ubiquitin chains may induce a conformational change of the RIG-I CARD domains to promote their intermolecular interactions, resulting in their oligomerization. High-resolution structural studies are required to understand how ubiquitin chains bind to RIG-I CARD domains, how the oligomerization occurs, and how it terminates to produce RIG-I tetramers.

Nonetheless, the crystal structures of RIG-I CARD domains and the model of RIG-I conformational changes induced by RNA ligand proposed by these studies provide insights into the early steps of RIG-I activation, and are encouraging for future work to determine the following steps of RIG-I activation. Based on the model proposed by these

papers, co-operative binding of ATP and dsRNA to the helicase domain is important for inducing the conformational changes to release CARD domains. A major remaining question is: what is the precise role of ATP hydrolysis. RIG-I may hydrolyze ATP in order to adopt an optimal conformation for the presentation of the CARDs or for maintaining an active conformation. This has not been answered by these studies using non-hydrolysible ATP analogs and transition state analog. It is also known that RIG-I uses ATP hydrolysis to translocate along dsRNA[67]. The precise function of this translocation is not clear. It is tempting to speculate that the ATP-hydrolysis-powered translocation arranges RIG-I molecules in optimized spatial positions and/or maintains RIG-I in an active form, such as a ubiquitin-bound tetramer. Further structure studies as well as single molecule studies focusing on the role of ATP hydrolysis should be informative. Structure studies on the active form of RIG-I, in complex with RNA, ATP and polyubiquitin, should also be very informative. Together structure studies will be helpful in providing an integrated picture of the complete multistage process of RIG-I activation.

Structural information of RIG-I may be helpful in determining the structures of MDA5 and LGP2. Compared to RIG-I, the most striking sequence differences in MDA5 are the significantly longer linker between CARD2 and the helicase domain, and some structure features of the helicase insertion domain. Structure-based functional differences may help explain mechanistic differences between MDA5 and RIG-I.

VI.3. Regulation of Ubiquitin-Dependent RIG-I Activation Mechanisms In Vivo

We estimated that approximately 10 ng of endogenous K63-Ub6 could be isolated from 20 million HEK293T cells using our protocol[339]. This is equivalent to approximately 6000 molecules of K63-Ub6 per cell. These Ub chains can activate RIG-I with an EC50 of approximately 50 pM, which is equivalent to ~15 molecules per cell. At first glance, this rough estimate seems to suggest that there should be abundant endogenous Ub chains to activate RIG-I(N), partly explaining why overexpression of RIG-I(N) is sufficient to induce IFNβ in the absence of viral infection. However, there are several issues worth considering before making a statement about the abundance of endogenous ubiquitin chains. First, this estimate was made for cells overexpressing RIG-I(N), which are different from resting cells. Second, forced cleavage of RIG-I in vivo (Figure 3.6D), generating its N-terminal fragments, was not sufficient to activate it without virus infection. There are two possible explanations for this observation. First, it is possible that N-terminal fragments generated in this way are still suppressed in vivo by the concomitantly generated C-terminal fragments containing helicase-RD domains in equal molar amount, such that even if ubiquitin chains are abundant, they cannot gain access to the CARDs. However, efficient suppression will require all N-terminal fragments to be tightly associated with C-terminal fragments without dissociating, which is unlikely because they can be easily separated in vitro. Alternatively and perhaps more likely, free K63 polyubiquitin chains free floating in resting cells are limiting, perhaps due to rapid disassembly by high levels of cellular DUB activity. These polyubiquitin chains may get a boost from incoming stimulation such as virus infection or RIG-I(N) overexpression

(the situation in which the aforementioned estimate was made), to achieve local and transient accumulation of these ubiquitin chains in the vicinity of RIG-I CARD domains. The mechanism of such a boost may be in the form of enhanced polyubiquitin synthesis, or protection from DUB activities. Notably, RIG-I CARD domains, can capture and protect K63 polyubiquitin, partly contributing to the polyubiquitin "boost". It is not clear whether there is enhanced synthesis of polyubiquitin chains as RIG-I activators, but this hypothesis is worth further investigation (discussed next).

Interestingly, a recent study provides another example of free polyubiquitin chain regulating antiviral immunity[347]. TRIM5 is an anti-retroviral protein that is also a RING-domain E3 ligase. TRIM5 was previously known to restrict retroviruses, including human immunodeficiency virus (HIV), by ubiquitinating viral capsid proteins and targeting them for proteasomal degradation. In the recent study, it was shown that HIV viral capsid strongly stimulates TRIM5 to synthesize free K63-linked polyubiquitin chains[347], which then activate the TAK1 kinase complex to trigger an innate immune response[148]. It is tempting to speculate that a similar mechanism for RIG-I also exits, in which virus infection enhances the synthesis of free polyubiquitin chains which serve as RIG-I activators. Several E3 ligases have been implicated in RIG-I activation, such as Trim25 and Riplet. To start to test this hypothesis, candidate E3s can be tested for their E3 ligase activity in resting and stimulated states. Polyubiquitin synthesis could also be regulated by the recruitment of E3s to RIG-I. Cellular localization of candidate E3s and RIG-I can be monitored. E3 ligase activity of candidate E3s should also be tested in the presence

and absence of RIG-I, to test the hypothesis that association with RIG-I could stimulate E3 activity.

VI.4. Regulation of MDA5-Mediated Antiviral Pathway

RIG-I and MDA5 share similar signaling pathways and adaptor molecules. Here I have shown that their activation mechanisms by ubiquitin binding also seem to be conserved. Yet, there are clear differences between these two proteins that are still not well understood.

RIG-I and MDA5 complement each other by responding to diverse types of nonself RNAs from different viruses. In addition to short (longer than ~20bp) blunt-end 5'-pppRNA, RIG-I can also be activated by dsRNA of intermediate length (~a few hundred base pair). Structure features of RNA ligands for MDA5 have not been well defined, except for "long double-stranded RNA". How do MDA5 and RIG-I distinguish the length of RNA ligands remain curious. Comparative structure studies of the MDA5 helicase and CTD with those of RIG-I should shed light on this question.

Endogenous RNA ligand for RIG-I during negative-strand RNA virus infection was likely viral genomic RNA[47]. Physiological RNA ligands for MDA5 can be characterized with cell-based virus infection models, such as established and described in

this dissertation. For example, after virus infection, MDA5 associated RNA could be isolated and tested for immunostimulatory activity in vivo and in vitro. Notably, in several cell lines, IFNβ production could be induced by transfection of RNA isolated from EMCV infected cells, but not by EMCV infection. Genetic manipulation of the virus would be useful in understanding the differences between RNA ligands generated by virus infection and by RNA transfection.

Although the activation of recombinant full length MDA5 in vitro is relatively robust, it appears that MDA5 purified after in vivo stimulation has weaker activity in the in vitro reconstitution assay (for example, Figure 5.16), while activated RIG-I isolated from SeV infected cells very potently activates IRF3 dimerization in vitro. It is possible that MDA5 activated with physiological ligands, in the purification conditions used here, is missing certain "cofactors". In order to understand the differences between MDA5 activation in the in vivo and the in vitro systems, physiological RNA ligand (for example, 293EMCV) should be characterized for its ability to activate MDA5 in vitro. Interestingly, MDA5 purified from HEK293T/MDA5 cells, when analyzed with gel filtration column, appeared bigger than its expected size. Identification of interacting partners should also provide starting points for further analysis of MDA5 regulation. Whether such co-factors or interacting partners are required for MDA5 oligomerization should also be tested.

The regulatory role of LGP2 in RIG-I and MDA5 pathways is still controversial because of conflicting results from genetic studies. It is not clear whether LGP2 positively or negatively regulates RIG-I, while in general, it appears that LGP2 may

positively regulate MDA5. Binding to RNA may be one of the mechanisms through which LGP2 function. Other mechanisms may also exist that do not require RNA binding[30, 53, 60, 62, 63, 348]. LGP2 might play a positive role in the MDA5 pathway by promoting RNA binding, ubiquitin binding, and oligomerization of MDA5. Both in vitro and in vivo MDA5 activation systems established in this study should facilitate the characterization of the role of LGP2 in MDA5 activation.

VI.5. MAVS Activation by RIG-I

Upon activation, MAVS forms prion-like aggregates on the outer mitochondrial membrane[85]. It was found that sub-stoichiometric amounts of RIG-I – ubiquitin chain complex can cause very rapid aggregation and activation of MAVS on the mitochondrial membrane. However, we have been unable to detect stable interaction between the CARD domains of RIG-I and that of MAVS in the presence or absence of K63 polyubiquitin chains. It remains to be determined how RIG-I tetramers become competent to trigger MAVS aggregation. RIG-I – ubiquitin chain complex might act like a catalyst in that it transiently contacts and induces a conformational change of the MAVS CARD, which in turn interacts with other MAVS to form functional aggregates. This mechanism allows for a rapid amplification of the signaling cascade upon detection of viral RNA, leading to a robust antiviral immune response. Further biochemical and structural analyses are needed to test this hypothesis.

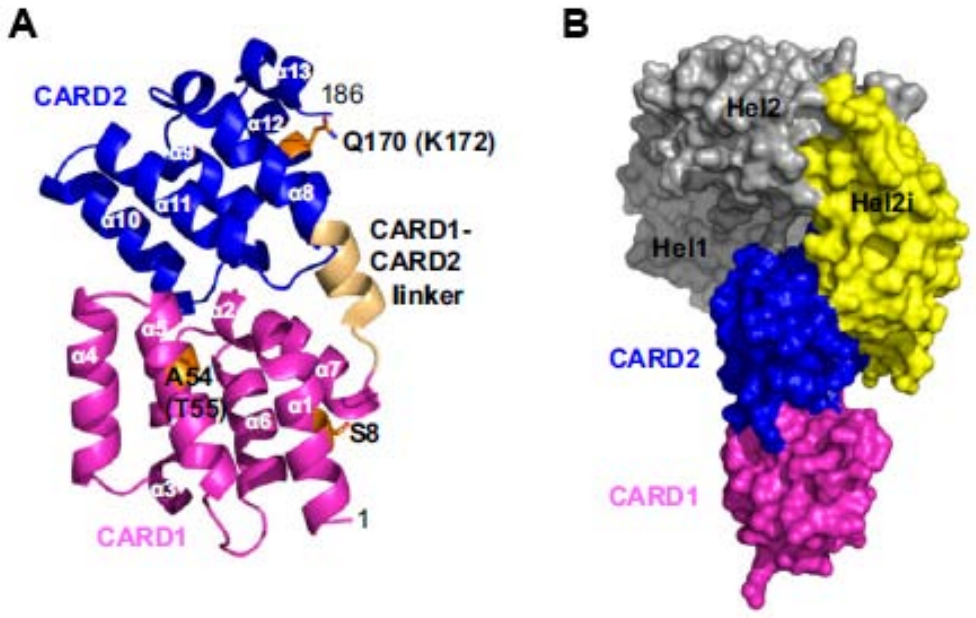

Figure 6.1. Structures of duck (*Anas platyrhynchos,* the mallard duck) RIG-I (dRIG-I) tandem CARDs and CARDs-helicase (modified from published work)[59].

(A-B) Ribbon diagram of dRIG-I tandem CARDs structure (A) and CARDs-helicase structure (B). CARD1 (magenta), CARD2 (blue), HEL2i (yellow), HEL1 and HEL2 (gray).

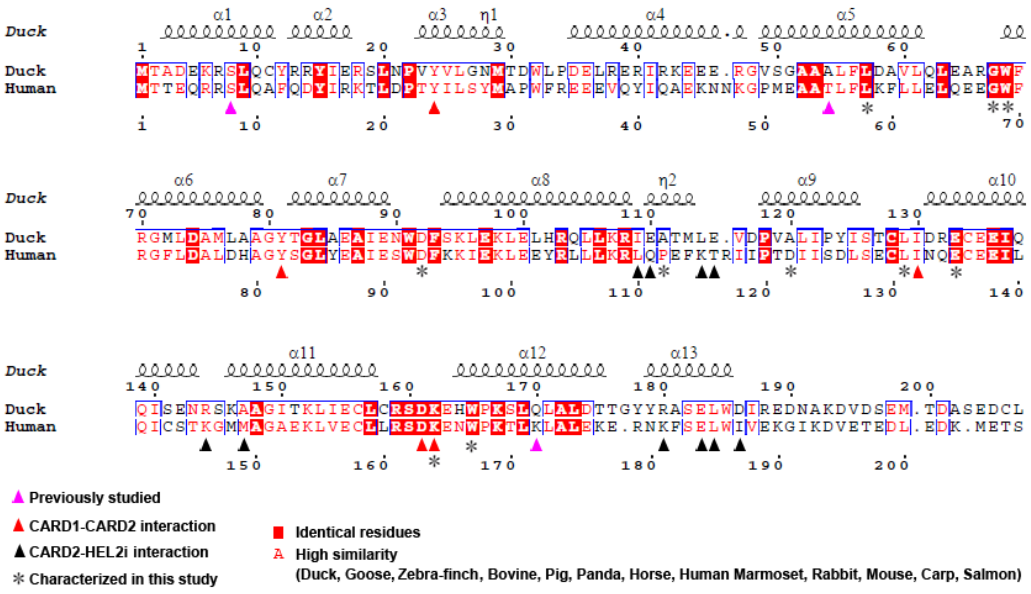

Figure 6.2. Sequence alignment of the CARD domains of RIG-I from duck and human.

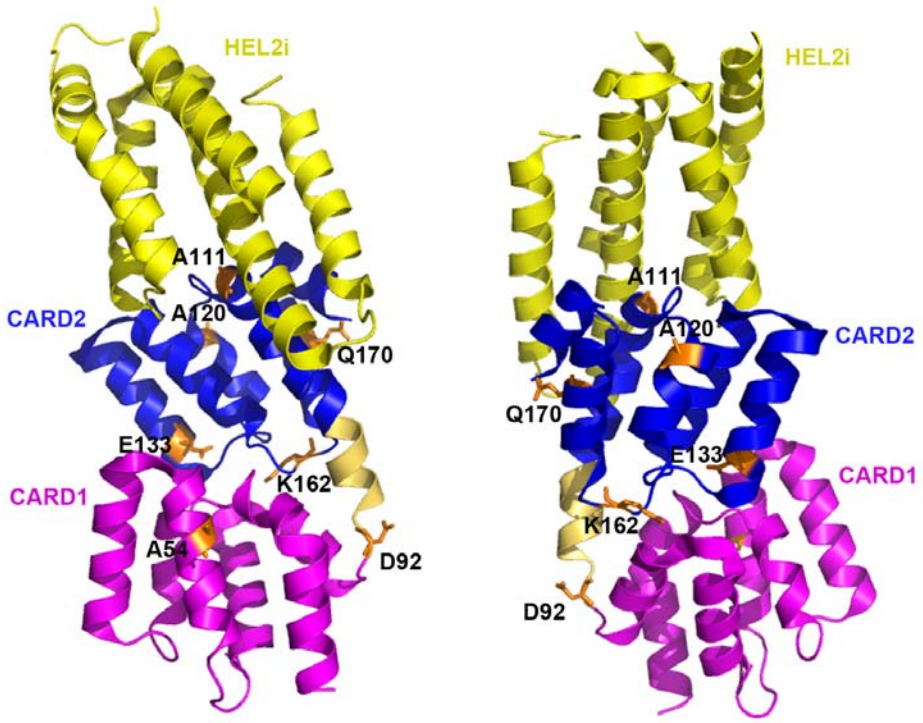

Figure 6.3. Residues characterized in this and previous studies in CARD mediating potential interactions.

Ribbon diagrams of dRIG-I tandem CARDs-HEL2i (left and right, rotated 180 around the vertical axis). Highlighted residues are described below.

A54 (T55 in human, same below): solvent-exposed.

D92 (D93): linker between CARD1 and CARD2.

A111 (P112): interface between CARD2 and HEL2i.

A120 (D122): maybe solvent-exposed.

E133 (E135): interface between CARD1 and CARD2.

K162 (K164): interface between CARD1 and CARD2.

Q170 (K172): close to the C-terminus of CARD2 that interacts with HEL2i.

APPENDIX A
List of Abbreviations

5'-ppp	5'-triphosphate
ATP	Adenosine triphosphate
bp	base pair
CARD	Caspase activation and recruitment
CYLD	Cylindromatosis protein
DD	death domain
DUB	deubiquitination enzyme
E1	ubiquitin-activating enzyme
E2	ubiquitin-conjugating enzyme
E3	ubiquitin protein ligase
EMCV	Encephalomyocarditis virus
GFP	green fluorescent protein
GST	glutathione S-transferase
HMW	high molecular weight
IB	immunoblotting
IFN	interferon
IκB	inhibitor of κB
IKK	IκB kinase
IL	interluekin
IP	immuno-precipitation

IRF	interferon regulatory factor
ISG	interferon-stimulated genes
IsoT	Iso-peptidase T
K63	lysine 63
KO	knock out
LGP	laboratory of genetics and physiology
MAPK	mitogen-activated protein kinase
MAVS	Mitochondrial antiviral-signaling protein
MDA	Melanoma Differentiation-Associated Gene
NEM	N-ethylmaleimide
NEMO	NF-κB essential modulator
NF-κB	nuclear factor κB
NLR	NOD-like receptor
NOD	Nucleotide-binding oligomerization domain
NZF	novel zinc finger
PAMP	pathogen-assocaited molecular pattern
PRR	pattern recognition receptor
RIG	retinoic acid-inducible gene
RLR	RIG-I like receptor
SDS-PAGE	sodium dodecyl sulfate polyacrylamide gel electrophoresis
SeV	Sendi virus
shRNA	small hairpin RNA

siRNA	small interfering RNA
TAK	transforming growth factor-β-activated kinase
TANK	TRAF family member-associated NF-κB activator
TBK	TANK-binding kinase
TLR	toll-like receptor
TNF	tumor necrosis factor
TRAF	TNF receptor associated factor
Ub	ubiquitin
UBC	ubiquitin-conjugating enzyme
Uev1A	ubiquitin-conjugating enzyme E2 variant 1 isoform A
WT	wild type

BIBLIOGRAPHY

1. Janeway, C.A., Jr. Approaching the asymptote? Evolution and revolution in immunology. *Cold Spring Harb Symp Quant Biol* **54 Pt 1**, 1-13 (1989).
2. Medzhitov, R. & Janeway, C., Jr. Innate immune recognition: mechanisms and pathways. *Immunol Rev* **173**, 89-97 (2000).
3. Fraser, I.P., Koziel, H. & Ezekowitz, R.A. The serum mannose-binding protein and the macrophage mannose receptor are pattern recognition molecules that link innate and adaptive immunity. *Semin Immunol* **10**, 363-72 (1998).
4. Yoneyama, M. et al. The RNA helicase RIG-I has an essential function in double-stranded RNA-induced innate antiviral responses. *Nat Immunol* **5**, 730-7 (2004).
5. Kang, D.C. et al. mda-5: An interferon-inducible putative RNA helicase with double-stranded RNA-dependent ATPase activity and melanoma growth-suppressive properties. *Proc Natl Acad Sci U S A* **99**, 637-42 (2002).
6. Chatziandreou, N., Young, D., Andrejeva, J., Goodbourn, S. & Randall, R.E. Differences in interferon sensitivity and biological properties of two related isolates of simian virus 5: a model for virus persistence. *Virology* **293**, 234-42 (2002).
7. Kovacsovics, M. et al. Overexpression of Helicard, a CARD-containing helicase cleaved during apoptosis, accelerates DNA degradation. *Curr Biol* **12**, 838-43 (2002).
8. Yoneyama, M. et al. Shared and unique functions of the DExD/H-box helicases RIG-I, MDA5, and LGP2 in antiviral innate immunity. *J Immunol* **175**, 2851-8 (2005).
9. Kato, H. et al. Cell type-specific involvement of RIG-I in antiviral response. *Immunity* **23**, 19-28 (2005).
10. Melchjorsen, J. et al. Activation of innate defense against a paramyxovirus is mediated by RIG-I and TLR7 and TLR8 in a cell-type-specific manner. *J Virol* **79**, 12944-51 (2005).
11. Li, K., Chen, Z., Kato, N., Gale, M., Jr. & Lemon, S.M. Distinct poly(I-C) and virus-activated signaling pathways leading to interferon-beta production in hepatocytes. *J Biol Chem* **280**, 16739-47 (2005).
12. Liu, P. et al. Retinoic acid-inducible gene I mediates early antiviral response and Toll-like receptor 3 expression in respiratory syncytial virus-infected airway epithelial cells. *J Virol* **81**, 1401-11 (2007).
13. Kang, D.C. et al. Expression analysis and genomic characterization of human melanoma differentiation associated gene-5, mda-5: a novel type I interferon-responsive apoptosis-inducing gene. *Oncogene* **23**, 1789-800 (2004).
14. Peltier, D.C., Simms, A., Farmer, J.R. & Miller, D.J. Human neuronal cells possess functional cytoplasmic and TLR-mediated innate immune pathways influenced by phosphatidylinositol-3 kinase signaling. *J Immunol* **184**, 7010-21 (2010).

15. Gack, M.U. et al. Roles of RIG-I N-terminal tandem CARD and splice variant in TRIM25-mediated antiviral signal transduction. *Proc Natl Acad Sci U S A* **105**, 16743-8 (2008).
16. Pothlichet, J. et al. Study of human RIG-I polymorphisms identifies two variants with an opposite impact on the antiviral immune response. *PLoS One* **4**, e7582 (2009).
17. Nistal-Villan, E. et al. Negative role of RIG-I serine 8 phosphorylation in the regulation of interferon-beta production. *J Biol Chem* **285**, 20252-61 (2010).
18. McCartney, S.A. et al. MDA-5 recognition of a murine norovirus. *PLoS Pathog* **4**, e1000108 (2008).
19. Roth-Cross, J.K., Bender, S.J. & Weiss, S.R. Murine coronavirus mouse hepatitis virus is recognized by MDA5 and induces type I interferon in brain macrophages/microglia. *J Virol* **82**, 9829-38 (2008).
20. Fredericksen, B.L., Keller, B.C., Fornek, J., Katze, M.G. & Gale, M., Jr. Establishment and maintenance of the innate antiviral response to West Nile Virus involves both RIG-I and MDA5 signaling through IPS-1. *J Virol* **82**, 609-16 (2008).
21. Gitlin, L. et al. Melanoma differentiation-associated gene 5 (MDA5) is involved in the innate immune response to Paramyxoviridae infection in vivo. *PLoS Pathog* **6**, e1000734 (2010).
22. Childs, K. et al. mda-5, but not RIG-I, is a common target for paramyxovirus V proteins. *Virology* **359**, 190-200 (2007).
23. Yount, J.S., Gitlin, L., Moran, T.M. & Lopez, C.B. MDA5 participates in the detection of paramyxovirus infection and is essential for the early activation of dendritic cells in response to Sendai Virus defective interfering particles. *J Immunol* **180**, 4910-8 (2008).
24. Garcin, D., Latorre, P. & Kolakofsky, D. Sendai virus C proteins counteract the interferon-mediated induction of an antiviral state. *J Virol* **73**, 6559-65 (1999).
25. Parisien, J.P. et al. A shared interface mediates paramyxovirus interference with antiviral RNA helicases MDA5 and LGP2. *J Virol* **83**, 7252-60 (2009).
26. Loo, Y.M. et al. Distinct RIG-I and MDA5 signaling by RNA viruses in innate immunity. *J Virol* **82**, 335-45 (2008).
27. Li, J., Liu, Y. & Zhang, X. Murine coronavirus induces type I interferon in oligodendrocytes through recognition by RIG-I and MDA5. *J Virol* **84**, 6472-82 (2010).
28. Ikegame, S. et al. Both RIG-I and MDA5 RNA helicases contribute to the induction of alpha/beta interferon in measles virus-infected human cells. *J Virol* **84**, 372-9 (2010).
29. Andrejeva, J. et al. The V proteins of paramyxoviruses bind the IFN-inducible RNA helicase, mda-5, and inhibit its activation of the IFN-beta promoter. *Proc Natl Acad Sci U S A* **101**, 17264-9 (2004).
30. Rothenfusser, S. et al. The RNA helicase Lgp2 inhibits TLR-independent sensing of viral replication by retinoic acid-inducible gene-I. *J Immunol* **175**, 5260-8 (2005).

31. Venkataraman, T. et al. Loss of DExD/H box RNA helicase LGP2 manifests disparate antiviral responses. *J Immunol* **178**, 6444-55 (2007).
32. Satoh, T. et al. LGP2 is a positive regulator of RIG-I- and MDA5-mediated antiviral responses. *Proc Natl Acad Sci U S A* **107**, 1512-7 (2010).
33. Yoneyama, M. & Fujita, T. RIG-I: critical regulator for virus-induced innate immunity. *Tanpakushitsu Kakusan Koso* **49**, 2571-8 (2004).
34. Marques, J.T. & Williams, B.R. Activation of the mammalian immune system by siRNAs. *Nat Biotechnol* **23**, 1399-405 (2005).
35. Kim, D.H. et al. Interferon induction by siRNAs and ssRNAs synthesized by phage polymerase. *Nat Biotechnol* **22**, 321-5 (2004).
36. Marques, J.T. et al. A structural basis for discriminating between self and nonself double-stranded RNAs in mammalian cells. *Nat Biotechnol* **24**, 559-65 (2006).
37. Hornung, V. et al. 5'-Triphosphate RNA is the ligand for RIG-I. *Science* **314**, 994-7 (2006).
38. Pichlmair, A. et al. RIG-I-mediated antiviral responses to single-stranded RNA bearing 5'-phosphates. *Science* **314**, 997-1001 (2006).
39. Lee, Y.F., Nomoto, A., Detjen, B.M. & Wimmer, E. A protein covalently linked to poliovirus genome RNA. *Proc Natl Acad Sci U S A* **74**, 59-63 (1977).
40. Habjan, M. et al. Processing of genome 5' termini as a strategy of negative-strand RNA viruses to avoid RIG-I-dependent interferon induction. *PLoS One* **3**, e2032 (2008).
41. Saito, T., Owen, D.M., Jiang, F., Marcotrigiano, J. & Gale, M., Jr. Innate immunity induced by composition-dependent RIG-I recognition of hepatitis C virus RNA. *Nature* **454**, 523-7 (2008).
42. Uzri, D. & Gehrke, L. Nucleotide sequences and modifications that determine RIG-I/RNA binding and signaling activities. *J Virol* **83**, 4174-84 (2009).
43. Kato, H. et al. Length-dependent recognition of double-stranded ribonucleic acids by retinoic acid-inducible gene-I and melanoma differentiation-associated gene 5. *J Exp Med* **205**, 1601-10 (2008).
44. Schlee, M. et al. Recognition of 5' triphosphate by RIG-I helicase requires short blunt double-stranded RNA as contained in panhandle of negative-strand virus. *Immunity* **31**, 25-34 (2009).
45. Schmidt, A. et al. 5'-triphosphate RNA requires base-paired structures to activate antiviral signaling via RIG-I. *Proc Natl Acad Sci U S A* **106**, 12067-72 (2009).
46. Takahasi, K. et al. Nonself RNA-sensing mechanism of RIG-I helicase and activation of antiviral immune responses. *Mol Cell* **29**, 428-40 (2008).
47. Rehwinkel, J. et al. RIG-I detects viral genomic RNA during negative-strand RNA virus infection. *Cell* **140**, 397-408 (2010).
48. Baum, A., Sachidanandam, R. & Garcia-Sastre, A. Preference of RIG-I for short viral RNA molecules in infected cells revealed by next-generation sequencing. *Proc Natl Acad Sci U S A* (2010).
49. Malathi, K., Dong, B., Gale, M., Jr. & Silverman, R.H. Small self-RNA generated by RNase L amplifies antiviral innate immunity. *Nature* **448**, 816-9 (2007).

50. Pichlmair, A. et al. Activation of MDA5 requires higher-order RNA structures generated during virus infection. *J Virol* **83**, 10761-9 (2009).
51. Zust, R. et al. Ribose 2'-O-methylation provides a molecular signature for the distinction of self and non-self mRNA dependent on the RNA sensor Mda5. *Nat Immunol* **12**, 137-43 (2011).
52. Luthra, P., Sun, D., Silverman, R.H. & He, B. Activation of IFN-{beta} expression by a viral mRNA through RNase L and MDA5. *Proc Natl Acad Sci U S A* **108**, 2118-23 (2011).
53. Saito, T. et al. Regulation of innate antiviral defenses through a shared repressor domain in RIG-I and LGP2. *Proc Natl Acad Sci U S A* **104**, 582-7 (2007).
54. Cui, S. et al. The C-terminal regulatory domain is the RNA 5'-triphosphate sensor of RIG-I. *Mol Cell* **29**, 169-79 (2008).
55. Lu, C. et al. The structural basis of 5' triphosphate double-stranded RNA recognition by RIG-I C-terminal domain. *Structure* **18**, 1032-43 (2010).
56. Wang, Y. et al. Structural and functional insights into 5'-ppp RNA pattern recognition by the innate immune receptor RIG-I. *Nat Struct Mol Biol* **17**, 781-7 (2010).
57. Jiang, F. et al. Structural basis of RNA recognition and activation by innate immune receptor RIG-I. *Nature* (2011).
58. Luo, D. et al. Structural Insights into RNA Recognition by RIG-I. *Cell* **147**, 409-22 (2011).
59. Kowalinski, E. et al. Structural Basis for the Activation of Innate Immune Pattern-Recognition Receptor RIG-I by Viral RNA. *Cell* **147**, 423-35 (2011).
60. Bamming, D. & Horvath, C.M. Regulation of signal transduction by enzymatically inactive antiviral RNA helicase proteins MDA5, RIG-I, and LGP2. *J Biol Chem* **284**, 9700-12 (2009).
61. Murali, A. et al. Structure and function of LGP2, a DEX(D/H) helicase that regulates the innate immunity response. *J Biol Chem* **283**, 15825-33 (2008).
62. Pippig, D.A. et al. The regulatory domain of the RIG-I family ATPase LGP2 senses double-stranded RNA. *Nucleic Acids Res* **37**, 2014-25 (2009).
63. Li, X. et al. The RIG-I-like receptor LGP2 recognizes the termini of double-stranded RNA. *J Biol Chem* **284**, 13881-91 (2009).
64. Li, X. et al. Structural basis of double-stranded RNA recognition by the RIG-I like receptor MDA5. *Arch Biochem Biophys* **488**, 23-33 (2009).
65. Takahasi, K. et al. Solution structures of cytosolic RNA sensor MDA5 and LGP2 C-terminal domains: identification of the RNA recognition loop in RIG-I-like receptors. *J Biol Chem* **284**, 17465-74 (2009).
66. Ranjith-Kumar, C.T. et al. Agonist and antagonist recognition by RIG-I, a cytoplasmic innate immunity receptor. *J Biol Chem* **284**, 1155-65 (2009).
67. Myong, S. et al. Cytosolic viral sensor RIG-I is a 5'-triphosphate-dependent translocase on double-stranded RNA. *Science* **323**, 1070-4 (2009).
68. Park, H.H. et al. The death domain superfamily in intracellular signaling of apoptosis and inflammation. *Annu Rev Immunol* **25**, 561-86 (2007).
69. Kawai, T. et al. IPS-1, an adaptor triggering RIG-I- and Mda5-mediated type I interferon induction. *Nat Immunol* **6**, 981-8 (2005).

70. Meylan, E. et al. Cardif is an adaptor protein in the RIG-I antiviral pathway and is targeted by hepatitis C virus. *Nature* **437**, 1167-72 (2005).
71. Seth, R.B., Sun, L., Ea, C.K. & Chen, Z.J. Identification and characterization of MAVS, a mitochondrial antiviral signaling protein that activates NF-kappaB and IRF 3. *Cell* **122**, 669-82 (2005).
72. Xu, L.G. et al. VISA is an adapter protein required for virus-triggered IFN-beta signaling. *Mol Cell* **19**, 727-40 (2005).
73. Gack, M.U. et al. TRIM25 RING-finger E3 ubiquitin ligase is essential for RIG-I-mediated antiviral activity. *Nature* **446**, 916-920 (2007).
74. Wang, P. et al. Caspase-12 controls West Nile virus infection via the viral RNA receptor RIG-I. *Nat Immunol* (2010).
75. Zhang, M. et al. Regulation of IkappaB kinase-related kinases and antiviral responses by tumor suppressor CYLD. *J Biol Chem* **283**, 18621-6 (2008).
76. Friedman, C.S. et al. The tumour suppressor CYLD is a negative regulator of RIG-I-mediated antiviral response. *EMBO Rep* **9**, 930-6 (2008).
77. Jounai, N. et al. The Atg5 Atg12 conjugate associates with innate antiviral immune responses. *Proc Natl Acad Sci U S A* **104**, 14050-5 (2007).
78. Kim, M.J., Hwang, S.Y., Imaizumi, T. & Yoo, J.Y. Negative feedback regulation of RIG-I-mediated antiviral signaling by interferon-induced ISG15 conjugation. *J Virol* **82**, 1474-83 (2008).
79. Arimoto, K., Konishi, H. & Shimotohno, K. UbcH8 regulates ubiquitin and ISG15 conjugation to RIG-I. *Mol Immunol* **45**, 1078-84 (2008).
80. Gack, M.U., Nistal-Villan, E., Inn, K.S., Garcia-Sastre, A. & Jung, J.U. Phosphorylation-mediated negative regulation of RIG-I antiviral activity. *J Virol* **84**, 3220-9 (2010).
81. Sun, Q. et al. The specific and essential role of MAVS in antiviral innate immune responses. *Immunity* **24**, 633-42 (2006).
82. Dixit, E. et al. Peroxisomes are signaling platforms for antiviral innate immunity. *Cell* **141**, 668-81 (2010).
83. Tang, E.D. & Wang, C.Y. MAVS self-association mediates antiviral innate immune signaling. *J Virol* **83**, 3420-8 (2009).
84. Baril, M., Racine, M.E., Penin, F. & Lamarre, D. MAVS dimer is a crucial signaling component of innate immunity and the target of hepatitis C virus NS3/4A protease. *J Virol* **83**, 1299-311 (2009).
85. Hou, F. et al. MAVS forms functional prion-like aggregates to activate and propagate antiviral innate immune response. *Cell* **146**, 448-61 (2011).
86. Balachandran, S., Thomas, E. & Barber, G.N. A FADD-dependent innate immune mechanism in mammalian cells. *Nature* **432**, 401-5 (2004).
87. Michallet, M.C. et al. TRADD protein is an essential component of the RIG-like helicase antiviral pathway. *Immunity* **28**, 651-61 (2008).
88. Ermolaeva, M.A. et al. Function of TRADD in tumor necrosis factor receptor 1 signaling and in TRIF-dependent inflammatory responses. *Nat Immunol* **9**, 1037-46 (2008).

89. Poeck, H. et al. Recognition of RNA virus by RIG-I results in activation of CARD9 and inflammasome signaling for interleukin 1 beta production. *Nat Immunol* **11**, 63-9 (2010).
90. Diao, F. et al. Negative regulation of MDA5- but not RIG-I-mediated innate antiviral signaling by the dihydroxyacetone kinase. *Proc Natl Acad Sci U S A* **104**, 11706-11 (2007).
91. Gao, D. et al. REUL is a novel E3 ubiquitin ligase and stimulator of retinoic-acid-inducible gene-I. *PLoS One* **4**, e5760 (2009).
92. Arimoto, K. et al. Negative regulation of the RIG-I signaling by the ubiquitin ligase RNF125. *Proc Natl Acad Sci U S A* **104**, 7500-5 (2007).
93. Oshiumi, H., Matsumoto, M., Hatakeyama, S. & Seya, T. Riplet/RNF135, a RING finger protein, ubiquitinates RIG-I to promote interferon-beta induction during the early phase of viral infection. *J Biol Chem* **284**, 807-17 (2009).
94. Castanier, C., Garcin, D., Vazquez, A. & Arnoult, D. Mitochondrial dynamics regulate the RIG-I-like receptor antiviral pathway. *EMBO Rep* **11**, 133-8 (2010).
95. Onoguchi, K. et al. Virus-infection or 5'ppp-RNA activates antiviral signal through redistribution of IPS-1 mediated by MFN1. *PLoS Pathog* **6**, e1001012 (2010).
96. Yasukawa, K. et al. Mitofusin 2 inhibits mitochondrial antiviral signaling. *Sci Signal* **2**, ra47 (2009).
97. Moore, C.B. et al. NLRX1 is a regulator of mitochondrial antiviral immunity. *Nature* **451**, 573-7 (2008).
98. Xu, L., Xiao, N., Liu, F., Ren, H. & Gu, J. Inhibition of RIG-I and MDA5-dependent antiviral response by gC1qR at mitochondria. *Proc Natl Acad Sci U S A* **106**, 1530-5 (2009).
99. You, F. et al. PCBP2 mediates degradation of the adaptor MAVS via the HECT ubiquitin ligase AIP4. *Nat Immunol* **10**, 1300-8 (2009).
100. Jia, Y. et al. Negative regulation of MAVS-mediated innate immune response by PSMA7. *J Immunol* **183**, 4241-8 (2009).
101. Kayagaki, N. et al. DUBA: a deubiquitinase that regulates type I interferon production. *Science* **318**, 1628-32 (2007).
102. Nakhaei, P. et al. The E3 ubiquitin ligase Triad3A negatively regulates the RIG-I/MAVS signaling pathway by targeting TRAF3 for degradation. *PLoS Pathog* **5**, e1000650 (2009).
103. Johnsen, I.B., Nguyen, T.T., Bergstroem, B., Fitzgerald, K.A. & Anthonsen, M.W. The tyrosine kinase c-Src enhances RIG-I (retinoic acid-inducible gene I)-elicited antiviral signaling. *J Biol Chem* **284**, 19122-31 (2009).
104. Cui, J. et al. NLRC5 negatively regulates the NF-kappaB and type I interferon signaling pathways. *Cell* **141**, 483-96 (2010).
105. An, H. et al. Phosphatase SHP-1 promotes TLR- and RIG-I-activated production of type I interferon by inhibiting the kinase IRAK1. *Nat Immunol* **9**, 542-50 (2008).
106. Lemaitre, B., Nicolas, E., Michaut, L., Reichhart, J.M. & Hoffmann, J.A. The dorsoventral regulatory gene cassette spatzle/Toll/cactus controls the potent antifungal response in Drosophila adults. *Cell* **86**, 973-83 (1996).

107. Belvin, M.P. & Anderson, K.V. A conserved signaling pathway: the Drosophila toll-dorsal pathway. *Annu Rev Cell Dev Biol* **12**, 393-416 (1996).
108. Jin, M.S. & Lee, J.O. Structures of the toll-like receptor family and its ligand complexes. *Immunity* **29**, 182-91 (2008).
109. Kubarenko, A., Frank, M. & Weber, A.N. Structure-function relationships of Toll-like receptor domains through homology modelling and molecular dynamics. *Biochem Soc Trans* **35**, 1515-8 (2007).
110. O'Neill, L.A., Fitzgerald, K.A. & Bowie, A.G. The Toll-IL-1 receptor adaptor family grows to five members. *Trends Immunol* **24**, 286-90 (2003).
111. Medzhitov, R., Preston-Hurlburt, P. & Janeway, C.A., Jr. A human homologue of the Drosophila Toll protein signals activation of adaptive immunity. *Nature* **388**, 394-7 (1997).
112. Poltorak, A. et al. Defective LPS signaling in C3H/HeJ and C57BL/10ScCr mice: mutations in Tlr4 gene. *Science* **282**, 2085-8 (1998).
113. Takeuchi, O. et al. Differential roles of TLR2 and TLR4 in recognition of gram-negative and gram-positive bacterial cell wall components. *Immunity* **11**, 443-51 (1999).
114. Hayashi, F. et al. The innate immune response to bacterial flagellin is mediated by Toll-like receptor 5. *Nature* **410**, 1099-103 (2001).
115. Uematsu, S. et al. Detection of pathogenic intestinal bacteria by Toll-like receptor 5 on intestinal CD11c+ lamina propria cells. *Nat Immunol* **7**, 868-74 (2006).
116. Uematsu, S. et al. Regulation of humoral and cellular gut immunity by lamina propria dendritic cells expressing Toll-like receptor 5. *Nat Immunol* **9**, 769-76 (2008).
117. Zhang, D. et al. A toll-like receptor that prevents infection by uropathogenic bacteria. *Science* **303**, 1522-6 (2004).
118. Yarovinsky, F. et al. TLR11 activation of dendritic cells by a protozoan profilin-like protein. *Science* **308**, 1626-9 (2005).
119. Alexopoulou, L., Holt, A.C., Medzhitov, R. & Flavell, R.A. Recognition of double-stranded RNA and activation of NF-kappaB by Toll-like receptor 3. *Nature* **413**, 732-8 (2001).
120. Edelmann, K.H. et al. Does Toll-like receptor 3 play a biological role in virus infections? *Virology* **322**, 231-8 (2004).
121. Le Goffic, R. et al. Detrimental contribution of the Toll-like receptor (TLR)3 to influenza A virus-induced acute pneumonia. *PLoS Pathog* **2**, e53 (2006).
122. Diebold, S.S. Recognition of viral single-stranded RNA by Toll-like receptors. *Adv Drug Deliv Rev* **60**, 813-23 (2008).
123. Diebold, S.S., Kaisho, T., Hemmi, H., Akira, S. & Reis e Sousa, C. Innate antiviral responses by means of TLR7-mediated recognition of single-stranded RNA. *Science* **303**, 1529-31 (2004).
124. Heil, F. et al. Species-specific recognition of single-stranded RNA via toll-like receptor 7 and 8. *Science* **303**, 1526-9 (2004).

125. Hornung, V. et al. Sequence-specific potent induction of IFN-alpha by short interfering RNA in plasmacytoid dendritic cells through TLR7. *Nat Med* **11**, 263-70 (2005).
126. Hemmi, H. et al. A Toll-like receptor recognizes bacterial DNA. *Nature* **408**, 740-5 (2000).
127. Haas, T. et al. The DNA sugar backbone 2' deoxyribose determines toll-like receptor 9 activation. *Immunity* **28**, 315-23 (2008).
128. Cella, M. et al. Plasmacytoid monocytes migrate to inflamed lymph nodes and produce large amounts of type I interferon. *Nat Med* **5**, 919-23 (1999).
129. Colonna, M., Krug, A. & Cella, M. Interferon-producing cells: on the front line in immune responses against pathogens. *Curr Opin Immunol* **14**, 373-9 (2002).
130. Kumagai, Y. et al. Alveolar macrophages are the primary interferon-alpha producer in pulmonary infection with RNA viruses. *Immunity* **27**, 240-52 (2007).
131. O'Neill, L.A. & Bowie, A.G. The family of five: TIR-domain-containing adaptors in Toll-like receptor signalling. *Nat Rev Immunol* **7**, 353-64 (2007).
132. Hemmi, H. et al. Small anti-viral compounds activate immune cells via the TLR7 MyD88-dependent signaling pathway. *Nat Immunol* **3**, 196-200 (2002).
133. Kawai, T. et al. Interferon-alpha induction through Toll-like receptors involves a direct interaction of IRF7 with MyD88 and TRAF6. *Nat Immunol* **5**, 1061-8 (2004).
134. Kawai, T. & Akira, S. TLR signaling. *Cell Death Differ* **13**, 816-25 (2006).
135. Kagan, J.C. & Medzhitov, R. Phosphoinositide-mediated adaptor recruitment controls Toll-like receptor signaling. *Cell* **125**, 943-55 (2006).
136. Yamamoto, M. et al. Role of adaptor TRIF in the MyD88-independent toll-like receptor signaling pathway. *Science* **301**, 640-3 (2003).
137. Yamamoto, M. et al. TRAM is specifically involved in the Toll-like receptor 4-mediated MyD88-independent signaling pathway. *Nat Immunol* **4**, 1144-50 (2003).
138. Kagan, J.C. et al. TRAM couples endocytosis of Toll-like receptor 4 to the induction of interferon-beta. *Nat Immunol* **9**, 361-8 (2008).
139. Carty, M. et al. The human adaptor SARM negatively regulates adaptor protein TRIF-dependent Toll-like receptor signaling. *Nat Immunol* **7**, 1074-81 (2006).
140. Lin, S.C., Lo, Y.C. & Wu, H. Helical assembly in the MyD88-IRAK4-IRAK2 complex in TLR/IL-1R signalling. *Nature* **465**, 885-90 (2010).
141. Kawagoe, T. et al. Sequential control of Toll-like receptor-dependent responses by IRAK1 and IRAK2. *Nat Immunol* **9**, 684-91 (2008).
142. Conze, D.B., Wu, C.J., Thomas, J.A., Landstrom, A. & Ashwell, J.D. Lys63-linked polyubiquitination of IRAK-1 is required for interleukin-1 receptor- and toll-like receptor-mediated NF-kappaB activation. *Mol Cell Biol* **28**, 3538-47 (2008).
143. Cao, Z., Xiong, J., Takeuchi, M., Kurama, T. & Goeddel, D.V. TRAF6 is a signal transducer for interleukin-1. *Nature* **383**, 443-6 (1996).
144. Hacker, H. et al. Immune cell activation by bacterial CpG-DNA through myeloid differentiation marker 88 and tumor necrosis factor receptor-associated factor (TRAF)6. *J Exp Med* **192**, 595-600 (2000).

145. Gohda, J., Matsumura, T. & Inoue, J. Cutting edge: TNFR-associated factor (TRAF) 6 is essential for MyD88-dependent pathway but not toll/IL-1 receptor domain-containing adaptor-inducing IFN-beta (TRIF)-dependent pathway in TLR signaling. *J Immunol* **173**, 2913-7 (2004).
146. Hacker, H. et al. Specificity in Toll-like receptor signalling through distinct effector functions of TRAF3 and TRAF6. *Nature* **439**, 204-7 (2006).
147. Deng, L. et al. Activation of the IkappaB kinase complex by TRAF6 requires a dimeric ubiquitin-conjugating enzyme complex and a unique polyubiquitin chain. *Cell* **103**, 351-61 (2000).
148. Xia, Z.P. et al. Direct activation of protein kinases by unanchored polyubiquitin chains. *Nature* **461**, 114-9 (2009).
149. Ea, C.K., Deng, L., Xia, Z.P., Pineda, G. & Chen, Z.J. Activation of IKK by TNFalpha requires site-specific ubiquitination of RIP1 and polyubiquitin binding by NEMO. *Mol Cell* **22**, 245-57 (2006).
150. Wu, C.J., Conze, D.B., Li, T., Srinivasula, S.M. & Ashwell, J.D. Sensing of Lys 63-linked polyubiquitination by NEMO is a key event in NF-kappaB activation [corrected]. *Nat Cell Biol* **8**, 398-406 (2006).
151. Rahighi, S. et al. Specific recognition of linear ubiquitin chains by NEMO is important for NF-kappaB activation. *Cell* **136**, 1098-109 (2009).
152. Tokunaga, F. et al. Involvement of linear polyubiquitylation of NEMO in NF-kappaB activation. *Nat Cell Biol* **11**, 123-32 (2009).
153. Gilliet, M., Cao, W. & Liu, Y.J. Plasmacytoid dendritic cells: sensing nucleic acids in viral infection and autoimmune diseases. *Nat Rev Immunol* **8**, 594-606 (2008).
154. Honda, K. et al. Spatiotemporal regulation of MyD88-IRF-7 signalling for robust type-I interferon induction. *Nature* **434**, 1035-40 (2005).
155. Honda, K. et al. Role of a transductional-transcriptional processor complex involving MyD88 and IRF-7 in Toll-like receptor signaling. *Proc Natl Acad Sci U S A* **101**, 15416-21 (2004).
156. Uematsu, S. et al. Interleukin-1 receptor-associated kinase-1 plays an essential role for Toll-like receptor (TLR)7- and TLR9-mediated interferon-{alpha} induction. *J Exp Med* **201**, 915-23 (2005).
157. Hoshino, K. et al. IkappaB kinase-alpha is critical for interferon-alpha production induced by Toll-like receptors 7 and 9. *Nature* **440**, 949-53 (2006).
158. Oganesyan, G. et al. Critical role of TRAF3 in the Toll-like receptor-dependent and -independent antiviral response. *Nature* **439**, 208-11 (2006).
159. Sato, S. et al. Toll/IL-1 receptor domain-containing adaptor inducing IFN-beta (TRIF) associates with TNF receptor-associated factor 6 and TANK-binding kinase 1, and activates two distinct transcription factors, NF-kappa B and IFN-regulatory factor-3, in the Toll-like receptor signaling. *J Immunol* **171**, 4304-10 (2003).
160. Jiang, Z., Mak, T.W., Sen, G. & Li, X. Toll-like receptor 3-mediated activation of NF-kappaB and IRF3 diverges at Toll-IL-1 receptor domain-containing adapter inducing IFN-beta. *Proc Natl Acad Sci U S A* **101**, 3533-8 (2004).

161. Meylan, E. et al. RIP1 is an essential mediator of Toll-like receptor 3-induced NF-kappa B activation. *Nat Immunol* **5**, 503-7 (2004).
162. Cusson-Hermance, N., Khurana, S., Lee, T.H., Fitzgerald, K.A. & Kelliher, M.A. Rip1 mediates the Trif-dependent toll-like receptor 3- and 4-induced NF-{kappa}B activation but does not contribute to interferon regulatory factor 3 activation. *J Biol Chem* **280**, 36560-6 (2005).
163. Pobezinskaya, Y.L. et al. The function of TRADD in signaling through tumor necrosis factor receptor 1 and TRIF-dependent Toll-like receptors. *Nat Immunol* **9**, 1047-54 (2008).
164. Huang, G., Shi, L.Z. & Chi, H. Regulation of JNK and p38 MAPK in the immune system: signal integration, propagation and termination. *Cytokine* **48**, 161-9 (2009).
165. Matsuzawa, A. et al. ROS-dependent activation of the TRAF6-ASK1-p38 pathway is selectively required for TLR4-mediated innate immunity. *Nat Immunol* **6**, 587-92 (2005).
166. Dumitru, C.D. et al. TNF-alpha induction by LPS is regulated posttranscriptionally via a Tpl2/ERK-dependent pathway. *Cell* **103**, 1071-83 (2000).
167. Kaiser, F. et al. TPL-2 negatively regulates interferon-beta production in macrophages and myeloid dendritic cells. *J Exp Med* **206**, 1863-71 (2009).
168. Kanneganti, T.D., Lamkanfi, M. & Nunez, G. Intracellular NOD-like receptors in host defense and disease. *Immunity* **27**, 549-59 (2007).
169. Ogura, Y. et al. A frameshift mutation in NOD2 associated with susceptibility to Crohn's disease. *Nature* **411**, 603-6 (2001).
170. Hugot, J.P. et al. Association of NOD2 leucine-rich repeat variants with susceptibility to Crohn's disease. *Nature* **411**, 599-603 (2001).
171. Kobayashi, K.S. et al. Nod2-dependent regulation of innate and adaptive immunity in the intestinal tract. *Science* **307**, 731-4 (2005).
172. Ting, J.P., Duncan, J.A. & Lei, Y. How the noninflammasome NLRs function in the innate immune system. *Science* **327**, 286-90 (2010).
173. Sabbah, A. et al. Activation of innate immune antiviral responses by Nod2. *Nat Immunol* **10**, 1073-80 (2009).
174. Chin, A.I. et al. Involvement of receptor-interacting protein 2 in innate and adaptive immune responses. *Nature* **416**, 190-4 (2002).
175. Kobayashi, K. et al. RICK/Rip2/CARDIAK mediates signalling for receptors of the innate and adaptive immune systems. *Nature* **416**, 194-9 (2002).
176. Park, J.H. et al. RICK/RIP2 mediates innate immune responses induced through Nod1 and Nod2 but not TLRs. *J Immunol* **178**, 2380-6 (2007).
177. Pan, Q. et al. MDP-induced interleukin-1beta processing requires Nod2 and CIAS1/NALP3. *J Leukoc Biol* **82**, 177-83 (2007).
178. Bertrand, M.J. et al. Cellular inhibitors of apoptosis cIAP1 and cIAP2 are required for innate immunity signaling by the pattern recognition receptors NOD1 and NOD2. *Immunity* **30**, 789-801 (2009).
179. Hasegawa, M. et al. A critical role of RICK/RIP2 polyubiquitination in Nod-induced NF-kappaB activation. *EMBO J* **27**, 373-83 (2008).

180. Hitotsumatsu, O. et al. The ubiquitin-editing enzyme A20 restricts nucleotide-binding oligomerization domain containing 2-triggered signals. *Immunity* **28**, 381-90 (2008).
181. Hsu, Y.M. et al. The adaptor protein CARD9 is required for innate immune responses to intracellular pathogens. *Nat Immunol* **8**, 198-205 (2007).
182. Hsu, L.C. et al. A NOD2-NALP1 complex mediates caspase-1-dependent IL-1beta secretion in response to Bacillus anthracis infection and muramyl dipeptide. *Proc Natl Acad Sci U S A* **105**, 7803-8 (2008).
183. Martinon, F., Burns, K. & Tschopp, J. The inflammasome: a molecular platform triggering activation of inflammatory caspases and processing of proIL-beta. *Mol Cell* **10**, 417-26 (2002).
184. Mariathasan, S. et al. Cryopyrin activates the inflammasome in response to toxins and ATP. *Nature* **440**, 228-32 (2006).
185. Kanneganti, T.D. et al. Bacterial RNA and small antiviral compounds activate caspase-1 through cryopyrin/Nalp3. *Nature* **440**, 233-6 (2006).
186. Sutterwala, F.S. et al. Critical role for NALP3/CIAS1/Cryopyrin in innate and adaptive immunity through its regulation of caspase-1. *Immunity* **24**, 317-27 (2006).
187. Gross, O. et al. Syk kinase signalling couples to the Nlrp3 inflammasome for anti-fungal host defence. *Nature* **459**, 433-6 (2009).
188. Muruve, D.A. et al. The inflammasome recognizes cytosolic microbial and host DNA and triggers an innate immune response. *Nature* **452**, 103-7 (2008).
189. Thomas, P.G. et al. The intracellular sensor NLRP3 mediates key innate and healing responses to influenza A virus via the regulation of caspase-1. *Immunity* **30**, 566-75 (2009).
190. Allen, I.C. et al. The NLRP3 inflammasome mediates in vivo innate immunity to influenza A virus through recognition of viral RNA. *Immunity* **30**, 556-65 (2009).
191. Martinon, F., Mayor, A. & Tschopp, J. The inflammasomes: guardians of the body. *Annu Rev Immunol* **27**, 229-65 (2009).
192. Tschopp, J. & Schroder, K. NLRP3 inflammasome activation: The convergence of multiple signalling pathways on ROS production? *Nat Rev Immunol* **10**, 210-5 (2010).
193. Agostini, L. et al. NALP3 forms an IL-1beta-processing inflammasome with increased activity in Muckle-Wells autoinflammatory disorder. *Immunity* **20**, 319-25 (2004).
194. Ishii, K.J. et al. A Toll-like receptor-independent antiviral response induced by double-stranded B-form DNA. *Nat Immunol* **7**, 40-8 (2006).
195. Stetson, D.B. & Medzhitov, R. Recognition of cytosolic DNA activates an IRF3-dependent innate immune response. *Immunity* **24**, 93-103 (2006).
196. Takaoka, A. et al. DAI (DLM-1/ZBP1) is a cytosolic DNA sensor and an activator of innate immune response. *Nature* **448**, 501-5 (2007).
197. Wang, Z. et al. Regulation of innate immune responses by DAI (DLM-1/ZBP1) and other DNA-sensing molecules. *Proc Natl Acad Sci U S A* **105**, 5477-82 (2008).

198. Kaiser, W.J., Upton, J.W. & Mocarski, E.S. Receptor-interacting protein homotypic interaction motif-dependent control of NF-kappa B activation via the DNA-dependent activator of IFN regulatory factors. *J Immunol* **181**, 6427-34 (2008).
199. Unterholzner, L. et al. IFI16 is an innate immune sensor for intracellular DNA. *Nat Immunol* **11**, 997-1004 (2010).
200. Ishikawa, H. & Barber, G.N. STING is an endoplasmic reticulum adaptor that facilitates innate immune signalling. *Nature* **455**, 674-8 (2008).
201. Ishikawa, H., Ma, Z. & Barber, G.N. STING regulates intracellular DNA-mediated, type I interferon-dependent innate immunity. *Nature* **461**, 788-92 (2009).
202. Zhong, B. et al. The adaptor protein MITA links virus-sensing receptors to IRF3 transcription factor activation. *Immunity* **29**, 538-50 (2008).
203. Tsuchida, T. et al. The ubiquitin ligase TRIM56 regulates innate immune responses to intracellular double-stranded DNA. *Immunity* **33**, 765-76 (2010).
204. Burckstummer, T. et al. An orthogonal proteomic-genomic screen identifies AIM2 as a cytoplasmic DNA sensor for the inflammasome. *Nat Immunol* **10**, 266-72 (2009).
205. Fernandes-Alnemri, T., Yu, J.W., Datta, P., Wu, J. & Alnemri, E.S. AIM2 activates the inflammasome and cell death in response to cytoplasmic DNA. *Nature* **458**, 509-13 (2009).
206. Hornung, V. et al. AIM2 recognizes cytosolic dsDNA and forms a caspase-1-activating inflammasome with ASC. *Nature* **458**, 514-8 (2009).
207. Roberts, T.L. et al. HIN-200 proteins regulate caspase activation in response to foreign cytoplasmic DNA. *Science* **323**, 1057-60 (2009).
208. Ablasser, A. et al. RIG-I-dependent sensing of poly(dA:dT) through the induction of an RNA polymerase III-transcribed RNA intermediate. *Nat Immunol* **10**, 1065-72 (2009).
209. Chiu, Y.H., Macmillan, J.B. & Chen, Z.J. RNA polymerase III detects cytosolic DNA and induces type I interferons through the RIG-I pathway. *Cell* **138**, 576-91 (2009).
210. Sato, M. et al. Distinct and essential roles of transcription factors IRF-3 and IRF-7 in response to viruses for IFN-alpha/beta gene induction. *Immunity* **13**, 539-48 (2000).
211. Honda, K. et al. IRF-7 is the master regulator of type-I interferon-dependent immune responses. *Nature* **434**, 772-7 (2005).
212. Panne, D., Maniatis, T. & Harrison, S.C. An atomic model of the interferon-beta enhanceosome. *Cell* **129**, 1111-23 (2007).
213. Saitoh, T. et al. Negative regulation of interferon-regulatory factor 3-dependent innate antiviral response by the prolyl isomerase Pin1. *Nat Immunol* **7**, 598-605 (2006).
214. Honda, K., Takaoka, A. & Taniguchi, T. Type I interferon [corrected] gene induction by the interferon regulatory factor family of transcription factors. *Immunity* **25**, 349-60 (2006).

215. Chau, T.L. et al. Are the IKKs and IKK-related kinases TBK1 and IKK-epsilon similarly activated? *Trends Biochem Sci* **33**, 171-80 (2008).
216. Zhao, T. et al. The NEMO adaptor bridges the nuclear factor-kappaB and interferon regulatory factor signaling pathways. *Nat Immunol* **8**, 592-600 (2007).
217. Shinohara, M.L. et al. Osteopontin expression is essential for interferon-alpha production by plasmacytoid dendritic cells. *Nat Immunol* **7**, 498-506 (2006).
218. Genin, P., Vaccaro, A. & Civas, A. The role of differential expression of human interferon--a genes in antiviral immunity. *Cytokine Growth Factor Rev* **20**, 283-95 (2009).
219. Colina, R. et al. Translational control of the innate immune response through IRF-7. *Nature* **452**, 323-8 (2008).
220. Savitsky, D., Tamura, T., Yanai, H. & Taniguchi, T. Regulation of immunity and oncogenesis by the IRF transcription factor family. *Cancer Immunol Immunother* **59**, 489-510 (2010).
221. Takaoka, A. et al. Integral role of IRF-5 in the gene induction programme activated by Toll-like receptors. *Nature* **434**, 243-9 (2005).
222. Balkhi, M.Y., Fitzgerald, K.A. & Pitha, P.M. IKKalpha negatively regulates IRF-5 function in a MyD88-TRAF6 pathway. *Cell Signal* **22**, 117-27 (2010).
223. Balkhi, M.Y., Fitzgerald, K.A. & Pitha, P.M. Functional regulation of MyD88-activated interferon regulatory factor 5 by K63-linked polyubiquitination. *Mol Cell Biol* **28**, 7296-308 (2008).
224. Tailor, P. et al. The feedback phase of type I interferon induction in dendritic cells requires interferon regulatory factor 8. *Immunity* **27**, 228-39 (2007).
225. Schmitz, F. et al. Interferon-regulatory-factor 1 controls Toll-like receptor 9-mediated IFN-beta production in myeloid dendritic cells. *Eur J Immunol* **37**, 315-27 (2007).
226. Mancuso, G. et al. Bacterial recognition by TLR7 in the lysosomes of conventional dendritic cells. *Nat Immunol* **10**, 587-94 (2009).
227. Yarilina, A., Park-Min, K.H., Antoniv, T., Hu, X. & Ivashkiv, L.B. TNF activates an IRF1-dependent autocrine loop leading to sustained expression of chemokines and STAT1-dependent type I interferon-response genes. *Nat Immunol* **9**, 378-87 (2008).
228. Taniguchi, T., Ogasawara, K., Takaoka, A. & Tanaka, N. IRF family of transcription factors as regulators of host defense. *Annu Rev Immunol* **19**, 623-55 (2001).
229. Darnell, J.E., Jr., Kerr, I.M. & Stark, G.R. Jak-STAT pathways and transcriptional activation in response to IFNs and other extracellular signaling proteins. *Science* **264**, 1415-21 (1994).
230. Maher, S.G., Romero-Weaver, A.L., Scarzello, A.J. & Gamero, A.M. Interferon: cellular executioner or white knight? *Curr Med Chem* **14**, 1279-89 (2007).
231. Stetson, D.B. & Medzhitov, R. Type I interferons in host defense. *Immunity* **25**, 373-81 (2006).
232. van Boxel-Dezaire, A.H., Rani, M.R. & Stark, G.R. Complex modulation of cell type-specific signaling in response to type I interferons. *Immunity* **25**, 361-72 (2006).

233. Santini, S.M. et al. Type I interferon as a powerful adjuvant for monocyte-derived dendritic cell development and activity in vitro and in Hu-PBL-SCID mice. *J Exp Med* **191**, 1777-88 (2000).
234. Le Bon, A. et al. Cross-priming of CD8+ T cells stimulated by virus-induced type I interferon. *Nat Immunol* **4**, 1009-15 (2003).
235. Lucas, M., Schachterle, W., Oberle, K., Aichele, P. & Diefenbach, A. Dendritic cells prime natural killer cells by trans-presenting interleukin 15. *Immunity* **26**, 503-17 (2007).
236. McCartney, S. et al. Distinct and complementary functions of MDA5 and TLR3 in poly(I:C)-mediated activation of mouse NK cells. *J Exp Med* **206**, 2967-76 (2009).
237. Lohoff, M. & Mak, T.W. Roles of interferon-regulatory factors in T-helper-cell differentiation. *Nat Rev Immunol* **5**, 125-35 (2005).
238. Marrack, P., Kappler, J. & Mitchell, T. Type I interferons keep activated T cells alive. *J Exp Med* **189**, 521-30 (1999).
239. Tough, D.F., Borrow, P. & Sprent, J. Induction of bystander T cell proliferation by viruses and type I interferon in vivo. *Science* **272**, 1947-50 (1996).
240. Le Bon, A. et al. Direct stimulation of T cells by type I IFN enhances the CD8+ T cell response during cross-priming. *J Immunol* **176**, 4682-9 (2006).
241. Pickart, C.M. Mechanisms underlying ubiquitination. *Annu Rev Biochem* **70**, 503-33 (2001).
242. Sun, S.C. Deubiquitylation and regulation of the immune response. *Nat Rev Immunol* **8**, 501-11 (2008).
243. Dikic, I., Wakatsuki, S. & Walters, K.J. Ubiquitin-binding domains - from structures to functions. *Nat Rev Mol Cell Biol* **10**, 659-71 (2009).
244. Kirisako, T. et al. A ubiquitin ligase complex assembles linear polyubiquitin chains. *EMBO J* **25**, 4877-87 (2006).
245. Xu, P. et al. Quantitative proteomics reveals the function of unconventional ubiquitin chains in proteasomal degradation. *Cell* **137**, 133-45 (2009).
246. Kerscher, O., Felberbaum, R. & Hochstrasser, M. Modification of proteins by ubiquitin and ubiquitin-like proteins. *Annu Rev Cell Dev Biol* **22**, 159-80 (2006).
247. Ye, Y. & Rape, M. Building ubiquitin chains: E2 enzymes at work. *Nat Rev Mol Cell Biol* **10**, 755-64 (2009).
248. Petroski, M.D. & Deshaies, R.J. Function and regulation of cullin-RING ubiquitin ligases. *Nat Rev Mol Cell Biol* **6**, 9-20 (2005).
249. Kawai, T. & Akira, S. The role of pattern-recognition receptors in innate immunity: update on Toll-like receptors. *Nat Immunol* **11**, 373-84 (2010).
250. Wang, C. et al. TAK1 is a ubiquitin-dependent kinase of MKK and IKK. *Nature* **412**, 346-51 (2001).
251. Kanayama, A. et al. TAB2 and TAB3 activate the NF-kappaB pathway through binding to polyubiquitin chains. *Mol Cell* **15**, 535-48 (2004).
252. Chang, M., Jin, W. & Sun, S.C. Peli1 facilitates TRIF-dependent Toll-like receptor signaling and proinflammatory cytokine production. *Nat Immunol* **10**, 1089-95 (2009).

253. Tseng, P.H. et al. Different modes of ubiquitination of the adaptor TRAF3 selectively activate the expression of type I interferons and proinflammatory cytokines. *Nat Immunol* **11**, 70-5 (2010).
254. Gonzalez-Navajas, J.M. et al. Interleukin 1 receptor signaling regulates DUBA expression and facilitates Toll-like receptor 9-driven antiinflammatory cytokine production. *J Exp Med* **207**, 2799-807 (2010).
255. Lin, S.C. et al. Molecular basis for the unique deubiquitinating activity of the NF-kappaB inhibitor A20. *J Mol Biol* **376**, 526-40 (2008).
256. Komander, D. & Barford, D. Structure of the A20 OTU domain and mechanistic insights into deubiquitination. *Biochem J* **409**, 77-85 (2008).
257. Komander, D. et al. The structure of the CYLD USP domain explains its specificity for Lys63-linked polyubiquitin and reveals a B box module. *Mol Cell* **29**, 451-64 (2008).
258. Harhaj, E.W. & Dixit, V.M. Deubiquitinases in the regulation of NF-kappaB signaling. *Cell Res* **21**, 22-39 (2011).
259. Wertz, I.E. et al. De-ubiquitination and ubiquitin ligase domains of A20 downregulate NF-kappaB signalling. *Nature* **430**, 694-9 (2004).
260. Bosanac, I. et al. Ubiquitin binding to A20 ZnF4 is required for modulation of NF-kappaB signaling. *Mol Cell* **40**, 548-57 (2010).
261. Boone, D.L. et al. The ubiquitin-modifying enzyme A20 is required for termination of Toll-like receptor responses. *Nat Immunol* **5**, 1052-60 (2004).
262. Turer, E.E. et al. Homeostatic MyD88-dependent signals cause lethal inflamMation in the absence of A20. *J Exp Med* **205**, 451-64 (2008).
263. Shembade, N., Ma, A. & Harhaj, E.W. Inhibition of NF-kappaB signaling by A20 through disruption of ubiquitin enzyme complexes. *Science* **327**, 1135-9 (2010).
264. Tavares, R.M. et al. The ubiquitin modifying enzyme A20 restricts B cell survival and prevents autoimmunity. *Immunity* **33**, 181-91 (2010).
265. Hovelmeyer, N. et al. A20 deficiency in B cells enhances B-cell proliferation and results in the development of autoantibodies. *Eur J Immunol* **41**, 595-601 (2011).
266. Chu, Y. et al. B cells lacking the tumor suppressor TNFAIP3/A20 display impaired differentiation and hyperactivation and cause inflammation and autoimmunity in aged mice. *Blood* **117**, 2227-36 (2011).
267. Coornaert, B. et al. T cell antigen receptor stimulation induces MALT1 paracaspase-mediated cleavage of the NF-kappaB inhibitor A20. *Nat Immunol* **9**, 263-71 (2008).
268. Duwel, M. et al. A20 negatively regulates T cell receptor signaling to NF-kappaB by cleaving Malt1 ubiquitin chains. *J Immunol* **182**, 7718-28 (2009).
269. Hong, B. et al. Mucosal and systemic anti-HIV immunity controlled by A20 in mouse dendritic cells. *J Clin Invest* **121**, 739-51 (2011).
270. Song, X.T. et al. A20 is an antigen presentation attenuator, and its inhibition overcomes regulatory T cell-mediated suppression. *Nat Med* **14**, 258-65 (2008).
271. Kovalenko, A. et al. The tumour suppressor CYLD negatively regulates NF-kappaB signalling by deubiquitination. *Nature* **424**, 801-5 (2003).

272. Trompouki, E. et al. CYLD is a deubiquitinating enzyme that negatively regulates NF-kappaB activation by TNFR family members. *Nature* **424**, 793-6 (2003).
273. Reiley, W.W. et al. Deubiquitinating enzyme CYLD negatively regulates the ubiquitin-dependent kinase Tak1 and prevents abnormal T cell responses. *J Exp Med* **204**, 1475-85 (2007).
274. Reiley, W.W. et al. Regulation of T cell development by the deubiquitinating enzyme CYLD. *Nat Immunol* **7**, 411-7 (2006).
275. Hovelmeyer, N. et al. Regulation of B cell homeostasis and activation by the tumor suppressor gene CYLD. *J Exp Med* **204**, 2615-27 (2007).
276. Jin, W. et al. Deubiquitinating enzyme CYLD regulates the peripheral development and naive phenotype maintenance of B cells. *J Biol Chem* **282**, 15884-93 (2007).
277. Zhang, M., Lee, A.J., Wu, X. & Sun, S.C. Regulation of antiviral innate immunity by deubiquitinase CYLD. *Cell Mol Immunol* (2011).
278. Han, C. et al. Integrin CD11b negatively regulates TLR-triggered inflammatory responses by activating Syk and promoting degradation of MyD88 and TRIF via Cbl-b. *Nat Immunol* **11**, 734-42 (2010).
279. Shi, M. et al. TRIM30 alpha negatively regulates TLR-mediated NF-kappa B activation by targeting TAB2 and TAB3 for degradation. *Nat Immunol* **9**, 369-77 (2008).
280. Yu, Y. & Hayward, G.S. The ubiquitin E3 ligase RAUL negatively regulates type i interferon through ubiquitination of the transcription factors IRF7 and IRF3. *Immunity* **33**, 863-77 (2010).
281. Virgin, H.W. & Levine, B. Autophagy genes in immunity. *Nat Immunol* **10**, 461-70 (2009).
282. Kirkin, V. et al. A role for NBR1 in autophagosomal degradation of ubiquitinated substrates. *Mol Cell* **33**, 505-16 (2009).
283. Kraft, C., Peter, M. & Hofmann, K. Selective autophagy: ubiquitin-mediated recognition and beyond. *Nat Cell Biol* **12**, 836-41 (2010).
284. Thurston, T.L., Ryzhakov, G., Bloor, S., von Muhlinen, N. & Randow, F. The TBK1 adaptor and autophagy receptor NDP52 restricts the proliferation of ubiquitin-coated bacteria. *Nat Immunol* **10**, 1215-21 (2009).
285. Zheng, Y.T. et al. The adaptor protein p62/SQSTM1 targets invading bacteria to the autophagy pathway. *J Immunol* **183**, 5909-16 (2009).
286. Wild, P. et al. Phosphorylation of the Autophagy Receptor Optineurin Restricts Salmonella Growth. *Science* (2011).
287. Ponpuak, M. et al. Delivery of cytosolic components by autophagic adaptor protein p62 endows autophagosomes with unique antimicrobial properties. *Immunity* **32**, 329-41 (2010).
288. van Niel, G., Wubbolts, R. & Stoorvogel, W. Endosomal sorting of MHC class II determines antigen presentation by dendritic cells. *Curr Opin Cell Biol* **20**, 437-44 (2008).
289. Shin, J.S. et al. Surface expression of MHC class II in dendritic cells is controlled by regulated ubiquitination. *Nature* **444**, 115-8 (2006).

290. van Niel, G. et al. Dendritic cells regulate exposure of MHC class II at their plasma membrane by oligoubiquitination. *Immunity* **25**, 885-94 (2006).
291. Matsuki, Y. et al. Novel regulation of MHC class II function in B cells. *EMBO J* **26**, 846-54 (2007).
292. Walseng, E. et al. Ubiquitination regulates MHC class II-peptide complex retention and degradation in dendritic cells. *Proc Natl Acad Sci U S A* **107**, 20465-70 (2010).
293. De Gassart, A. et al. MHC class II stabilization at the surface of human dendritic cells is the result of maturation-dependent MARCH I down-regulation. *Proc Natl Acad Sci U S A* **105**, 3491-6 (2008).
294. Thibodeau, J. et al. Interleukin-10-induced MARCH1 mediates intracellular sequestration of MHC class II in monocytes. *Eur J Immunol* **38**, 1225-30 (2008).
295. Tze, L.E. et al. CD83 increases MHC II and CD86 on dendritic cells by opposing IL-10-driven MARCH1-mediated ubiquitination and degradation. *J Exp Med* **208**, 149-65 (2011).
296. Lilley, B.N. & Ploegh, H.L. A membrane protein required for dislocation of misfolded proteins from the ER. *Nature* **429**, 834-40 (2004).
297. Ye, Y., Shibata, Y., Yun, C., Ron, D. & Rapoport, T.A. A membrane protein complex mediates retro-translocation from the ER lumen into the cytosol. *Nature* **429**, 841-7 (2004).
298. Stagg, H.R. et al. The TRC8 E3 ligase ubiquitinates MHC class I molecules before dislocation from the ER. *J Cell Biol* **186**, 685-92 (2009).
299. Burr, M.L. et al. HRD1 and UBE2J1 target misfolded MHC class I heavy chains for endoplasmic reticulum-associated degradation. *Proc Natl Acad Sci U S A* **108**, 2034-9 (2011).
300. Sun, L., Deng, L., Ea, C.K., Xia, Z.P. & Chen, Z.J. The TRAF6 ubiquitin ligase and TAK1 kinase mediate IKK activation by BCL10 and MALT1 in T lymphocytes. *Mol Cell* **14**, 289-301 (2004).
301. Stempin, C.C. et al. The E3 ubiquitin ligase mindbomb homolog 2 (Drosophila) (MIB2) controls B-cell CLL/lymphoma 10 (BCL10)-dependent NF-{kappa}B activation. *J Biol Chem* (2011).
302. King, C.G. et al. Cutting edge: requirement for TRAF6 in the induction of T cell anergy. *J Immunol* **180**, 34-8 (2008).
303. Mueller, D.L. E3 ubiquitin ligases as T cell anergy factors. *Nat Immunol* **5**, 883-90 (2004).
304. Nurieva, R.I. et al. The E3 ubiquitin ligase GRAIL regulates T cell tolerance and regulatory T cell function by mediating T cell receptor-CD3 degradation. *Immunity* **32**, 670-80 (2010).
305. Vardhana, S., Choudhuri, K., Varma, R. & Dustin, M.L. Essential role of ubiquitin and TSG101 protein in formation and function of the central supramolecular activation cluster. *Immunity* **32**, 531-40 (2010).
306. Huang, H. et al. K33-linked polyubiquitination of T cell receptor-zeta regulates proteolysis-independent T cell signaling. *Immunity* **33**, 60-70 (2010).
307. Chang, M. et al. The ubiquitin ligase Peli1 negatively regulates T cell activation and prevents autoimmunity. *Nat Immunol* **12**, 1002-9 (2011).

308. Vallabhapurapu, S. et al. Nonredundant and complementary functions of TRAF2 and TRAF3 in a ubiquitination cascade that activates NIK-dependent alternative NF-kappaB signaling. *Nat Immunol* **9**, 1364-70 (2008).
309. Matsuzawa, A. et al. Essential cytoplasmic translocation of a cytokine receptor-assembled signaling complex. *Science* **321**, 663-8 (2008).
310. Neumann, M. & Naumann, M. Beyond IkappaBs: alternative regulation of NF-kappaB activity. *FASEB J* **21**, 2642-54 (2007).
311. Dolganiuc, A. et al. Hepatitis C core and nonstructural 3 proteins trigger toll-like receptor 2-mediated pathways and inflammatory activation. *Gastroenterology* **127**, 1513-24 (2004).
312. Kurt-Jones, E.A. et al. Pattern recognition receptors TLR4 and CD14 mediate response to respiratory syncytial virus. *Nat Immunol* **1**, 398-401 (2000).
313. Jude, B.A. et al. Subversion of the innate immune system by a retrovirus. *Nat Immunol* **4**, 573-8 (2003).
314. Bieback, K. et al. Hemagglutinin protein of wild-type measles virus activates toll-like receptor 2 signaling. *J Virol* **76**, 8729-36 (2002).
315. Compton, T. et al. Human cytomegalovirus activates inflammatory cytokine responses via CD14 and Toll-like receptor 2. *J Virol* **77**, 4588-96 (2003).
316. Lund, J., Sato, A., Akira, S., Medzhitov, R. & Iwasaki, A. Toll-like receptor 9-mediated recognition of Herpes simplex virus-2 by plasmacytoid dendritic cells. *J Exp Med* **198**, 513-20 (2003).
317. Lund, J.M. et al. Recognition of single-stranded RNA viruses by Toll-like receptor 7. *Proc Natl Acad Sci U S A* **101**, 5598-603 (2004).
318. Barton, G.M., Kagan, J.C. & Medzhitov, R. Intracellular localization of Toll-like receptor 9 prevents recognition of self DNA but facilitates access to viral DNA. *Nat Immunol* **7**, 49-56 (2006).
319. Kariko, K., Buckstein, M., Ni, H. & Weissman, D. Suppression of RNA recognition by Toll-like receptors: the impact of nucleoside modification and the evolutionary origin of RNA. *Immunity* **23**, 165-75 (2005).
320. Colby, C. & Duesberg, P.H. Double-stranded RNA in vaccinia virus infected cells. *Nature* **222**, 940-4 (1969).
321. Marcus, P.I. & Sekellick, M.J. Defective interfering particles with covalently linked [+/-]RNA induce interferon. *Nature* **266**, 815-9 (1977).
322. Tsai, R.Y. & Reed, R.R. Using a eukaryotic GST fusion vector for proteins difficult to express in E. coli. *Biotechniques* **23**, 794-6, 798, 800 (1997).
323. He, J. & Chang, L.J. Functional characterization of hepatoma-specific stem cell antigen-2. *Mol Carcinog* **40**, 90-103 (2004).
324. Xu, M., Skaug, B., Zeng, W. & Chen, Z.J. A ubiquitin replacement strategy in human cells reveals distinct mechanisms of IKK activation by TNFalpha and IL-1beta. *Mol Cell* **36**, 302-14 (2009).
325. Pickart, C.M. & Raasi, S. Controlled synthesis of polyubiquitin chains. *Methods Enzymol* **399**, 21-36 (2005).
326. Alberti, S., Halfmann, R., King, O., Kapila, A. & Lindquist, S. A systematic survey identifies prions and illuminates sequence features of prionogenic proteins. *Cell* **137**, 146-58 (2009).

327. Padrick, S.B. et al. Determination of protein complex stoichiometry through multisignal sedimentation velocity experiments. *Anal Biochem* **407**, 89-103 (2010).
328. Balbo, A. et al. Studying multiprotein complexes by multisignal sedimentation velocity analytical ultracentrifugation. *Proc Natl Acad Sci U S A* **102**, 81-6 (2005).
329. Altschul, S.F. et al. Gapped BLAST and PSI-BLAST: a new generation of protein database search programs. *Nucleic Acids Res* **25**, 3389-402 (1997).
330. Frickey, T. & Lupas, A. CLANS: a Java application for visualizing protein families based on pairwise similarity. *Bioinformatics* **20**, 3702-4 (2004).
331. Holm, L., Kaariainen, S., Rosenstrom, P. & Schenkel, A. Searching protein structure databases with DaliLite v.3. *Bioinformatics* **24**, 2780-1 (2008).
332. Retief, J.D. Phylogenetic analysis using PHYLIP. *Methods Mol Biol* **132**, 243-58 (2000).
333. Zeng, W., Xu, M., Liu, S., Sun, L. & Chen, Z.J. Key role of Ubc5 and lysine-63 polyubiquitination in viral activation of IRF3. *Mol Cell* **36**, 315-25 (2009).
334. Kaiser, S.E. et al. Protein standard absolute quantification (PSAQ) method for the measurement of cellular ubiquitin pools. *Nat Methods* **8**, 691-6 (2011).
335. Mimnaugh, E.G., Chen, H.Y., Davie, J.R., Celis, J.E. & Neckers, L. Rapid deubiquitination of nucleosomal histones in human tumor cells caused by proteasome inhibitors and stress response inducers: effects on replication, transcription, translation, and the cellular stress response. *Biochemistry* **36**, 14418-29 (1997).
336. Terrell, J., Shih, S., Dunn, R. & Hicke, L. A function for monoubiquitination in the internalization of a G protein-coupled receptor. *Mol Cell* **1**, 193-202 (1998).
337. Wu, Z.H., Shi, Y., Tibbetts, R.S. & Miyamoto, S. Molecular linkage between the kinase ATM and NF-kappaB signaling in response to genotoxic stimuli. *Science* **311**, 1141-6 (2006).
338. Li, M. et al. Mono- versus polyubiquitination: differential control of p53 fate by Mdm2. *Science* **302**, 1972-5 (2003).
339. Zeng, W. et al. Reconstitution of the RIG-I pathway reveals a signaling role of unanchored polyubiquitin chains in innate immunity. *Cell* **141**, 315-30 (2010).
340. Reyes-Turcu, F.E. et al. The ubiquitin binding domain ZnF UBP recognizes the C-terminal diglycine motif of unanchored ubiquitin. *Cell* **124**, 1197-208 (2006).
341. Frias-Staheli, N. et al. Ovarian tumor domain-containing viral proteases evade ubiquitin- and ISG15-dependent innate immune responses. *Cell Host Microbe* **2**, 404-16 (2007).
342. Meyer, H.H., Wang, Y. & Warren, G. Direct binding of ubiquitin conjugates by the mammalian p97 adaptor complexes, p47 and Ufd1-Npl4. *EMBO J* **21**, 5645-52 (2002).
343. Hofmann, R.M. & Pickart, C.M. Noncanonical MMS2-encoded ubiquitin-conjugating enzyme functions in assembly of novel polyubiquitin chains for DNA repair. *Cell* **96**, 645-53 (1999).
344. Yamamoto, M. et al. Key function for the Ubc13 E2 ubiquitin-conjugating enzyme in immune receptor signaling. *Nat Immunol* **7**, 962-70 (2006).

345. Kato, H. et al. Differential roles of MDA5 and RIG-I helicases in the recognition of RNA viruses. *Nature* **441**, 101-5 (2006).
346. Lu, C., Ranjith-Kumar, C.T., Hao, L., Kao, C.C. & Li, P. Crystal structure of RIG-I C-terminal domain bound to blunt-ended double-strand RNA without 5' triphosphate. *Nucleic Acids Res* **39**, 1565-75 (2011).
347. Pertel, T. et al. TRIM5 is an innate immune sensor for the retrovirus capsid lattice. *Nature* **472**, 361-365 (2011).
348. Komuro, A. & Horvath, C.M. RNA- and virus-independent inhibition of antiviral signaling by RNA helicase LGP2. *J Virol* **80**, 12332-42 (2006).